University of Wollongong Thesis Collection   University of Wollongong Thesis Collections

2004

The effect of welding parameters on levels of diffusible hydrogen in weld metal deposited using gas shielded rutile flux cored wires

Miroslav Pitrun
University of Wollongong

THE EFFECT OF WELDING PARAMETERS ON LEVELS OF DIFFUSIBLE HYDROGEN IN WELD METAL DEPOSITED USING GAS SHIELDED RUTILE FLUX CORED WIRES

A thesis submitted in fulfillment of the requirements for the award of the degree of

DOCTOR OF PHILOSOPHY

from

THE UNIVERSITY OF WOLLONGONG

by

MIROSLAV PITRUN, M.Sc.

Department of Materials Engineering

2004

Declaration

I hereby declare that this submission is my own work and that, to the best of my knowledge and belief, it contains no material previously published or written by another person nor material which to a substantial extent has been accepted for the award of any other degree or diploma of a university or other institute of higher learning, except where due acknowledgment is made in the text.

_____

Miroslav Pitrun, M.Sc.

March 2004

Acknowledgments

Abstract

Hydrogen assisted cold cracking (HACC) represents a significant threat to the integrity of welded steel constructions. HACC occurs at near ambient or lower temperatures and may be delayed for several hours, or even days, after welding is completed.

Significant advances in developing thermomechanically controlled processed steels, with reduced carbon and alloy content, resulted in steels that are more resistant to HACC in the heat affected zone (HAZ). This has enabled the use of lower preheat temperatures during fabrication of welded structures. However, the improvement in the resistance of the HAZ to HACC has shifted the problem of cold cracking to the weld metal.

The objective of this current work was to establish the effect of flux cored arc welding (FCAW) welding parameters, such as welding current, contact-tip to workpiece distance (CTWD) and shielding gas type, on diffusible hydrogen (H_D) content for single run, bead-on-plate welds using low strength seamed and seamless gas shielded rutile wires of E71 T-1 classification. The work has shown that under most conditions investigated, the weld metal H_D levels for the seamed rutile wire were above the 10 ml/100g specified by the consumable's classification (H10). The measured range of diffusible hydrogen for the H10 wire was 8.3 to 17.0 ml/100g, with the highest hydrogen content being obtained at the lowest welding current of 280 A, shortest CTWD of 15 mm and deposited using 75Ar-25CO$_2$ shielding gas. In contrast, the seamless wire met requirements of the H5 classification ($H_D \leq$5 ml/100g) for all welding conditions investigated, with a range of H_D levels of 0.9 to 3.5 ml/100g.

In general, lower H_D levels were achieved when using CO_2 shielding gas, although the effect is less significant with the H5 seamless rutile wire.

The work included an investigation of arc characteristics under typical welding conditions, using high speed digital imaging and laser backlighting, in order to provide information on metal transfer and arc length. Several tests were carried out using the H10 consumable. It was established that the amount of heat generated by resistive heating of the wire prior to melting can exert a strong influence on the weld metal H_D content and is more pronounced in welds deposited using 75Ar-25CO_2. The measured arc length was reduced significantly when welding under CO_2 shielding gas. Despite suggestions in the literature there was no evidence of a change in metal transfer mode to spray transfer on increasing the welding current from 280 to 320 A, transfer mode was globular for all conditions used.

Following the weld metal diffusible hydrogen testing and welding arc imaging work, the weld metal susceptibility to cold cracking was assessed using the gapped bead-on-plate (G-BOP) test at different preheat temperatures. For this part of the work, identical welding parameters those used for the diffusible hydrogen testing were selected. It was found that the H5 wire weld deposits did not reveal any cracking at ambient temperature, whereas all the welds deposited using the H10 wire exhibited cold cracking with no preheat. Weld metal deposited using 75Ar-25CO_2 shielding gas resulted in higher susceptibility to cold cracking than with CO_2, which correlated to lower H_D levels the CO_2 tests. Besides the higher hydrogen content, it was also found that higher weld metal hardness corresponded to the greater crack susceptibility in the welds deposited using 75Ar-25CO_2 shielding gas. These factors are considered to contribute to higher susceptibility to transverse cold cracking compared with CO_2 shielding gas.

Although the overall results indicate that the weld metal susceptibility to cold cracking corresponds to the relevant levels of H_D, this relationship was found to be ambiguous in welds deposited at the shortest CTWD of 15 mm, using CO_2 shielding gas at all welding currents investigated. While the amount of diffusible hydrogen was marginally increased from 11.7 to 12.8 ml/100g, resulting from the welding current increase from 280 to 320 A, the amount of cold cracking at room temperature was significantly decreased from 89 to 25 %RTC. This is explained by a significant difference in the cross section of the weld beads, suggesting a need to more closely evaluate the G-BOP testing, particularly examining the effects of weld bead profiles on the weld susceptibility to HACC.

Preheat was found to decrease the amount of cold cracking in the H10 welds and it was concluded that preheat significantly reduces the main contributor to decrease the H_D in the weld metal. Although the cracking susceptibility of welds using 75Ar-25CO$_2$ shielding gas decreased more slowly with an increasing preheat temperature, compare to those deposited using CO_2, no cracking was observed at 120 °C in welds under both shielding gases. This indicates that the same welding consumable (H10) deposited using different shielding gases can result in a different response to preheat temperature.

Based on the results of this work, a number of changes are proposed to hydrogen testing standards AS 3752-1996 and ISO 3690-2000, particularly with respect to the effects of CTWD and shielding gases on levels of diffusible hydrogen in weld metal deposited using gas shielded rutile flux-cored wire.

Contents

CHAPTER 1

Introduction

Hydrogen assisted cold cracking (HACC), also known as cold or delayed cracking, represents one of the most common defects encountered in the welding industry today and, because of its importance, it has been the subject of much research for many years. It is well known that HACC may occur in steels during manufacture and during service in sour conditions. However, HACC also occurs during steel fabrication as a result of welding. This type of cracking can initiate several hours, or even days, after completion of welding. In structural steels, HACC takes place near or below ambient temperatures, but is unlikely to occur where temperatures above 150 °C are maintained. In practice, it is difficult to predict the time delay to the onset of cracking and therefore the incidence of HACC may be often overlooked, especially where the final inspection is carried out immediately or shortly after welding.

Despite more than fifty years of scientific investigation conducted around the world, HACC remains a significant phenomenon that compromises the integrity of welded structures. Cold cracking in weldments can be present either in the parent metal heat affected zone (HAZ) or in the weld metal itself. Possibly the most known case of hydrogen cracking occurrence in Australia was a collapse of the Kings Bridge early 1960s, when the initiating defect for the final fracture was identified as HAZ hydrogen cracks. Steel high carbon equivalent, inadequate preheat, control of consumable conditions and inspection were identified as the major multi-factor causes of the bridge collapse.

Although significant progress has been made in understanding the influence of process parameters on susceptibility of particular weld systems to hydrogen cracking in the HAZ, a comprehensive understanding of the mechanism(s) of weld metal HACC remains a subject of considerable scientific enquiry.

It is well established that hydrogen can be absorbed into the HAZ and weld metal during the welding process. The absorbed hydrogen can then interact with residual stresses to initiate and propagate cold cracking in the HAZ of the parent metal, where susceptible microstructures can develop as a result of the rapid cooling rate. Relatively recent developments in steel processing have resulted in a new generation of thermo-mechanically controlled process (TMCP) low carbon and low alloy steels with reduced carbon equivalents. As a result, the weldability of these steels has been markedly improved [Swinn et al. 1995], with HAZ microstructures that are less vulnerable to the effects of hydrogen [Yurioka and Suzuki 1990].

The improved weldability of TMCP steels, facilitating lower preheat temperature requirements, was a major advance in the technology of structural steel. Although HACC in HAZ still occurs, the lower carbon-equivalent steel has shifted its susceptibility from HAZ to the weld metal. Thus the weld metal has become more vulnerable to cracking. Hydrogen cracking within the weld metal has therefore become a more noticeable, and potentially greater threat to welding industry since it is more difficult to control the as-cast microstructures of weld metals, which derive mechanical properties from a relatively highly alloyed composition with substantial non-metallic inclusion contents. The weld metal chemistry must provide a structure with mechanical properties that match those provided by modern TMCP steels. Therefore, the effect on resistance to hydrogen cracking is an important variable dictating the welding consumable selection.

The most effective way to avoid HACC is a reduction of hydrogen level in the weldment, either through the selection of an appropriate preheat temperature and/or employing a low hydrogen welding process and consumable. From the practical perspective, and acknowledging the availability of welding processes generating relatively low levels of

hydrogen in weldment, predictive systems have been established to provide guidance on the susceptibility of welds to HACC in the parent metal HAZ. However, no such systems consider the likelihood of weld metal HACC. Fabricators of welded steel constructions have little information to guide them towards using welding methods which minimize the risk of hydrogen cracking in weld metals. The current welding standards AWS D1.1, EN 1011.2, AS/NZS 1554.1 and AS/NZS 1554.4 are based entirely on the avoidance of cold cracking in the HAZ, with the assumption that following these standards will also minimize weld metal hydrogen cracking. However, even when we know that in principal the same factors influence the risk of hydrogen cracking in weld metal as in HAZ (namely stress, hydrogen levels and susceptible microstructure), it appears that the relationship between weld procedure, weld materials and hydrogen cracking in weld metal differs from that for HAZ [Pargeter 1992]. A significant international research effort is ongoing to better understand weld metal hydrogen cracking with a view to developing guidance for consumable manufacturers and fabricators, so that the risk of weld metal HACC can be minimized.

In comparison with manual metal arc welding (MMAW), gas metal arc welding (GMAW) using solid wires and flux cored arc welding (FCAW) processes generate considerable interest in the welding industry. Due to their high deposition rates, duty cycle and weld metal recovery, the continuous wire processes are recognised as more economically attractive alternatives to MMAW. However, besides welding current these processes have an additional set of welding parameters that influence the final weldment hydrogen content. These include contact tip to work distance, wire feed speed and the shielding gases used. These welding parameters are more significant in the case of FCAW than in the GMAW processes due to influence of the included flux which results in additional reactions occurring within the plasma

arc. The interactions between parameters are complex and the mechanism of weld metal cold cracking that may result is yet to be fully determined.

The objectives of this document are:

    a) to review current knowledge with respect to weld metal HACC, both from phenomenological and mechanistic viewpoint,

    b) to consider important practical issues such as the measurement of diffusible hydrogen in weld metal as a function of the welding parameters for the FCAW process using gas shielded flux cored wires, and

    c) to investigate HACC susceptibility in rutile FCAW weld deposits as a function of welding parameters and preheat conditions.

The current work was concerned primarily with the determination of interactions between welding parameters with two commonly used shielding gases and their effect on hydrogen concentration in the deposited weld metal. The effects of various welding conditions on arc transfer characteristics were also examined using a high-speed digital imaging system.

The experimental work was based on the gas-shielded FCAW process using rutile, low strength welding consumables (AWS 5.20 E71 T-1 classification, equivalent to AS 2203.1 ETP-GMp-W503A CM1), with nominal hydrogen contents of 5 and 10 ml/100g of deposited weld metal. The reason for the selection of this consumable type is its wide spread use for fabrication of C or C-Mn, low strength steels in general fabrication application in Australia.

The inclusion of consumables with the same classification, but different nominal hydrogen levels, has provided an opportunity to evaluate the role of hydrogen in low strength weld metal on propensity to HACC. Susceptibility to transverse weld metal hydrogen cracking was investigated using the gapped bead-on-plate (G-BOP) test.

CHAPTER 2

Hydrogen in Ferritic Steels

In the last few decades, it is encouraging that more and more engineers have recognised that potential cracking problems in ferritic steel weldments must be considered in combination with the mechanical properties when materials are being selected for a given application. This is generally known as considering the weldability. However, there is no simple universal procedure which enables the engineer to reach a verdict on weldability of a selected steel by procedure qualification and/or by carrying out selected cracking tests, even if the mechanical properties may be satisfactory to the requirements of design strength. Material weldability is defined in Australian Standard AS 2812-1985 as: "the capacity of metal to be welded, under the fabrication condition imposed, into a specific, suitably designed structure and to perform satisfactorily in the intended service". It is apparent from this definition that an engineer must consider more steps than just to accept a qualified welding procedure for a given application. For example, the initial welding procedure qualification is often carried out under laboratory conditions, but the main purpose of the welding procedure is its successful application and the performance of the resulting welds under service conditions. It is during the actual production fabrication that factors not present during the procedure qualification may be introduced.

The intention of this study was to acquire some fundamental insight into HACC as it has been shown to occur when welding low strength (250 MPa yield strength) C-Mn steel using rutile FCAW matching strength consumable.

2.1 HYDROGEN ABSORPTION DURING ARC WELDING

Hydrogen is by far the most abundant element in the universe and makes up about 90 % of the universe by weight. Hydrogen is the lightest known gas with molecular weight of 2.016 and

density of 0.0972 g/l. Hydrogen, in the form of the diatomic gas H_2, is also characteristic by a high thermal conductivity, similar to that of helium. This feature is advantageous for some welding application, where hydrogen is added to inert gases to increase the heat input for operations involving cutting and gouging [ASM Handbook Vol.6].

It is generally agreed that hydrogen can exist in iron or steel in two different forms, as molecular or atomic hydrogen. Hydrogen, in atomic form is a transient element, which continually moves within the steel even at ambient temperatures. Similar to nitrogen, hydrogen is an interstitial element forming an interstitial solid solution. Hydrogen can be dissolved into the parent and weld metal causing embrittlement. In addition to welding hydrogen may be introduced by electroplating and reactions within the hydrogen storage vessels [Schwinn et al. 1995, Moore and McIntyre 1998], such as hydrocrackers and desulphurisers [Pargeter 1993].

During welding processes, the weld pool may become saturated with gas from the surrounding atmosphere, and this can be detrimental to the weld quality through formation of weld porosity, or increased susceptibility to weld cracking. The nature of fusion welding is such that thermodynamic equilibrium between the liquid metal of the weld pool and its gaseous atmosphere is rarely possible [Lancaster 1999]. While oxy-acetylene welds usually contain very little hydrogen of 2-3 ml/100g [Séférian 1962], the hydrogen of welds deposited using arc processes is much greater, with the actual content depending predominately on the nature of the electrode coating and/or the composition of shielding gas. Hence, the gaseous atmosphere interacts within the arc plasma column, thereby affecting the base and filler material entering the molten weld pool.

The humidity in ambient atmosphere, moisture absorbed into electrode coating and hydrogenous compounds, when raised to high temperature in the plasma arc, tend to dissociate over the molten weld pool through decomposition of water vapour to hydrogen atoms [Hirai et al. 1974] according to Equation 2.1:

$$2H_2O(g) \leftrightarrow 2H_2(g) + O_2(g) \qquad\qquad (2.\ 1)$$

This reaction can be further complicated by various shielding gas compositions and consumable flux formulation systems. The amount of diffusible hydrogen, H_D, in the weld metal [Hirai et al. 1974] is then given as:

$$H_D = H - (H_R + H_E) \qquad\qquad (2.\ 2)$$

where:　　　　H_D　　= diffusible hydrogen

　　　　　　　H　　= dissolved hydrogen

　　　　　　　H_R　　= residual hydrogen

　　　　　　　H_E　　= escaped hydrogen into ambient atmosphere

Sievert's law, Equation 2.3, defines the relationship between dissolved hydrogen and hydrogen in the atmosphere of the arc. The dissolved gas is proportional to the square root of the gas pressure. The thermodynamic equilibrium constant, K_1 , is defined as:

$$K_1 = \frac{p_H}{\sqrt{p_{H2}}} \qquad\qquad (2.\ 3)$$

where:　　　　K_1　　= constant

　　　　　　　p_H　　= partial pressure of atomic hydrogen

　　　　　　　p_{H2}　　= partial pressure of molecular hydrogen

Since the concentration of atomic hydrogen is proportional to the partial pressure, the Equation 2.3 can be also written as:

$$K_1 = \frac{H}{\sqrt{p_{H2}}} \qquad (2.4)$$

hence,

$$H = K_1 \times \sqrt{p_{H2}} \qquad (2.5)$$

From Equation 2.5, the volume of dissolved hydrogen measured in ml/100g of weld metal is a function of partial pressure [Gedeon and Eager 1990].

Once the basic principals of gas-metal chemical reactions within the arc and weld pool are understood, particularly for gas shielded welding processes, it is possible to alter shielding gas compositions to influence the welding arc performance [Vaidya 2002].

The primary role of the shielding gas is to protect the molten metal from atmospheric nitrogen, oxygen and hydrogen. In gas shielded welding processes, the gas used has not only a substantial influence on the arc stability [Vaidya 2002] forming continuous metal transfer during welding, but also significantly affects the weld metal mechanical and metallurgical properties [Stenbacka et al. 1989].

Hydrogen is a diatomic gas and when heated to high temperatures, such as in the arc plasma, it dissociates into atomic hydrogen. Once in monatomic form the hydrogen is easily absorbed into the weld pool. A theoretical model illustrating the monatomic and diatomic hydrogen absorption at different points across the weld pool was proposed [Gedeon and Eager 1990] as shown in Figure 2. 1. The model was constructed with the assumption that the calculated

values result from a hydrogen dissociation temperature of 2500 °C and that temperature is uniform across the weld pool.
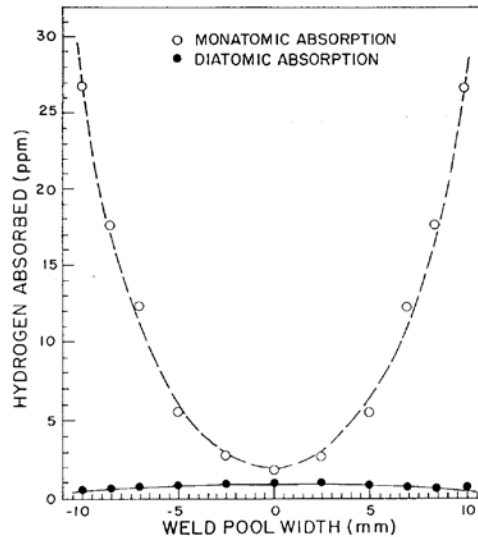
Figure 2. 1   Theoretical hydrogen absorption of monatomic and diatomic hydrogen as a function across the weld pool, assuming a dissociation temperature of 2500 °C and added hydrogen to argon shielding gas (after Gedeon and Eager, 1990).

The model shows maximum hydrogen absorption around the outer edges of the weld pool dominated by monatomic hydrogen instead of Sievert's law which suggests that maximum absorption should occur in the high temperature region – the centre of the weld pool [Gedeon and Eager 1990]. However, it is likely that hydrogen absorption is more complicated, such that the use of a simple dissociation temperature may not be representative of the large temperature gradients existing across the weld pool. Furthermore, variations in temperature and hydrogen distribution across the plasma arc column are likely to be influential [Li and North 1992].

2.1.1   Sources of Hydrogen During Welding

Studies by Lee et al. (1998) and Pokhodnya (1996) have categorized the sources of hydrogen into the following groups:

a)   organic materials and adsorbed moisture in electrode coating and fluxes,

b)   residual hydrogen-bearing lubricants on welding consumables, e.g. flux cored wire

c)   moisture in shielding gas,

d)   moisture in ambient atmosphere,

e)   incidental hydrogenous material, e.g. paint, grease, condensation, anti-spatter fluids or sprays, and

f)   hydrogen already residing in bare steel.

The significance of each of these groups as a source of hydrogen in welding has been the subject of numerous studies, particularly in the case of the FCAW welding process where studies have been conducted to determine the level of contribution of hydrogen content in the weld deposits [Kiefer 1996; Sierdzinski et al. 1998; Davidson 1998 and Harvig et al. 1999]. From a consumable manufacturer's perspective, reducing the amount of weld metal hydrogen is best approached by modifying the hydrocarbon drawing compounds (lubricants) and the formulation of compounds in the flux system to reduce the potential for hydrogen pickup from hydrogenous compounds such as organic lubricants and water, as demonstrated by Sierdzinski et al. (1998).

Figure 2. 2 illustrates how the moisture and hydrogen from various sources can enter the flux-cored arc welding pool.
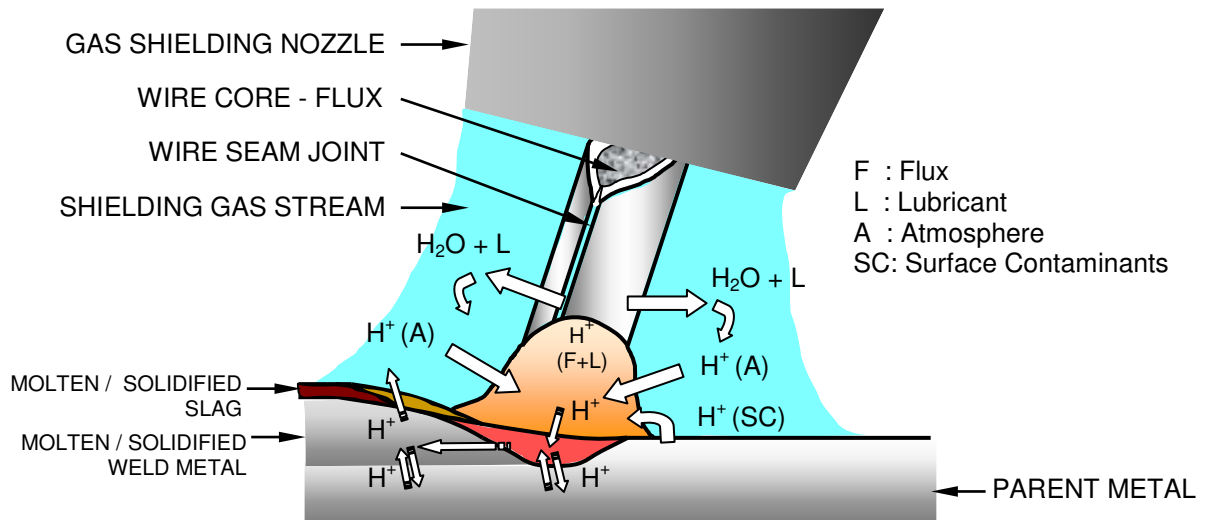
Figure 2. 2   Sources of hydrogen in the gas shielded FCAW process.

From the processing perspective, Harvig et al. (1999) examined the effects of atmospheric moisture during storage on hydrogen content of welds deposited by FCAW wires and concluded that all examined wires (rutile and basic to a lesser degree) are susceptible to an increase of hydrogen levels with an increase of atmospheric moisture. Further, long term exposure tests at normal atmospheric conditions where electrodes were stored for one year in their original containers inside an air-conditioned room, have produced weld deposits with higher diffusible hydrogen levels.

Often it is the presence of incidental hydrogenous materials that is most likely to increase the level of diffusible hydrogen. Welding standards [AS/NZS 1554 Parts 1 and 4] clearly recognize this fact by advising proper use of anti-spatter fluids with particular care, so as to

avoid contaminating any area in or near the weld zone. Such contamination will increase the weld metal hydrogen level.

The use of lower hydrogen or low moisture absorption consumables, the observation of proper material handling procedures and the selection of correct welding materials and procedures, are just some of the approaches that can be used to help minimize the risk of HACC. Their importance has to be assessed in combination, along with the joint geometry which affects the residual stresses within the weldment.

2.1.2   Solubility and Diffusion of Hydrogen in Steel

An important feature of hydrogen is its ability to diffuse through the iron lattice structure at elevated or even at room temperature. Hydrogen can pass through the iron lattice in the atomic form, where it has smaller dimensions than the interstices in the iron lattice.

Iron lattice structure can exist in two forms; as the face-centered cubic (F.C.C.) metal structure of austenite (γ-Fe) and the body-centered cubic (B.C.C.) structure of ferrite (α-Fe), as shown in Figure 2. 3.

F.C.C.   B.C.C.
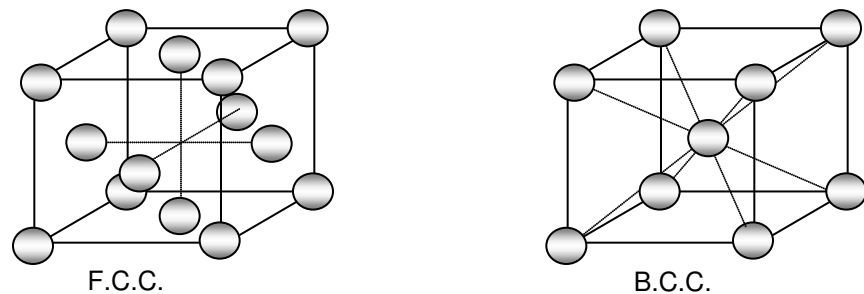
Figure 2. 3   Atomic arrangement for face-centred cubic austenite (γ-Fe) and body-centred cubic ferrite (α-Fe) structures.

A packing factor is defined as the ratio between the volume of atoms within the volume of the unit cell, and for (γ-Fe) and (α-Fe) the packing factors are 0.74 and 0.68, respectively [van Vlack 1964]. The austenite has a larger inter-atomic spacing than does ferrite. Atomic interstitial hydrogen has a lower diffusivity through closely packed face-centered cubic (F.C.C.) metal structure of austenite (γ-Fe) than in ferrite (α-Fe) with a body-centered cubic (B.C.C.) structure. Thus allowing greater degree for solubility of interstitial hydrogen in austenite than in ferrite.

Hydrogen diffusivity is not only the function of atomic structure, as it varies over the range of temperatures, as shown in Figure 2. 4.   Where hydrogen diffusion remains linear with decreasing temperature in the case of austenitic steels, a sudden decrease of hydrogen diffusion is noticeable in ferritic steels below 100-150 °C down to room temperature due to trapping effect of microstructural features, to be discussed later in this Chapter.
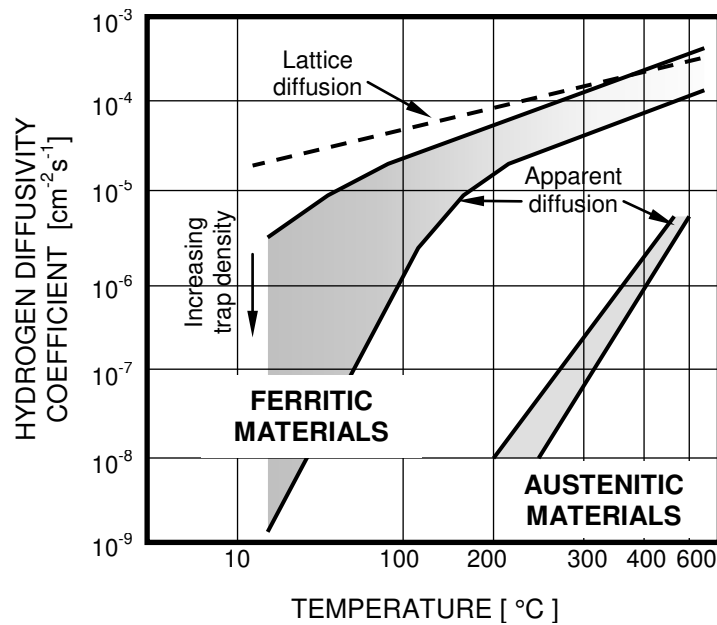
Figure 2. 4   Hydrogen diffusivity coefficient as a function of temperature for ferritic and austenitic steels.

Hydrogen solubility is also a function of temperature and corresponding metallurgical phase transformations during cooling. This is shown diagrammatically in Figure 2. 5.
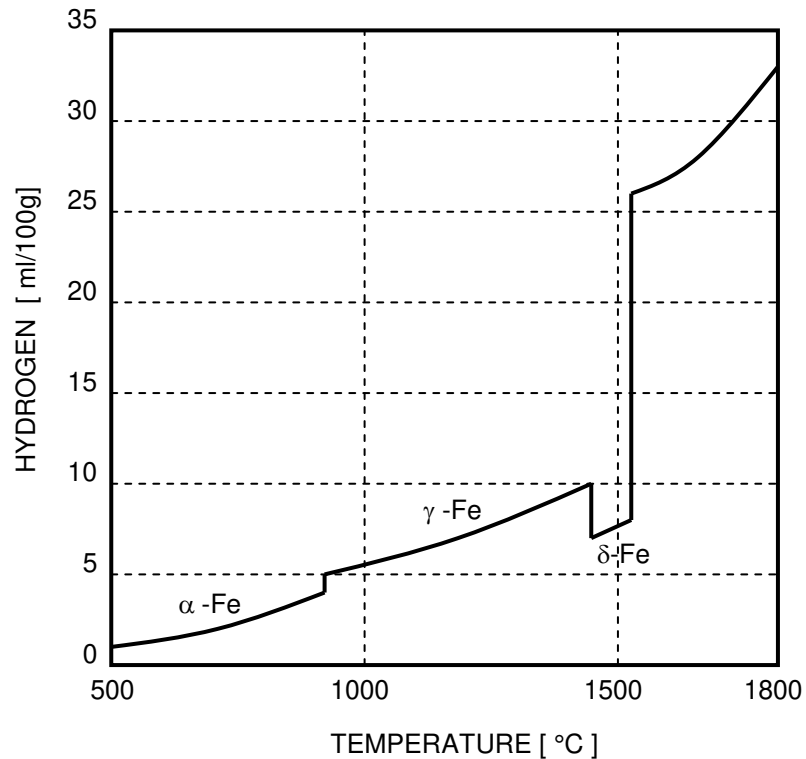
Figure 2. 5   Graph illustrating the equilibrium solubility of hydrogen in iron in the solid and liquid states as a function of temperature at atmospheric pressure (after Séférian 1962).

2.2   HYDROGEN TRANSPORT

Once the welding is completed and the weld metal is solidifying, absorbed hydrogen escapes by diffusion into the atmosphere and into the HAZ of parent metal, but a proportion remains within the solidified weld metal.

The hydrogen present in the weld metal is commonly classified into two types:

a) Diffusible hydrogen, which is dissolved in the steel in an atomic or ionic form and is able to evolve from the weldment after welding and cooling to ambient temperature.

b) Residual hydrogen, also known as stable hydrogen, which does not evolve from the weldment at ambient temperature.

A total hydrogen content is then a sum of diffusible and residual hydrogen [Mikula 1994].

The amount of dissolved hydrogen depends on the partial pressure of hydrogen in the arc atmosphere and this pressure is determined primarily by the humidity in the ambient atmosphere and by the moisture absorbed in the consumable flux [Hirai et al. 1974]. In order to cause hydrogen embrittlement of steel, hydrogen must be transported through the vapor phase, absorbed and transported internally by lattice diffusion or by dislocation motion [Hirth 1980, Li and Liu 1992].

Transformation of γ-Fe to α-Fe usually occurs first in the re-austenitised HAZ region because of the direction of the temperature gradient. This tends to drive hydrogen back towards the weld fusion boundary region [Yurioka and Suzuki 1990 and French 1998] since its solubility in α-Fe is less than in γ-Fe. However, this does not take into account the fact that hydrogen may not be homogeneously distributed in the parent steel and the weld metal [Olson et al. 1996].

The damaging effects of hydrogen in materials have been recognized for more than a century [Pokhodnya and Shvachko 1970]. However, there is still considerable controversy [Vasudevan et al. 1981 and Lynch 1992] about the existing hypotheses for a single mechanism for

hydrogen embrittlement of steels. Some of the important models developed since the early 1940's are described below [Yurioka and Suzuki 1990 and Mikula 1994]:

a) Internal planar pressure theory, based on the decrease of hydrogen solubility as a function of temperature decrease and the associated increase in hydrogen gas pressure in microvoids or pores [Zapfee and Sims 1941].

b) Adsorption theory or surface energy mechanism, which proposes a lowering of the surface free energy at the tips of micro-pores leading into reduction in the stress levels due to hydrogen absorption [Petch and Stables 1952].

c) De-cohesion theory, which suggests that accumulated hydrogen interacts with dislocations in areas of triaxial stress to lower the cohesive strength [Troiano 1962 and Graville 1967].

d) Slip softening model or interaction theory between faults in crystalline structure and hydrogen, which suggests that a sufficient concentration of dissolved hydrogen in the lattice just ahead of crack tip representing stress intensity leads into fracture modes determined by the microsturucture, crack-tip intensity and amount of hydrogen present [Beacham 1972]. This model unifies several theories, excluding the internal planar and adsorption theories.

e) Enhanced adsorption theory at the crack tip by Lynch (1988). This model supports the injection of dislocations from crack tips [Shvachko 2000], thereby promoting the microvoid coalescence of cracks with voids ahead of existing crack front accompanied by a plastic flow.

Each of these theories can explain observed behaviour for certain materials tested under specific conditions, but they are by no means universal. This supports the view that no single mechanism exists which can be universally applied [Vasudevan et al. 1981].

For the above hypotheses a number of schematic models for hydrogen crack formation have been suggested by Pokhodnya (1996), based on the following modes of hydrogen transfer in steels and weld joints:

a) diffusion in the field of a concentration gradient,

b) diffusion in the stress field,

c) thermal diffusion,

d) surface diffusion,

e) diffusion along microstructural defects, and

f) transfer by dislocations.

Pokhodnya (1996) has proposed that hydrogen embrittlement from the initial stage to crack formation can be described by the following steps, and as shown schematically in Figure 2. 6.

1. Presence of dislocations   (size: 10^{-7} mm)
2. Super-dislocation – sub-microcrack   (size: 10^{-6} …10^{-5} mm)
3. Critical sub-microcrack   (size: 10^{-4} mm)
4. Micro-crack   (size: 10^{-3} …10^{-1} mm)
5. Macro-crack   (size: 1 mm)
6. Cracks in structures   (size: 1 …10 mm)

(1)   (2)   (3)

(4)   (5)   (6)
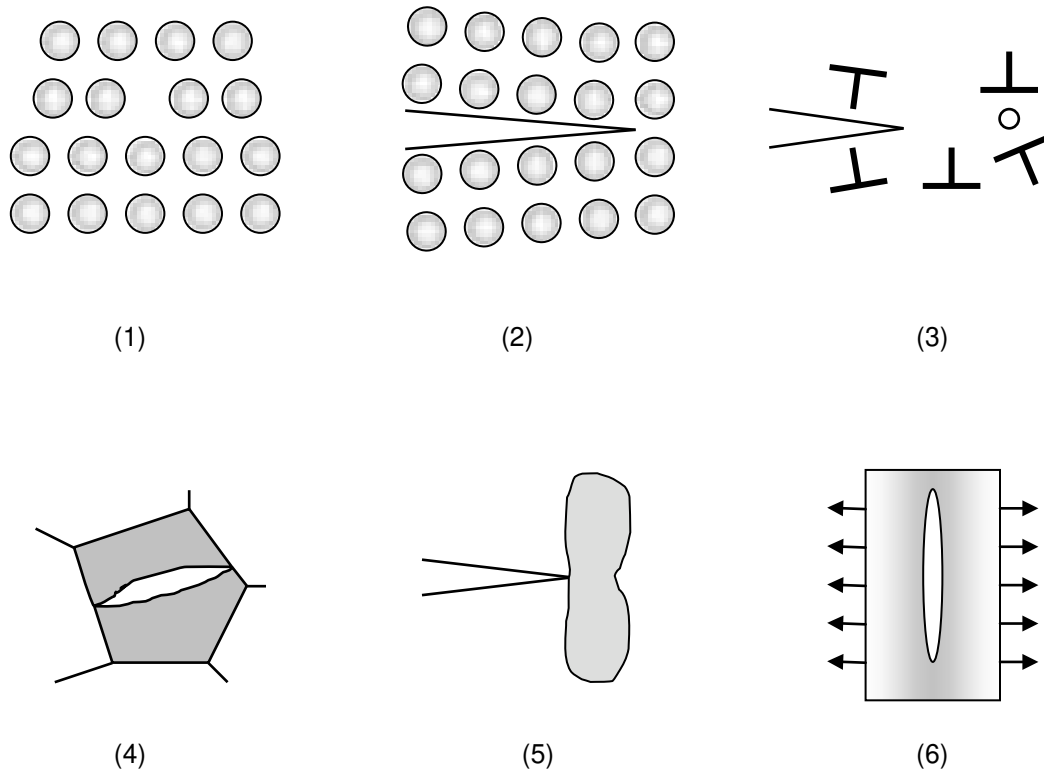
Figure 2. 6   Schematic diagram of the mechanism of hydrogen embrittlement from the initial stage, commencing at a disclocation (1), and progressing through to the final crack (6) (after Pokhodnya 1996).

A summary of hydrogen transport process through stages of diffusion or dislocation mechanism was proposed by Thompson and Bernstein (1980), as schematically shown in Figure 2. 7.
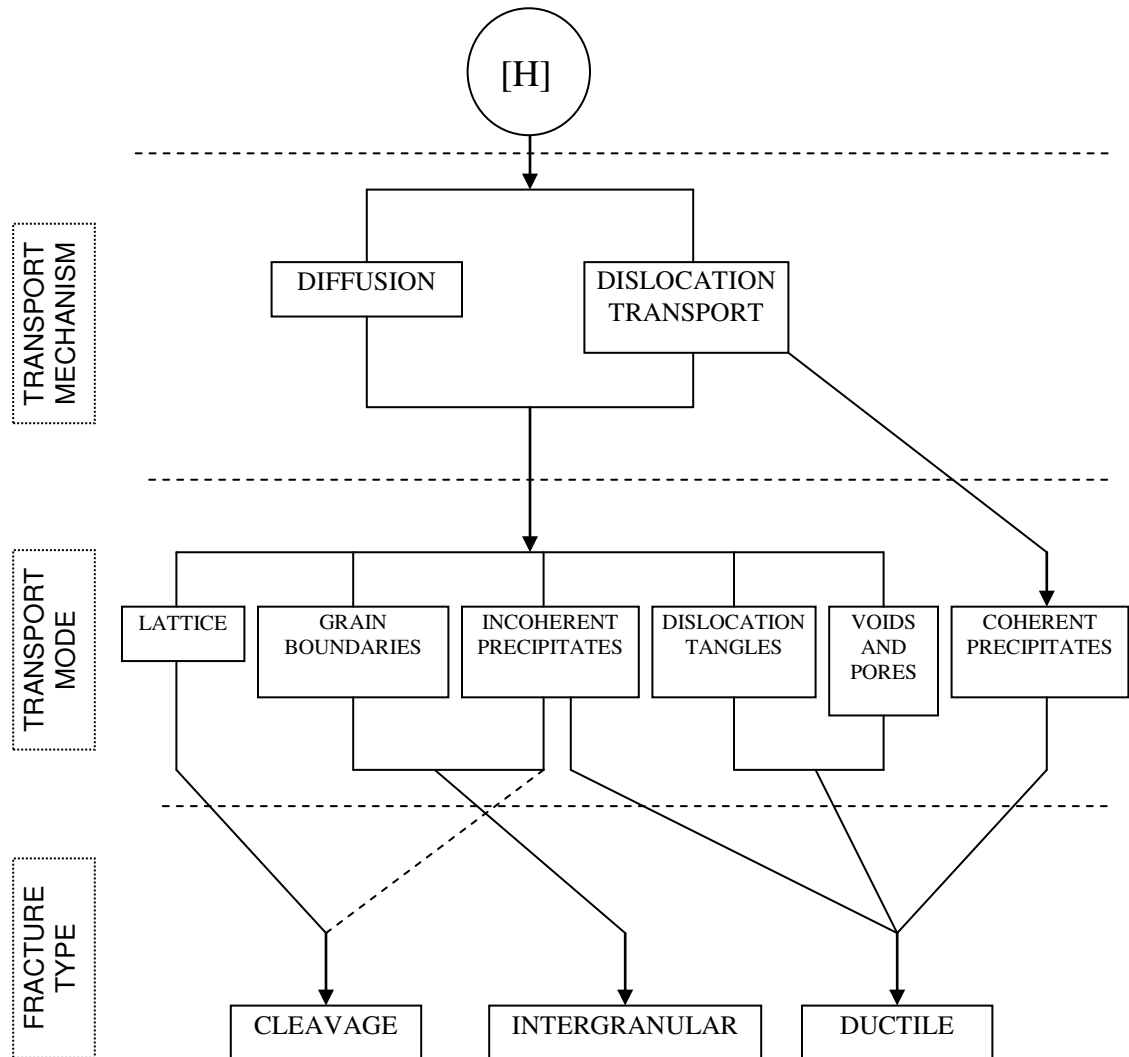
Figure 2. 7   Flow chart illustrating hydrogen transport by diffusion or dislocations, thereby leading to accumulation at microstructural features and finally resulting in fracture type (after Thompson and Bernstein 1980).

2.2.1 Thermal Cycle During Welding

Welding processes are characterized by rapid heating cycles generated by the welding arc. Once the welding arc moves away from the molten region, solidification and cooling of the fused metal takes place. The characteristics of this thermal cycle play an important role in determining the mechanical, chemical and microstructural properties of the weldment, but also the level of hydrogen introduced during welding process.

The temperature – time cycle occurring at any particular point in the weld during the passing of the welding arc consists of a short heating phase, when the temperature rises very rapidly to a peak temperature, Tp, and followed by a more extended cooling phase. Where Tp is approximately the same throughout the weld metal, various regions of the parent metal experience different peak temperatures, as shown in Figure 2. 8.
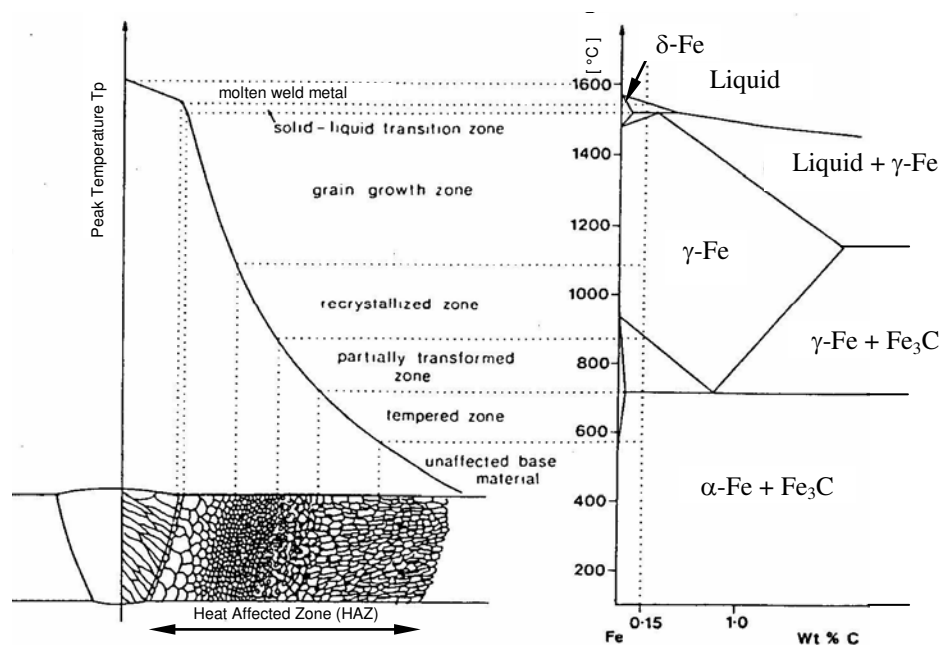
Figure 2. 8   Schematic diagram showing the microstructural gradient established by butt welding of 0.15C steel with 0.15C filler and its relationship to the peak temperature reached and the corresponding phase(s) indicated by the the Fe-Fe$_3$C phase diagram (after Easterling 1983).

As previously discussed molecular hydrogen breaks down to atomic form at the high arc plasma temperatures within the welding arc. Hydrogen ions are then absorbed into the molten weld pool, and transported through the weld metal and into the parent metal HAZ by diffusion. This diffusion stage is particularly important where the weldment experiences a longer cooling phase, causing austenitic grain growth in the HAZ during the austenitization stage.

The final microstructure of the weld metal will depend on the interactions between following variables:

a) initial chemical composition of parent and weld metals,

b) cooling rates or time spent through transformation region (γ-Fe $\rightarrow$ α-Fe), and

c) heat input resulting in different degree of weld metal dilution.

A weld metal may be considered a miniature casting, where solidification follows the fundamentals of casting solidification. However, cooling rates for weld metal will be expected to be higher due to the excellent heat transfer through the parent metal, in comparison to the relatively poor heat transfer through a typical casting mold. In comparison to the casting, weld metal therefore experiences greater temperature gradient between the weld fusion boundary and its centerline. In contrast with the casting of molten metal into a mold, a higher degree of stirring action can be expected in the weld metal as a result of arc induced effects such as the Marangoni forces [Shiralli and Mills 1993]. Where solidification develops by heterogeneous nucleation at the mold wall of a casting, weld metal solidification occurs by epitaxial growth from the weld fusion boundary.

Initially, solidification is continued by planar grain growth, according to the temperature gradient developed by heat transfer away from the weld pool and into the parent metal. However, with a decrease in the temperature gradient and an increase of constitutional super-cooling by segregation, the crystal growth process changes to cellular growth, cellular dendritic, columnar dendritic and eventually equiaxed dendritic grain growth [Savage et al. 1976]. Schematic illustration of weld metal microstructures developed at the solid-liquid interface and the temperature gradients are shown in Figure 2. 9.

2.2.2   Hydrogen Distribution

Hydrogen transport in weld metal is more complex than the parent metal since the weld metal microstructures are 'as cast' structures with considerable chemical and structural heterogeneity, including the presence of non-metallic inclusions. The hydrogen diffusion process through the metallurgically inhomogeneous weld metal can be locally varied by second phase particles, inclusions, microvoids, pores, lattice imperfections and other microstructural features, which can act as preferential sites for hydrogen entrapment [Olson et al. 1996 and Davidson et al. 1996].

It is known that the diffusivity of hydrogen in α-Fe is faster than in γ-Fe and that it decreases with decreasing temperature. However, at lower temperatures of less than 200 °C, diffusivity in α-Fe decreases more markedly as illustrated earlier in Figure 2. 4.
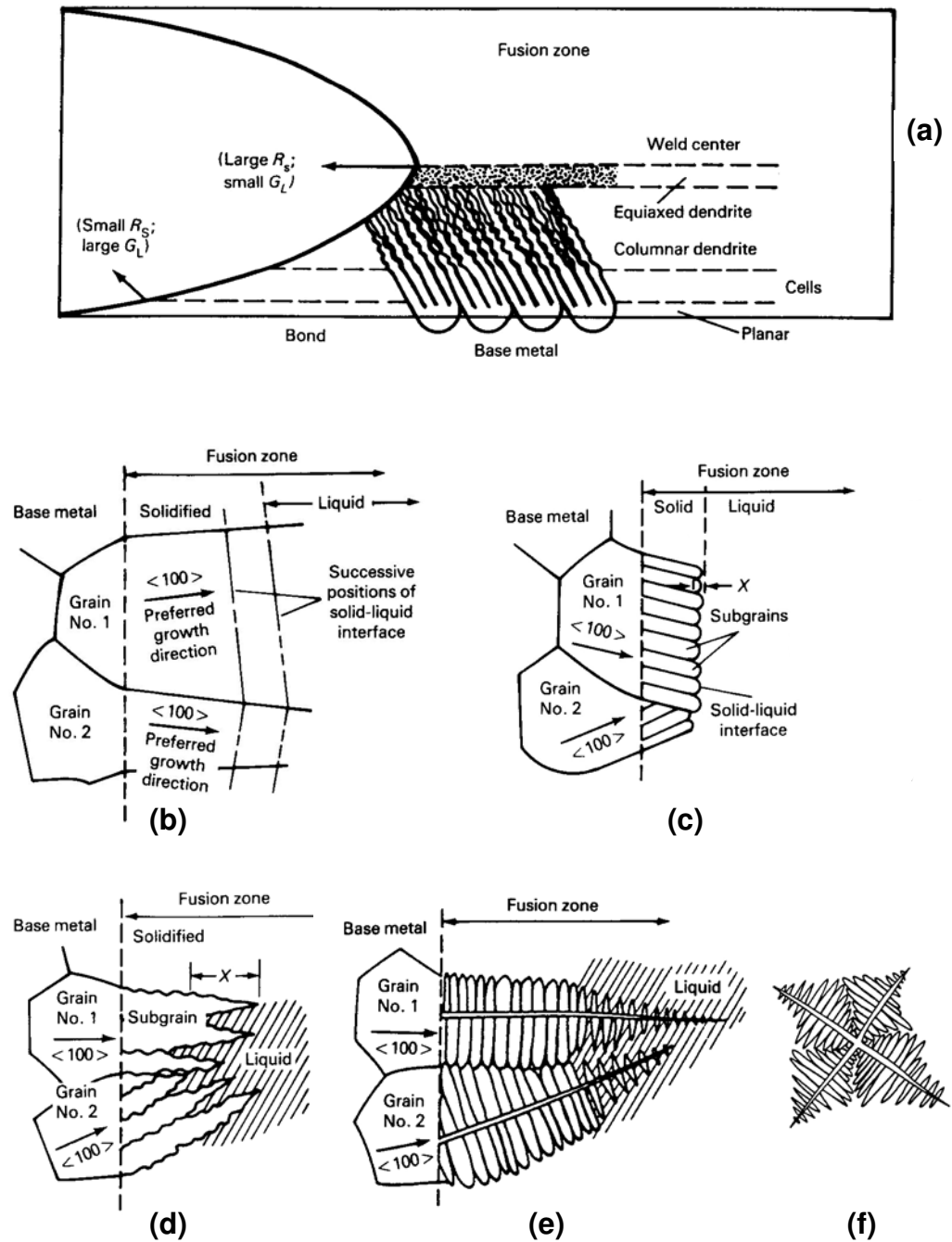
Figure 2. 9   Schematic diagram showing various types of microstructures that form in response to variation of solidification mode around the weld pool. Typical microstructural growth developed in solid-liquid interface (a); Planar (b), cellular (c), cellular-dendritic (d) columnar-dendritic (e) and equixed dendritic (f) (after ASM Handbook Vol.6).

The presence of hydrogen traps retards the evolution of hydrogen from the weld [Pussegoda et al. 1997] and decreases the hydrogen diffusivity [Olson et al. 1996]. A description of lattice diffusivity as a function of the measured amount and densities of traps present was developed by Oriani (1970), who also confirmed this phenomenon by numerical modeling.

Hydrogen diffusivity change as a function of temperature, type of trap sites and their volume has been extensively examined [Choo et al. 1981, Lee and Lee 1983 and Pussegoda et al. 1997]. With increasing amount of percentage volume of traps, the hydrogen diffusivity decreases [Pussegoda et al. 1997] and weld metal will produce lower levels of diffusible hydrogen content [Olson et al. 1996]. However, the number of trap sites that can be used to trap diffusible hydrogen is limited by the detrimental effect of excessive non-metallic inclusions characterized by low fracture toughness, often resulting in the onset of HACC [Pressouyre 1980]. Therefore, the design and use of hydrogen traps should not be based solely on the suppression of diffusible hydrogen in weld metal, but rather to promote a more uniform distribution of hydrogen in the weld metal so that a high local accumulation of hydrogen at crack initiation sites can be prevented.

During weld metal solidification, when hydrogen is mobile and travels through the weldment due to the different hydrogen concentration gradients, hydrogen can be attracted to various types of trap sites. Traps are classified as "irreversible" if they act purely as hydrogen sinks and "reversible", if they accept hydrogen, but act as a hydrogen source under certain circumstances [Pressouyre 1980].

Types of traps, grouped into "irreversible", "reversible" and "very reversible" categories, and their relevant ranges of binding energies and are listed in Table 2. 1 [Olson et al. 1996 and Davidson et al. 1996].

Table 2. 1   Types of hydrogen traps with their relevant binding energies and release temperatures.

HYDROGEN TRAP	Binding Energy $[kJmol^{-1}]$	Release Temperature $[\,°C\,]$
Very reversible: (i.e. interstitial lattice sites, elastic stress field, dislocations)	7.7	-
Reversible: (i.e. Ti substitutional atom, grain boundaries, dislocations ferrite / carbide and ferrite / cementite interfaces, tempered martensite)	17 - 36	112 - 270
Irreversible: (i.e.microvoids, Fe_2O_3, Fe_3O_4, MnS, Al_2O_3, or SiO_2, TiC, Ce_2O_3)	35 - 112	305 - 750

A reduction of susceptibility of ferritic weld deposits to HACC, can be achieved by considering the following factors [Olson et al. 1996]:

a) hydrogen-trap binding energy,

b) the trap density,

c) the martensite start temperature in weld metal, M_{WM} , and

d) the cooling rate $\Delta t_{8/5}$.

The increase or decrease of the resistance to HACC depends on the nature and distribution of the traps [Davidson et al. 1996]. Diffusible hydrogen content in a weld metal decreases with hydrogen-traps that have increasing binding energy from 60 kJmol^{-1} for dislocations, 80 kJmol^{-1} for Al_2O_3 inclusions, 100 kJmol^{-1} for TiC particles and 120 kJmol^{-1} for rare earth additions (e.g. Ce_2O_3,). Therefore, weld metals containing high binding energy traps may have improved resistance to HACC. Olson et al. (1996) suggest that by the proper use of hydrogen traps with appropriate morphology, number and their uniform distribution, it is possible to trap a large portion of hydrogen in the weld metal, thereby immobilizing the hydrogen and preventing it from reaching and accumulating at potentially critical sites for the initiation of cold cracking. Reversible traps, whose binding energy is <60 kJmol^{-1} , will not be able to prevent hydrogen cracking since hydrogen can be transported by moving "reversible" dislocations, which can then act as crack initiators [Olson et al. 1996].

Another method of improving the resistance to HACC by hydrogen trapping in weld metal has been suggested for HSLA steels susceptible to cold cracking [Hart and Evans 1997, Park et al. 2002]. Weld samples, containing increased levels of retained austenite demonstrate an increased resistance to HACC due to the capacity of γ-Fe to act as a hydrogen sink due to lower diffusivity of hydrogen in γ-Fe phase. The beneficial effect of this phenomenon was observed by Leonard et al. (2000) who found that weld metal microstructures of duplex stainless steel that contain larger a ratio of γ-Fe : α-Fe show reduced susceptibility to hydrogen cracking. Cracking in each of the high ferrite welds was transgranular in nature, propagating through the ferrite phase and arresting at ferrite-austenite boundaries.

The concept of controlled levels of γ-Fe phase provides a metallurgical alternative for the management of hydrogen distribution throughout the weld metal.

Tarlinski (1974) employed a sophisticated laser beam mass spectrographic method to measure the microscopic distribution of diffusible hydrogen horizontally across the weld bead and HAZ. Maximum hydrogen levels were observed at the weld pool fusion regions, Figure 2. 10.
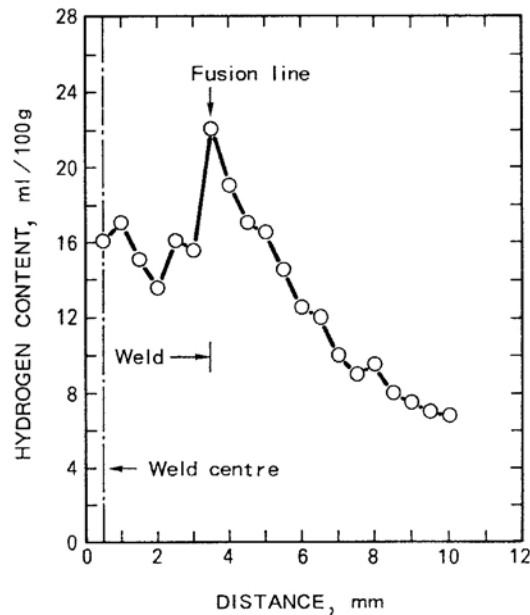
Figure 2. 10   Graph showing hydrogen distribution horizontally across the weld, as measured by laser beam mass spectrometry (after Tarlinski 1974).

The results of this early experimental work were in agreement with the theoretical model constructed for the weld pool by Gedeon and Eager (1990), Olson et al. (1996) and recent work by Smith II et al. (2001-1) using laser ablation/mass spectrometry. It appears that weld metal hydrogen content rises at the fusion line and gradually decreases further away throughout the parent metal HAZ. The hydrogen content of the HAZ rises because of hydrogen diffusion into the parent metal. This mechanism is illustrated in Figure 2. 11.
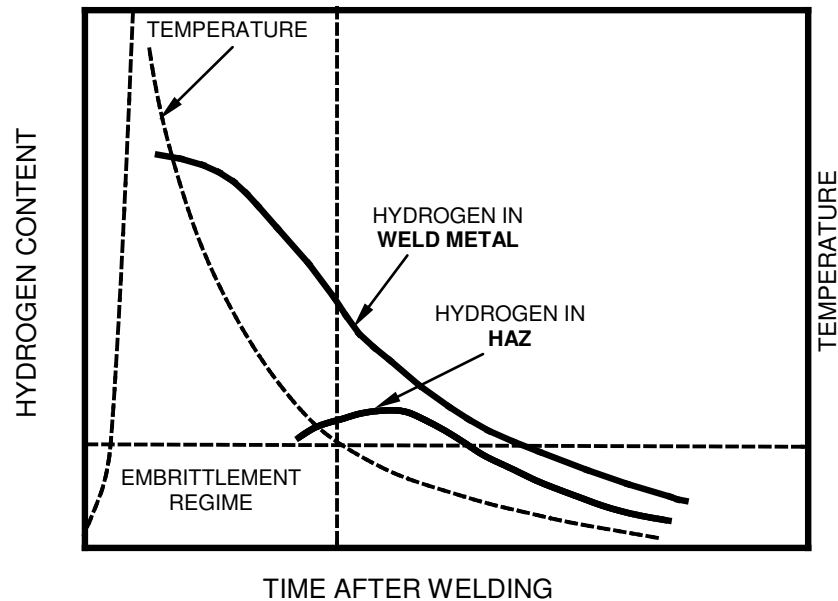
Figure 2. 11   Schematic illustration of the change of hydrogen content in the weld metal and the parent metal HAZ following solidification (after Matsuda et al. 1985).

The final hydrogen distribution at ambient temperature across the weld metal and parent metal regions will depend on factors such as welding consumable hydrogen content [Vasudevan et al. 1981], initial preheat temperature, welding process used, arc energy, heat input, cooling rates and metallurgical and chemical properties of both weld and parent metal. These variables are interrelated and variation of one or several may result in a change in the distribution of hydrogen.

2.2.3   Hydrogen Prediction Models

The experimental analysis of hydrogen distribution in welds using various extraction methods can be complemented by hydrogen diffusion models [Yurioka and Suzuki 1990].

Most hydrogen diffusion models are two-dimensional, are applied in a transverse direction across the weld, and have been designed using an average hydrogen concentration assumption. These models have been found to be useful for estimating expected hydrogen levels and prescribing preheat conditions necessary to avoid cold cracking in single pass welds.

However, such an approach is less appropriate in the multi-pass welds, where the geometry and thermal history of each of the weld passes varies [Pussegoda et al. 1997] and results in a variation of hydrogen concentration throughout the weld thickness [Coe and Chano 1975].

A prediction model for HACC in weld MMAW metal was developed using experimental results from a modified Y-groove Tekken test [Alcantara and Rogerson 1984]. This model defines crack susceptibility in terms of a total real crack length and weld metal area by an average cracking coefficient (ACC). Using the measured diffusible hydrogen levels of multi-pass weld deposit, arc energy (expressed in terms of heat input; kJ/mm) and measured ACC, a tertiary diagram can be constructed, for a particular plate thickness, electrode classification and preheat temperature. This enables the description of a crack/no crack condition at any selected arc energy or consumable hydrogen level. This model appears to be restricted to the variables of plate composition, thickness and electrode type and cannot be used universally for other combinations.

Mathematical methods are providing more flexible options for the development of hydrogen prediction models. Yurioka et al. (1979) proposed to evaluate a hydrogen activity coefficient (γ) from the diffusion coefficient (D) based on Fick's second law of diffusion [Tchaikovsky and Squires 1996], as shown in Equation 2.6:

$$D = \frac{\pi}{4} \times \frac{M^2}{AC_0^2 t} \tag{2.6}$$

where: D = diffusion coefficient [mm^2/s]

                        C_0 = hydrogen collected at the specimen surface [g/mm^2]

                        M = mass of hydrogen diffused into a specimen [g]

                        A = diffusion surface area [mm^2]

                        t = diffusion time [s]

The diffusion coefficient 'D', calculated in Equation 2.6, is the result of a complex real process of transportation of hydrogen mass. Consequently, it can be applied to the calculation of the actual hydrogen activity coefficient, γ , as well as to the simulation of the distribution of diffusible hydrogen in steel weldments.

Following Yurioka et al. (1979), and not considering hydrogen trapping effect,

$$\frac{D}{\gamma} = \text{const.} \tag{2.7}$$

By substituting Equation 2.6 into 2.7, the hydrogen activity coefficient (γ) can be expressed in Equation 2.8 as following:

$$\gamma = \frac{1}{0.14^{[-\frac{3200}{RT}]}} \times \frac{\pi}{4} \times \frac{M^2}{AC_0^2 t} \tag{2.8}$$

where: R = 1.9872 cal/mol K

                        T = 293.16 [K]

Following work by Yurioka et al. (1979), the study by Tchaikovsky and Squires (1996) showed that diffusion (D) and activity (γ) coefficients fall with increasing strain from 0 % to 6.5 % at 20 °C, for a deposited MMAW weld using AS 1553.1 E4113 welding consumable.

For known boundary conditions of diffusion time (t), thickness and hydrogen concentration, the mass of hydrogen that diffused into a specimen can be described using the Laplace transformation, as follows:

$$M_t = \int_0^L C(x,t) \, dx \qquad\qquad (2.\,9)$$

where: M_t = mass of hydrogen diffused into a specimen over the time [g]

    C   = hydrogen concentration

    x   = distance [mm]

    t   = time [s]

    L   = specimen thickness [mm]

A two dimensional mesh diffusion model was developed by Pussegoda et al. (1997) using the assumption that Fick's law of diffusion applies and that hydrogen diffusion is driven by the concentration gradient. From this model, the hydrogen concentration at a node from a grid in the subsequent time step (n+1) is given by:

$$C_{i,j,n+1} = C_{i,j,n} + [D\Delta t/\Delta x^2] \times [C_{i+1,j} + C_{i-1,j} + C_{i,j+1} + C_{i,j-1} - 4C_{i,j}]_n \qquad (2.\,10)$$

where: $C_{i,j}$ = hydrogen concentration at a node of the grid

    n   = subsequent step

    Δt = time steps between grids [mm]

    Δx = definable pitch (distance) [mm]

New computer technology may enable the modelling of hydrogen diffusion at a microscopic level [Bergheau et al. 1997], incorporating the effects of non-metallic inclusions and other types of hydrogen traps and their densities [Hirth 1980 and Olson et al. 1996]. Improved computer models for post heat treatment for hydrogen removal are also likely [Kyte and Chew 1979]. A precise microscopic definition of hydrogen diffusion in weld metal and parent metal microstructures, and their subsequent insertion into three-dimensional macroscopic models, has a great potential to enhance the accuracy and understanding of hydrogen prediction models.

2.2.4 Heat Affected Zone and Weld Metal

The metallurgical concept of hydrogen distribution between the parent metal HAZ and weld metal was earlier described by Granjon (1971). The hydrogen diffusion behaviour during the formation of martensite and/or ferrite in low alloy steel weld metal can be described by a simple relationship described by Olson et al. (1996), Equation 2.11:

$$\Delta M_S = M_{WM} - M_{HAZ} \tag{2. 11}$$

where: ΔM_S = change in martensite start temperature [°C]

M_{WM} = martensite start temperature of weld metal [°C]

M_{HAZ} = martensite start temperature of parent metal HAZ [°C]

Case (a):   if $\Delta M_S > 0$, hydrogen will accumulate in the parent metal HAZ

Case (b):   if $\Delta M_S < 0$, hydrogen will accumulate in the weld metal

The concept was based on different austenite (γ-Fe) – martensite (M) and/or ferrite (α-Fe) transformation temperatures between weld metal and HAZ, as illustrated in Figure 2. 12.
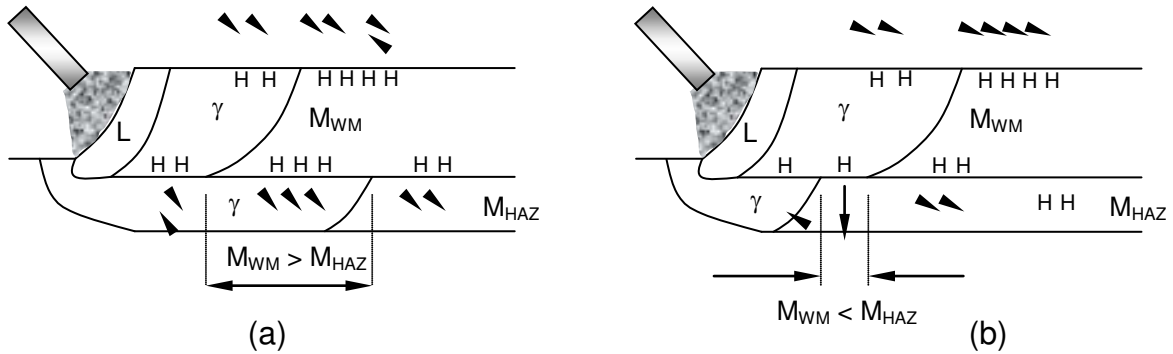
Figure 2. 12   A schematic illustration showing hydrogen diffusion and the effect of different γ-Fe / M and/or α-Fe transformation temperature. Hydrogen cracking susceptibility greater in the HAZ (a) and greater in the weld metal (b) (after Olson 1996).

The lower the M_{WM} temperature is, the longer time for hydrogen is available to reside in the weld metal. This also means that the available temperature range for effective hydrogen diffusion and trapping in the martensitic/ferritic phase becomes narrower and the suppression of diffusible hydrogen content becomes less effective.

2.3   MEASUREMENTS OF DIFFUSIBLE HYDROGEN

As the welding industry becomes more aware of hydrogen-related problems, and more familiar with diffusible hydrogen testing procedures, then the consumable specifications and testing standards are gradually becoming essential tools for the welding engineer to use in conjunction with the welding standards. The procedures and methodology used to determine the consumable hydrogen levels are described in detail in international standard ISO 3690-

2000 and are incorporated in many national standards such as ANSI/AWS A4.3-93, JIS Z3118-1992, EN758 and AS/NZS 3752-1996.

It is important to recognize that the selection of welding parameters at which the welding consumables are tested for hydrogen levels are currently at the discretion of the consumable manufacturers, and are usually within the range of welding parameters delivering the best running characteristic for the consumable tested.

2.3.1   Consumable Hydrogen Classifications

Selection of the correct welding consumable for a given application requires an understanding of the classification systems given in consumable specification standards.

Although the various hydrogen testing standards have many similarities in definitions and formulations for calculating the hydrogen levels, historically these standards have adopted different hydrogen benchmark levels, as shown in Table 2. 2.

Table 2. 2   A comparison of the benchmarks for diffusible hydrogen content, as determined by the testing standards ISO 3690-2000, ANSI/AWS A4.3-93, JIS Z3118-1992 and AS/NZS 3752-1996.

	IIW ISO 3690	ANSI/AWS A4.3-93	JIS Z3211* and JIS Z3212	AS/NZS 3752-1996
Hydrogen Levels	Diffusible weld metal hydrogen [ml/100g]			
Controlled	≤15	≤16	≤15*, ≤15, ≤12	≤15
Low	≤10	≤8	≤10, ≤9, ≤7	≤10
Very Low	≤5	≤4	≤6	≤5
(Under consideration)		≤2		

It should be noted that where the International Institute of Welding (IIW) Commission II adopted a linear scale increment of hydrogen levels by units of 5 (5-10-15 ml/100g), the American Welding Society currently uses logarithmic scale (4-8-16 ml/100g) of deposited weld metal. It is claimed that an incremental improvement in hydrogen cracking resistance following the AWS benchmarks, from 16 to 8 ml/100g, is equal to the improvement from 8 to 4 ml/100g [Kotecki 1992], according to the logarithmic relationship between critical cracking stress and total hydrogen determined by the hydrogen cracking implant test method [Evans et al. 1971]. The logarithmic scale also leaves open a possibility for further equivalent incremental improvements in hydrogen cracking resistance down to 2 ml/100g or less. This possibility of new lower hydrogen level is, however, not possible for a linear scale increment of 5 ml/100g, as used by the international standard ISO 3690-2000 and the Australian Standard AS/NZS 3752-1996. That is, a consumable with hydrogen classification of 0 ml/100g is clearly unrealistic. Hence, a new smaller increment than 5 ml/100g would be required [Kotecki 1992]. Another approach in hydrogen benchmarking is adopted in JIS Z3118-1992, where the step from low to very low consumable classification requires only 1 ml/100g of hydrogen content decrease from ≤7 to ≤6 ml/100g of weld metal. Considering the reproducibility of the diffusible hydrogen tests to be no better than ±1 ml/100g, this benchmarking scale may be described as unrealistic [Kotecki 1996].

It should be noted that a welding engineer, when selecting a welding consumable on the basis of diffusible hydrogen levels, is only guided by the arbitrary groupings as shown in Table 2. 2. When selecting a consumable from 'low' level group H10, the consumable may have actual hydrogen levels of 5.1 or 9.8 ml/100g, although both meet the requirement of ≤10 ml/100g. A similar concept applies when selecting a consumable from the 'very low' group, where the

actual hydrogen content may be 4.9 ml/100g, which is insignificantly lower than a consumable containing 5.1 ml/100g but is classified within the 'low' hydrogen group. The accuracy limits of measurement or variation due to selection of welding parameters during testing may easily overlap two groups.

Despite these factors, steel manufacturers and welding standards are adopting these hydrogen level benchmarks. A standard will recommend a welding consumable with a given hydrogen classification for a particular material to be welded. The consumable hydrogen classification is described as an essential variable in welding standards AS/NZS 1554.1-2000 and ANSI/AWS D1.1-2000. Any deviation, especially a change from hydrogen controlled to a non-hydrogen controlled consumable, or any increase in hydrogen classification and requires re-qualification of welding procedure.

2.3.2   Single weld bead diffusible hydrogen test

The welding consumable to be tested is used to deposit a single weld bead under closely monitored welding and atmospheric conditions as specified by the relevant hydrogen testing standards mentioned previously. Once the welded sample is rapidly quenched to minimize effusion of hydrogen from the deposited weld, it is quickly cooled down in icy water and stored at 78 °C, or lower, until the sample is required for further preparation and final hydrogen analysis.

It should be noted that the aim of the hydrogen testing method is to determine the hydrogen level obtained under extreme welding conditions, with most of hydrogen preserved in the weld metal, and not under varying and often uncontrollable in-situ welding and atmospheric conditions.

Regardless of the test method used a test sample containing a single weld bead is prepared. Test piece size and welding fixtures are determined by heat inputs derived from the welding processes used. Welding fixtures must be made from copper blocks, thereby allowing the test sample to rapidly cool and minimize the hydrogen effusion from the welded test piece. An example of recommended welding jig for the production of test welds with a heat input ≤2 kJ/mm [ISO 3690-2000] is shown in Figure 2. 13.
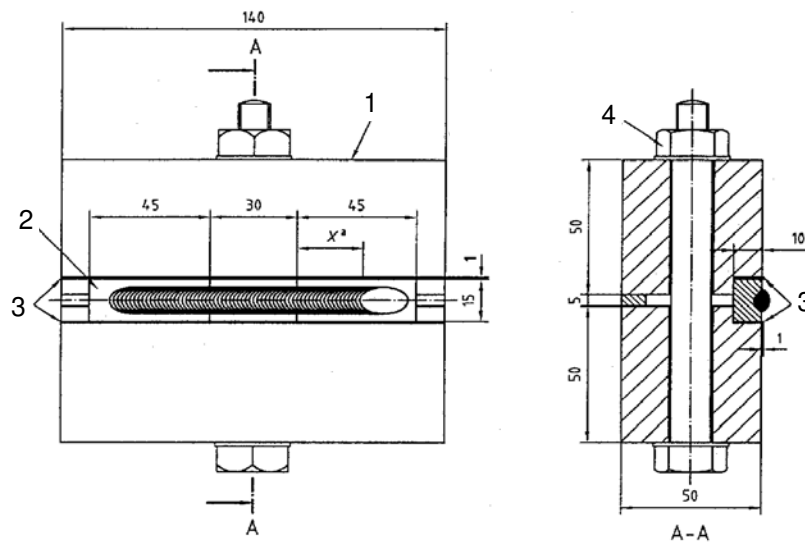
Figure 2. 13   A schematic illustration of the welding jig and test piece assembly required by ISO 3690-2000 for weld deposits made with a heat input of up to 2 kJ/mm. (1: copper block, 2: test sample, 3: copper shim, 4: tightening mechanism).

The choice of fixture, with or without water cooling channels, and assembly depends on arc energy involved and the resultant weld pool size on welded assembly shown in Figure 2. 14.
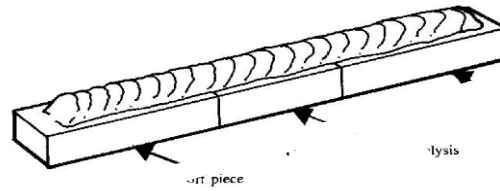
Figure 2. 14   An illustration of the welded test piece assembly, showing run-on, centre (used for analysis) and run-off pieces.

In accordance with ISO 3690-2000, the test pieces shall be prepared from a plain carbon steel with a carbon content of not more than 0.18 % and sulphur content of not more than 0.02 %. It is important that the test pieces have a uniform width to obtain proper clamping. Copper shims are also used for this purpose. Proper contact between the copper shims and copper block at the bottom of the sample is essential for ensuring adequate and reproducible cooling rates. It is expected that poor clamping conditions give higher hydrogen levels. For example, work by van Wortel (1993) showed that inadequate clamping conditions were responsible for an increase in measured diffusible hydrogen levels from a specified nominal hydrogen content of 5 ml/100g, to measured levels of 14 ml/100g or higher for basic coated electrodes. This phenomenon is explained by unsatisfactory clamping conditions of the welded sample, resulting in significantly lower cooling rates. It is suggested that after the completion of welding, when the welded sample is immediately water quenched, the sample is still in the fully austenitic structure and most likely over-saturated by diffusible hydrogen. Proper clamping of the sample can be visually detected after welding. Uncolored clamping regions are the indications of a optimal clamping arrangements. Any surface oxide discoloration (yellow or blue) of the welded sample sidewalls, which are in contact with the copper jig or shims, are a sign of unacceptable clamping affecting the accuracy of test.

It is recommended that the centre sections shall be degassed at 650 °C ±10 °C for 1 hour, carried out in vacuum or in electrical furnace filled with dry inert gas. However, testing standard ISO 3690-2000 also permits degassing after machining or in air when this is followed by complete removal of surface oxide by subsequent machining. Although not mandatory, a consideration should be given to degas run-on and run-off pieces as well [ISO 3690-2000].

Once the welding is completed, the jig with the clamped welded test piece is quickly released and the weld is immediately quenched to a sub-zero temperature, cleaned and broken apart. The sample then may be stored at dry ice or liquid nitrogen temperatures until required for analysis. Such prepared samples may be stored for up to 3 days (at –78 °C in CO_2) or for a number of weeks (at –198 °C in liquid N) before analysis, if necessary.

2.3.2.1 Deposited Weld Metal

The obtained data can be presented in term of diffusible hydrogen level in weld metal 'deposited' or 'fused' metal. This is schematically as shown in Figure 2. 15:

Figure 2. 15   Schematic illustration showing the definition of (a) deposited and (b) fused weld metals.

Where the diffusible hydrogen is to be expressed in terms of deposited weld metal, the diffusible hydrogen concentration is then calculated using Equations 2.12 and 2.13 [ISO 3690-2000]:

$$H_D = V \times \frac{100}{m_D} \tag{2.12}$$

where: H_D = diffusible hydrogen of deposited weld metal [ml/100g]

              V = volume of hydrogen collected [ml]

              m_D = mass deposited weld metal [g]

and

$$m_D = m_2 - m_1 \tag{2.13}$$

where: m_1 = mass sample prior welding [g]

              m_2 = mass of welded sample [g]

Consumable manufacturers, welding fabricators and welding standards refer mostly to hydrogen measurements defined in terms of deposited weld metal (ml of hydrogen per 100 g of deposited weld metal), although hydrogen measurements expressed in terms of fused metal are also obtainable from the same sample.

2.3.2.2   Fused Weld Metal

Where the diffusible hydrogen is to be expressed in terms of concentration in the fused metal (see Figure 2. 15 (b)), it is necessary to measure the cross-sectional area of the fused with deposited weld metal. The areas are to be measured on the ends of the welded samples and then averaging the results. Diffusible hydrogen in the fused weld is calculated following Equation 2.14 [ISO 3690-2000]:

$$H_F = H_D \times 0.9 \times \frac{A_D\,(avg)}{A_F\,(avg)} \tag{2.14}$$

where: H_D = diffusible hydrogen of deposited weld metal [ml/100g]

              H_F = diffusible hydrogen of fused weld metal [1g/tonne = 1.11ml/100g]

              $A_{D(avg)}$ = average area of deposited weld metal [mm^2]

              $A_{F(avg)}$ = average area of fused weld metal [mm^2]

When comparing the deposited and fused weld metal hydrogen values, Equations 2.12 and 2.14 respectively, it is apparent that diffusible hydrogen measured as deposited weld metal hydrogen is greater than that calculated fused for the weld metal hydrogen. After conducting a series of tests using MMAW welding process and comparing the results of deposited and fused weld metal hydrogen values, Pokhodnya (1996) concluded that hydrogen content of fused weld metal is 2-3 times lower. The relationship between the deposited and fused weld metals is diagrammatically shown in Figure 2. 16.
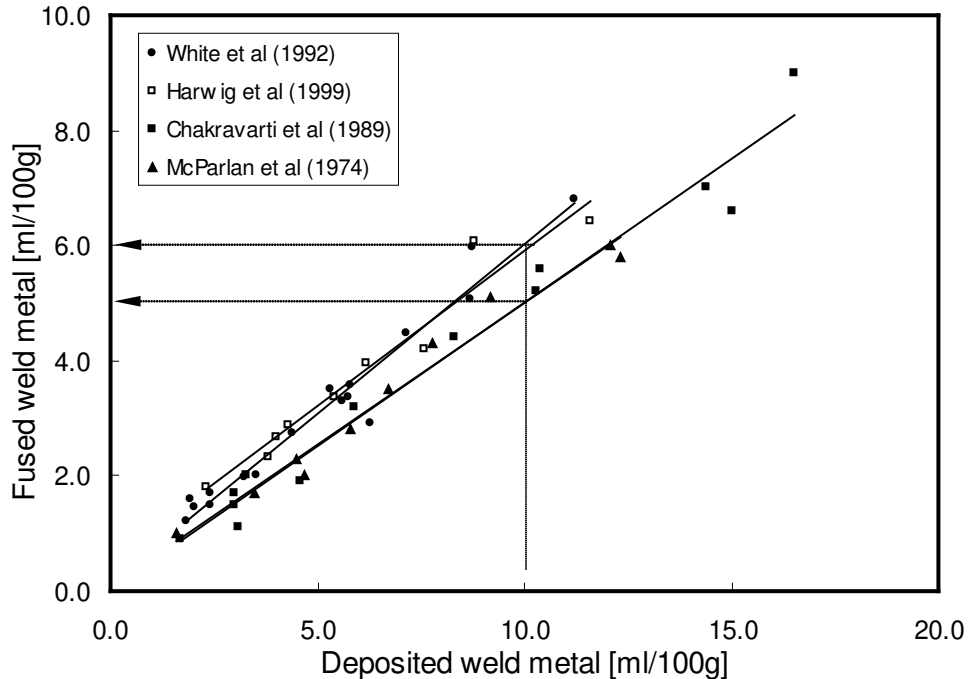
Figure 2. 16   Relationship between deposited and fused weld metal for FCAW rutile wires E71T-1 H5 and H10 (after White et al. (1992), Harwig et al. (1999), Chakravarti et al. (1989) and McParlan et al. (1976)).

The diagram illustrates that the levels of fused weld metal are approximately 2 times lower than the deposited weld metal hydrogen levels. From the relationship found between deposited and fused weld metal shown above, it appears to be possible to predict value of fused metal.

Trend lines of this work, Chakravarti et al. (1989) and McParlan et al. (1976) are identical, whereas the results of White et al. (1992) and Harwig et al. (1999) are noticeably positioned higher. To determine the exact cause for this shift may prove to be difficult, considering the wide range of welding consumables, variations in weld metals dilution, different shielding gases and welding variables used in each project.

To determine the fused weld metal additional equipment is required, such as sophisticated and expensive digital image-analyzing microscope to analyze the weld cross-sectional areas. Therefore, the consumable manufacturers, the welding industry and the welding standards commonly recommend the more simplistic hydrogen values measured in ml/100g of deposited weld metal.

2.3.3   Testing Methods

Currently there are three widely accepted testing methods for measuring diffusible hydrogen content extracted from a weld sample:

a) glycerin [H_{JIS}] method,

b) mercury method [H_{IIW}], and

c) gas chromatographic method [H_{C-G}].

All of the above methods determine diffusible hydrogen content in ferritic weld metal deposited using arc welding processes with filler metal. All three methods are based on a collection of hydrogen evolved from the welded sample through analytical apparatus, followed by the calculation of results. In addition to the above methods, there are other more

advanced methods, which enable the measurement of diffusible and residual hydrogen and involve shorter periods of time for testing. Some of these more advanced methods will be discussed later on in this Chapter.

Collection of hydrogen over mercury is currently referred as the 'primary' or 'reference' method. However, mercury can vaporize even at room temperature causing a health concern as mentioned in all hydrogen testing standards. Therefore, different sealing fluids other than mercury, such as glycerin and alcohol, have been used as alternatives. These, however, can partially absorb hydrogen from tests and from moisture in atmosphere, becoming hydrogenated and resulting in differences between 20-50 % when comparing with the mercury method [Pokhodnya 1996]. The relationship between primary and gas chromatography methods have been studied by a number of projects [Coe 1972, IIW doc. II-698-74 and IIW doc. II-1073-86] which established three different correlation equations, with only small differences among them [Kotecki 1992]. Ultimately, two correction coefficients were established and implemented in the Japanese standard [JIS Z3118-1992]. Assuming that the results of mercury and gas chromatography methods are yielding the same diffusible hydrogen values ($H_{IIW} = H_{C-G}$), the relationship between the mercury and glycerin methods adopted by ISO 3690-2000 employs the following correction coefficients,

$$H_{C-G} = 1.27 \times H_{JIS} + 2.19 \tag{2.15}$$

For gas chromatography method, Equation 2.16 applies:

$$H_{C-G} = 2 \times H_{JIS} + 0.3 \tag{2.16}$$

where: H_{IIW} = hydrogen level measured using mercury method

H_{JIS} = hydrogen level measured using glycerin method

H_{C-G} = hydrogen level measured using gas chromatography method

Since the correlation has been established in the Japanese testing standards JIS Z3118-1992, the H_{JIS} method using glycerin has been widely used [Lee et al. 1998] and is also regarded as being safer when comparing with the mercury method, particularly when a weld sample is to be immersed in at 45 °C for 48 hours.

Glycerin is susceptible to the absorption of hydrogen [Kotecki 1992]. This could potentially require a change in the correlation formulas, which could then affect the hydrogen measurement results. Repeatedly used glycerin will become more and more saturated by hydrogen, resulting in a distortion of a correct hydrogen measurement. This is perhaps the major concern for the testing laboratories when selecting a reliable testing method for hydrogen testing of welding consumables.

The testing standards also require the recording and reporting of atmospheric conditions during welding of samples. In addition to that, ANSI/AWS A4.3-93 also specifies atmospheric conditions for welding the test pieces at the time of testing. The standard specifies limits of 1.43 g of water per kg of dry air, or a moisture partial pressure of 1.635 mmHg, and the test specimens must be welded at or above these conditions to validate the testing. These conditions, at the atmospheric temperature of 20 °C, represent a low relative humidity of only 10 %.

Knowledge of the welding consumable mechanical properties and chemical composition required to match the parent metal properties is not the only factor in the process of selecting a welding consumable. Even when the consumable complies with these criteria, a need to assess the consumable from the point of view of hydrogen cracking is essential. Welding consumable manufacturers can assist with supplying the relevant information on request and, if

economically justified may even supply a certificate on the same batch number. The customer may even specify exactly what hydrogen levels the consumable should have for a given application. It is, however, important to understand that the different welding parameters used by the fabricator and those used in the hydrogen testing may not be the same and so hydrogen related problems may still occur. As specified in the AS/NZS 3752-1996, the weld shall be made using an amperage set in the mid-range of that recommended by the manufacturer and at an arc voltage conducive to optimum weld metal transfer. This is clearly inadequate for controlling hydrogen levels and therefore should be recognized by the fabricator as a guide only.

The current work will closely consider the importance of welding parameters with respect to determining the hydrogen content in two rutile flux cored wires of ANSI/AWS A5.20-95 E71 T-1 classification, but with different nominal diffusible hydrogen contents of 5 and 10 ml/100g of deposited weld metal.

2.3.3.1 Glycerin Method

The accuracy of this method was studied in the early 1980s by the AWS A5 committee. Several task groups conducted a series of round-robin tests to assess the glycerin, mercury and gas chromatography methods with main focus on their reliability, reproducibility and validity [Kotecki 1992]. The results clearly showed concerns about the glycerin method with very poor reproducibility, with both virgin and hydrogenated glycerin when comparing with the results of mercury and gas chromatography methods. Inter-laboratory results for glycerin method, while using the virgin glycerin, showed an average of 3.2 ml/100g. For hydrogenated glycerin, the test results were marginally higher, and averaging 5.0 ml/100g of diffusible hydrogen.

However, the individual test results from the participating laboratories using the hydrogenated glycerin were producing very wide range of diffusible hydrogen measurements between 3.2 and 11.4 ml/100g.

The measuring apparatus for this method is schematically shown in Figure 2. 17. In comparison with the other hydrogen measuring methods, the glycerin method is relatively simple.
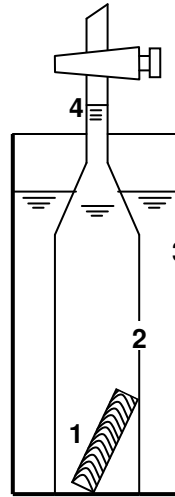
Figure 2. 17   Illustration of the hydrogen measuring apparatus for the glycerin method. (1-sample, 2-hydrogen collecting tube, 3-glycerin container, 4-hydrogen collecting tube) (after IIW doc.No: II-1073-86).

2.3.3.2   Mercury Method

In principle, the mercury method is similar to the glycerin method, but more sophisticated in the collecting apparatus as shown Figure 2. 18. The volume of evolved and collected hydrogen is determined by measurement of the length 'C' of the gas column, shown schematically in Figure 2. 19.
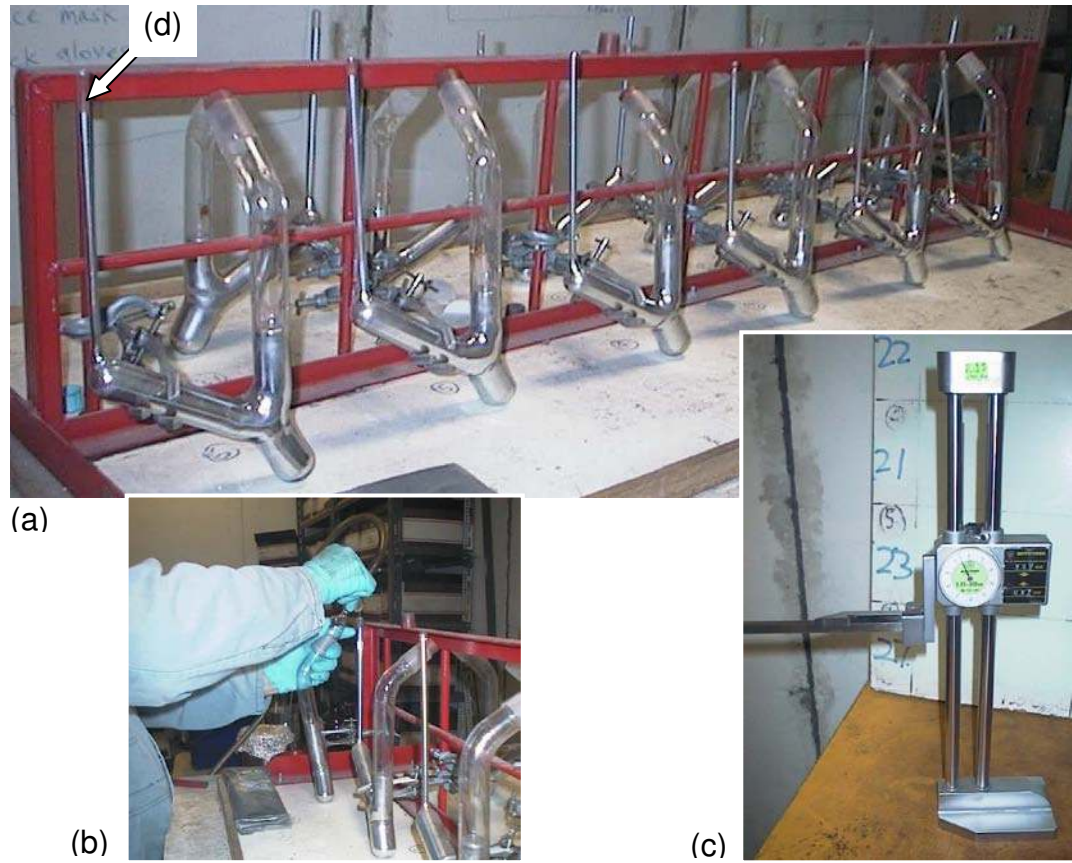
Figure 2. 18   Photographs showing the diffusible hydrogen collecting apparatus used for the mercury method. (a) Assembly of burettes known as Y-tubes for collection of multiple samples, (b) extraction of air from the burette, (c) height gauge for hydrogen column measurements above mercury shown in a precision bore tube (d) (courtesy of Lincoln Electrical laboratories, Sydney, Australia).
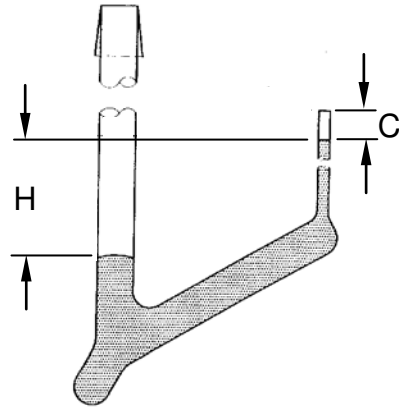
Figure 2. 19   Diffusible hydrogen collecting apparatus, 'Y' tube; H-head of mercury, C-length of hydrogen column above mercury (after AS/NZ 3752-1996).

The volume of hydrogen displacement as measured in the precision bore tube, corrected to standard temperature and pressure, is given by Equation 2.17 (ISO 3690-2000):

$$V = \frac{273 \times (P - H) \times (\pi r^2 \times C)}{760 \times (273+T) \times 1000} \qquad (2.\,17)$$

where: V   = volume of hydrogen collected [mm]

P   = barometric pressure of mercury [mm]

H   = pressure exerted by mercury in Y- tube [mm]

C   = length of gas column above mercury [mm]

r   = radius of the capillary precision tube [mm]

T   = room temperature at the time of hydrogen testing [°C]

The toxicity of the mercury method remains a health concern in testing laboratories and extra care must be taken during the testing procedure. All available testing standards for hydrogen determination refer to this method as the reference method. However, gas chromatography has

been shown to produce a similar margin error in diffusible hydrogen test results and should be considered as being capable of providing equivalent results [Kotecki 1992].

2.3.3.3 Gas Chromatography Method

Testing standards ANSI/AWS A4.3-93 and AS/NZS 3752-1996 both allow for the use of either the mercury or gas chromatography methods to calculate the weld metal hydrogen content, without any need for a correction factor.

The gas apparatus for collection of hydrogen using the gas chromatography method is more sophisticated than for the mercury method. It requires sealing the prepared samples into capsules of a sampler. After this, a number of combinations of temperature and time may be used to extract the diffusible hydrogen (see Table 2. 3).

Table 2. 3   The approved combinations of temperature and holding time for the gas chromatography method, in accordance with AS/NZS 3752-1996.

Holding temperature [°C]	Holding time [hrs]
45 ± 3	72 (+5, -0)
80 ± 3	18 (+2, -0)
150 ± 3	6 (+1, -0)

After completion of the holding period and cooling down to ambient temperature, the sampler is then connected to the gas chromatography analyser, calibrated as part of a standard procedure prior to every test. High purity argon as a carrier gas transports the hydrogen

evolved from the samples through the system. The amount of hydrogen volume 'V' is then detected by the instrument and recorded by the analyser. Figure 2. 20 shows the Oerlikon-Yanako hydrogen analyser model G-1006, of which a gas flow route diagram is shown schematically in Figure 2. 21.

Figure 2. 20   Photograph showing hydrogen and argon bottles connected to a hydrogen analyzer, shown on right (courtesy of CIGWELD Pty Ltd laboratories, Melbourne, Australia)
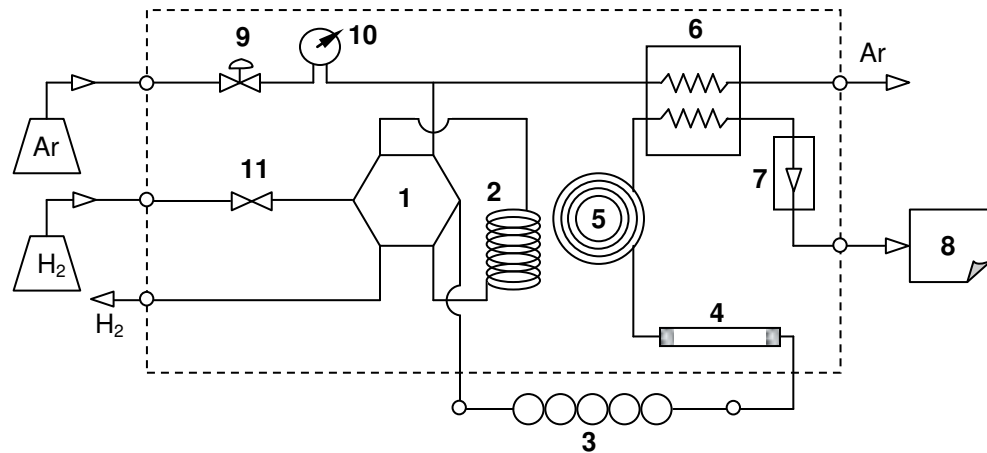
Figure 2. 21   Flow route diagram for hydrogen measuring apparatus used for gas chromatography procedure. (1-measuring valve, 2-hydrogen measuring tube, 3-sampler, 4-dehumidifier, 5-separation column, 6-detector, 7-flow meter, 8-recorder, 9-pressure regulating valve, 10-pressure gauge, 11-stop valve)

2.3.3.4   Hot Extraction Method

The choice of temperature is an important factor when to determine not only the evolution time but amount of hydrogen evolved. Where the glycerin and mercury hydrogen testing methods employ mostly ambient holding temperatures, the gas chromatography method allows for increases in the holding temperature up to 150 °C in order to accelerate the hydrogen effusion from the sample and thereby reduce the holding time down to 6 hours. However, the holding time can be reduced significantly by using the vacuum hot extraction or carrier gas hot extraction (HE) method, as shown in Figure 2. 22.
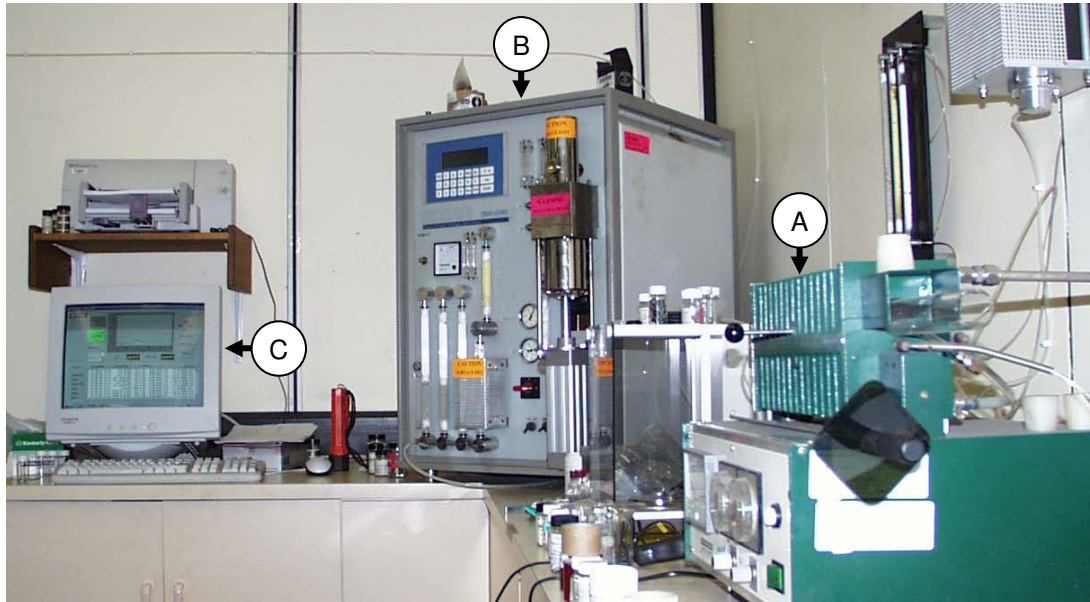
Figure 2. 22   Photograph showing the carrier gas hot extraction apparatus Eltra ONH-2000 analyser. A: furnace, B: analyzer unit, C: integrator/computer (courtesy of BHP-Billion laboratories, Port Kembla, Australia)

In principle, the hot extraction procedure is very similar to that of gas chromatography method. In the hot extraction method, the sample is placed into heated furnace up to 400 °C in a constant stream of high purity argon as carrier gas. At such a high temperature, the carrier gas removes hydrogen extracted from the sample within minutes and takes it through an analyzer which converts the carrier and hydrogen gas mixture to a volume of hydrogen, by reference to a calibration based on the injection of high purity hydrogen of a known volume.

Release of residual hydrogen is thought to become significant above about 400 °C (ISO 3690-2000). This residual hydrogen would normally remain in the sample at room temperature, permanently trapped in the microstructure of the weld deposit.

There appears to be some conjecture as to the influence of relatively high temperature (400 °C) on the amount of hydrogen desorbed during testing and the amount remaining 'trapped' in the microstructure as residual hydrogen. The accuracy of the HE method was recently considered in an Australian study by examining the hydrogen levels in weld deposits using a rutile flux cored wire E71T-1 [Nolan and Pitrun 2003]. The results of this study showed that the HE method was removing more hydrogen as 'diffusible hydrogen' than the mercury and gas chromatography test methods. However, the difference of 0.2 - 0.3 ml/100g was considered insignificant and certainly well within the generally accepted accuracy level of ±1 ml/100g of deposited weld metal. The authors suggest that the commercial, environmental and safety benefits of using the HE method, which can provide results in less than half an hour, far outweigh any risk associated with enhanced hydrogen desorption due to the higher test temperature at 400 °C.

2.3.3.5   Newly Developed Methods

To quantify the effects of hydrogen on cracking and its management in the weldment, new methods of hydrogen testing are still emerging. Some of them are in the very early stages of development [Lanford 1996], but show promise for measurements of hydrogen concentration profiles in solid samples using MeV ion beam analysis techniques. Two ion beam methods are based on a nuclear reaction analysis (NRA) and on elastic recoil detection (ERD). It is clear

that these methods have some unique characteristics, but their application in the control of hydrogen in welding has yet has to be established.

Another development is based on developing a spectrographic sensor to monitor and predict the weld metal diffusible hydrogen levels [Wong et al. 1996]. Very good results were obtained when the spectrometer was able to measure a relative intensity with results correlating to the ANSI/AWS A4.3-93.

A hydrogen sensor was successfully developed by Albert et al. (1997) using a conductive polymer electrode. The results of this work also indicate that this new method is reliable and as consistent as results obtained from gas chromatography.

Another sophisticated method capable of detecting the absolute hydrogen concentration in the weld arc plasma, involves using a high resolution spectrograph [Weber 1996]. In this method, an optical lens points directly into the weld arc through a bundle of high temperature resistant optical fibers and transfers the light into a monochromator where it is broken into component wavelengths. Data are graphed as diode versus wavelength, from which the amount of hydrogen is calculated. However, no correlation was presented between this and other conventional methods used for determination of diffusible hydrogen content in deposited weld metal.

A hydrogen sensor capable of generating hydrogen results in less than an hour and allowing in-situ analysis on the welded structure was also successfully developed using an opto-electronic diffusible hydrogen sensor [Smith II et al. 2001-1]. When comparing the experimental and gas chromatography method on nineteen specimens, the calibrated apparatus was found to have a good fit to measure data with a correlation coefficient r = 0.970.

In order to determine hydrogen levels in different areas of the weld, two methods based on laser ablation/mass spectrometry [LA/MS] and laser ablation/gas chromatography [LA/GC] were developed [Smith II et al. 2001-2]. Although the LA/GC method was successful in quantitative differentiation of hydrogen levels in different areas of the weld, its resolution was not as high as for the LA/MS method due to the longer ablation periods required to produce a detectable signals.

These recent developments of advanced analytical methods for hydrogen measurements show great potential for use in distinguishing between total and local hydrogen distribution, particularly in the case of multiple pass welding that is employed for welding thick wall sections.

2.3.4   Accuracy and Reproducibility of Testing

Although one can recognize the benefits selecting a consumable from a 'very low' hydrogen consumable group, the accuracy and reproducibility limits of hydrogen testing methods as determined by the standards can often overlap two neighboring hydrogen classification groups.

Other than JIS Z3118-1992, none of the other testing standards, ISO 3690-2000, ANSI/AWS A4.3-93 and AS/NZS 3752-1996, allow for the use of the glycerin method. Where the most recent international standard ISO 3690-2000 accepts the mercury method as the primary and reference method, the standard also acknowledges the mercury method as being time-consuming, particularly when carried out at a temperature of 25 °C ±5 °C. Therefore, in order to reduce the hydrogen evolution time, it allows for heating the weld sample to 45 °C, 150 °C and higher temperatures. This increase in test temperature is accompanied by an undesirable

and significant increase in the health hazard. As a result, ISO 3690-2000 permits alternative and more rapid and safer methods, but these methods must provide a proper correlation in terms of accuracy and reproducibility of the diffusible hydrogen results obtained with the primary method at ambient temperature.

All testing standards unanimously recognize the need for calibration of an analytical instrument by the injection of a known volume of hydrogen into the system, according to the manufacturers procedure. When considering alternative methods to mercury, the standards also recommend the determination of the accuracy of the method (instrument) at three hydrogen levels for weld metal (5, 10 and 15 ml/100g). It is recommended that nine repeat determinations be carried out using both the rapid and the primary method. The accuracy of the rapid method is then assessed by the statistical significance of the difference in means of the two sets of results (ISO 3690-2000). If the probability of the difference not due to chance is >95 %, then the difference in means is probably significant. The most common statistics used when comparing means is the 't' value defined as follows Equation 2.18:

$$t = \frac{(\bar{x}_R - \bar{x}_P)}{\sqrt{\dfrac{s^2_R}{n_R} + \dfrac{s^2_P}{n_P}}} \tag{2. 18}$$

where: $\bar{x}_R, s_R, n_R$ = mean, standard deviation, number of samples - rapid method

$\bar{x}_P, s_P, n_P$ = mean, standard deviation, number of samples - primary

The 't' value is subsequently applied to statistical tables, where for the number of degrees of freedom involved ($n_P + n_R - 2$), the probability of this value having arisen by chance will be

given. If the difference in means is judged to have arisen by chance, then the two methods may be assumed to give identical testing results.

When using the primary mercury method, the reproducibility and/or accuracy of hydrogen testing for a welding consumable containing 10 ml/100g of hydrogen, was found to be within ±1 ml/100g representing 10 %, most probably due to variation of welding parameters and individual welding consumable [Bailey et al. 1995].

2.3.5 Multiple Weld Pass - Hydrogen Distribution Measurements

The conventional hydrogen measurement methods of mercury, gas chromatography and glycerin are for application to a single pass weld deposit only. The hydrogen measurements obtained from these single pass tests represent maximum values for a particular consumable welded at particular welding conditions with very fast cooling rates achieved by immersing the samples into ice water immediately after the completion of welding and quenched into liquid nitrogen. This procedure minimizes hydrogen evolution from the test sample.

The main influence on hydrogen concentration is certainly the welding consumable, where the initial hydrogen content in each weld pass should be the same. However, from a practical point of view, the welding of thicker wall sections by multi-pass welding requires such measurements of hydrogen content be reconsidered with respect to other variables affecting the hydrogen distribution across the multi-pass weld. The hydrogen concentration of each weld pass will vary according to the thermal regime experienced during and after each subsequent weld pass as observed by Kuebler et al. (2000).

It is expected that a multi-pass weld would consist of regions of as deposited weld metal, as well as sections that have been subject to one or more reheating cycles and re-melted weld metal. Repeated thermal cycles will affect not only the weld metal microstructure, resulting in non-uniform distribution of various microstructural constituents [French 1998], but also the hydrogen distribution within the weld metal [Kasuaya et al. 2001]. Hydrogen diffusion rates in weld metal may also be affected [Pargeter 1992] due to the heterogeneity of weld metal microstructure, particularly with respect to the high inclusion content.

While the sequence and location of individual weld beads may be controlled to enable the refinement of weld metal and HAZ microstructures [Kiefer 1995], controlled deposition sequences should also be able to control the amount and distribution of hydrogen throughout a multi-pass weld.

Variation of one of the welding parameters such as preheating temperature or the heat input, are likely to changes the weld metal cooling rate and alter the hydrogen concentration. These changes are also likely to alter the residual stress and weld metal microstructure [Davidson et al. 1996, Dixon and Taylor 1996, DeLoach et al. 1999]. Elevating preheat temperature and heat input reduces weld metal cooling rates resulting in reduced hydrogen concentration [Lin and Perng 1997] through enhanced effusion. However, in terms of weld metal microstructure, factors such as hydrogen trap binding energy and their density can affect the hydrogen effusion locally as well [Olson et al. 1996].

Methods of measuring hydrogen levels in multipass welding are more intricate. Various techniques of measuring hydrogen distribution in multi-pass welds were reviewed by Yurioka and Suzuki (1990) and include:

a) micro-printing of polished cross-section through a neodymium film or nuclear emulsion silver bromide,

b) bubble counting on the polished weld cross-section covered by a film of glycerin,

c) laser beam spot fusion followed by mass spectrographic analysis of evaporated hydrogen, and

d) weld sample micro-sectioning at different weld zones at low temperature to minimize the rapid effusion of hydrogen out of a sample.

Another method to obtain the hydrogen concentrations through a multi-pass weld is by extracting a sample directly from the molten weld pool using a glass tube and then immediately quenched in ice water followed by liquid nitrogen [Thibau and Bala 1983]. The results of this technique were compatible to the hydrogen results obtained from a conventional weld samples extracted by machining, while maintaining the sample <20 °C during the machining operation [Kasuaya et al. 2001].

An analytical model was constructed to determine the hydrogen distribution in a 90 mm thick multi-pass weld [Nishito et al. 1975], using parameters such as diffusion time, temperature and weld depth. The results of hydrogen distribution were similar to the experimental values of diffusible hydrogen distribution in 55 mm and 40 mm thick welds by Takahashi et al. (1979) and Kasuaya et al. (2001), respectively as shown in Figure 2. 23.
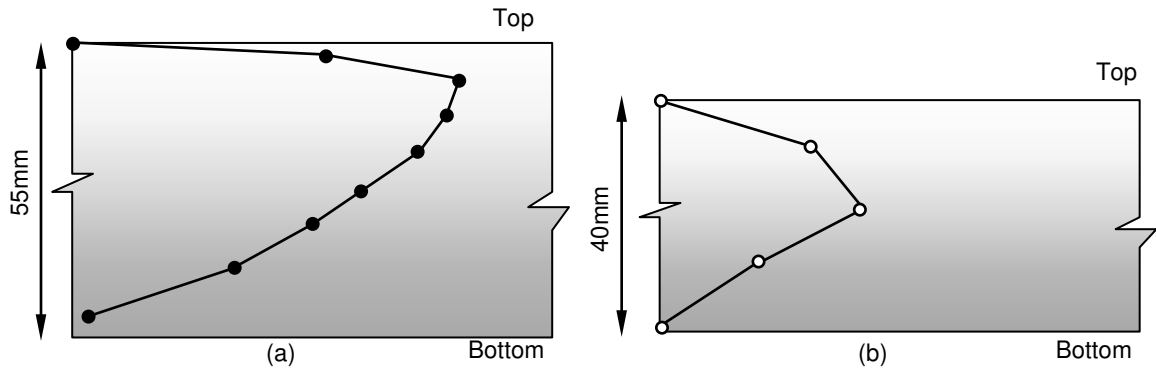
Figure 2. 23   A schematic illustration of hydrogen distribution in 55mm and 40mm thick

welds (after Takahashi et al. (1979) and Kasuaya et al. (2001))   [not to scale]

Another analytical model of hydrogen diffusion in multi-pass welded joints was developed by

Kasuaya et al. (2001), considering hydrogen content, diffusion coefficient, time and material

thickness. Very good correlation, a difference of <5 %, was found between defining the

thermal history in a welded joint using a series of mathematical equations and comparing the

experimental data.

The results from the existing studies examining the hydrogen distribution through the multi-

pass weld deposits, show that the weld sequence and the frequency and locations of weld

deposits should be taken into account when assessing the hydrogen distribution in welds with

large wall thicknesses. This may be particularly important in the case of repair welding of

thick wall sections accompanied by high restraint levels.

CHAPTER 3

Hydrogen Assisted Cold Cracking (HACC)

In comparison to austenitic steels, ferritic steels are characterised by higher susceptibility to hydrogen cracking and higher crack growth rates [Vigilante et al. 1996]. This is a result of their different lattice structures, whereby the less closely packed structure of ferrite (α-Fe) with body-centered cubic (B.C.C.) allows greater mobility of hydrogen atoms.

Different materials react differently to hydrogen absorption. Table 3. 1 gives the order of susceptibility to hydrogen embrittlement of a range of metals [Smithell Metals Book 1983] commonly used in the welding industry.

Table 3. 1   Susceptibility of some common materials to hydrogen embrittlement.

Susceptibility (Ranking in decreasing order)	Material
High	- High strength steels at high yield strength - High strength nickel steels - Medium strength and low strength steels - Iron-silicon single crystals - Cobalt alloys
Low	- Austenitic stainless steels; 310, 304
Little or none	- Stabilized stainless steels - Aluminium alloys - Molybdenum

As mentioned earlier, hydrogen assisted cold cracking can occur either in the parent metal HAZ or weld metal, where a sufficient amount of hydrogen is introduced into the restrained welded joint and transported to a critical site characterized by susceptible microstructure, then cracking can be initiated in the HAZ or the weld metal.

Traditionally, processing factors such as preheat temperature, plate thickness, selection of welding process, welding consumable strength and nominal hydrogen content, are chosen to avoid HACC in the HAZ of the parent plate, as specified in the welding standards. It is usually a consequence of inadequate preheat temperature that weld metal transverse cracking is encountered in welding thick plates [Jones and Hart 1983]. Increasing weld metal strength also increases the propensity for this type of cracking [Pussegoda et al. 1997] by effectively increasing the level of residual stresses. When the welded joint is thick, the delay times for cracking can be quite high (several days) as hydrogen must first be transported to the location where the stress or strain state is most severe.

Hydrogen distribution is not uniform and varies for the different compositions and microstructures in the weld metal and HAZ [French 1998]. High stress intensity generates a large plastic zone within the hydrogen-rich weld metal microstructure where the HACC is then more likely to occur [Yurioka and Suzuki 1990]. As mentioned in the Introduction, modern steels have become more resistant to HAZ hydrogen cracking as a result of reduced alloying content and the introduction of TMCP technology. As a consequence, it is becoming increasingly important to develop reliable testing methods that provide accurate data for avoidance of weld metal hydrogen cracking. The methodical assessment of the HACC phenomenon in weld metal is an ongoing but relatively new area of study. Therefore, independent management procedures for avoiding HACC in the weld metal are yet to be developed.

Although the factors that control weld metal hydrogen cracking are recognized, it is still very difficult to predict it in practice [Vuik 1993 and Kinsey 2000]. Although there are guidelines and welding standards for avoidance of HACC in HAZ [AS/NZS 1554.1-2000, AS/NZS

1554.4-1995, AWS D1.1-2000 and EN 1011.2-2001], a universal and reliable model for HACC avoidance in the weld metal is expected to be more complex and harder to achieve than for hydrogen cracking in parent metal [Uwer and Höhne 1991].

3.1   HYDROGEN CRACKING OF WELDED JOINTS

In general, it is accepted that HACC in welded ferritic steels occurs at near to normal ambient temperature as a result of three main inter-related factors:

  I. hydrogen concentration in the weld joint,

  II. local residual stresses acting on the weld joint raising from joint restraint and thermal contraction during cooling, and

  III. crack susceptible HAZ and/or weld metal microstructures.

For HACC to occur all three must overlap as shown in Figure 3. 1.
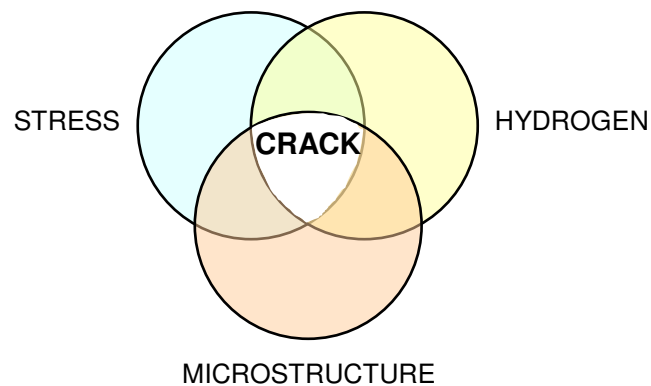
Figure 3. 1 An illustration of three interacting factors responsible for HACC: stress, hydrogen present and susceptible microstructure (after Hart 1999).

The magnitude of each factor and its significance within this 3-way interactive relationship is yet to be fully determined for weld metal hydrogen cracking. However, by selecting very low hydrogen containing welding consumable, selecting weld configurations with less restraint and opting for consumables with microstructures that are less susceptible to cold cracking, we can potentially reduce the overlapping area and perhaps gain control of HACC occurrence in welded joints.

Hydrogen cracking can be initiated in the weld metal or its HAZ, and depends on transformation behaviour, as described by Granjon (1971) and as shown in Figure 2.12. In principle, a region with delayed transformation or cooling can maintain hydrogen mobility for longer and may be characterized by increased cracking susceptibility during a continuous temperature decrease;

1. HAZ cracking: When the martensitic transformation in weld metal occurs at a higher temperature than the parent metal, then the diffusible hydrogen will segregate predominantly in the parent metal HAZ resulting in underbead cracking.

2. Weld metal cracking: when the transformation temperature of parent metal HAZ is higher than for the weld metal then it is likely that hydrogen will be trapped within the weld metal, thereby increasing cracking propensity in the weld metal.

The location of cracks will also depend on other factors such as relative hardenability, carbon and alloy content of the weld and parent metals and the direction of the principle weld joint restraint forces [Lancaster 1999].

Hydrogen cracking can be transferred from parent metal HAZ to weld metal as a result of higher restraints at the weld [Barbaro 1999], especially when welding thick plate sections [Alam et al. 1996] since the greater the thickness, the higher the restraint intensity. Higher restraint intensities and lower heat inputs also can create faster stress build up and this is expected to shift cracking susceptibility from the HAZ to the weld metal [Hoffmeister et al. 1987].

Hydrogen cracks can be initiated in regions containing stress concentrators, such as a lack of fusion, notches, weld root of the fillet weld or weld joint misalignment. Regarding their orientation, cold cracks can be either longitudinal or transverse, where there are high longitudinal restraint forces [Lancaster 1999]. The cracks can be surface breaking or contained below the surface. The various types of orientations of hydrogen associated cold cracks can be described and defined according to their location in the welded joints, as shown in Figure 3. 2.

1 -TRANSVERSE CRACK IN WELD METAL (surface breaking or sub-surface)
2 -TRANSVERSE CRACK IN HAZ
3 - HAZ, TOE CRACK
4 - WELD METAL ROOT CRACK
5 - ROOT CRACK IN HAZ
6 - UNDERBEAD CRACK
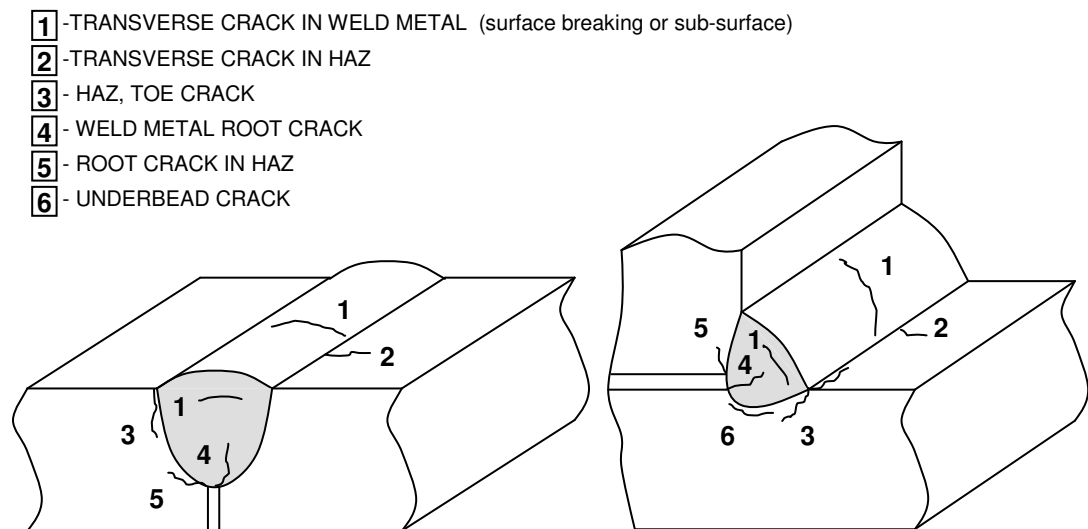
Figure 3. 2   Schematic illustration of typical crack locations associated with the HACC.

The primary aim of this work was to investigate the effect of welding parameters on weld metal hydrogen levels and its influence on transverse weld metal cracking (described in Figure 3. 2 as type [1]).

3.1.1   Heat Affected Zone

Over the years, research on hydrogen induced cracking has focused predominantly on weldability of steel, with regard to the avoidance of cracking in the parent metal HAZ. Generally, it was found that HAZ hardness depends on hardenability of steel, which is predominantly a function of steel chemical composition and cooling rate.

A typical example of steel composition affecting cold cracking behaviour would be a lamellar tearing initiated by partially removed inclusions remaining in the banded layers present in rolled steel. In these layers, known for lower through-thickness ductility, cracking can occur as a result of high restraint joint configurations which develop high residual stresses during weld metal solidification. These stresses act transversally to the rolling direction of steel and result in subsurface cracking along the parent metal HAZ, as shown in Figure 3. 3.
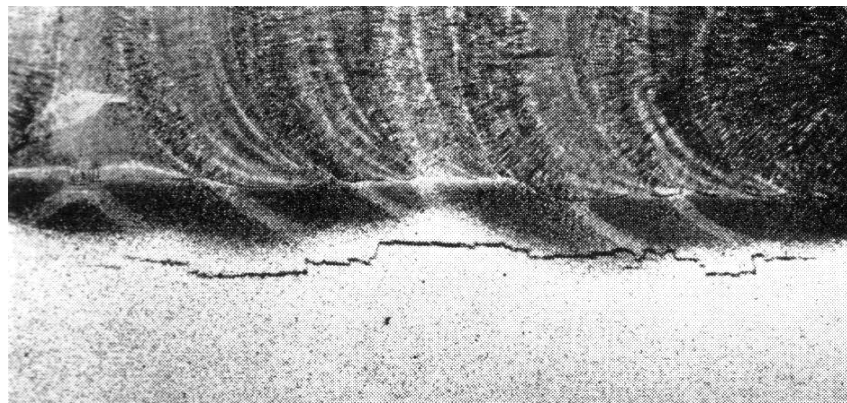
Figure 3. 3   A micrograph showing typical sub-surface lamellar tear (after Farrar and Dolby 1969).

The new generation of TMCP steels is characterized by lean chemistry within the steel. Mainly via better control of carbide forming elements, the risk of hydrogen cracking in the steel HAZ was gradually diminished. This is driven by a reduction in the carbon and carbon equivalent levels [Kinsey 2000].

However, HAZ cracking can still occur. Examples of HACC at the weld toe and root of a single weld pass are shown in Figure 3. 4, and of HACC in a multi-pass welds of low strength low hydrogen welding consumable in Figure 3. 5.
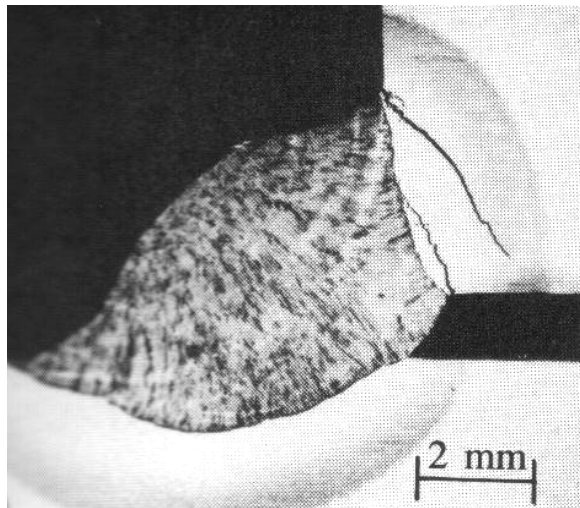
Figure 3. 4   A typical HAZ cracks initiating in weld root as well in weld toe caused by an excessive root gap (after Bailey et al. 1995).
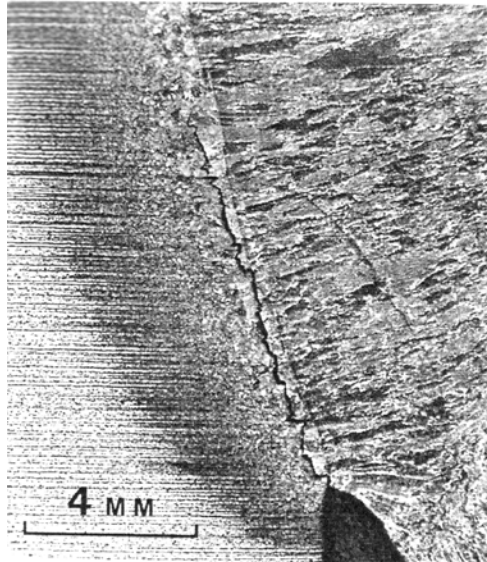
Figure 3. 5   A micrograph showing root HAZ cracks in a mutli-pass weld of 100 mm boiler steel, welded using a low hydrogen welding consumable with a single bevel preparation (after Suzuki and Yurioka 1982).

The hydrogen cracking in HAZ is usually underbead and present in the grain-coarsened regions of HAZ containing large coarse grains, as shown in detail in Figure 3. 6.
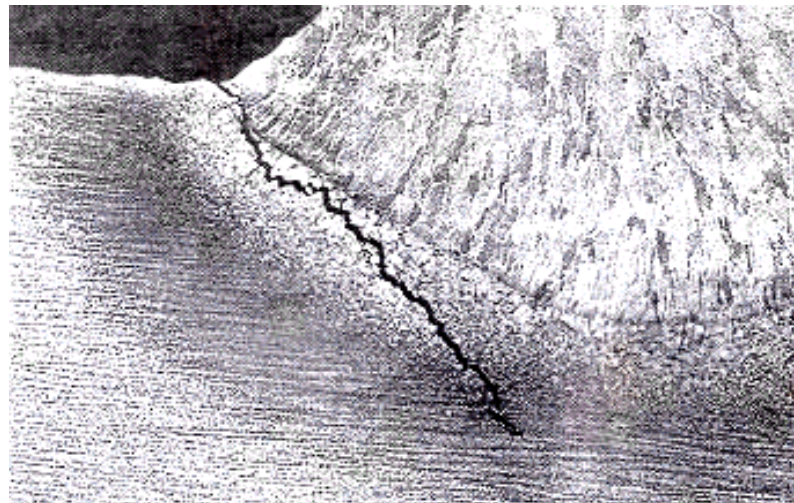
Figure 3. 6   A micrograph showing HACC in the coarse region of parent metal HAZ (after Bailey et al. 1995).

There is no doubt the incidence of hydrogen cracking in HAZ is decreasing [Edwards and Liu 1990], predominantly due to steel development, decreasing hydrogen levels of consumables and well disseminated knowledge to avoid HAZ cracking in the welding industry. The guidance provided by well established welding standards, such as AS/NZS 1554.1-2000 and ANSI/AWS D1.1-2000 and other for structures and pressure vessels fabrication, have resulted in a much improved understanding of the importance of HACC and a consequent decrease in its occurrence.

3.1.2   Weld Metal

The improvements of weldability in HAZ have had the effect of shifting HACC to the weld metal, which is generally more highly alloyed and characterised by considerable microstructural heterogeneity. While the industry guidelines developed for HACC in HAZ provide some important background information on factors vital to suppress the existence of HACC, they cannot be applied directly to the care of weld metal cold cracking. For this reason, development of predictive methods for weld metal HACC is currently a topic of considerable international interest.

In general, the susceptibility of weld metal to hydrogen cracking appears to increase with an increase in weld metal strength, hydrogen content and section thickness increase [Hart 1999]. Cracking is often accompanied by a high degree of plastic strain and cracks are therefore located in such microstructural regions where intense plastic strain is accumulating [Nevasmaa 2002].

One of the very common defects found in the ferritic steel weld deposits is a 'fish-eye' as shown in Figure 3. 7.
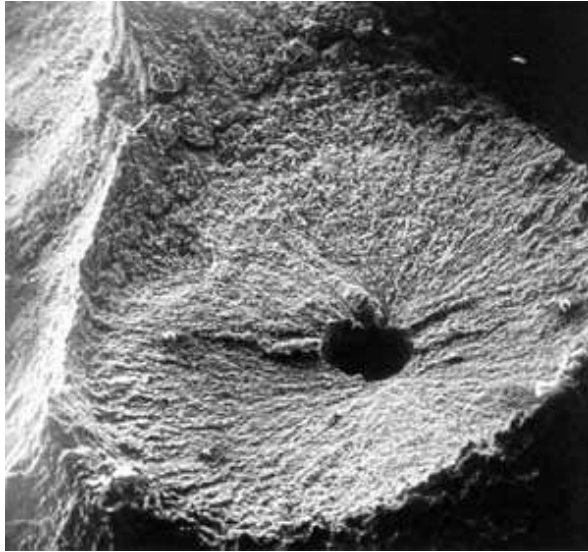
Figure 3. 7   SEM micrograph showing a typical 'fish-eye' hydrogen crack initiating at the centre (after http://www.twi.co.uk).

This defect is observed when a ferritic steel weld metal region contains an excessive amount hydrogen and is plastically strained at a low strain rate at ambient temperature. The fish-eye comprises of two regions. At the centre, the "pupil" of the eye is a spherically shaped pore or inclusion and the outer region, the "iris", has fractured due to local hydrogen embrittlement in a quasi-cleavage mode, in a pattern radiating away from the "pupil" (http://www.twi.co.uk).

It is important to note that it is a common practice that the consumable manufacturers, prior to mechanical testing of all weld metal samples, heat treat the test coupons immediately after welding to remove hydrogen from the weld deposit, thus minimizing the occurrence of this fish-eye defect.

Chevron cracking, sometimes called staircase cracking, can be found in multi-pass weld deposits, such as the submerged arc weld shown in Figure 3. 8 [Lancaster 1999], but it has also been observed in MMAW weld deposits [Mota and Apps 1982].

Figure 3. 8   A photograph of a typical pattern of chevron cracking in a longitudinal section revealing 45° angle with the plane of the plates in a butt joint (after http://www.twi.co.uk).

Chevron cracking is a type of hydrogen cracking which can be eliminated by decreasing the hydrogen levels caused by moisture contaminated flux [Allen et al. 1982].

The formation of chevron cracking mechanism is schematically shown in Figure 3. 9.
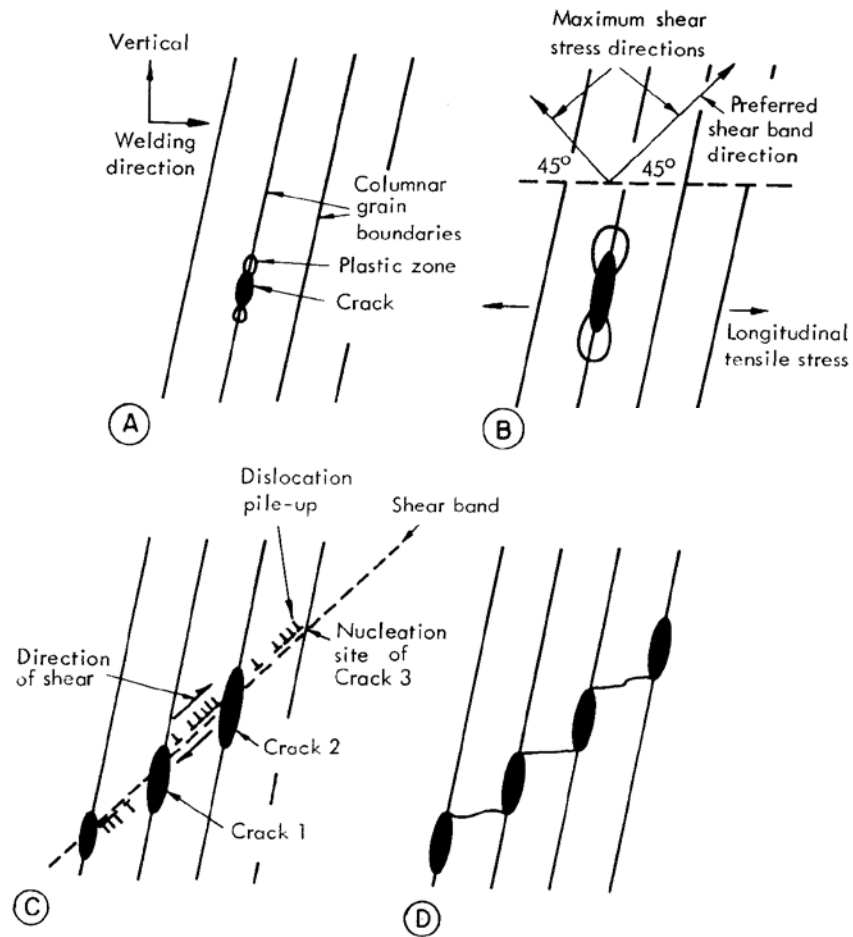
Figure 3. 9   A schematic illustration of the proposed mechanism of chevron crack formation with dislocation shear bands. (A) - Micro-crack nucleation, (B) - blunting and arrest, (C) - crack formation with shear band, (D) - macro-crack formation (after Allen et al. 1982).

Chevron cracking is characterized by high level of axial stress in the direction of the weld, causing slip bands at an angle of 45° in the direction of welding. Local concentration of plastic

strain in the inter-granular polygonal ferrite and a critical amount of hydrogen are thought to be the two main factors in development of chevron cracking [Hrivňák 1992].

Severe weld metal hydrogen cracking in a plane perpendicular to the welding direction has been reported in 60 mm thick multi-pass weld SAW and FCAW welds deposited without and with preheat application, are shown in Figure 3. 10, respectively. Interestingly, no cracking was observed in the HAZ in either work by Abson (1995) or Kuebler et al. (2000).
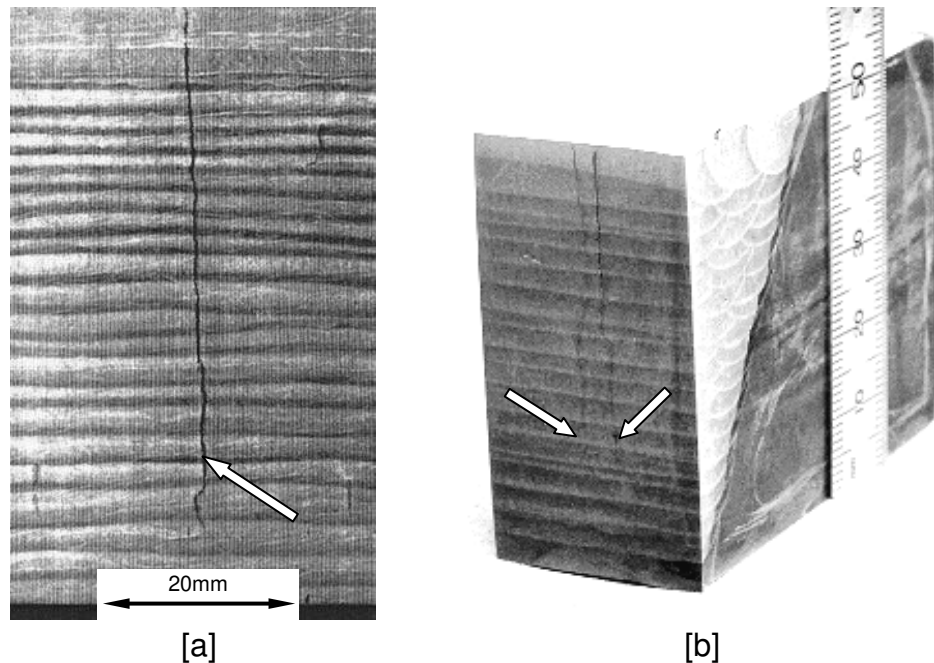
Figure 3. 10   Photographs showing typical transverse cracking in multi-pass weld deposits (after [a]: Abson 1995 and [b]: Kuebler at al 2000).

In recent years, more and more scientific data are becoming available in relation to weld metal hydrogen cracking. There appear to be some similarities between occurrences of weld metal and HAZ cold cracking. However, it is more complex than the case of HAZ cracking [Yurioka and Suzuki 1990].

3.1.3   Steel Hardenability

In general, weldability is improved by reducing the carbon content and carbon equivalent and by minimizing alloy content of welded steel [Lancaster 1999]. Historically, carbon was considered to be the most cost effective element to strengthen structural steels. However, it results in several negative effects with respect to other properties such as toughness, ductility and weldability. It is traditionally considered to be the most potent of the crack promoting alloying elements through its effect on steel hardenability [Hart 1991].

The influence of chemical composition on weldability is usually described quantitatively in terms of carbon equivalent formulae. Carbon equivalent numbers (CE) can be calculated from various empirical formulae to represent the relative influence of the combined effects of significant compositional elements in a hardenable steel influencing the material's hardenability and weldability. Several carbon equivalent based formulae have been developed in the last decades for use in the determination of crack susceptibility in HAZ [Lundin et al. 1990, Yurioka and Suzuki 1990]. All these formulae show that a reduction in the carbon content results in improved steel weldability. However, there is presently no effective parameter for weld metal crack susceptibility, particularly in thick walled sections where cracking is more likely to occur [Barbaro 1999].

The two formulae that are perhaps the most widely adopted in welding standards in Australia [AS/NZS 1554 Parts 1 and 4] are the CE_{IIW} and Pcm formulae. They predict hardenability and therefore susceptibility to cold cracking, and are used to determine the required preheat temperature to avoid HACC in the parent metal.

The first, Equation 3.1, defines the material carbon equivalent (CE) relates composition to hardenability. It was developed originally for semi-killed steels [Bailey et al. 1995] and adopted by the International Institute of Welding (IIW) and is as follows:

$$CE_{IIW} = C + \frac{Mn}{6} + \frac{Cr+Mo+V}{5} + \frac{Cu+Ni}{15} \tag{3. 1}$$

The second formula, Equation 3.2 was developed [Ito and Bessyo 1968] to take into account further elements such as silicon and boron, considering that boron makes the steel more hardenable [McMahon 1980, Bang and Ahn 1997, WTIA TN 1]:

$$Pcm = C + \frac{Mn+Cu+Cr}{20} + \frac{Si}{30} + \frac{Ni}{60} + \frac{Mo}{15} + \frac{V}{10} + 5B \tag{3. 2}$$

The Pcm formula has been adopted for welding of quenched and tempered (QT) steels with carbon content not exceeding more than 0.11 % [Düren 1990]. High strength steels are characterized by high CE_{IIW}, resulting in high hardenability. Consequently, the Pcm formula gives more weight to C and B content and is more appropriate for low alloy, quenched and tempered steels than the CE_{IIW} formula. The Pcm parameter was also described to be more appropriate for the HAZ hydrogen cracking behaviour of modern low carbon equivalent steels than CE_{IIW} [Martharu and Hart 1985].

There are other carbon equivalent formulae suggested by numerous authors such as Ceq, CEN, CET, CEw focused on different levels of C and other alloying elements effecting weldability and hardenability of steels.

3.1.4 Preheat and Inter-pass Temperature

Where microstructure and hardness control cannot be ensured, limitation of hydrogen content is the necessary step to avoid cold cracking. The first step is to select a welding process and consumable that produces weld deposits characterized by very low hydrogen levels. However, high structural restraints may still be the major factor to consider when HACC is a concern. As mentioned earlier in Chapter 2, diffusivity of hydrogen is slowed by fast cooling rates and rapidly decreasing temperature of the weldment. The hydrogen then remains in weld metal and HAZ, thus subsequently causing hydrogen embrittlement at lower temperature. By slowing down this fast and detrimental process, we can therefore minimize the risk of HACC. This is done by the application of a preheating treatment as an effective practical method of decreasing cooling rates and allowing a longer time for hydrogen to effuse from the weldment.

Selection of an appropriate preheat level is based on the level of hydrogen present, the stresses associated with the joint configuration, material strength, composition and thickness and its susceptibility to hydrogen embrittlement, particularly in an association with fast cooling rates. In order to avoid cold cracking, it is not just the level of preheating temperature, but also cooling time down before reaching 100 °C complying with condition that $t_{100} \geq (t_{100})_{cr}$, where t_{100} is the cooling rate to 100 °C and $(t_{100})_{cr}$ is the critical time within which cracking can be prevented under the welding condition described by the cracking index (CI) [Yurioka et al. 1983]. The same affect can be achieved by maintenance of inter-pass temperature. Hence, by implementing an appropriate preheat and inter-pass temperature, such that the actual duration time of cooling down to 100 °C is exceeding the $(t_{100})_{cr}$ parameter, cracking may be avoided. Hydrogen cracking can occur if the welding parameters, such as preheat or inter-pass temperature and heat input, result in the condition, $t_{100} < (t_{100})_{cr}$. Figure 3. 11 represents a

schematic illustration of Yurioka's crack prediction model. This model considers the effect of changes in plate thickness and chemistry, welding consumable, welding parameters and hydrogen content to avoid hydrogen cracking.
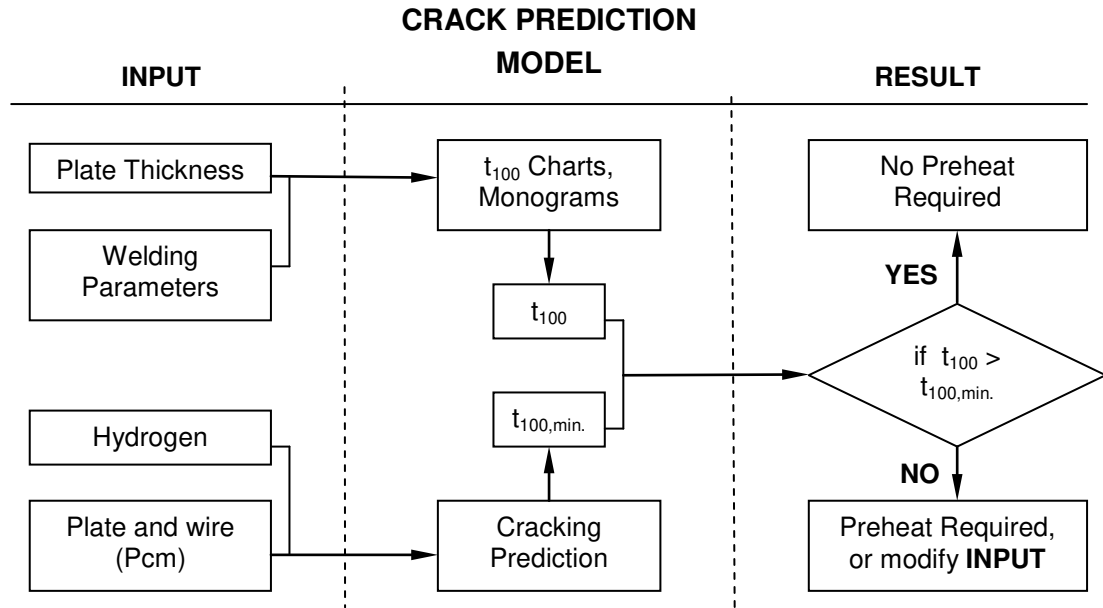
Figure 3. 11   A hydrogen prediction model determining the preheat requirements based on the condition that $t_{100} \geq (t_{100})_{cr}$ (after Yurioka et al. 1983).

In contrast to the above model, a mathematical formula was established by Okuda et al. (1987) for the critical preheat temperature, Tc, using multiple regression analysis, with the assumption that the tensile strength is known and the diffusible hydrogen content is also quantifiable by gas chromatographic method, Equation 3.3:

$$T_c = 0.524 \times \sigma B + 277 \times \log[H_D]_{G\text{-}C} - 482 \tag{3. 3}$$

where: T_c = critical preheat temperature [°C]

             σB = weld metal tensile strength [MPa]

             $[H_D]_{G\text{-}C}$ = diffusible hydrogen level of weld metal measured by gas chromatography method [ml/100g]

This was successfully validated by joining two plates with a weld metal containing very low diffusible hydrogen content of <5 ml/100g, with thickness ranging from 20-80 mm for a minimum temperature of $1.15T_c$. It highlights that preheating and inter-pass temperatures are strongly related not just to weld metal diffusible hydrogen levels, but also to its tensile strength.

As described in the standards AS/NZS 1554.1-2000, AS/NZS 1554.4-1995 and AWS D1.1-2000 for structural welding, the most significant factors when considering HACC susceptibility are the thickness, the chemical composition (expressed often in terms of CE_{IIW} and Pcm of the weldment), the heat input for a given welding process and the welding parameters used. Less significance is given to the surface heat transfer affected by ambient temperature and/or drafts. In order to avoid HAZ cold cracking in a particular material, welding standards use different prediction of preheat temperatures. Based on different types of carbon equivalents for these materials, a comparison of welding standards was undertaken in a number of studies to assess the adequacy of their predictive preheat temperatures [Yurioka and Kasuya 1995, Yurioka 2002]. Although they were categorized in terms like appropriate, conservative, probably conservative and too conservative, these reviews concluded that none of the preheat temperatures were found to be inadequate [Yurioka 2002]. These variations of preheat temperatures for the welding of high strength quenched tempered steel AS 3597 Gr.700 (Bisalloy 80) joined together by a single 'V' butt weld using high strength FCAW basic and/or rutile wire are plotted from different sources and are shown in Figure 3. 12. Though they may appear to have different temperatures ranges for preheat selection at particular plate thickness range, the preheat temperatures may still be adequate for avoidance of hydrogen cracking in parent metal.
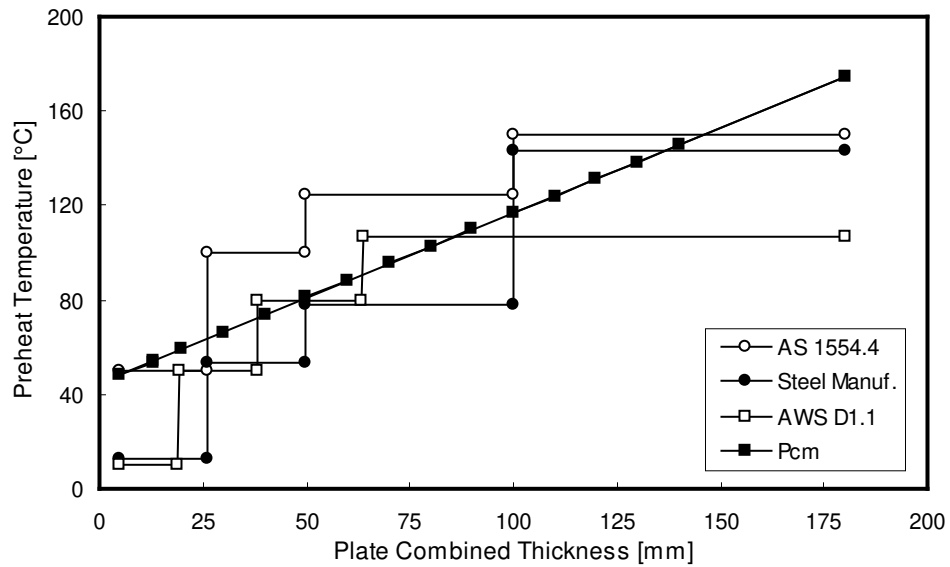
Figure 3. 12   A graph showing the method for prediction of preheat temperatures for welding of high strength low alloy AS 3597-1993 Gr.700 (Bisalloy 80) plate.

It is clear that methods differ not only in determining at what combined plate thickness the preheat temperature should be increased, but also in the respective preheat temperatures. When looking at combined plate thickness of 50mm, higher preheat temperature range 100-120 °C recommended by AS/NZS1554.4 - 1995 can be described as more conservative than other methods. However, the Australian steel manufacturer's recommendation [Bisalloy Steels 1997] for preheating is in a lower temperature range between 50-75 °C, which is significantly lower than the preheat level required by the welding standards.

Increased preheat and/or inter-pass temperatures result in lower cooling rates and reduced residual stresses. They also affect the mechanical properties of weld deposits [DeLoach et al. 1999], reducing HAZ hardness in both high strength low alloy and plain carbon steels [Graville 1978] but, most importantly, minimizing the risk of HACC in HAZ and weld deposits [Lee and Kang 1997].

A number of projects studying the effect of preheat temperature on cold cracking concluded that low or inadequate preheat and inter-pass temperature with fast cooling rates are the main contributors to cold cracking [Abson 1995, Lee et al. 1998, Kinsey 1998, Lee and Kang 2003]. The results of these studies showed that where the HAZs of various base plate steels were resistant to hydrogen induced cracking, even without preheat, severe hydrogen cracking was observed in the weld metal. While reduced cooling rates are advantageous since they allow hydrogen to escape from weldment, a study by DeLoach et al. (1999) also found that increased cooling rates resulted in an increase of the weld metal yield strength and impact values. However, at critical cooling rates of 70 °C/s obtained without preheating, transverse cracking was observed in a 50 mm thick plate section using GMAW process.

The results of above the experimental research work, and of other work that has illustrated HACC in weld metal deposited using recommended preheat temperature for low [Visman 2002] and high [Kuebler 2000] strength rutile flux cored wires with low diffusible hydrogen levels of ≤10 ml/100g, highlight the need to develop a model to predict preheat temperatures with consideration of avoiding HACC in weld metal.

3.2   EFFECT OF HYDROGEN

The sequence leading to hydrogen cold cracking in ferritic steels can described as follows:

a) Hydrogen enters the arc atmosphere via moisture contaminated flux or shielding gas, or surface contamination on materials and consumable surfaces. The hydrogen is then converted to monatomic hydrogen at high temperatures experienced in the arc.

b) First hydrogen is absorbed into the molten weld pool. The weld metal and/or HAZ becomes supersaturated in hydrogen as it cools down. During cooling, the hydrogen is initially soaked up in the austenite phase where is has comparatively high solubility. As the structure transforms to the ferritic/martensitic structure, the atomic hydrogen is less soluble and therefore is driven to points of discontinuity, such as prior austenite grain boundaries and second phase particles.

c) The external restraints generate residual stresses due to shrinkage strains and transformation changes. The hydrogen then may contribute to cracking by lowering the cohesive strength within the lattice or by adding to the localized stresses at the discontinuity.

The crack initiation mechanism may be time dependent since the hydrogen must diffuse through the lattice. Cracking is then initiated at the critical location, in HAZ and/or weld metal, with a specific combination of hydrogen concentration, localized stresses and susceptible microstructure.

The reduction of steel ductility at temperature below 200 °C, for hydrogen containing and hydrogen free specimen is demonstrated in Figure 3. 13, with the maximum embrittlement for a low carbon steel occurring at the temperature between –50 °C and +150 °C [Pokhodnya et al. 2000]. The embrittlement caused by hydrogen on a welded joint below 200 °C is due to physical interactions between interstitial hydrogen and the lattice structure. This reaction is reversible only once the hydrogen is removed by heat treatment, which can lead to recovery of steel ductility to normal levels [Lancaster 1999]. Softening the microstucture by tempering, the microstructure then becomes less susceptible to cracking [Bailey et al. 1995].
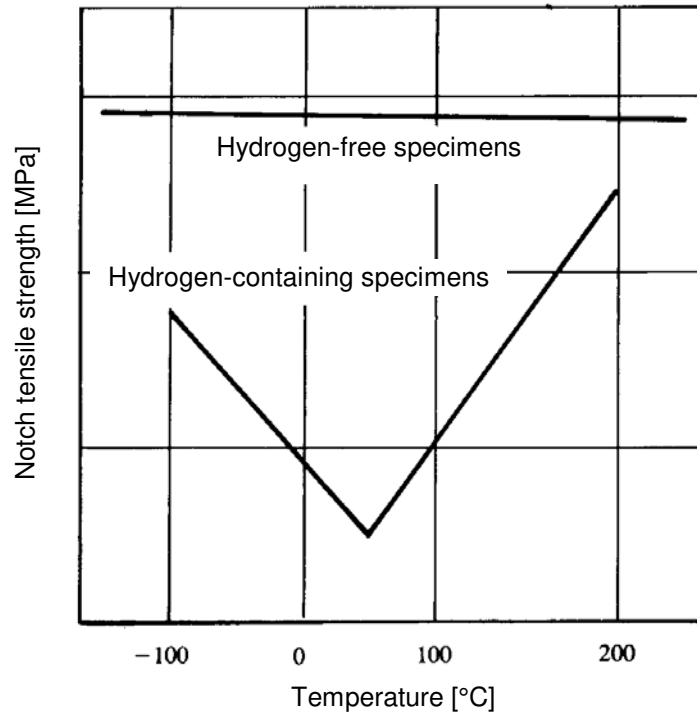
Figure 3. 13   Graph showing the notch tensile strength of hydrogen-free and hydrogen-containing steel, with minimum at values close to ambient temperature (after Bailey et al. 1995).

To predict the hydrogen concentration during and after welding, a computer model was developed by Pussegoda et al. (1997). From the modeling, it was found that hydrogen concentration peaked 24 hours after the start of welding near the tip of a notch. Work by Alexandrov (2002), examining the behaviour of diffusible hydrogen in welded joints by using mathematical modelling, concluded that the equilibrium solubility of diffusible hydrogen in the normalized ferrite-pearlite microstructure of base metal is four to five times lower than in HAZ. This is most likely due to the austenite formation in parent metal HAZ which causes considerable increase of the local concentration of diffusible hydrogen in HAZ. In the case of weld metal, the hydrogen concentration during cooling to room temperature is controlled by the level of alloying of under-cooled austenite [Alexandrov 2003].

It is known that hydrogen effuses out of the weld over a period of days or weeks at room temperature, so the risk of cracking gradually disappears. However, the period after which the cracking is unlikely to occur has yet to be defined and is an important part of research into hydrogen cracking. Therefore, it is a common industrial practice that non-destructive testing (NDT) for the detection of hydrogen cracking in a weldment be delayed for at least 48 hours after completion of welding. However, the time to fracture may vary, even when using the same welding consumable, since change of welding parameters and atmospheric conditions may affect hydrogen content, weld metal microstructure, mechanical properties and therefore HACC susceptibility.

The work by Beachem (1972) revealed that the time to fracture and the fracture modes are both dependent on the hydrogen level. In general, low hydrogen weld metal requires a long incubation period (several hours) and fracture occurs by brittle intergranular fracture (IG) and/or the quasi-cleavage (QC) mechanism. At high hydrogen levels, microvoid coalescence (MVC) was the predominant mechanism, and it occurred after a short incubation time. These results are illustrated in the Beacham (1972) diagram, shown in Figure 3. 14, which was constructed from hydrogen charged, quenched and tempered steel, assuming a homogenous hydrogen distribution. The diagram demonstrates the combination of stress intensity and hydrogen concentration just after welding at point 'A'. As time passes, hydrogen accumulates at the notch tip located in weld or the weld toe. When the hydrogen concentration reaches the critical level at point 'B', a crack is initiated. In a self-restraint weld, residual stress is relaxed and stress intensity decreases with crack growth, and eventually the crack stops (dashed line). In external weld cracking tests, the stress intensity continues to increase and the crack growth rate is accelerated as the crack grows in the form of MVC (solid line).
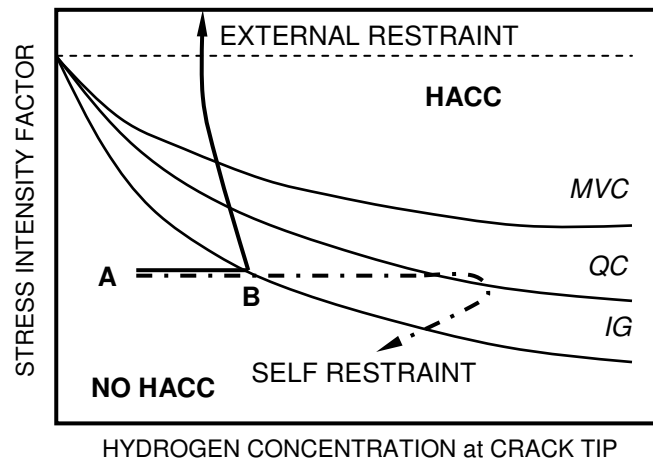
Figure 3. 14   The Beacham diagram, representing the relationship between hydrogen concentration and stress intensity factor (after Beacham 1972).

At low stress intensity factors, IG can be still a predominant fracture mode where hydrogen concentrations are high [Gedeon and Eagar 1990/1], a behaviour that is promoted by increasing oxygen content [Matsuda et al. 1985]. The IG mode is replaced by the QC and MVC modes at higher stress intensities [Vasudenan 1981, Yurioka and Suzuki 1990].

The IG, QC and MVC modes are shown schematically in Figure 3. 15.
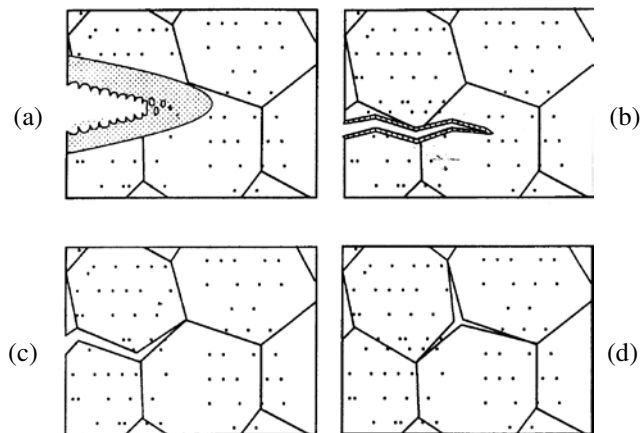
Figure 3. 15   Schematic diagrams of microscopic fracture modes. (a) MVC with high stress intensity factor, (b) QC intermediate stress intensity factor, (c) IG with low stress intensity factor and (d) IG with assisted hydrogen pressure (after Lee et al. 1998).

However, it should be noted that hydrogen is not homogeneously distributed in the parent steel and the weld metal [Olson et al. 1996]. Hydrogen will be found not only in the host lattice, but also segregated to atomic and microstructural imperfections such as vacancies, voids, solute atoms, dislocations, grain boundaries and second phase particles. All of these can act as hydrogen sinks, where hydrogen atoms can accumulate.

The combination of a stress concentrator and hydrogen may nucleate a crack if the stresses are present [Suzuki 1978, Thibau and Bala 1983]. The kinetics and morphology of hydrogen crack growth is influenced by microstructural features, hydrogen content, strain rate, temperature and stress intensity [Yurioka and Suzuki 1990] and HACC can vary for the same material, depending on the hydrogen concentration at the crack tip and the stress intensity factor [Davidson et al. 1996]. Increased stress intensity levels can lead to a change in the fracture mode from brittle intergranular fracture (IG) to quasi-cleavage (QC) and finally transgranular microvoid coalescence (MVC) [Beachem 1972].

In order to avoid or minimize the hydrogen concentrations that lead to embrittlement of a welded joint, a good welding procedure would recommend as 'compulsory' the post heat treatment of a completed weld [Okumura and Horikawa 1971]. Preferably, the post heat treatment should be carried out immediately from preheat and/or inter-pass temperatures. This however, is not always possible in practice, particularly in the welding of large sections where it may be impractical to maintain a preheat temperature above 200 °C. In the extreme cases, with high levels of joint restraint and a susceptible microstructure, a welding procedure should control weld pass deposition rate, the time elapsing between weld passes and perhaps, in large sections, carry out the post heat treatment in stages.

3.3   EFFECT OF RESIDUAL STRESS

Residual stresses are the result of manufacturing and fabricating of a weldment. Any heat treatment or welding process induces residual stresses, which have a major effect on overall performance of a component in service [Bergheau et al. 1997 and Pussegoda et al. 1997].

There are a number of factors affecting the presence of residual stresses including:

a)   non-uniform heating or cooling across the weldment,

b)   constraints or rigidity imposed on the joint by the structural configuration,

c)   presence of previous welding when repair is required,

d)   external loads used to ensure fit-up,

e)   thermal expansion and different transient temperatures, and

f)   transformation from austenite (γ-Fe) to ferrite (α-Fe) (see Figure 3. 16).
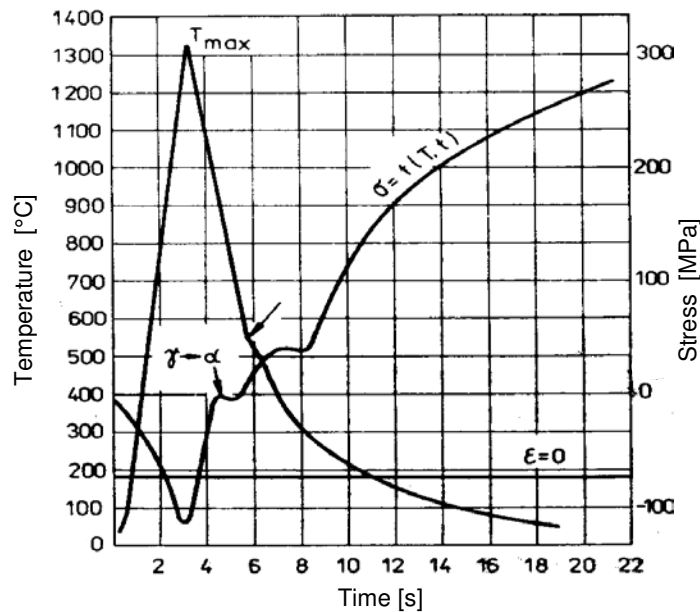
Figure 3. 16   A graphical representation of stresses induced through the thermal cycle, observed during transformation from austenite to ferrite (after Easterling 1983).

The type (tensile or compressive) and magnitudes of the residual stresses are affected by the interaction of these factors.

In simplistic terms, the three most important sources of residual stress in welded joints [Lin and Perng 1997] are:

a) shrinkage of the weld metal during solidification,

b) shrinkage of the weld heat affected zone during cooling, and

c) phase transformations in both the weld metal and the HAZ.

In order to minimize the detrimental effects of residual stresses in welded joints, particularly where there is significant amount of hydrogen present, it is vital to avoid high restraints in joints by appropriate design, and to avoid local stress raisers, such as excessive weld joint root gaps and weld undercuts. In addition to these design related factors, consideration should be also given to carrying out immediate post heat treatment to promote hydrogen effusion from the weld, thereby mitigating against cold cracking.

3.3.1   Stress Fields Distribution

During the welding, the temperature field in the weldment is not distributed homogeneously through the thickness of weld. The weld outer surface and weld adjacent to a plate along its fusion line cool more rapidly than the weld interior. This is demonstrated in a two-dimensional model of thermal transverse stresses in a plate shown in Figure 3. 17.
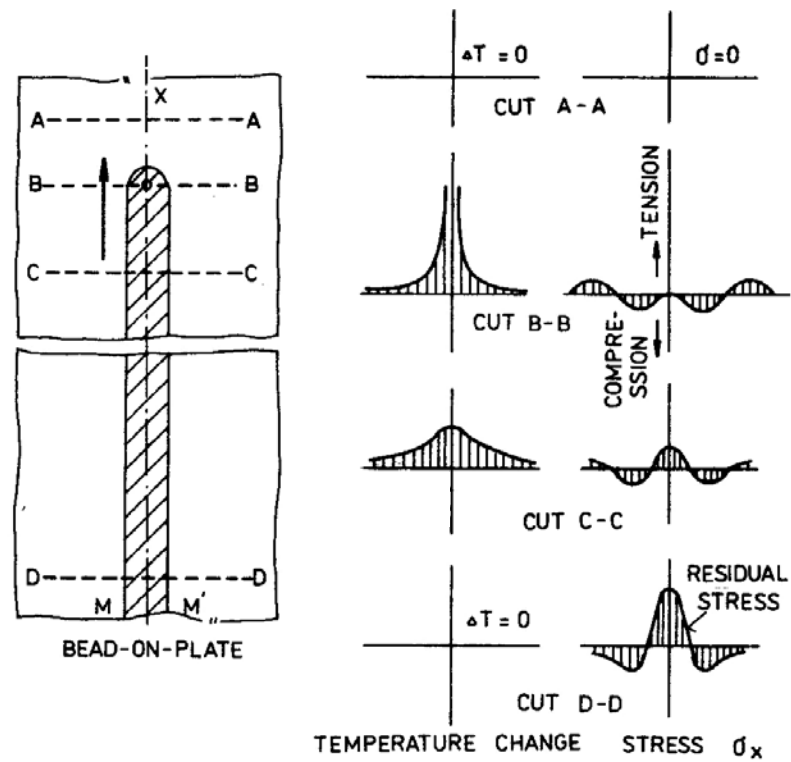
Figure 3. 17   Schematic representation of temperature and transverse stresses during welding (after ASM Welding Handbook Vol.6, 1993).

Every weld pass generates a thermally non-linear induced loading, which result in residual stress after welding [Shim et al. 1992]. This is particularly important in a case of large plates being welded together by multiple passes. The residual stresses transverse and longitudinal to the weld axis are shown in Figure 3. 18.
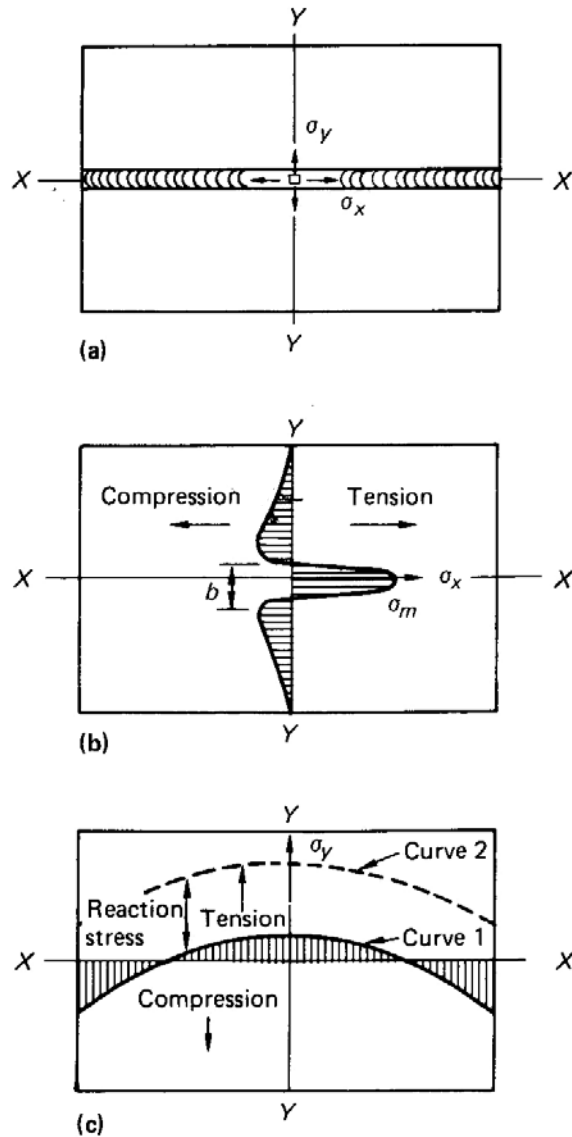
Figure 3. 18   An illustration of typical residual stress distribution in a butt weld (after ASM Welding Handbook Vol.6, 1993).

The longitudinal stresses, measured through the plate thickness, were found to be higher than the transverse residual stresses [Gunnet 1958], resulting in the tendency for transverse cracking in weld metal to occur. Generally, higher residual stresses are developed as the thickness increases because structural rigidity is higher and therefore there is less opportunity

for accommodation of the stresses by longitudinal or transverse distortion of the plate [Stout 1985].

There are several methods for measuring residual stresses in welded joints, including hole – drilling technique, X-ray diffraction, FEM modeling and neutron diffraction, which is said to enable penetration of the steel to a depth of about 30 mm [Ripley 2002]. All of these methods have been shown to give good agreement between each other.

3.3.2   Multi-pass Weld Deposits

When welding thinner section plates, most of the residual stresses build up during the first run, usually resulting in visible distortion in both longitudinal and transverse directions. However, in thick section plates there is a progressive intensification of stresses by each subsequent weld deposit as the joint is built up.

The longitudinal and transverse residual stresses, measured vertically through 55 mm thick butt weld, are shown in Figure 3. 19 [Takahashi et al. 1979].
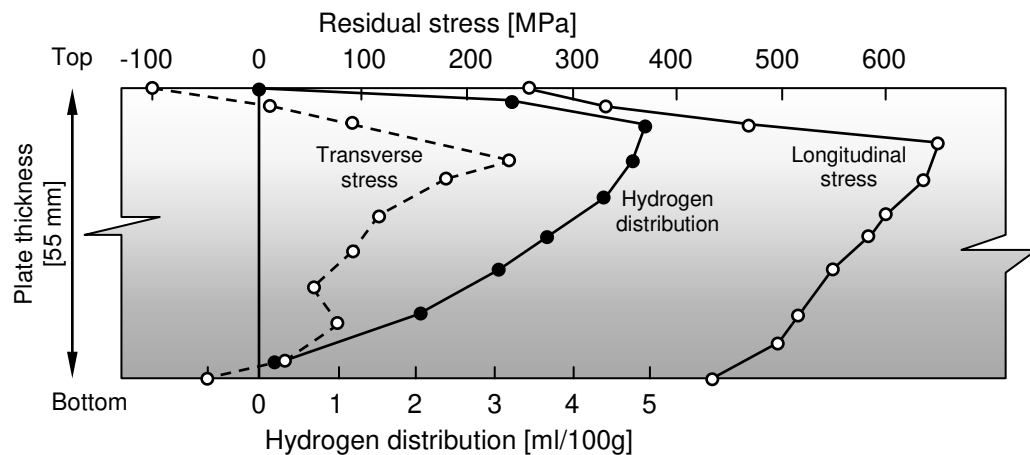
Figure 3. 19   An illustration of longitudinal and transverse residual stress distribution through 55 mm thick plate (after Takahashi et al. 1979)   [not to scale]

Longitudinal stress was found to be significantly higher than transverse stress through the entire plate thickness, with both peaking at a depth of about 10 mm below the top surface. It is important to note that the residual stresses and hydrogen distribution were found to be maximum in approximately the same depth from the plate top surface.

It is not just plate thickness, but also plate width, which affects the residual stresses in a moderate thickness of 10 mm [Lancaster 1999]. Wider plates revealed higher longitudinal tensile residual stresses in the weld and lower compression residual stresses in the joined plates. Narrower plates show a decrease and increase of longitudinal stresses in weld and plates, respectively.

The application of preheat decreases the weld cooling rate, allowing more hydrogen to diffuse out (as described in detail in Chapter 2). Increased preheat temperature also reduces residual stresses in the weld deposit when welding thick section high strength steel [Lee et al. 1998]. An increase of preheat and inter-pass temperatures from 30 °C to 100-120 °C welding using FCAW process for 50 mm thick plate has been shown to result in a decrease in the range of residual stresses from 40-60 MPa to 30-40 MPa, respectively [Lee et al. 1998].

Modelling of residual stresses and temperature distribution in large wall thicknesses is of particular interest for analysis of cold cracking. Finite element computer packages such Sysweld® and ABAQUS® are used to carry out numerical simulations that examine interactions between all the physical phenomena involved, including metallurgical transformations, plastic stresses and strains, and hydrogen diffusion rates [Smith and Blunt 1993, Roelens, Bergheau et al. 1997]. The results from such computer models give reasonable correlation with calculated stress distributions in both longitudinal and transverse directions

[Hong et al. 1998] and confirm experimental data obtained using the conventional blind-hole drilling strain gauging method [Shim et al. 1992].

3.4   EFFECT OF MICROSTRUCTURE

The microstructure developed during welding is one of the principle factors that determines the susceptibility to HACC in weld deposits.

The microstructure of ferritic steel weld metal, in general, is significantly more complicated than that of the steel it joins. Unlike the plate material produced under controlled thermal processing routes, which is usually a combination of fine ferritic–pearlitic microstructure at lower strength or bainitic–martensitic microstructure in HSLA steels, the weld metal largely consists of an unrefined solidification structure, generated through high cooling rates. As a result, the weld metal can contain microstructural constituents unlikely to occur in the parent steel.

During weld metal solidification, and during subsequent solid state transformations on cooling, the following microstructures can develop with relevant agreed abbreviations [ASM Welding Handbook Vol.6, 1993]:

PF	- primary ferrite
PF(G)	- grain boundary ferrite
PF(I)	- polygonal inter-granular ferrite
FS	- ferrite with second phase
FS(NA)	- ferrite non-aligned second phase
FS(A)	- ferrite aligned second phase
FS(SP)	- ferrite side plates (Widmanstätten)
FS(B)	- bainite
AF	- acicular ferrite
FC	- ferrite carbide aggregate
M	- martensite

The classification of different morphologies of microstructure found in ferritic steel weld metals was developed by the International Institute of Welding (IIW) and published as the 'Guide to the light microscope examination of ferritic steel weld metals' [IIW doc.No: IX-1533-88]. The above nomenclature has been adopted in the current work.

Factors affecting the formation of ferritic weld metal microstructures are the alloy composition [Tyagi et al. 1996, Grong and Kluken 1992], heat input [Wegrzyn 1992] (which affects the cooling rate particularly during γ-Fe $\rightarrow$ α-Fe transformation), the oxygen / inclusion content [Komizo and Fukuda] and the nature of segregation in the weld metal. Formation of structures in low carbon weld metal and nucleation of various microstructures is presented in the continuous cooling transformation (CCT) diagram presented in Figure 3. 20.
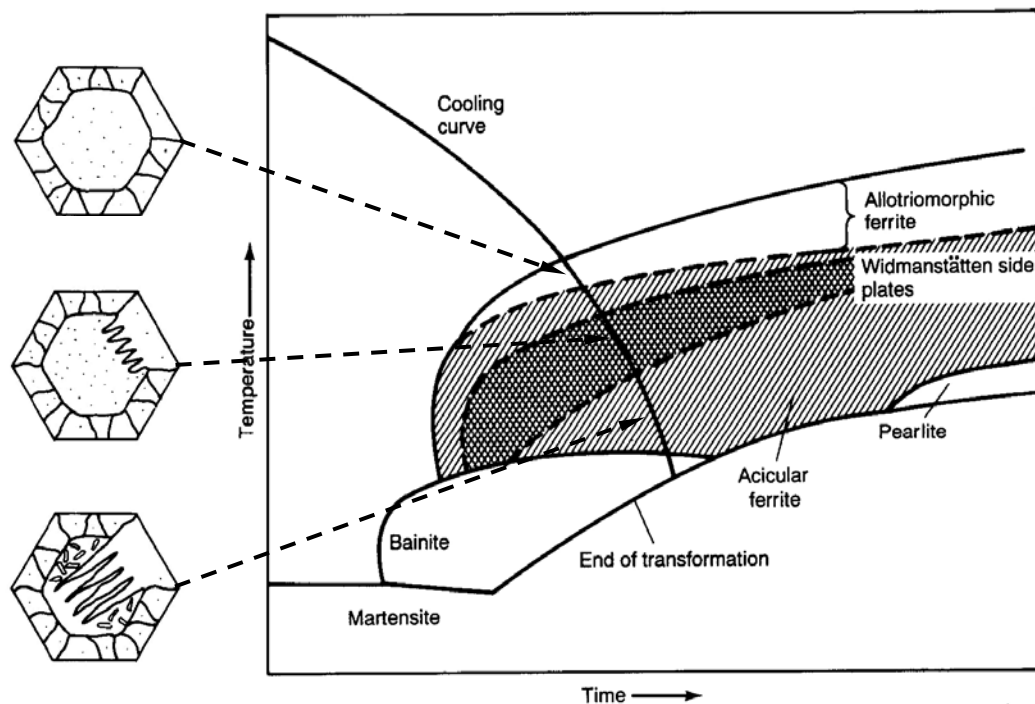
Figure 3. 20   Schematic illustration of a weld CCT diagram, showing of microstructural development during cooling (after ASM Welding Handbook Vol.6, 1993).

A schematic illustration of the development of ferritic weld metal microstructure is shown in Figure 3. 21. The original austenite grains (a), transform to grain boundary ferrite (b), and then other ferritic microstructural constituents (c).

(a)   (b)   (c)
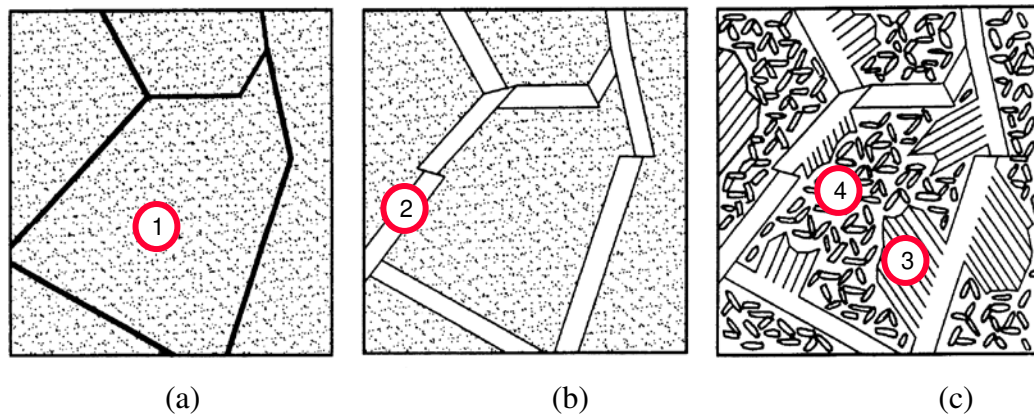
Figure 3. 21   A schematic illustration of microstructural development in weld metal on cooling from delta ferrite (δ-Fe), undergoing: (a) - solid state transformation to austenite γ-Fe grains [1], (b) – formation of grain boundary ferrite PF(G) [2] on the prior austenite grain boundaries and (c) – initiation of ferrite with second phase FS(SP), usually being Widmanstätten side plates [3] growing into the austenitic grains from PF(G) and (c) formation of acicular ferrite AF [4] (terminology by IIW doc.No: IX-1533-88, after French 1998).

Hydrogen cracking is commonly found to propagate along prior austenite grain boundaries [Thibau and Bala 1983, Pargeter 1992], although it has also been found to propagate through acicular ferrite AF [Bailey et al. 1995]. Regions containing ferrite with second phase FS(SP), which provide a relatively easy cleavage path over considerable distances [French 1998], can also be susceptible to hydrogen cracking.

In general, large grain size with low angle grain boundaries offer the lowest resistance to cleavage crack propagation [Nakamura and Furubayashi 1990]. On the other hand, small

grains and high angle grain boundaries require high energy for cleavage since cracks must frequently change direction [French 1998 and Davidson et al. 1996].

As cooling proceeds the first ferrite nucleates at the prior austenite grain boundaries to form grain boundary ferrite PF(G). Being on the grain boundaries, this potentially offers an easy cleavage path depending, of course, on the orientation of the boundaries and the grain size. Therefore, PF(G) is considered to be deleterious to cleavage fracture initiation and propagation, and has been implicated as a contributing factor in hydrogen induced intergranular fracture [Davidson et al. 1996; and Wang and Apps 1991]. PF(G) is reported to be more susceptible to cracking than AF [Wildash et al. 2000 and Alam et al. 1997].

Acicular ferrite forming within the austenite grains, and consisting of fine interlocking lathes of ferrite separated by high angle boundaries, is generally characterized by higher toughness than other as-deposited constituents [French 1998]. Acicular ferrite laths are known to nucleate on intragranular inclusions, such titanium monoxide (TiO) and galaxite ($MnO\text{-}Al_2O_3$) [Liu 1992]. As a result, AF offers higher resistance to hydrogen crack propagation than PF(G) [Wildash et al. 1999]. AF is most resistant to hydrogen cracking when it is in the form of finely dispersed acicular ferrite. Such fine AF is promoted by fluoride-basic type agglomerated flux [Pokhodnya 1996]. Although AF is generally regarded as a desirable, fracture-resistant microstructure, the non-metallic inclusions which contribute to its formation [Abson 1989], can act as sites for void creation by local plastic yielding in the presence of a high hydrogen concentration and high stress intensity [Alam et al. 1997].

Heat input influences the proportion of intra-granularly nucleated components [French and Bosworth 1997]. By increasing the heat input from 1.1 $kJmm^{-1}$ to 2.6 $kJmm^{-1}$, AF has been

shown to decrease markedly, with an associated increase in the propagation of PF(I), PF(G) and Widmanstätten ferrite side plates FS. Therefore, an increase of cooling rates suppress the content of coarse-grained PF(G) and promote the formation of AF. The proportion of each constituent contained within the weld metal microstructure is usually assessed quantitatively by optical microscopy. However, computational modelling based on thermophysical data, welding parameters and chemical composition of metal can also be used to determine the relative amounts of microstructural constituents, such as PF(G), AF and FS(SP) via derived phase diagrams and CTT curves [Mundra et al. 1997]. The calculated volumes of microstructures from such modeling, compared with the experimental results, showed very good correlation.

Weld metal microstructure is markedly affected by alloy components, such as C, Mn, Cr, Mo or Ni promote fine proeutectoid ferrite [Evan 1989]. However, an increased content of sulfur in the form of manganese sulfite inclusions, playing the role of hydrogen sinks, has been shown to result in an increased amount of hydrogen cracks in weld metal [Thibau and Bala 1983]. As expected, carbon and hydrogen were both found to enhance the nucleation stages of cracking. The control of oxygen uptake affects the content and density of oxide inclusions at prior austenite grain boundaries [Shinozaki et al. 1990] and also plays a significant role in formation of AF [Wegrzyn 1992]. For gas shielded FCAW ferritic weld deposits, the oxygen levels are also affected by the shielding gas composition [Tyagi et al. 1996], where mixed shielded gases Ar-CO_2 have lower potential to oxidize weld metal than CO_2 as discussed in Chapter 4.4.6. Further, basic flux systems for consumables give a lower oxygen content in weld metal than rutile consumables. CO_2 gas also produces lower weld metal oxygen and

therefore lower volume fractions of inclusions are to be expected [Kuwana and Sato 1990, French 1998; Powell and Herfurth 1998].

Reduction of oxygen in weld metal results in a lower content of non-metallic inclusions [Wildash et al. 2000], whereas higher oxygen contents usually lead to more and larger inclusions, therefore promoting crack initiation by cleavage fracture [Hughes and Ritter 1995]. Inclusion sizes over 1 mm in diameter were described as initiators of cleavage fracture [French 1998]. The introduction of a small concentration of Ti (0.005 %) produces relatively small inclusions of size <0.4 mm diameter, and this can promote formation of AF and therefore enhance cleavage fracture resistance [French 1998]. Titanium addition enhances the formation of acicular ferrite and weld metal notch toughness [Evans 1995 and Koseki et al. 1997].

Increased alloy content and low levels of oxygen content in weld metal may shift or delay the γ-Fe $\rightarrow$ α-Fe transformation down and to the right, as shown in Figure 3. 22. This can result in a further increase of fine-grained ferrite in the weld metal.
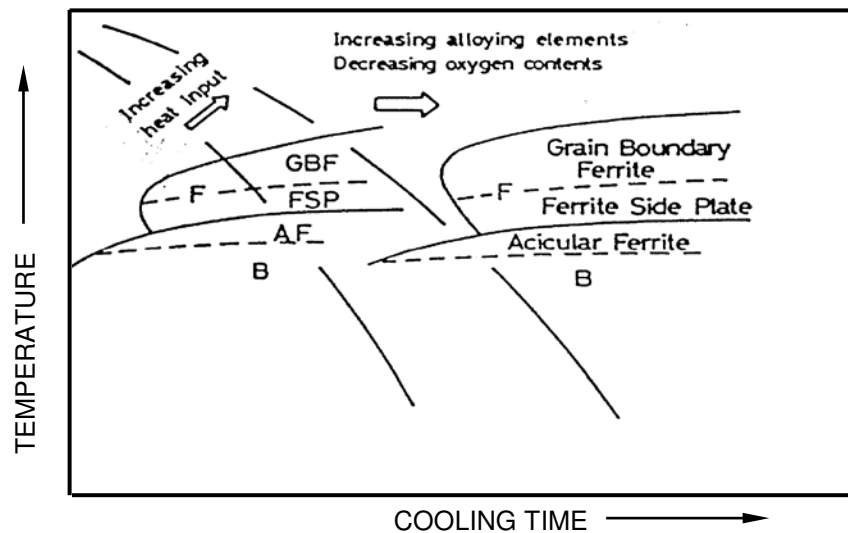
Figure 3. 22   Weld metal CTT diagram showing the effect of increasing alloy content and decreasing oxygen content (after Komizo and Fukuda).

In contrast with the single pass weld, multi-pass welds also consist of regions of as-deposited and reheated regions for a given weld joint. In the case of multi-pass welds, re-heated weld zones can be divided into coarse and fine-grained zones. The coarse zones are situated close to the new weld deposit due to re-austenitizing and grain growth of γ-Fe. This also effects the hydrogen diffusion rates during the welding regime (cooling or re-heating) [Pussegoda et al. 1997].

The resistance to cleavage fracture in multi-pass deposits can be similar or higher than that exhibited by as-deposited weld. The tempered fine-grained zones are highly resistant to cleavage fracture [Wang and Apps 1991, French and Bosworth 1997 and French 1998], but not immune to the effects of hydrogen embrittlement [Lee and Kang 1997].

Large individual weld deposits in multi-pass welds can reduce the tempering effects that result from subsequent weld passes [Kiefer 1995]. Unrecrystalised regions of weld metal, which contain coarse proeutectoid ferrite "veins" along the columnar grain boundaries, are known to possess low fracture toughness and can act as initiation sites [Barbaro 1999] and/or crack propagation paths [Thibau and Bala 1983] for transverse hydrogen cracking. A typical example of hydrogen crack in C-Mn steel weld deposit, following large grain boundary ferrite is shown in Figure 3. 23.

Large columnar austenitic grains will result in enhanced grain boundary segregation, particularly of S and P which are known to cause embrittlement resulting in weld metal cracking preferably within grain boundary ferrite veins [Alam et al. 1997 and Hoffmeister et al. 1987]. However, for high restraint conditions cracks will tend to propagate across the grains rather than following the grain boundary structures [Lee and Kang 1997].
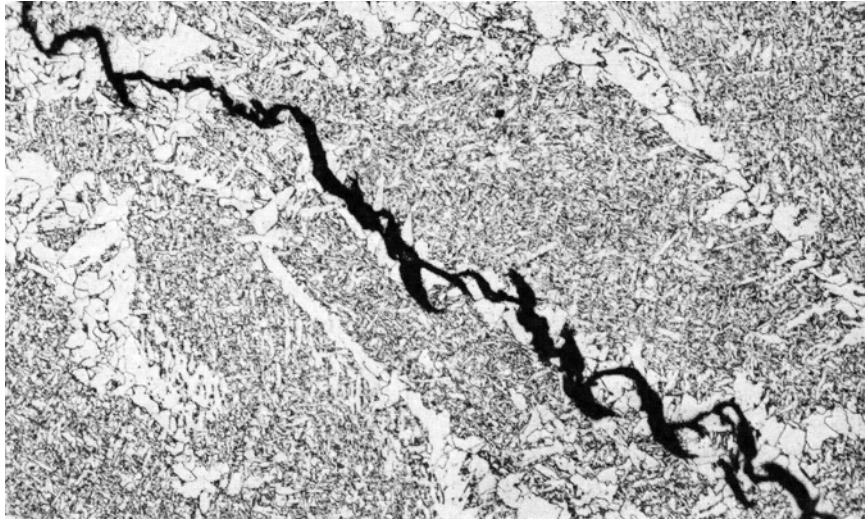
Figure 3. 23　　　Micrograph showing weld metal microstructure of a C-Mn steel deposited using SAW with high heat input of 5 kJ/mm. Note the hydrogen crack running along the prior austenite grain boundaries (after Pargeter 1992).

In general, weld metal mechanical properties of rutile flux-cored wires cannot match the basic flux-cored weld metal properties, particularly with respect to low temperature impact properties. This is due to their rutile slag system which gives relatively high weld metal oxygen levels, and results in a significant increase of large non-metallic inclusions in the weld metal [French 1998]. This lowers the cleavage resistance and promotes susceptibility to hydrogen cracking.

In the current work, the focus was to study the effects of welding parameters on levels diffusible hydrogen in rutile flux-cored weld deposits, as obtained from the G-BOP testing. G-BOP test samples were produced under different welding parameters for two low strength rutile E71 T-1 seamless and seamed wires with nominal weld metal hydrogen levels of 5 and 10 ml/100g, respectively.

3.5 EFFECT OF WALL THICKNESS

When steel is welded the parent metal adjacent to the deposited weld metal is heated rapidly to high temperatures approaching the melting point and rapidly cooled by heat transfer into the parent steel. This thermal cycle consists from three stages, such as heating time, maximum temperature, Tmax, and cooling rate, as shown in Figure 3. 24 [Hrivňák 1992]. The rate of cooling depends on the section thickness, the preheat temperature and the heat input from the welding process.
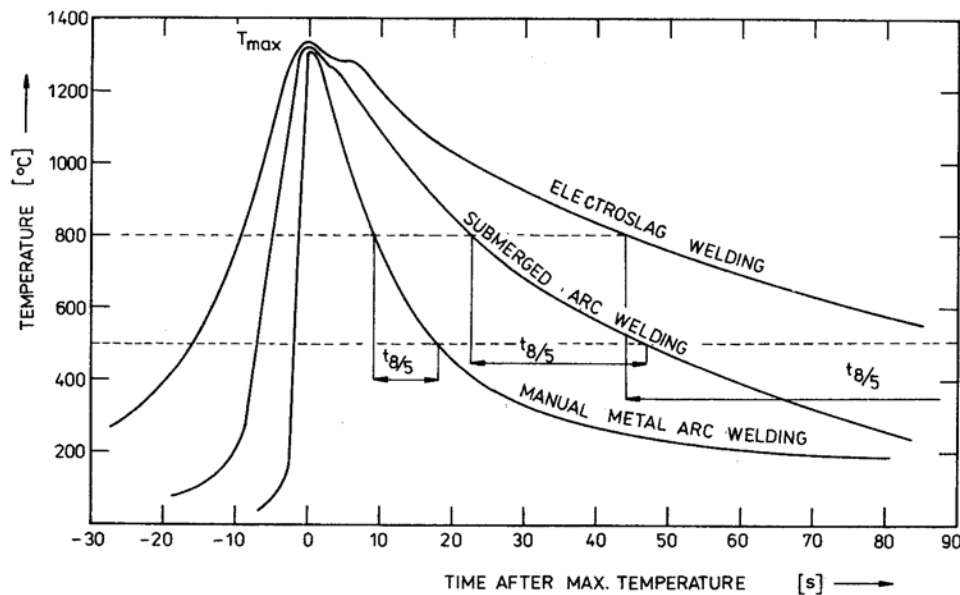
Figure 3. 24   Graph showing typical shapes of thermal cycles resulting from various welding methods (after Hrivňák 1992).

Cooling times, $t_{8/5,}$ measured between 800 °C and 500°C, increase with the use of welding processes that generate higher heat input. This results in variation in weld metal microstructure and hydrogen levels.

Since any welded joint consists of two or more connecting plates it is the combined thickness, which determines the weld metal cooling rates. The combined thickness is defined as a sum of thickness of plate being joined by weld. The carbon equivalent, selected welding process/consumable and combined thickness, can be used in a predictive system to give a minimum preheat and inter-pass temperature required for avoidance of HACC in HAZ [AS/NZS 1554.1-2000]. When welding large wall thickness without preheat, high cooling rates are expected and this can result in increased risk of HACC by promoting the formation of harder, and therefore more susceptible microstructures, and reducing the effusion of hydrogen from the weld metal. Figure 3. 25 shows hydrogen effusion of hydrogen from various plate thickness at different temperatures.
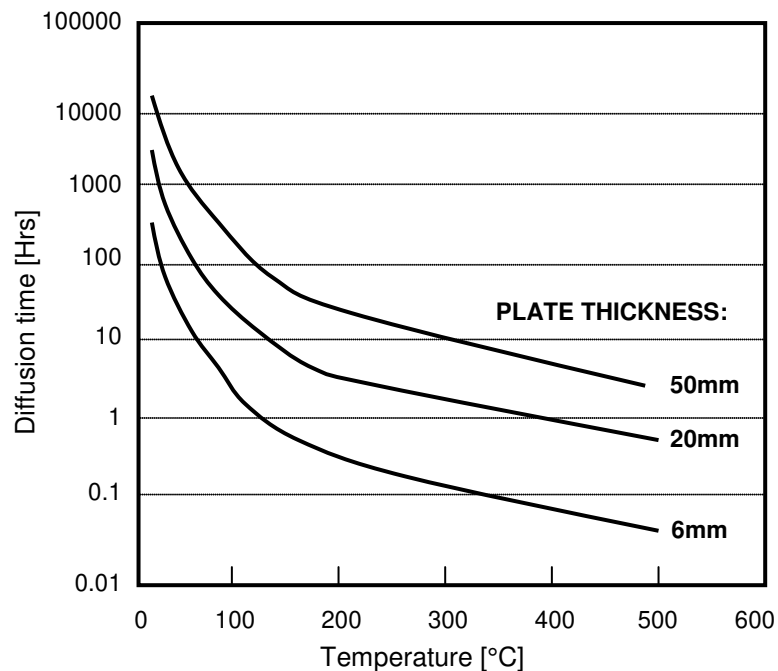
Figure 3. 25   Graph showing the relationship between hydrogen effusion and temperature at different plate thicknesses (after Ito and Bessyo 1968).

From the relationship between temperature and diffusion time it is apparent that hydrogen can slowly diffuse out of a weldment at ambient temperature, and hence reduce the risk of HACC. However, particularly when welding large wall thicknesses, this process can take several days. During this time, residual stresses can result in cracking well before the trapped hydrogen will diffuse out of the welded joint.

When welding large wall thicknesses, especially in a self-restrained conditions such as full penetration 'T' butt welds and weld repairs, consideration should be given to increasing the preheat temperature to minimize occurrences of HACC. Quantitative allowance for three levels of restraint intensity is provided in ANSI/AWS D1.1-2000, Table XI-1,2 for a given susceptibility index grouping as a function of hydrogen levels, composition parameter (Pcm) and plate thickness.

The current welding standards agree in principle to allowing an increase of plate thickness from the test plate to the actual plate. For example, AS/NZS 3992-1998 for welding procedure and personnel qualification allows for the actual plate thickness to be double that of qualifying weld. For an example, the standards used to approve welding procedures may allow the welding tests on 25 mm thick plate and permit welding up 50 mm. However, this may not prevent cracking of the thicker joints [Gregory 1991]. This underlines the importance of making the welding procedure qualification test realistic, so that conditions of restraint match those in the component to be welded. Although this may be a costly exercise, it is nevertheless a valuable one, particularly when welding large wall thicknesses (>50 mm) and for repair welding.

In the case of structural welding, AS/NZS 1554.1-2000 appears to be more conservative, allowing only an increase of 1.5 times from the qualification test plate thickness. However, no upper limit of plate thickness is specified for butt joint welding with welded plate thickness over 36 mm.

AWS D1.1-2000 for structural welding has a combination of allowing double the actual plate/pipe thickness from the nominal thickness, and specifies unlimited restriction of actual thickness when the welded test plate is ≥ 1 inch (25.4 mm).

An option for avoiding welding thick plates during the welding procedure qualification is often an appealing option for the fabricator. However, one must not neglect or underestimate the risk of cracking in the weld metal, especially when there is increasing evidence that hydrogen cracking in thick sections is a significant problem and yet not sufficiently addressed in current welding standards.

In the case of welding thicker sections, where multiple weld deposits are required, hydrogen concentration builds up in successive layers of a multi-pass weld. After a weld pass is deposited, hydrogen continuously diffuses out from the weld. When another weld pass is deposited over the first pass, the temperature in the first pass is immediately increased thereby assisting hydrogen diffusion from the weldment as well as introducing more hydrogen from the last pass. However, the diffusion distance to the surface of the weld is increased further with each weld pass and the complete removal of hydrogen from the first deposit is less likely due to the greater thickness through which it must diffuse. As further weld passes are made, they are effectively increasing the distance for the effusion resulting in hydrogen enriched regions within the weld body. Increasing and maintaining preheat and inter-pass temperatures,

with increased time between each pass, will result in more extensive removal of hydrogen. However, where high levels of productivity are required, control of these factors is often seen as a costly and avoidable procedure.

There is a minimum plate thickness required for the commencement of transverse cracking [Barbaro 1999]. The weld metal cold cracking risk is progressively decreased with weld thickness reduction and become insignificant below 10 mm, regardless of weld metal strength and hydrogen content [Nevasmaa 2003]. In another work, a gradual weld thickness decrease from 50 mm down to 20 mm, resulted in a decrease the amount of transverse weld metal cracking until no cracking was evident in the 20 mm thick weld [Kuebler et al. 2000].

A number of research projects have recently been conducted to examine the presence of hydrogen cracking in thick multi-layer deposits. The extent of cracking initiated from artificial defects was examined using MMAW and SAW high strength low alloy multi layer welds on 'T' butt joints using 20x35 mm thick plates [Ritchburn et al. 2000]. Other work [Lee and Kang 1997] studied the effects of welding parameters on fully restrained 'V' butt welds of 50 mm thick plate, made from a low strength material (EH36) using the SAW process. This work revealed sub-surface transverse hydrogen cracks in the weld metal, detected in the upper part of the deposit at a constant depth from the top of weld surface [Lee and Kang 1997].

Similar results were obtained on fully restrained 'V' butt welds of 50 mm thick plate using the FCAW consumable E80T1-K2 [Lee et al. 1998]. In this case, transverse cracks were detected for <30 °C preheat and inter-pass temperature, but no cracks appeared where a preheat of 100-120 °C was employed. All cracks were sub-surface, at various depths between 9.0-27.0 mm away from the weld surface. Another study using 50 mm thick high strength EN 10113-1993

Gr.420ML steel and three flux cored wires (containing 10 ml/100g of diffusible hydrogen), found that HACC was confined to the weld metal for preheat and inter-pass temperatures of 70 °C [Kinsey 1998]. However, no cracking was observed for conditions with higher preheat temperature and/or lower hydrogen levels in the weld metal. The combination of diffusible hydrogen and high longitudinal stresses, resulted in transverse hydrogen cracking in a 50 mm thick plate welded with high strength basic and rutile flux cored wires [Kuebler et al. 2000]. In a study of crack distribution, welded samples were progressively machined by milling through the 50 mm thickness in 1 mm steps beginning at the top surface. Each newly machined weld surface was examined for cracking by magnetic particle inspection. The location, length and crack density, defined as a number of cracks per each weld metal surface varying through the depth was recorded. The hydrogen distributions measured through a 50 mm thick weld [Takahashi et al. 1979 and Kasuaya et al. 2001] were closely corresponding to hydrogen crack density distribution plotted by Kuebler et al. (2000) and shown in Figure 3. 26.
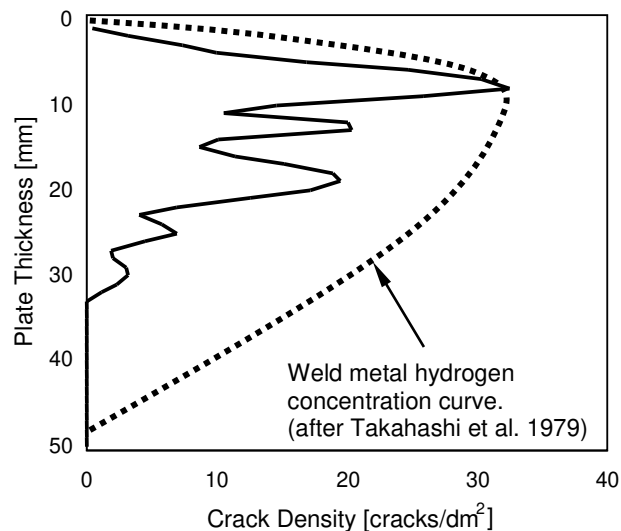
Figure 3. 26   A plot of crack density in the weld metal through a 50 mm thick plate (X-Y plane) at preheat and inter-pass temperature of 140 °C / 140 °C (after Kuebler et al. 2000).

When examining the crack location in longitudinal and transverse directions, the cracking appeared to be non-uniformly distributed. However, as shown in Figure 3. 27, many of the transverse cracks appeared to be aligned with individual weld passes. This observation was thought to support the theory that a multi-pass weld consists of weld regions experiencing different thermal cycles, resulting in different elapsed times between the weld passes and a variation of cooling rates.
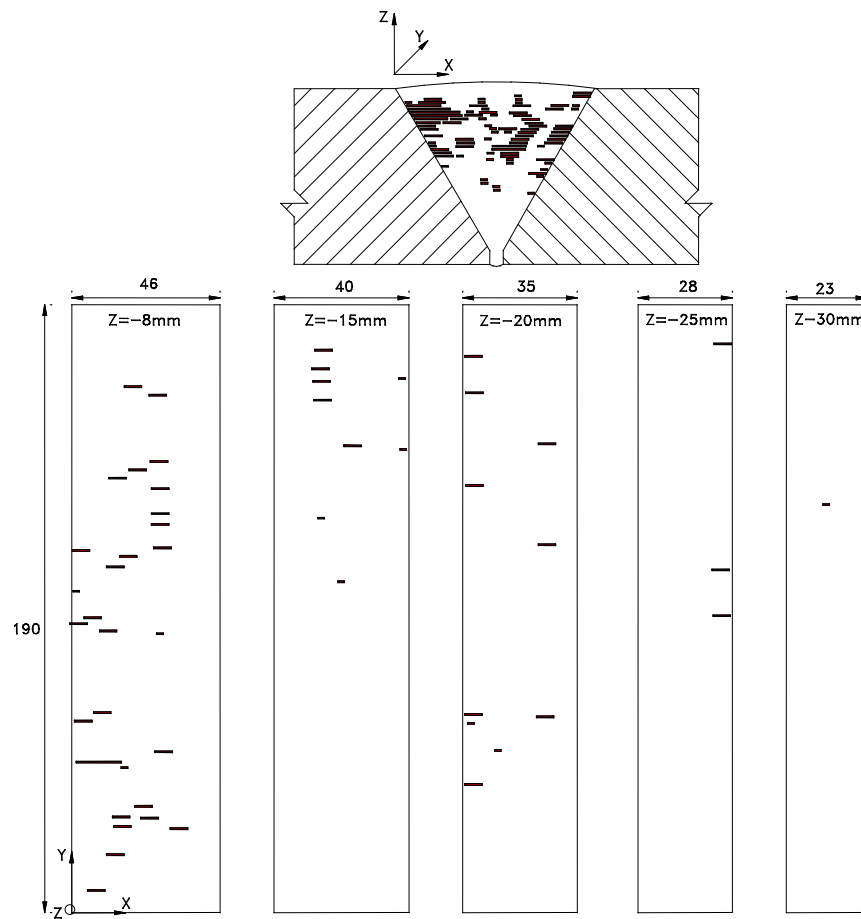
Figure 3. 27   Schematic illustration of transverse crack distribution in weld metal at various depths (8, 15, 20 and 25 mm), as shown in plane view Y-X. The smaller diagram above represents crack indications translated to the weld cross-section in Z-X plane (after Kuebler et al. 2000).   [not to scale]

Transverse weld metal cracking was also found after welding of 50 mm thick HSLA weldments fabricated by GMAW, a process known for generating very low levels of diffusible hydrogen [DeLoach et al. 1999]. In this work the hydrogen was measured to be 3.5 ml/100g at a nominal heat input of 1.2 kJmm^{-1} and a 15 °C preheat and inter-pass temperature.

In summary, low heat input and low preheat and inter-pass temperatures significantly increase the weld cooling rates, thereby reducing the time for removal of hydrogen from the weld by diffusion mechanism. A combination of local hydrogen concentration and high residual stresses through large wall thicknesses increase , the risk of weld metal HACC, particularly where if susceptible weld metal microstructures are present.

3.6   ASSESSMENT OF HACC SUSCEPTIBILITY

3.6.1   Weldability Tests

The first test methods for cold cracking emerged in the 1940s [Reeve 1940], when the formation of martensite in the HAZ was the main cause of cracking. Following World War II, the progressive development of hydrogen induced cracking tests for a range of weld configurations and applications continued. These tests became gradually more sophisticated and some were designed specifically for the investigation of the mechanism of hydrogen assisted cold cracking and for the proper selection of welding materials and welding conditions to avoid HACC during welding fabrication.

Where a test method has been developed for a specific application, careful consideration should be given to its validity with respect to other applications. Historically, the most of the

methods were designed to simulate some particular application in which cracking was experienced. The main objective of weldability tests is to examine the effects of various factors on cracking susceptibility, including parent metal composition, type of welding consumable, preheat temperature and other welding conditions.

The basic idea of all testing methods is to obtain a reliable and representative indication of crack susceptibility in relation to a defined set of test criteria. Cold cracking tests are used to:

a) examine sensitivity to welding variables and other surrounding conditions that effect hydrogen cracking,

b) examine the relationship between welding consumable and parent metal,

c) provide a preliminary examination of the cracking mechanism, and

d) establish welding conditions that avoid or minimize hydrogen cracking for a particular given combination of welding process, consumable and parent metal.

In view of the crack location, testing methods for susceptibility to HACC are divided into two groups, those that study HACC in HAZ or weld metal. Although the earlier tests were developed primarily to measure susceptibility to HAZ cracking, several tests have been designed specifically for weld metal cracking, or both as shown in Table 3. 2.

Table 3. 2   A listing of the various testing methods for determining hydrogen cracking in parent metal HAZ and weld metal.

TEST	Mode of Cracking Imposed		Weld Pass	Reference:
	HAZ	Weld Metal		
Reeve restraint cracking	x		S	Reeve (1940)
Non-restraint fillet	x		S	Tanaka et al. (1972)
Tekken (Y groove)	x		S	Kihara et al. (1962)
Controlled thermal severity (CTS)	x		S	Cottrell (1953)
Implant	x		S	Granjon (1969)
Tensile restraint cracking (TRC)	x		S	Suzuki et al. (1964)
Longitudinal bead - tensile restraint (LB-TRC)		x	S	Matsuda et al. (1979)
Longitudinal restraint cracking		x	S	Wang et al. (1991)
Lehigh (U groove) restraint cracking	x	x	S	Stout et al. (1946)
Lehigh (slot grove) restraint cracking	x	x	S	Vasudevan et al. (1981)
Welding Institute of Canada (WIC)	x	x	S	Pick et al. (1982)
Rigid restraint cracking (RRC)	x		S/M	Satoh (1968)
H slit restraint cracking	x		S/M	Watanabe et al. (1962)
Gapped bead on plate (G-BOP)		x	S/M	McParlan et al. (1976)
Cruciform	x		M	Horikawa et al. (1976)
Cranfield	x		M	Jubb et al. (1969)
V groove weld		x	M	Okuda et al. (1987)
Circular patch (BWRA)	x	x	M	Caplan et al. (1976)

Notes:
S = single
M = multiple

The majority of these test were designed predominantly as small scale laboratory tests, using a single weld pass. Other, more expensive weldability tests were designed for multi-pass welds that consider the interacting effects of thermal cycles, changes of thermal stresses and increase in restraint associated with welding progression through the plate thickness. A number of

studies have comprehensively reviewed the most commonly used weldability testing methods, which are widely utilized for both HAZ and weld metal susceptibility to cold cracking [Yurioka and Suzuki 1990, Davidson 1995 and Graville 1995, Hoffmeister and Matthiä 1990].

Although one can appreciate the fundamental differences between the testing methods, particularly in view of the different levels of restraint imposed, a number of cracking tests have proven to be the most reliable, including the Lehigh, CTS, G-BOP, Implant and Tekken tests. A number of these tests have been accepted internationally in American [API 4009-1977], British [BS7363-1990], French [NF A89-100-1991] and Japanese [JIS Z3158-1996] standards.

3.6.2   Gap Bead-On-Plate Test (G-BOP)

Often transverse cracking can occur when welding over a small gap that acts as a stress concentrator. It is usually associated with poor fit up in highly restraint joints that can lead to hydrogen transverse cracking.

A typical example of a gap initiating HACC is shown in Figure 3. 28, where a severe transverse crack had initiated in the un-fused land between the run-off plate attached to a 50 mm thick plate [Kuebler et al. 2000]. This crack appeared after 5 days of completion of welding and was therefore recognized as HACC, similar to those cracks in position 2 (after 5 days) and in position 3 (after 34 days).
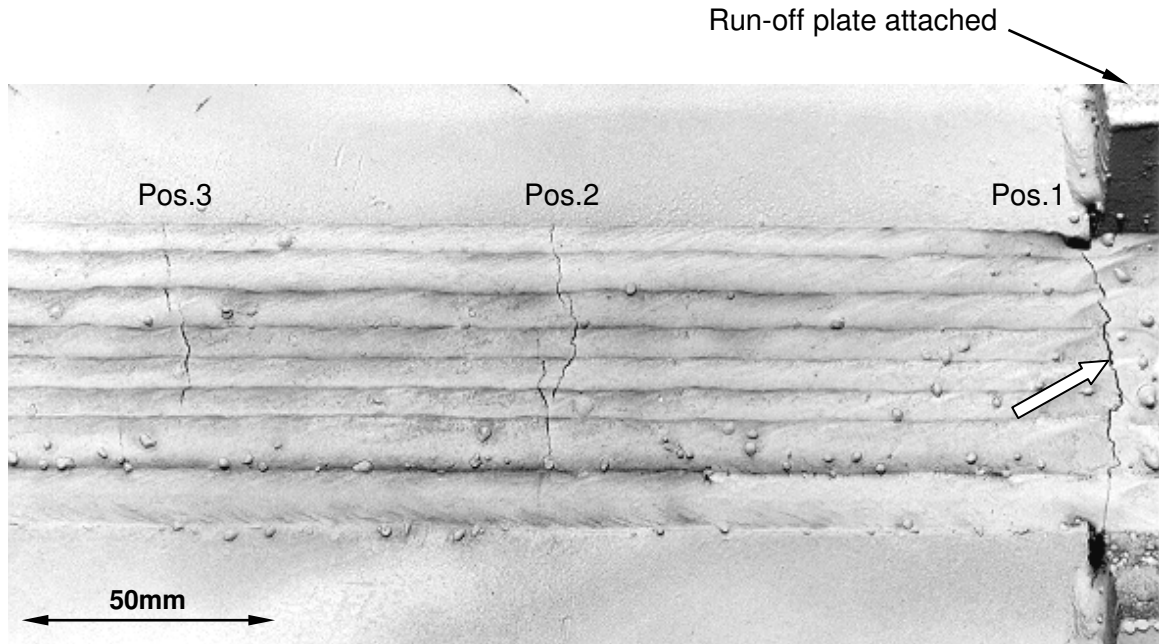
Figure 3. 28   Photograph of typical transverse cracking in weld metal. Note position 1, where the hydrogen crack (arrowed) had initiated at the unfused land between run-off and 50 mm thick plate (after Kuebler et al. 2000).

In the early 1960s, The Brown-Boveri test was introduced to examine cracking sensitivity. The test sample consisted of several machined thick plates bolted together, initially designed for austenitic stainless steels, but later applied to other materials [Séférian 1962]. During the early 1970s, Makara (1971) at E.O. Paton Welding Institute designed a test piece with an artificial notch that enabled initiation of a cold crack in a transverse direction to the weld. Following this concept, the effect of a self-restraint gaped bead-on-plate test (G-BOP) was later established by Graville and McParlan (1974), in which a gap underneath the weld introduces a large stress concentration assisting initiation of transverse weld metal cracking.

This early work, conducted by applying various levels of preheat temperature, proved that this test was suitable for the determination of cold cracking susceptibility. The results showed that

by increasing preheat temperature, cracking was gradually suppressed, presumably due to extended time for diffusion of hydrogen out of the weld at higher preheat temperatures. The mechanism of cold cracking was also confirmed by use of the G-BOP of test through measurement of the stress level variation across the gap. This work illustrated the typical delay characteristics of cold cracking over time [Graville and McParlan 1974].

The test sample consists of two 50 mm thick steel blocks, one of which has a machined 0.75 mm deep recess. The blocks are clamped together to prevent any relative movement and a bead is deposited along the top surface over the gap as shown in Figure 3. 29.
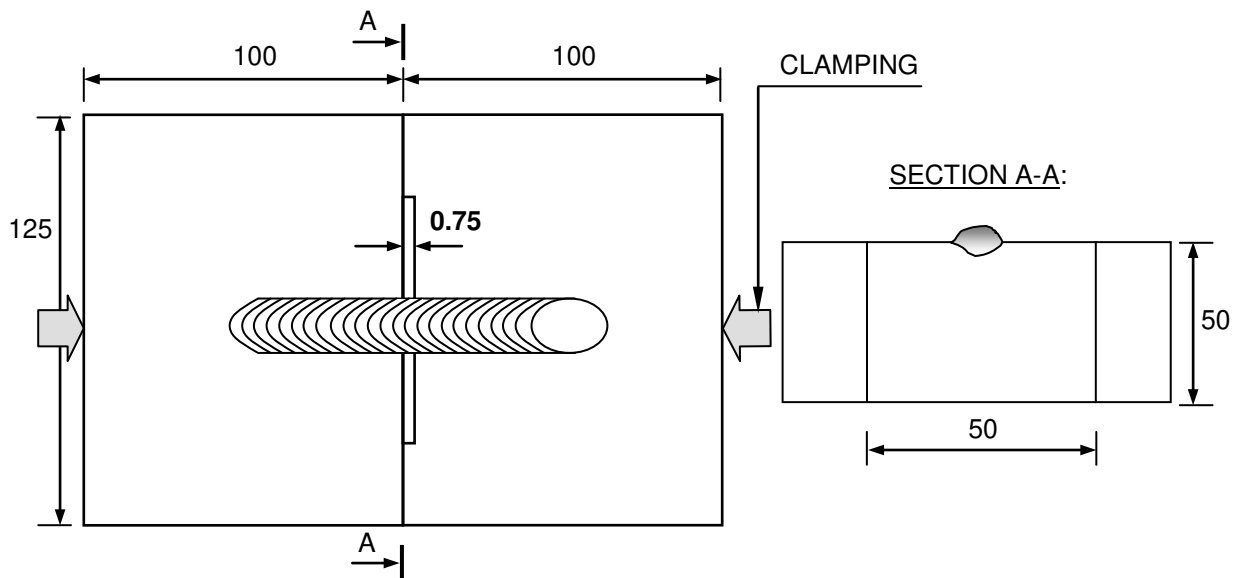
Figure 3. 29   A diagram of the G-BOP test configuration (after Graville and McParlan 1974). Note: all dimensions in millimeters.   [not to scale]

After welding, the blocks are left in clamps for a minimum of 48 hours to provide necessary restraint and to allow hydrogen cracking to develop. The welds are then heated to a dull red heat in the vicinity of the gap to allow heat tinting of the fracture surfaces. The samples are the

allowed to cool to room temperature and are then broken open revealing the fracture surfaces in weld [Graville and McParlan 1974]. Any cracks that developed in the weld metal during the dwell time of 48 hours are heat tinted, revealing a dark blue or gray discoloration of the fracture surface. Any non-cracked weld metal cross-section reveals a fresh fracture appearance characterized by a fresh light gray colour.

Several researchers later modified the test, as summarized in Table 3. 3. These modifications predominantly included variations of test block dimensions, incubation periods, clamping forces and releasing of clamps.

Table 3. 3   A listing of G-BOP testing parameters used in various studies.

	Graville et al. (1974)	McParlan et al. (1976)	Chakravarti et al. (1989)	Hart (1989)	Graville et al. (1995)	Atkins et al. (2002)
Test sample size (W x L x T) [mm]	125x100x50	125x100x50	115x115x61	125x100x50	125x125x50	100x100x50
Incubation period [hrs]	>48	24	24 + 24♣	>20	>24	>48
Clamping force/torque	♠	♠	10.3Nmm^{-2}	57Nm	♠	Torque♠
Clamp release	Unk.	Prior heating	Prior heating	After heating	Prior heating	Prior heating
Testing block	As received	As received	As received	Buttered	As received	As received

Notes:

♣ Additional time allowed after removal of clamps.

♠ Not specified.

The effect of weld metal dilution on the G-BOP test was studied by Hart (1986), through the buttering of test plates, as shown in Figure 3. 30. This modification is particularly applicable for cracking assessment of low alloy multi-pass welds.
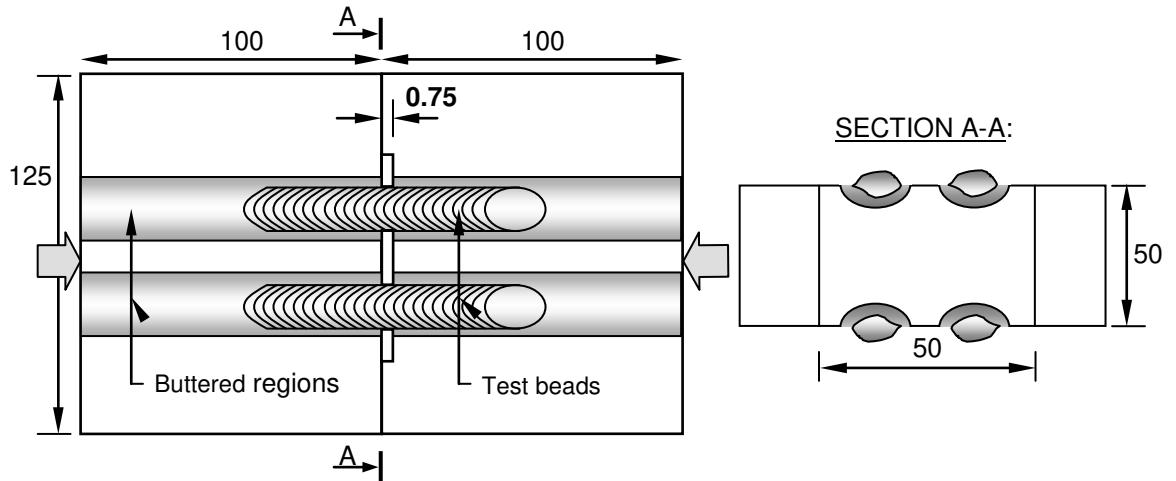
Figure 3. 30   A schematic illustration of a modified G-BOP test using buttering prior to the actual test welds (after Hart 1986). Note: all dimensions in millimeters.

Further modification of the testing procedure allowed rotation of blocks to deposit 4 weld beads, or eight of welded on both sides as shown in Figure 3. 31 [Graville et al. 1995].
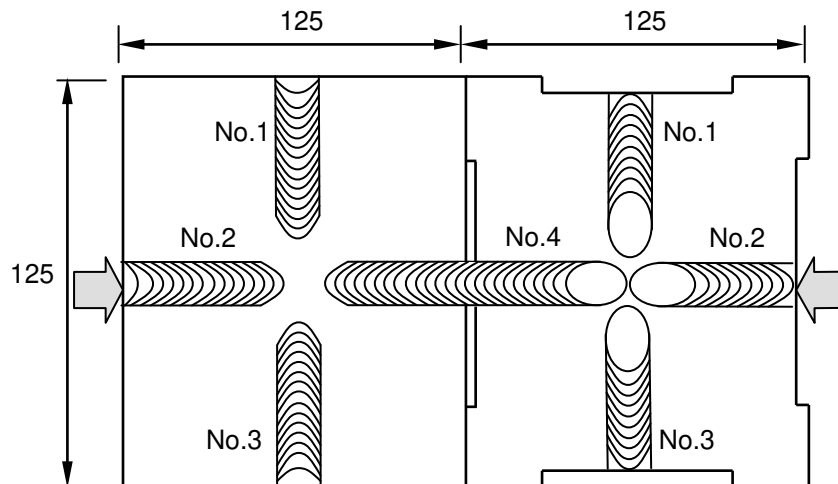
Figure 3. 31   An illustration of the current G-BOP test block designed that allows four weld beads to be deposited on each test block (after Graville et al. 1995). Note: all dimensions in millimeters.   [not to scale]

The incubation period originally proposed by Graville and McParlan (1974) of >48 hours has also been modified. Different incubation periods in testing procedures varied from a minimum of 20 hours to over 48 hours, with the most common being ≥24 hours period. Considering that transverse cracking was observed to occur within a few hours after welding, as shown in Figure 3. 32, the incubation period of 24 hour was generally found to acceptable for this test by all research studies carried out to date.
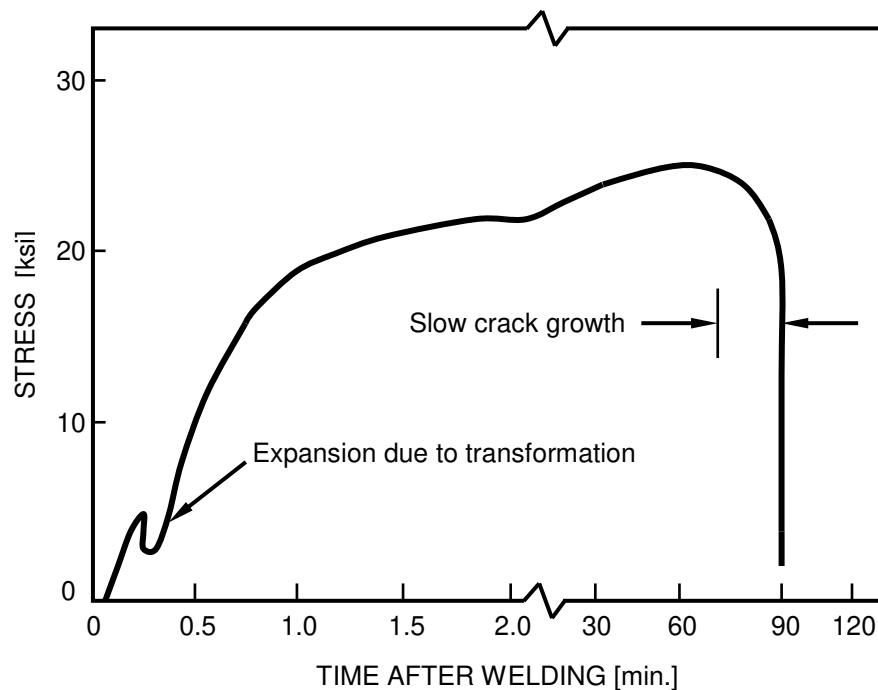
Figure 3. 32   Graph showing the typical development of stress in a G-BOP test, showing the time of crack initiation and growth (after Graville et al. 1974).

As discussed earlier in this Chapter 2, the transformation temperatures from austenite to ferrite/martensite is also accompanied with thermal stress changes [McParlan et al. 1976]. A typical temperature versus stress curve recorded on an instrumented G-BOP test block is shown in Figure 3. 33.
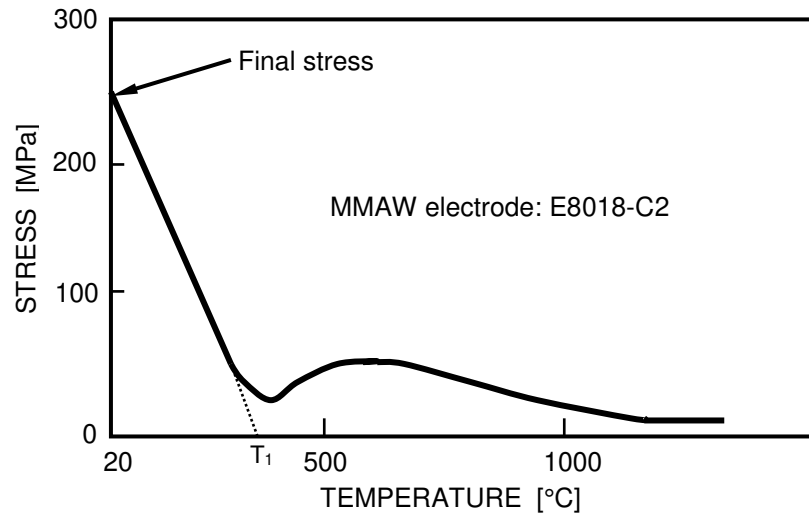
Figure 3. 33   Graph showing typical longitudinal stress evolution against cooling temperature in a G-BOP test weld (after McParlan et al. 1976).

As previously discussed, an increase of preheat temperature will result in a decrease in the weld metal cooling rate. A typical curve of cooling rate for G-BOP test is shown in Figure 3. 34.
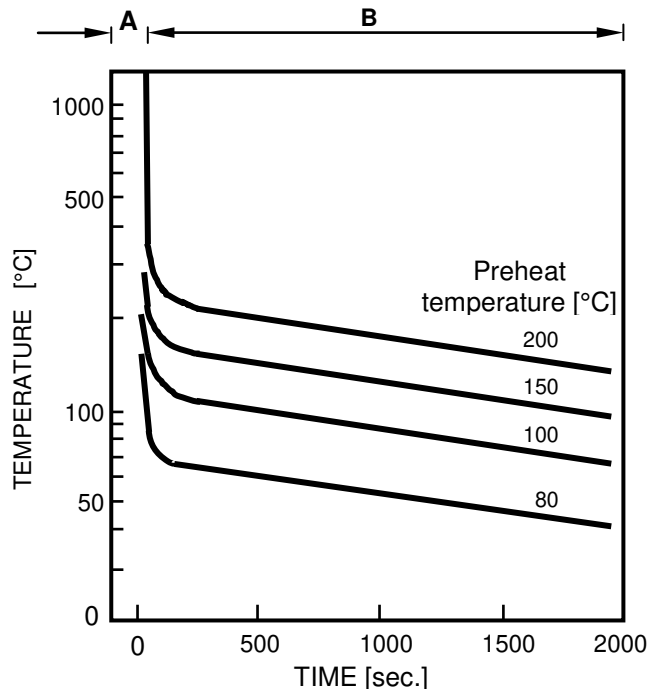
Figure 3. 34   Graph showing typical cooling curves for G-BOP test welds at various preheat temperatures and at energy heat input of all test bead of about 1 kJ/mm (after McParlan et al. 1976).

It can be defined as having two stages [McParlan et al. 1976]; Stage 'A', where the weld metal cools rapidly within the first few minutes to a temperature close to the preheat temperature of the test block, and Stage 'B' where the rate of cooling reduces and is driven toward ambient temperature by radiation heat loss of the G-BOP test blocks. This demonstrates that the G-BOP test block is large enough to disregard the heat intake by the weld.

Cooling rates of weld deposits are defined by the time taken to cool across a given temperature range, for a given application. The temperature range 800 to 500 °C is widely used for the study of microstructural changes and transformational effects. The range 300 to 100 °C is more commonly used for the study of HACC when considering the effusion of hydrogen down to 100 °C. A comparison of typical cooling times between $t_{8/5}$ and $t_{3/1}$ is shown in Figure 3. 35.
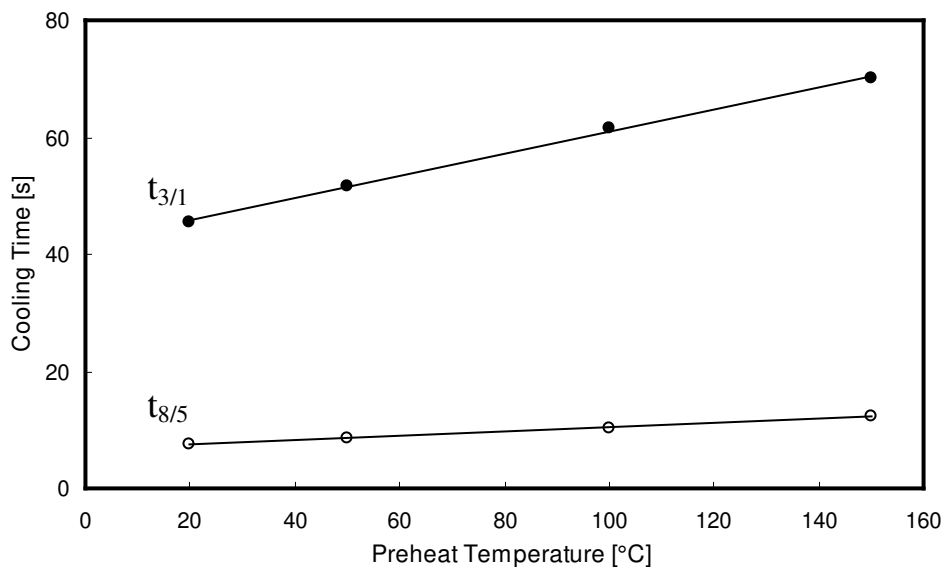
Figure 3. 35   Graph showing the relationship between cooling times $t_{3/1}$ and $t_{8/5}$ at different preheat levels, as measured from G-BOP tests (after Chakravarti et al. 1989).

As mentioned previously, two blocks are clamped together to prevent relative movement. The magnitude of the clamping force used to constrain the test sample parts was also found to vary across the previous studies. No reference to clamping force is given in the early test developmental work [Graville et al. 1974 and McParlan et al. 1976] and in recent studies by Graville et al. (1995), it is claimed that the clamping force is insignificant with respect to the testing procedure. Other studies have used a pneumatic clamp with measurable clamping force [Chakravarti et al. 1989] and/or torque [Hart 1989] to tighten a holding clamp to 10.3 Nmm^{-2} and 57 Nm, respectively. These studies have not indicated any error due to the different clamping forces used. However, considering that all of these studies were carried out using different welding conditions, consumables and materials, it is not possible to make definitive conclusions regarding the effect of clamping force.

The G-BOP test method is primarily used to assess the welding consumable susceptibility to cold cracking [Graville et al. 1974]. However, this test can also be applied to the study of the effects of weld metal hardness in relation to HACC [Graville et al. 1995]. Multiple purpose application of the G-BOP was also demonstrated through a study of parent metal dilution in a weld metal examining different degree of dilutions defined by WTIA TN 16 and DuPONT et al. (1995). Lazor and Graville (1983) investigated the effects of alloying elements and confirmed the susceptibility to weld metal transverse cracking using a series of parent metals ranging from carbon to low alloy steels. In order to minimize the dilution effects, a modified G-BOP test enable the study of the effects of weld metal composition without influence of dilution with parent metal. This is done by pre-fabrication of buttered G-BOP test samples, particular applicable for study of hydrogen cracking in alloyed and multi-pass weld deposits [Hart 1989].

The G-BOP test defines the percentage of cracking at room temperature, or at preheat temperatures above 20 °C. This parameter is known as room temperature cracking (RTC). However, in the case of high consumables containing higher levels of diffusible hydrogen, usually represented by 100 % RTC, this parameter is inadequate [Hart 1989]. Therefore, a parameter known as 10 % crack preheat temperature (10 % CPT), defined as the preheat temperature required to limit cracking to ≤10 %, was found to be more applicable [Hart 1989 and Chakravarti et al. 1989]. This parameter may be useful where two consumables containing a similar amount of diffusible hydrogen in their weld deposits may exhibit 100 % RTC, but may have different responsiveness to an increase in preheat temperature, resulting in 10 % CPT at two different preheat temperatures. Another useful parameter is the critical preheat temperature (CPT), at which cracking percentage is expected to be <5 % using extrapolation [Graville et al. 1995].

The G-BOP test was initially designed to examine transverse hydrogen cracking in weld metal affected by variation of preheat temperature in the restrained condition. One advantage of using preheat as an essential variable is its main influence on the level of hydrogen retained at low temperatures. The G-BOP test was found to be a quick and inexpensive 'go' or 'no-go' comparative method to compare consumables with respect to susceptibility to cold cracking, since the test can be readily conducted without sophisticated metallographic facilities [Graville 1986].

The standard procedure can be enhanced by an instrumented G-BOP test. This can be achieved by recording temperature history and cooling rates, ($t_{3/1}$ or $t_{8/5}$) using Pt-Pt/13 %Rh high temperature thermocouples plunged into the molten weld just behind the welding arc [Chakravarti et al. 1989]. Longitudinal stresses across the gap during the weld bead cooling

can also be recorded [Graville et al. 1974 and Chen 1999]. An instrumented G-BOP test, for measuring stress across the gap is shown in Figure 3. 36.
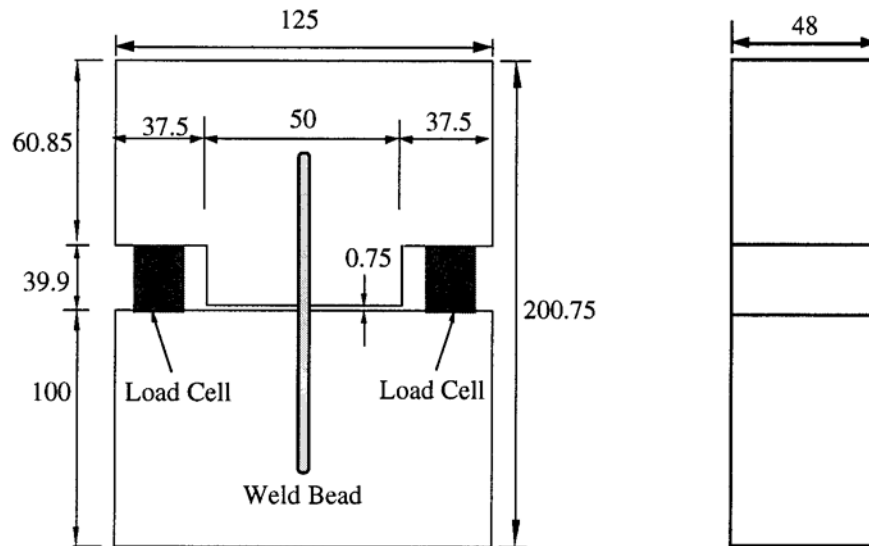
Figure 3. 36   Schematic diagram of instrumented G–BOP test blocks with two load cells located between the blocks for longitudinal stress measurements. All dimensions are in millimeters (after Chen 1999). Note: all dimensions in millimeters.   [not to scale]

The main aim of the current work was to investigate the sensitivity of seamed and seamless low strength rutile E71 T-1 flux cored wires with manufacturer's specified hydrogen levels of H10 and H5, respectively, to transverse cold cracking using the G-BOP test as shown in Figure 3. 31.

The main objectives of the current work were to study:

a) the effects of hydrogen content in deposited weld metal in rutile flux cored welding consumable with specified hydrogen benchmarks as 10 and 5 ml/100g of weld metal, with respect to varying levels of preheat temperatures on cracking behaviour,

b) the effects of welding variables such as welding current, wire feed speed and CTWD, on cracking behaviour, and

c) the effects of shielding gases on cracking behaviour.

3.7   NON-DESTRUCTIVE TESTING OF HACC

Incidents of weld metal hydrogen cracking are rarely reported, other than for hydrogen-rich weld deposits (eg Moomba-Sydney pipeline using cellulose electrodes). This may be due to the practical difficulties with non-destructive testing of thick weld sections, but sometimes due to inspection programs excluding the risks or the time delay associated with hydrogen cracking. The long delay times for hydrogen cracking have important implications for the credibility of the inspection process since an inspection carried out too soon after welding may not reveal delayed cracks [Pussegoda et al. 1997].

This section will provide some background to the non-destructive testing methods used for detection of volumetric planar defects, such as hydrogen cracks in welded joints.

3.7.1   Ultrasonic Examination

The ultrasonic testing method for examining welded joints is described in the Australian standard AS 2207-1994. This non-destructive testing method is capable of detecting planar and volumetric defects. However, meaningful and reliable results from ultrasonic examination require highly qualified and experienced operators that know how to interpret the test data. For example, in relation to detection of hydrogen cracks this method is highly sensitive to their orientation, the presence of other volumetric reflectors close to the crack and the skill of the

operator [Irving 1998]. Planar defects such as transverse hydrogen cracks present in thick section welds can be readily detected [DeLoach et al. 1999] but difficult to size even by highly qualified operators [Dixon and Taylor 1996]. Taking into account the intricacy of the ultrasonic testing which requires highly trained and experienced operators, this method for inspection of critical applications should be encouraged, particularly for an examination of transverse cold cracking [Ritter et al. 2002].

The validity of ultrasonic examination in thick section high strength MMAW and SAW welds with planar defects was examined by Ditchburn et al. (2000). In order to encourage the formation of hydrogen cracking, a number of artificial defects (slots and shims) were introduced in the weld region prior to welding. The inspection procedure focused on the detection of transverse and longitudinal cracking in "T" butt weld joints, using two ultrasonic techniques, the P-scan and conventional manual method using A-scan. In terms of sensitivity and detectability inspection was able to detect defects larger than 2 mm in height or length. However, the two methods revealed dissimilar results [Ditchburn et al. 2000]. Where the automated P-scan method failed to detect some large transverse defects (L18.0 x H13.4 mm), the manual method failed to detect one longitudinal defect (L5.0 x H0.5 mm) that was detected by P-scan. The authors concluded that, in general, the defect sizes were not well predicted by either of the ultrasonic testing methods used. This was confirmed by results from magnetic particle testing where sectioned machined surfaces were progressively tested every 0.5 mm of planar depth. The defects were found to be within a 5-10 mm range in the weld longitudinal direction of the ultrasonically detected defect locations.

Time-of-flight-diffraction (TOFD) is another ultrasonic method that allows detection of volumetric defects. This method complements other ultrasonic methods and can provide a

permanent image when required, enabling the operator to record the ultrasonically scanned D-scan images, which is a projection of weld in the through thickness indicating the positions of defects. The TOFD technique has been used to investigate the presence of hydrogen cracking in 50 mm thick plate [Harrison 2001] and was shown to be capable of detecting defects of <1 mm in size.

3.7.2 Radiographic Examination

In principle, the radiography method is intended for detection of volumetric defects and it has been accepted as one of the most reliable methods. Despite its health and safety concerns, this method is still commonly used in structural applications, predominantly in the pressure vessel industry, due to its simplicity and relatively competitive cost compared to other techniques used to detect volumetric defects.

However, there are some drawbacks associated with the practical application of this method for detection of planar defects, such as hydrogen cracks either in weld metal or parent metal HAZ. Firstly, flaw detectibility deteriorates as radiographed joint thickness is increased, and secondly, as the angle between the planar flaw and the radiographic beam increases then the detectibility decreases. Finally, it is not suitable for complex joint configurations, such as cruciform or tee butt joints.

This technique is able to detect both transverse and longitudinal cracks, but they may be missed if they are fine or not aligned parallel to the beam [Dixon and Taylor 1996]. This restricts the use of this method to situations where predictability of position and orientation of planar defects is high.

This concern was examined by Munns and Scheinder (1999), who studied the performance of various radiography methods using X-ray or Cobalt-60 sources on large planar welding flaws. Typical defects included in the study were lack of sidewall fusion, centerline solidification cracking, and weld metal and HAZ hydrogen cracking in welded joints with thickness ranging from 50 to 125 mm. The authors were able to establish that, for a particular flaw, under specific radiographic conditions, it is possible to estimate the margin of defect detectibility rather than simply stating whether the defect exists or not. This method, however, is yet to be further developed and is not widely accepted by testing authorities and industry.

3.7.3   Acoustic Emission Examination

Radiographic and ultrasonic techniques have been developed for detecting existing volumetric and planar defects in materials and/or welds. However, the acoustic emission (AE) method, described in detail by Vasudevan et al. (1981), has been found to be more suitable to real-time defect monitoring. The AE is a transient elastic wave generated by the rapid release of energy within a material as a result of fracture initiation and propagation. This energy can be recorded by a transducer attached to the sample during or after completion of welding and continuous temperature decrease.

Acoustic signals emitted during crack initiation and propagation [Fals and Trevisan 1998] have shown that hydrogen assisted cold cracking propagates in a discontinuous manner [Yurioka and Suzuki 1990].

Hydrogen cold cracking monitoring using AE been has been successfully correlated with theoretical models [Racko 1987] and used in the laboratory conditions on various instrumented cracking testing methods [Vasudevan et al. 1981, Fals and Trevisan 1998].

AE testing has also been found to be as effective method for studying hydrogen embrittlement in electrochemically charged samples [Fang et al. 1995].

3.8 PREVENTION OF WELD METAL HACC

The methods used for the prevention of HACC in HAZ, outlined in various welding standards, have been used to reduce the incidence of weld metal HACC. Although these methods can be generally applied with some success, the welding of thick sections and the use of low carbon equivalent materials [Hart 1978], high restraint conditions [Suzuki and Yurioka 1983, Lee et al. 1998] and high input [Pargeter 1992] create conditions where by the mechanism of weld metal hydrogen cracking may not be adequately controlled by the direct application of requirements for avoiding HAZ cracking [Kuebler et al. 2000].

In the absence of reliable guidance for avoidance of hydrogen in weld metal, hydrogen cracking may be minimised by taking one or more of the following precautions:

a) minimization of diffusible hydrogen content through the use of a low hydrogen welding process,

b) use of low hydrogen, high ductility welding consumables,

c) careful handling and storage of welding consumables to prevent their exposure to humid environments and subsequent uptake of atmospheric moisture and thereby maintaining the low hydrogen potential of the welding consumable, following recommended re-drying procedure for baking the consumables, and disregarding any

consumable showing rust appearance on the wire surface (applicable primarily for GMAW, FCAW and FCAW processes),

d) selection of high quality shielding gases containing minimum level of moisture,

e) if possible, selection of parent metal with lower carbon equivalent to improve the material weldability,

f) cleaning surfaces of parent metal prior commencement of welding,

g) selection of joint design, fit up and deposition sequence to minimize cumulative stresses,

h) application of sufficient preheating of parent metal before and during welding to slow down the cooling rates (note that for tack welds preheat is essential),

i) avoidance use of short inter-pass times during welding of multi-pass weld deposits of large wall thicknesses when preheating is continuously maintained,

j) use of higher heat input by deposition of large weld beads. (Note that a small root run in a butt joint may be more susceptible to cracking than subsequent larger deposits, and

k) selection of immediate post heating for hydrogen release, or if necessary, a post weld heat treatment for removal of residual stresses.

A successful welding procedure qualification, utilizing all the above preventative measures is certainly the first positive step to providing evidence of weld-parent metal weldability. The welding procedure can then be employed for a specific application. However, there may be

circumstances where the atmospheric conditions, large wall thickness, higher restraint levels in the welded joint may expose the qualified procedure to unexpected failure due to hydrogen assisted cold cracking. Here, in these extreme situations a consideration should be also given to conduct 'realistic welding trials', simulating the actual conditions expected during welding (level of restraint, wall thickness and atmospheric conditions), or use of higher temperatures for preheat than those recommended by the welding standards. This concept of carrying out 'realistic welding trials' may be seen as an expensive precaution, but it is certainly worthwhile in some severe applications and undoubtedly less expensive than the costs associated with repair of HACC occurring in the actual welds.

CHAPTER 4

HACC in FCAW Welds

4.1   HISTORY OF THE DEVELOPMENT OF FCAW

The origin of the arc welding process can be traced back to the early 19th century, when in 1808, Davy and Ritter produced the first electric discharge, obtained between two carbon electrodes [Saf & Airliquide]. Because the discharge bent upwards, due to the effect of the hot gases, it was named "arc". Some years later in 1888, Benardos and Olszewski were granted patent No. 12984 registered for carbon arc welding [www.weldinghistory.org]. Finally in 1907, O. Kjellberg applied for a patent dealing with the covered electrode what we know today as manual metal arc electrode [www.weldinghistory.org].

Perhaps the first significant steps in the application of shielding gases to the welding process came in 1930, when two U.S patents were issued on the use of inert shielding gases for welding. The first patent, issued to H. M. Hobart described the use of helium with carbon or metallic arcs. The other patent, issued to P. K. Devers, described the use of argon and its mixtures for arc processes [www.weldinghistory.org].

During World War II, the gas manufacturing company Praxair acquired the rights to the invention of shielding gases, and started an extensive research and development program to expand the application of the technology. As a result of this research effort, Praxair commercially introduced the process then know as HELIARC process (in 1946), and what is known today as Gas Tungsten Arc Welding (GTAW). In 1950, a patent was issued to Air Reduction Co. Inc. (Airco) covering a process later known as Gas Metal Arc Welding (GMAW) or Metal Inert Gas (MIG) and Metal Active Gas (MAG) [www.weldinghistory.org]. At that time, the process was better known as SIGMA (Shielded Inert Gas Metal Arc). During

the 1950s, further development of gas mixtures, wire chemistry, and equipment systems improved and expanded the application range of the GMAW process. This work led to the rapid growth of GMAW during the next thirty years and eventually to its wide spread use today. Furthermore, this development work provided the groundwork for the invention of gas shielded Flux Cored Arc Welding (FCAW) by Arthur Bernard and patented in the late 1957 [Ferree 1992, http://www.welding.com]. His patent was assigned to the National Cylinder Gas Co. (NCG). In 1959, self shielded Flux Cored Arc Welding was introduced by Landis and Patton in 1959, US Patent 2,909,778 [Quintana and Kotecki 2000] from where the processes were further developed and widely introduced for industrial use.

The application of the FCAW process has been continuously expanding in recent years and around the world [Stemvers 2001]. Although the properties and benefits of these wires are becoming better known [Jones 1982], their application range needs to develop further in line with the progression of new materials available.

4.2   FCAW PROCESS

As in the case for other arc welding processes, FCAW is vulnerable with regard to hydrogen uptake by the weld deposit. The scientific effort to understand how welding parameters and other associated factors influence hydrogen behaviour in FCAW weldments and the weld metal quality is an ongoing process, mainly due to new developments in flux cored wires [Sierdzinski and Ferree 1998, Ebert 1998, Dallam et al. 2000]. A number of new and large research projects are underway around the world which involve research institutions, steel producers, consumable manufactures and even fabricators, who are collaborating in an effort

to clarify how hydrogen influences HACC in FCAW welds. The common aim of this work is to determine the influential factors affecting the hydrogen content in the weld metal generated by the flux cored wires and to communicate the outcomes to the industry.

Flux Cored Arc Welding (FCAW) can be self-shielded or gas shielded. It is frequently referred to as flux cored welding (FCW). The gas shielded process is shown schematically in Figure 4. 1.
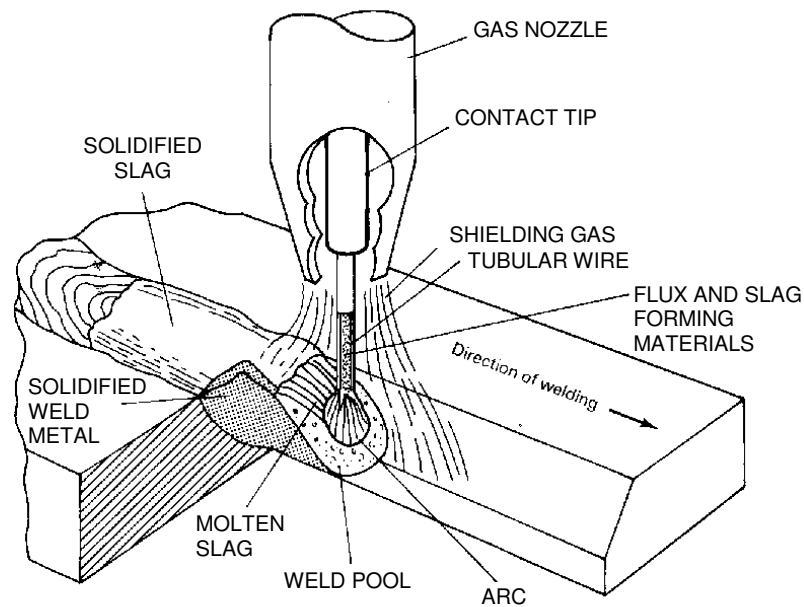
Figure 4. 1   A schematic illustration of the gas shielded FCAW process (after ASM Welding Handbook, Vol. 6, 1993).

FCAW process combines the productivity benefits of continuous wire feeding (similar to GMAW process) with self-contained flux to create a high deposition rate. Deposition rate is often used as a measure of potential productivity [Jones 1982], although many other factors contribute to operator duty cycle and hence productivity [Blackman et al. 2002]. A graph of comparative deposition rates of different welding processes is shown in Figure 4. 2.
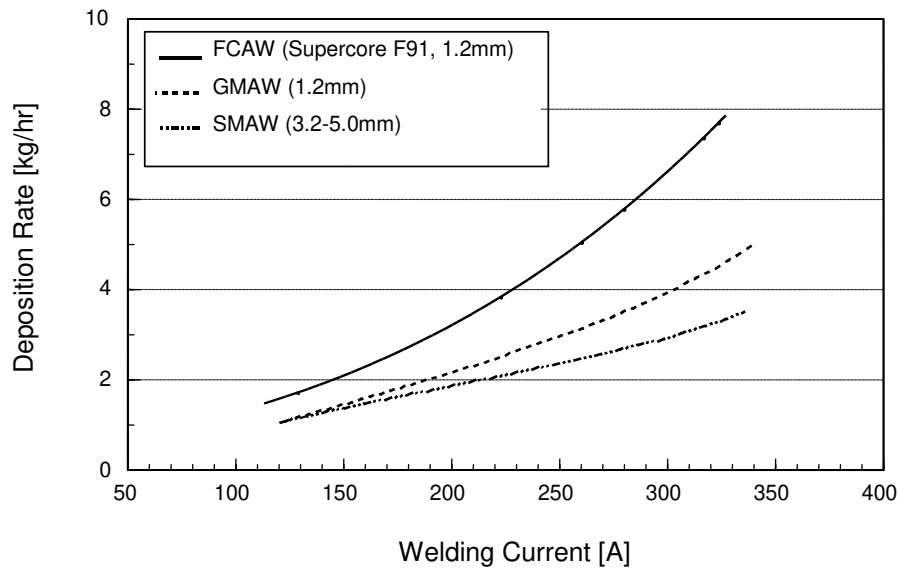
Figure 4. 2   Deposition rate of FCAW process compared with MMAW (SMAW) and GMAW processes (after Zhang et al. 2001).

In comparison with the GMAW process, FCAW consumables are generally more forgiving, and are often specified by welding engineers and fabricators, particularly for complex structures or in-situ fixed pipes involving out-of-position welding.

Flux cored welding process has several benefits relative to other welding processes:

a)   all position capability compared with GMAW,

b)   good quality weld metal deposit. More tolerant to mill scale and less sensitive to inter-run cold overlap than GMAW,

c)   deeper penetration than GMAW and MMAW,

d)   higher deposition rates than Manual Metal Arc Welding (MMAW),

e)   lower operator skill required than for GMAW, and

f)   metallurgical benefits that can be gained from the presence of flux when compared to GMAW.

The disadvantages of the FCAW welding process include:

a) potential for irregular wire feeding resulting in burnback and damage of contact tip,

b) requirement for removal of slag after each welding pass, and

c) increased fume formation during welding in comparison to GMAW and MMAW processes.

The use of flux cored wires has grown significantly in recent years [Stemvers 2001] with their successful application in pipeline, structural, shipbuilding, offshore constructions, petrochemical and power generation industries.

4.3   FCAW CONSUMABLES

Gas shielded flux cored wires are commonly used to weld carbon, carbon – manganese, high strength low alloy, stainless and some superalloy nickel-based steels. Despite the obvious advantages [Jones 1982], the operational limits of flux-cored consumables should be well understood, particularly with respect to weld metal mechanical properties and levels of diffusible hydrogen content. Typical diffusible hydrogen contents in the flux-cored arc weld deposits may vary from very low to high, mainly as a function of the type of consumable used, as shown in Figure 4. 3.

Flux cored wires are generally manufactured using a drawing process, where a thin sheath material is firstly rolled into "U" shape, which very fine premixed fluxes are then continuously poured into. Gradually, through a set of rolls, the filled groove is then formed into a round tube.
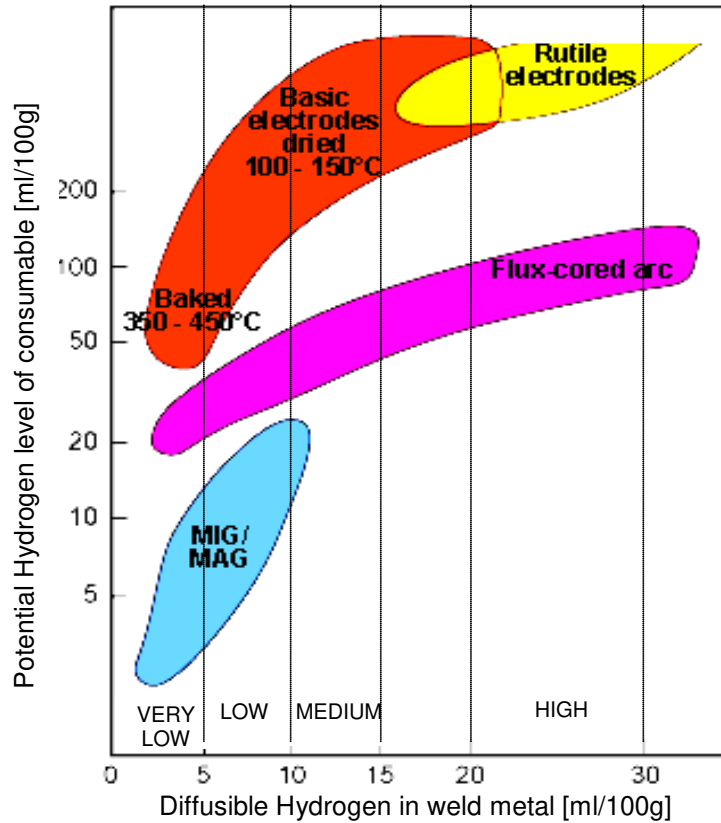
Figure 4. 3   Graph showing the range of hydrogen content expected in various welding processes (after Bailey et al. 1995).

The diameter of this tube is then reduced further through a drawing and rolling operation to a required final wire diameter. These wire diameters typically range from 0.9 to 2.4 mm.

Perhaps the most widely accepted worldwide standard for carbon steel flux cored wires is specification for steel electrodes for flux cored arc welding [ANSI/AWS A5.20-95]. The consumables classified under this specification are intended for FCAW, either with or without an external shielding gas. The standard differentiates the consumables by their mechanical properties, recommended welding position, polarity and their application. The ANSI/AWS A5.20-95 classification system is shown in Figure 4. 4.

Designates an electrode

This designator is either 6 or 7. It indicates the minimum tensile strength (in psi x 10,000)

This designator is either 0 (flat) or 1 (all positions). It indicates the position of welding for which the consumable is intended.

This designator indicates that this consumable is flux cored wire.

This designator is some number 1–14 or letter G (external shielding, no CVN are specified) with, or without an S (suitable for single pass only).

An M designator is indicates mixed (Ar/CO_2) shielding gas. If M is not shown, then the electrode is used with either CO_2 or self shielded.

Designates that the consumable meets the requirements for improved toughness (27J @ -40°C).

Designates that the consumable meets the requirements of weld metal diffusible hydrogen per 100g (H4, H8 or H16).

EXXT-XMJ HX

Figure 4. 4   A description of the classification system for carbon steel electrodes for flux cored arc welding (after ANSI/AWS A5.20-95).

Apart from ANSI/AWS A5.20-95, there are a number of different production technologies available which meet the standard specification. In principle, there are two major groups, characterized by different cross sectional structure of the wires. The first consists of various types of seam joints and the second is a seamless wire which promises to be an effective way of minimizing hydrogen potential in the family of FCAW wires [Quintana and Kotecki 2000]. It should be noted that the seamed flux cored wires have a several types of joints, as shown in Figure 4. 5, which potentially can provide a passage for moisture pickup or residual lubricants during the wire manufacturing process, as shown in Figure 4. 6. This is a valid concern since hygroscopic flux materials are sometimes used in the core as well. With respect to the details of the manufacturing method for seamed wires, such as type of lubricant used and the flux composition, these generally are considered to be proprietary and not widely published.
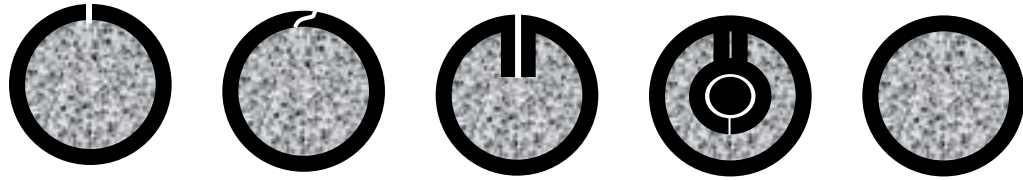
Figure 4. 5   A schematic illustration of the different designs of tubular flux cored wires (after Sato et al. 1997).
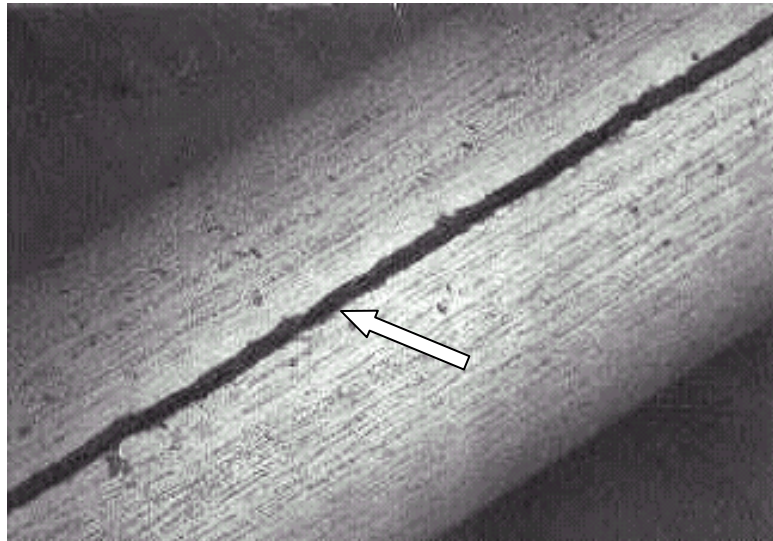
Figure 4. 6   A photograph showing a typical longitudinal seam joint in a tubular flux-cored wire (after Czarnecki, Phoenix International).

There are three major groups of gas shielded FCAW wires used for welding of carbon and carbon-manganese steels. Each group of wires is characterized by the mode of metal transfer which depends to a large extent on the flux system used, as shown schematically in Figure 4. 7.
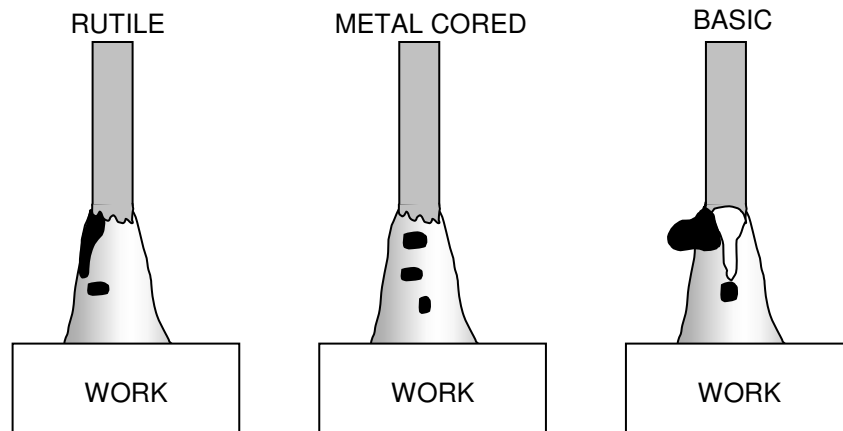
Figure 4. 7   Schematic representation of metal transfer types observed with flux cored wires (after Norrish 1992).

Rutile group:

Rutile wires are the most commonly used amongst the flux cored wires and have been widely used for over 17 years [Sierdzinski and Ferree 1998]. Rutile fluxes have a slag system based on TiO_2 and provide an arc that typically characterized by a fine metal spray transfer with a small amount of spatter. Slag usually covers the surface of the weld pool evenly, producing beads with smooth profile and surface appearance. The rate of deposition is high, welding is possible in all positions at high welding currents and the rate of weld metal recovery is high (usually 85-90 %). A wide range of rutile E71T-1 FCAW wires is available to fabricators, but their diffusible hydrogen levels can range from product to product between 3-15 ml/100g depending on their hydrogen classification. However, in order to meet the more stringent requirements of commercial fabricators, manufacturers are focusing on developed of rutile wires with reduced diffusible hydrogen levels down to <5 ml/100g [Sierdzinski and Ferree 1998].

Metal core group:

Metal core wires are known for their high efficiency. This is due to additional ingredients added into their core in the form of metal powders. The deposition rate is very high (about 95 %) and there is a minimal amount of slag. They are suitable for welding of large wall thickness weldments, using high welding currents and they typically produce weld metal deposits with lower hydrogen levels.

Basic group:

Basic wires have a flux mainly composed of de-oxidants such as MgO, $CaCO_3$, CaF_2, and CaO. They result in excellent mechanical properties in the deposited metal and produce microscopically clean weld metals with improved fracture toughness and therefore crack resistance. Basic type E70 T-5 wires produce the lowest diffusible hydrogen levels of <3 ml/100g. However, welding with basic wires tends to be characterized by a harsh, globular metal transfer mode. The basic flux formulation gives irregular dip transfer at low welding currents and non-axial globular transfer at high welding currents. A typical feature of the arc is a 'flux finger' of unmelted flux projecting from the wire downwards into the plasma arc [Norrish 1992]. In comparison with rutile wires, they usually produce a large amount of spatter and are limited to use in welding in flat and horizontal positions only.

It is important to understand that the classifications listed in the consumable standards, such as ANSI/AWS A5.20-95 and Australian AS 2203.1-1990, define these three groups in more detail according to their usability characteristics. Some wires are recommended only for single pass welding while others are recommended for multiple-pass welding.

Both American and Australian standards (ANSI/AWS A5.20-95 and AS 2203.1-1990) for flux cored electrodes for arc welding also refer to methods for the determination of diffusible hydrogen levels in accordance with ANSI/AWS A4.3-93 and AS/NZS 3752-1996, respectively, grouping the consumables into three categories as listed in Chapter 2, Table 2.2.

Fluxes containing a particular mixture of minerals can introduce a considerable amount of hydrogen, since these flux formulations can absorb significant moisture if stored in a humid environment and unprotected for long period of time [Harwig et al. 1999]. The issue of consumable handling and the associated potential of fluxes to absorb the moisture from atmospheric conditions has been well described and implemented in ANSI/AWS A5.20-95, Section A8.2. However, the Australian standard AS 2203.1-1990 does not account for this important matter.

4.4   EFFECT OF WELDING PARAMETERS

There are a number of important process parameters that affect diffusible hydrogen levels, including welding current and voltage. The effect of these and other welding parameters on diffusible hydrogen levels in flux cored wires has been the subject of previous work [White et al. 1992, Kurokawa et al. 1998]. However, some recent cases of transverse weld metal HACC in low strength structural steel fabrication in Australia, BHP Port Kembla and the study by Visman (2002) have highlighted the need for more work on understanding how the welding parameters affect HACC, particularly in the case of rutile weld deposits.

It is important to recognize that, in comparison with manual metal arc electrodes, semi-automated gas shielded processes such as flux cored arc welding have an additional set of

welding parameters that can influence hydrogen content, including contact tip-to-work distance (CTWD) and shielding gas. It is known in the industry that these welding parameters can influence not only the operating characteristics of flux cored wires, but also the weld metal mechanical properties [Konkol et al. 1998, French et al. 1997]. In combination with adverse welding conditions, particular combinations of welding parameters can result in weld deposits that exhibit susceptibility to HACC. This has been observed for welding of thick section plates under simulated conditions using recommended preheat temperature and both high [Kuebler et al. 2000] and low strength rutile flux cored wires [Lee et al. 1998, Visman 2002].

Predominantly, it is the consumable type, its hydrogen classification and the applied preheat and inter-pass temperatures that are recognized by the welding standards as being the most reliable controlling parameters for HACC in thick section plate welding. Another processing variable that is not currently acknowledged in any of welding standards is the inter-pass time. The study by Pargeter (1992) concluded that an increase in inter-pass time lessens the risk of HACC and, along with preheat and inter-pass temperatures, should form a part of any hydrogen cracking predictive system.

It is often the case that, although a successful welding procedure qualification may be carried out under controlled preheat and inter-pass temperatures (with all welding parameters monitored and recorded by a welding supervisor), parameters such as welding current and CTWD may vary during the production welding, resulting in different levels of hydrogen in weld deposits.

The welding standards prescribe the allowable changes for the "essential variables". The range for each essential variable listed in the welding standards allows the welding operator to vary

the welding variables during the production welding. However, this has the potential to adversely affect the weld metal integrity and diffusible hydrogen content. Further there are some inconsistencies in the way that various standards prescribe such allowable variations. For example, where the structural welding standards AS/NZS 1554.1-2000 and ANSI/AWS D1.1-2000 specify a maximum variation of ±10 % for welding current, the pressure equipment standard AS/NZS 3992-1998 refers to a variation between transfer arc modes, without specific reference to welding current.

In another example, the structural steel welding standards AS/NZS 1554.1-2000 and AS/NZS 1554.4-1995 allow CTWD to vary 20 %, whereas structural welding standard ANSI/AWS D1.1-2000 and pressure equipment standard for welding procedure qualification, AS/NZS 3992-1998, both omit CTWD as an essential variable.

It should be also noted that when classifying or qualifying welding consumables, manufacturers currently measure and report the weld metal hydrogen levels under a single set of welding parameters. However, fabricators may use completely different welding parameters and weld joint configurations, resulting in different levels of hydrogen and different degrees of restraint for the production of welds in industrial operations.

These welding parameters should be included in any hydrogen cracking predictive system in order to avoid misunderstanding between a specific set of welding condition at the time of testing and the actual and often different welding conditions during production.

The main aim of the current work was to develop an understanding of how individual welding variables in the FCAW process affect changes in arc transfer behaviour, levels of diffusible hydrogen and the occurrence of cold cracking in weld metal in laboratory conditions.

4.4.1 Welding Current

The electrical resistance of most metals increases with increasing temperature, where the ratio of the change of resistance per degree change of temperature to the resistance at some defined temperature is referred to as the temperature coefficient of resistance, α. Temperature rise along the wire leaving the contact tip is not only due to resistance heating caused by an increase of CTWD, resulting in a longer period of a wire element in the resistive heating zone (RHZ), but also due to I^2R loss. It might be said that the greater the welding current, the greater the heat energy, Q, generated. However, in order to maintain arc stability at higher setting of welding current, welding machines automatically increase wire feed speed (WFS), which results in greater burn-off rate of the wire. This subsequently counteracts the resistance heating effect by reducing the time available for temperature increase due to resistive heating, (t_{RHZ}). An exact relationship between welding current and t_{RHZ} is not possible without an accurate assessment of arc dimensions.

When studying the effects of increasing welding current between 160-260 A, using rutile E71 T-1 wire and 80Ar-20CO_2 shielding gas, White et al. (1992) found that the hydrogen content in the weld metal increased linearly. Further, the increase in the welding current, resulted in a change in the metal transfer mode within the arc from globular to drop and then to stream spray transfer. The results of this work, conducted using 1.2 mm diameter flux cored wire, indicated that a transition in metal transfer mode at higher welding currents may facilitate greater absorption of hydrogen as a result of the increased area per unit volume of a fine spray of molten droplets. It should be noted that without recording of arc images by White et al. (1992), it is most likely that the metal arc transfer differentiation was observed only by naked eye. This method would be quite inadequate to determine the droplet formation and their size

precisely. Similarly, a study by Harwig et al. (1999) on the same wire classification, wire diameter and shielding gas also found that weld diffusible hydrogen content increased almost linearly as the welding current increased. However, in this case the decrease of weld metal hydrogen content was explained in term of increasing time in the electrode extension. When time in resistive heating, t_{RHZ} , was maintained constant, the hydrogen content was recorded to be slightly higher with welds made at higher WFS. Hence, a temperature profile in the wire extension was suggested to be responsible for this effect, and not the metal transfer mode.

Keeping the CTWD constant, an increase in welding current will result in an increase in temperature in the wire. The temperature distribution was proposed by Jilong and Apps (1982), and shown in Figure 4. 8.
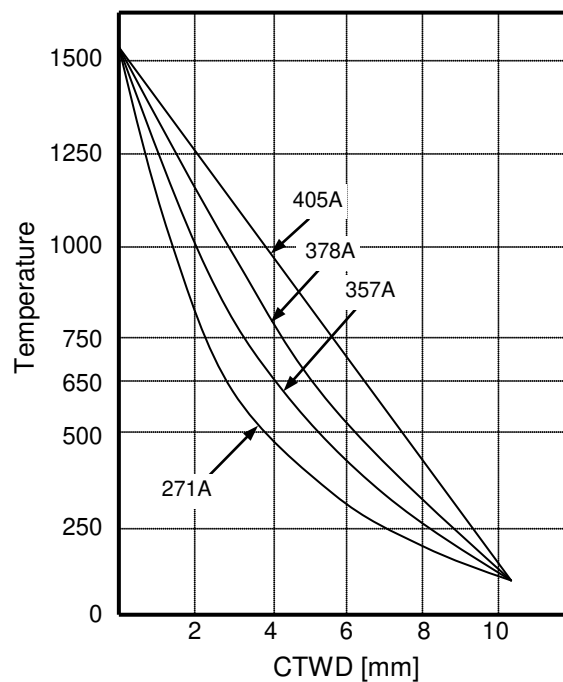

Figure 4. 8   Graph showing solid wire temperature distribution from contact tip to 10mm CTWD (after Jilong et al. 1982).

It can be seen that the relationship between the temperature distribution and a gradual increase of welding current from 271 to 405 A shows that the wire temperature increases linearly only at the highest welding current of 405 A. A decrease in welding current distorts the temperature distribution to an exponential relationship.

For basic E71 T-5 wires with much lower hydrogen levels of <5 ml/100g, increasing welding current has been shown to have no significant effect on weld metal hydrogen content between 160-260 A [White et al. 1992]. A similar effect, with only a marginal increase of hydrogen levels, was also suggested by Sierdzinski and Ferree (1998) for a newly developed rutile wire E71 T-1 deposited using shielding gas 75Ar-25CO_2 and with weld deposit hydrogen levels of <4 ml/100g. This observation would suggest that wires with very low nominal hydrogen levels, either basic or rutile, are less sensitive to welding current variation. This was also confirmed by examining larger wires (1.6 mm diameter) with the same shielding gas, 75Ar-25CO_2 [Pitrun et al. 2001]. No significant changes in weld metal diffusible hydrogen levels were recorded with variation of welding currents in the range 250-350 A for commercially available rutile and basic flux cored wires classified with nominal hydrogen levels of <5 ml/100g. Interestingly, when welding with CO_2 shielding gas, the measured weld metal hydrogen concentrations were found to be independent of welding current. In the same study this was also true for rutile wires with higher nominal hydrogen levels of <10 ml/100g.

4.4.2   Arc Voltage

Arc voltage has also been found to affect the levels of diffusible weld metal hydrogen [Kiefer 1996]. Arc voltage is proportional to the arc length and has an effect on arc stability, spatter

occurrence and bead geometry. It is defined as an accumulation of the following voltage drops [Villafuerte 1999]:

$$V = V_{cable} + V_{contact} + V_{CTWD} + V_{arc} \qquad\qquad (4.\ 1)$$

where: V_{cable} = voltage drop through the cable and torch couplings

$V_{contact}$ = voltage drop between the contact tip and wire

V_{CTWD} = voltage drop along the wire extension CTWD

V_{arc} = voltage drop across the plasma arc column

Voltage increase from 22 to 28 V has been shown to increase weld metal hydrogen content by about 40 % for a given setting [Kiefer 1996]. Although no arc images were recorded to determine the arc length, it was concluded that higher voltage produces a longer arc that subsequently increases exposure of metal droplets to hydrogen from the shielding gas and/or atmospheric conditions. Other work investigating the effects of arc voltage on weld metal hydrogen content also confirmed the relationship between arc voltage and diffusible hydrogen content [Kuebler 2003]. This experiment was carried out using a rutile wire (classification AWS 5.29 E81T1-Ni1). The constant welding conditions included a welding current of 200 A, $75Ar$-$25CO_2$ shielding gas and a CTWD of 20 mm, while arc voltage was increased from 27 to 33 V. The increase in voltage resulted in the diffusible hydrogen content increase in weld metal from 4.0 to 5.6 ml/100g, representing a 40 % increase.

4.4.3   Heat Input

Heat input, preheat temperature and combined plate thickness control weld metal cooling rate and microstructure, and therefore susceptibility of HAZ to hydrogen cracking [Alcantra and Rogerson 1984 and Bailey et al. 1995].

Arc energy is the energy supplied by the welding arc to the parent metal without consideration of the process used. It is calculated following Equation 4.2:

$$E = \frac{I \times V \times 60}{v} \times 1000 \qquad\qquad (4.2)$$

where: E   = arc energy [kJ/mm]

   I   = welding current [A]

   V   = arc voltage [V]

   v   = travel speed [mm/min.]

Heat input is the arc energy going into the parent metal, but also considers the effects of process efficiency. It is apparent that the level of heat input varies between welding processes as a result of differing thermal arc efficiencies, η, for each welding process. Therefore, in calculating heat input for a given welding process, the arc efficiency of that process must be taken into consideration (EN 1011.1-1998). It is calculated by multiplying the arc energy by an efficiency coefficient, η, specific to the welding process, as follows:

   Submerged arc welding (SAW)   : 1.0
   Manual metal arc welding (MMAW) : 0.8
   Gas metal arc welding (GMAW)   : 0.8
   Flux cored arc welding (FCAW)   : 0.8
   Gas tungsten arc welding (GTAW)   : 0.6

The use of heat input values in the assessment of weldability, as presented in welding standards, involves the determination of a minimum preheat temperature required to minimize the risk of cracking in the HAZ. For the same material and combined thickness, it is possible to select a lower minimum preheat temperature by using a welding process characterized by higher heat input. Selection of lower heat input process and inter-pass temperature allow the weld bead to cool more quickly, resulting in more hydrogen in the weld and increased risk of HACC. On the other hand, for a given combined plate thickness, high heat input combined with high preheat temperatures causes a larger weld pool that cools more slowly [Lancaster 1999], allowing hydrogen more time to effuse from the weld [Dixon and Taylor 1996]. For MMAW welding process, it has been shown that hydrogen levels of the deposited weld metal decrease linearly with increasing heat input via reduction in traverse speed [Pokhodnya 1996].

The effect of heat input on diffusible hydrogen levels were also studied by Kuebler et al. (2000) for the FCAW welding process. Heat input was varied via traverse speed, at constant welding current, voltage and CTWD. The results of this work concluded that both basic and rutile wires were susceptible to variations in weld metal diffusible hydrogen at content different heat inputs, with the effect being more noticeable for rutile wire, as shown in Figure 4. 9. Maximum hydrogen levels were observed at heat input of 0.95 kJ/mm, which represented traverse speed of 550 mm/min. An increase in heat input between 0.95 - 1.17 kJ/mm resulted in a significant drop of weld metal hydrogen levels. However, any further increase of heat input beyond 1.17 kJ/mm had a little effect on the levels of weld metal hydrogen.
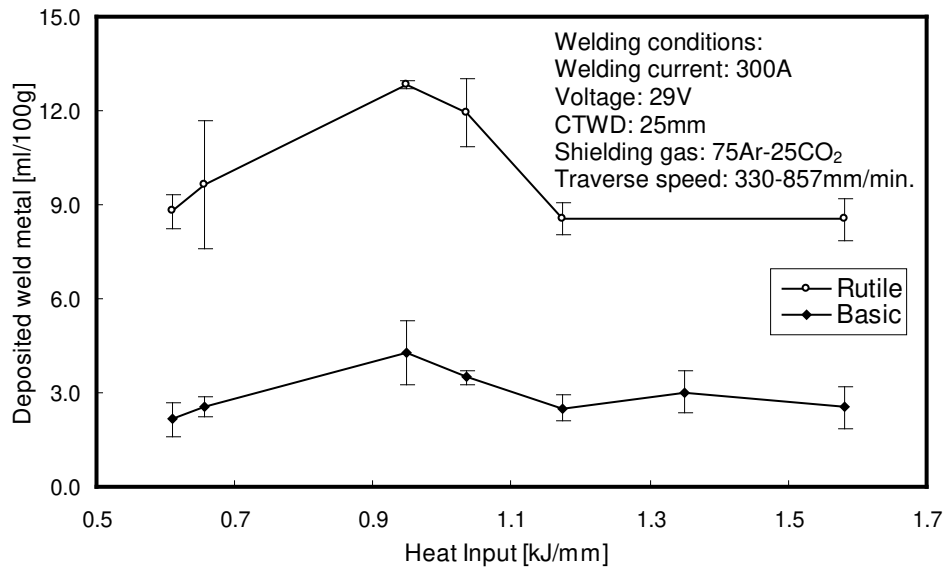
Figure 4. 9   Graph showing the influence of heat input values (varying traverse speed)
                   on levels of weld metal diffusible hydrogen (after Kuebler at al. 2000).

Although this observation supported the theory that larger weld bead size increases the time

for hydrogen escape from the weld, there was no experimental work done in more controlled

conditions to support this suggestion.

The arc energy is likely to have a significant influence on cooling time and $t_{8/5}$ (cooling time

through the transformation temperature range 800-500 °C). The following Equation 4.3

describes the relationship between the arc energy and initial preheat temperature [Uwer and

Degenkolbe 1976].

$$t_{8/5} = \frac{\eta}{2\pi\lambda} \times \frac{V_x I}{v} \times \left(\frac{1}{500\text{-}T_0} - \frac{1}{800\text{-}T_0} \right) \tag{4.3}$$

where: T_o = initial (preheat) temperature [°C]

              η = thermal arc coefficient

              λ = thermal conductivity of the steel [J/s cm°C]

An increase of heat input results in lower cooling rate, which in turn affects hydrogen levels. This is true not only for single weld deposits, but also for multi-pass welds in thick sections [Kinsey 1998]. Weld bead size influences hydrogen levels, but also the mechanical properties of the deposited weld [Schumann and French 1994]. Higher heat inputs via introduction of a weave-bead technique have been shown to result in a higher proportion of reheated material and improved impact properties. An increase of heat input is usually associated with an increase of weld metal size resulting in a reduction of weld metal hardness [Alcantara and Rogerson 1984]. This is most likely due to lower cooling rates, allowing a development of a coarser weld metal microstructure, typical for high heat input welding processes. However, excessively high heat inputs of 5 kJ/mm used for multi-pass weld deposits have been shown to result in hydrogen cracking in weld metal [Pargeter 1992]. This is counter intuitive to common experience for HAZ cracking, where the preheat temperature may even be relaxed using high heat input processes.

A change of parameters, within the "essential variable" tolerances given in ANSI/AWS D1.1-2000 (e.g. ±10 % welding current, ±7 % voltage) has been shown to result in an increase in hydrogen levels by over 3 ml/100g [Kiefer 1996]. These findings demonstrate that use of the heat input formula on its own is not an adequate way to control hydrogen levels in the weld and therefore to avoid or minimize the occurrence of weld metal HACC.

4.4.4   Preheat and Inter-pass Temperature

In order to allow more hydrogen to diffuse out from a thick section plate joint, it is essential to decrease cooling rates. As mentioned in Chapter 3, this can be achieved by the selection of

automatic processes with high arc energies, such as electroslag welding (ESW) or the SAW process, and/or by the introduction of preheat and inter-pass temperatures.

The level of hydrogen content in the weld metal is highly dependent on the thermal history, the heat input and, in particular, the preheat temperature, all of which govern weld cooling rate. By reducing cooling rates, preheating facilitates control of microstructural transformation in the parent metal and enables reduction of diffusible hydrogen levels in the weldment. A change in welding conditions that result in an increase of cooling times, either in $t_{3/1}$ or $t_{8/5}$, should be considered when the aim is to avoid hydrogen cold cracking.

In many instances it is also necessary to control the inter-pass temperature. This temperature is measured immediately before starting another weld deposit. Either a minimum or maximum may be specified in welding procedure. Where preheat is required to avoid cold cracking, the inter-pass temperature is a minimum, and is at least equal to the preheat temperature. When welding quenched and tempered steels, a maximum inter-pass temperature (maximum heat input) is required in order to minimize grain growth and tempering effects, thereby achieving the required mechanical properties, as illustrated in Figure 4. 10.
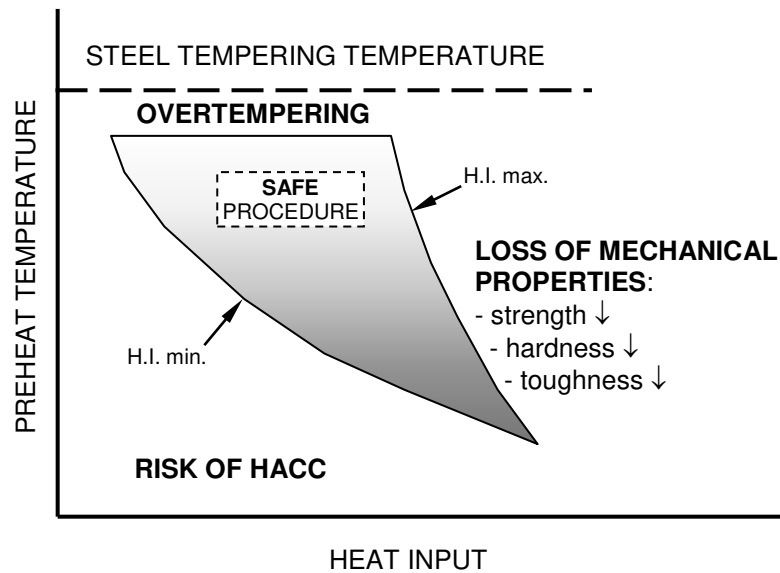
Figure 4. 10   A schematic diagram showing the limitation of maximum and minimum weld heat inputs for welding of quenched and tempered steels (after WTIA TN 15).

The effects of various preheat/inter-pass temperatures in 50 mm thick steel using FCAW wires were studied by Kinsey (1998) and Lee et al. (1998). Although the levels of diffusible hydrogen in weld metal were >5 ml/100g, the results of these studies revealed sub-surface transverse hydrogen cracking in the no preheat / inter-pass cases only. Both authors suggest that the hardness of weld metal depends on the preheating / inter-pass temperature and when the preheating / inter-pass temperatures are low, the weld metal becomes more susceptible to transverse cracking. Transverse hydrogen cracking has also been reported by DeLoach et al. (2000) in 50 mm thick, high strength 'V' butt welds deposited using GMAW process using a low preheat / inter-pass temperature of 15/15 °C.

Boundary lines for critical inter-pass temperatures in low strength C-Mn steel were established by Pargeter (1992). This work reported an increasing risk of weld metal hydrogen cracking at higher heat inputs, with decreasing inter-pass time. This is thought to be due to the reduction

of time for hydrogen escape and larger hydrogen diffusion distance from the centre of larger weld beads. This work concluded that, for welding with a low strength C-Mn consumable (H_D = 6 ml/100g) at heat input of 3 kJ/mm, 20 minutes inter-pass time, and with a minimum of 70 °C inter-pass temperature, weld deposits should be free from HACC. A reduction in inter-pass time from 20 to 10 minutes resulted in an increase of 50 °C in the preheat required to prevent cold cracking in weld metal (H_D = 7 ml/100g) deposited using heat input of 3 kJ/mm. A higher critical inter-pass temperature was observed for 50 mm than for 30 mm thick plate.

4.4.5 Contact Tip-to-Work Distance

Contact tip-to-work distance (CTWD), also sometimes referred to as electrode stick out (ESO), is defined as the distance between the end of the contact tip and the work piece. A schematic diagram of CTWD is shown in Figure 4. 11. CTWD includes the wire length from the contact tip, to the point where it enters the welding arc, and the arc length.
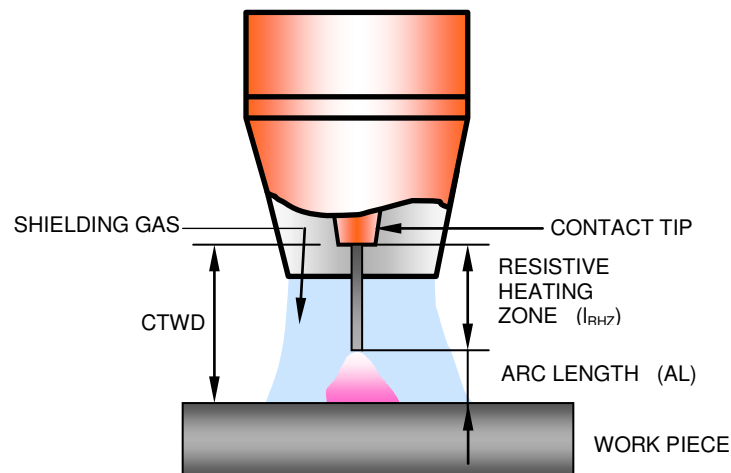

Figure 4. 11   Schematic diagram of CTWD, commonly referred as to electrode stick-out.

Not all welding standards appear to have adequately addressed the importance of CTWD in designing welding procedures. The CTWD has been recognized in the structural steel welding standard AS/NZS 1554.1-2000 as an essential variable for semi-automated welding processes such as GMAW, SAW and FCAW. Here, any change of CTWD of more than ±20 % would require re-qualification of welding procedure.

However, ANSI/AWS D1.1-2000 and the pressure vessel equipment standard AS/NZS 3992-1998, both exclude the CTWD as an essential variable. Despite this omission, it is clear that CTWD should be considered as an important factor, since the bulk of evidence available suggests that any change of CTWD affects the diffusible hydrogen in FCAW deposits, particularly for rutile wires. Previous work has shown that CTWD can significantly influence the weld hydrogen content, with levels of hydrogen decreasing with increasing CTWD for a range of rutile wires from different manufacturers [Pitrun et al. 2001]. This was found to be related to an increase in the time the wire spent in the resistive heating zone, t_{RHZ}, facilitating the removal of moisture and burn-off of lubricant residues. This work confirmed the results of earlier investigations by White et al. (1992) and Kiefer (1996). With a shorter CTWD and with higher welding current (higher wire feed speed), there is less time available to evaporate any residual moisture or decompose any hydrogen-bearing materials (such as residual lubricant from the wire surface) and this results in higher levels of diffusible hydrogen in weld deposits.

Contrary to these studies, work by Harwig et al. (1999) suggests the CTWD has no significant influence on levels of weld metal diffusible hydrogen at constant welding current while maintaining constant arc length of 6.35 mm. These findings suggest that keeping constant arc length, it is possible to maintain the weld metal hydrogen levels unchanged regardless of CTWD variation. However, it is important to note that in order to maintain an acceptable

characteristic of arc metal transfer (at arc length of 6.35 mm), the arc voltage must have been adjusted to maintain constant welding current. This suggests that diffusible hydrogen may be dependent not just on the welding current [Harwig et al. 1999], but also on arc voltage.

In the case of basic wires of type E71T-5, the weld metal hydrogen concentration has been shown to remain almost unchanged with variation in CTWD [White et al. 1992]. A similar effect was observed for basic E71T-5 consumables and E71T-1 seamless rutile type wires (total of 4 wires examined), with nominal hydrogen levels of <5 ml/100g [Pitrun et al. 2001]. However, a change in the CTWD from 25 to 15 mm resulted in a difference of about 1 ml/100g, which represented an average increase of about 50 % in hydrogen content. This work suggests that the mechanism by which CTWD changes diffusible hydrogen levels in weld deposits using basic E71T-5 consumables may be similar to that of rutile E71T-1 wires, and therefore cannot be discounted. This is particularly important for high strength weld metal [Kuebler 2000], where hydrogen cracking was found in weld deposits using high strength FCAW consumable AWS A5.29 E110 T-5, with diffusible hydrogen level of less than 5 ml/100g obtained with CTWD of 25 mm.

An empirical formula, Equation 4.4, calculating levels of diffusible hydrogen in weld metal as a function of CTWD and other welding parameters for the FCAW process is presented below [Kiefer 1996]:

$$H_D = \frac{\sqrt{H_{wt}} \times DP^{(1.86 + 0.014V + 0.036d)} \times A^{(0.6112 + 0.013d)}}{5045 \times d^{4.15}} \qquad (4.4)$$

where: H_D = diffusible hydrogen of deposited weld metal [ml/100g]

           Hwt   = hydrogen of wire tested [ppm]

           DP   = dew point [K] (K=°C+273)

V   = voltage [V]

d   = contact tip-to-work distance CTWD [mm]

A   = welding current [A]

It should be noted that, in practice, maintaining constant CTWD is very difficult, since welding is often performed manually with complex and out-of-position weld configurations, and this can result in fluctuations of hydrogen content throughout a given weld section.

Given the conflicting results and lack of detailed study of inter-relation between critical factors, such as arc length and welding current influencing the wire heat energy, further study is required to more clearly define the effect of CTWD.

Fabricators and welding engineers would benefit greatly from a set of recommendations from consumable manufacturers that provide guidance of expected hydrogen levels for different CTWD for a given process / consumable combination [Davidson and Phillips 1999, Sato et al. 1997].

4.4.6   Shielding Gas

There are a wide range of shielding gas types available for continuous gas shielded processes, and their effects on GMAW have been well documented [Lucas 1992, Irving 1994 and Stenbacka et al. 1989]. It is well known that the shielding gases have a pronounced effect on arc characteristics, mode of metal transfer, weld bead dimensions, penetration and wetting properties of molten weld pool, weld metal mechanical properties and weld metal microstructure [Schumann and French 1995, Francis et al. 1990].

As described earlier in Chapter 4.2, gas shielded FCAW is a semi-automatic arc process with continuous consumable feeding that is shielded by an externally supplied gas. Traditionally, shielding gases for FCAW wires were predominantly selected to optimize mechanical properties, welder appeal and costs.

The main function of shielding gas is to stabilize and protect the plasma arc from the surrounding atmosphere, and beneficially influence subsequent reactions with the plasma arc. The chemical composition of shielding gas has a significant influence on arc initiation, surrounding plasma physical dimensions, its temperature [Onsøien 1995] and therefore the wetting ability of the arc. For the FCAW process, commonly used shielding gases include welding grade CO_2 and various ratios of mixed gas Ar-CO_2 (usually up to 25 % CO_2).

Argon has a lower thermal conductivity compared to CO_2 at typical arc temperatures, resulting in expansion of the plasma column beyond the molten wire tip and extension upwards, as shown diagrammatically in Figure 4. 12 (b).
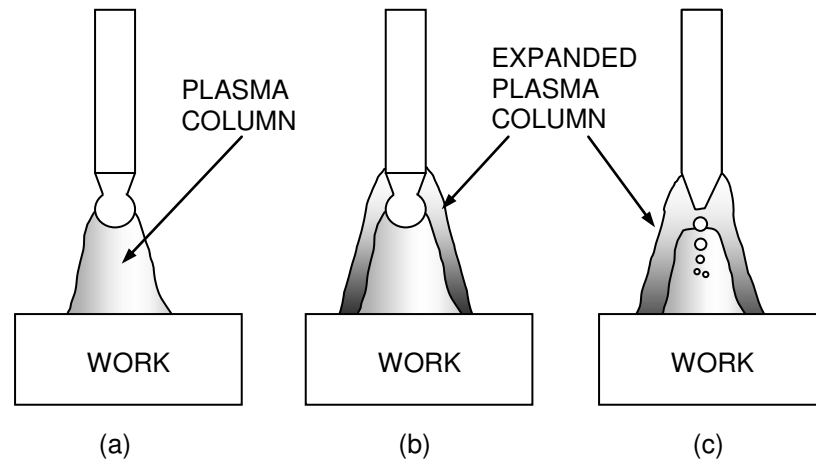
Figure 4. 12   A schematic illustration showing; (a) typical narrow plasma column of high thermal conductivity gases like He and CO_2, (b) typical plasma column of low thermal conductivity gas such as Ar, resulting in its expansion upwards and (c) spray transfer containing fine droplets (after Vaidya 2002).

This heating process will melt wire more rapidly and with a combination of increasing welding current [Norrish 1992], this will create a fast stream of fine droplets impinging on the base plate. It is generally accepted that increasing additions of CO_2 to Ar will progressively shift the fine spray metal transfer mode to more globular [Stenbacka et al. 1989], while reducing the arc stability, and increasing spatter generation and welding fume emissions. Welding fume generation rate (WFR) was found to be significantly reduced by 50 % when CO_2 content was decreased from 25 to 5 % in an Ar-CO_2 mixed shielding gas [Ferree 1995].

A shielding gas with higher content of CO_2 also becomes more oxidizing, resulting in a reduction of Mn and Si from carbon steel and low-alloy steel flux cored and metal cored wires and decreased hardenability, and resulting in a decrease in the proportion of acicular ferrite [Schumann and French 1994]. When using gas shielded flux-cored wires, the single shielding gas CO_2 has also been shown to control the hydrogen increase in the deposited weld metal at increasingly higher humidity atmospheric conditions [Kiefer 1996].

The less reactive Ar-CO_2 mixed gases produce less weld metal penetration, but usually weld deposits are accompanied with better impact toughness properties than those deposited using the more oxidizing 100 %CO_2 gas.

The oxygen potential (OP), generally defined as the oxidizing effect of the shielding gas and/or its significance to the oxygen content of weld metal, also influences the amount of weld surface slag, fluidity of the weld pool and the mechanical properties of the weld metal [Stenbacka et al. 1989]. An empirical formula, Equation 4.5, that defines the oxidation potential for mixed shielding gases containing ≤25 %CO_2 was proposed by Norrish and Richardson (1988). This was proposed as a method of estimating how the oxygen content of weld metal is affected by different gas mixtures:

$$OP = O_2 + \frac{\%CO_2}{2} \qquad (4.5)$$

Calculated values of OP for a given Ar-CO_2 ratios are given in Table 4. 1.

Table 4. 1   Oxidation potential values for a given Ar-CO_2 shielding gas mixture.

Gas mixture [%]		OP
Ar	**CO$_2$**	
100	0	0
98	2	1
95	5	2.5
85	15	7.5
82	18	9
80	20	10
75	25	12.5
0	100	50

The calculated values of OP listed in Table 4. 1 are shown diagrammatically in Figure 4. 13.
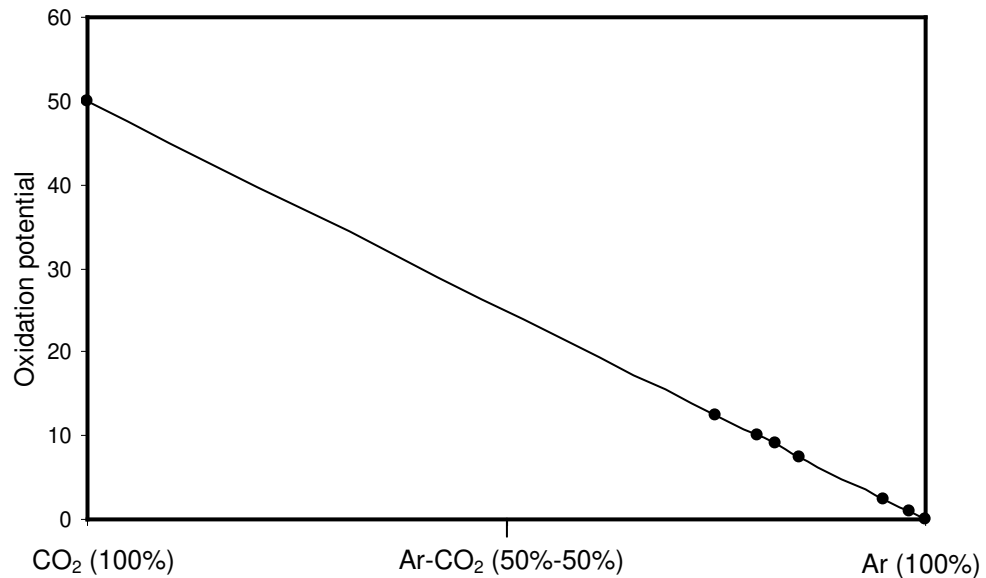

Figure 4. 13   Graph showing the oxidation potential for commercially available shielding gases used for the FCAW process.

It can be seen that a rapid increase of oxidation potential is apparent for mixture gas containing maximum percentage of more than 25 %CO_2. Any further increase of CO_2 leads to impaired metal transfer through the arc and an increase in the amount of spatter [Stenbacka et al. 1989].

Moisture content in the atmosphere is known to contribute to an increase of diffusible hydrogen levels in weld metal [Hirai et al. 1974, Siewert 1985, and McKeown 1985]. Moisture in shielding gases required for the FCAW process can act in a similar way. Therefore, it is important to use dry shielding gases and dry wires when aiming to minimize the hydrogen content in weld deposits for all gas shielded semi-automatic welding processes. Experimental results of work by Wong et al. (1996), when varying the amount of hydrogen content (up to 1 %) introduced into 98Ar-2O_2 shielding gas (measured as a relative intensity

H_2/Ar) resulted in a significant increase of weld metal diffusible hydrogen content. Previous work by Gedeon and Eagar (1990/1) studied the addition of hydrogen up to 2 % into 98Ar-$2O_2$ shielding gas and found also significant increase from 2 to 8 ml/100g of diffusible hydrogen in weld metal with increasing hydrogen. Similar results were found during a study of hydrogen increase in CO_2, where diffusible hydrogen content had also increased [Matsushita et al. 2000]. However, to obtain an increase of 7 ml/100g of diffusible hydrogen in the 100 %CO_2 shielding gas, an addition of 4 % hydrogen was required to be mixed with the CO_2 shielding gas.

It is important to note that gas manufacturers are well aware of the damaging effects of moisture content in the shielding gases, which may contribute to an increase of hydrogen levels and sometimes lead to increased risk of HACC. The maximum allowable moisture contents for various shielding gases are also specified in the relevant standards for shielding gas for welding, such as AS 4882-2003.

When comparing GMAW with the FCAW process, it is important to recognize that for the FCAW process, shielding gases are formulated with consideration of the flux composition of the wires with the aim being to produce specific operating characteristics. The shielding gas is an essential factor influencing the wire-shielding gas reaction occurring within the FCAW plasma arc.

A shielding gas consisting of 100 % CO_2 is generally used for low to medium grade applications and produces a relatively high consumable loss in form of high levels of spatter. Mixtures of Ar-CO_2 are used when positional welding capabilities and better mechanical properties are required. The most popular ratio of Ar-CO_2 mixed gas in the United States is

75-25, in Europe it is 82-18 and in Japan, where the cost of argon is prohibitive, the most popular shielding gas is 100 %CO_2 [Irving 1994].

In the case of rutile deposits, increasing Ar percentage in three gas mixtures (Ar-CO_2: 75-25, 90-10, 95-5) has been shown to result in an increase in the recovery of alloying elements, an increase in yield and tensile strength [Sierdzinski and Ferree 1998] and improvement of low temperature toughness [Schumann and French 1994].

Extensive work by van der Mee (2001) considered the effects of atmospheric storage conditions and the influence of two types of shielding gases, CO_2 and 80Ar-20CO_2 , on weld metal diffusible hydrogen levels for eight commercially available rutile E71 T-1 wires. This work found that for welding in CO_2 compared to the mixed gas Ar-CO_2, the weld metal diffusible hydrogen levels increased for 4, decreased for 2 and remained unchanged for the other 2 of the tested rutile wires. Wires with an identical classification, E71 T-1, but produced by different manufacturers, were found to react differently to a given shielding gas, resulting in different levels of diffusible hydrogen content in the weld metals. Other work by Pitrun et al. (2001) studied the effects of shielding gases on diffusible weld metal hydrogen for four rutile E71 T-1 and two basic T-5 wires, and found an increase of hydrogen levels in all six cases when welding under mixed 75Ar-25CO_2 shielding gas rather than CO_2.

The main aim of the current work (with respect to shielding gas effects) is to examine the effects of CO_2 and 75Ar-25CO_2 mixed shielding gases on characteristics of the metal arc transfer and their influence on diffusible weld metal levels in welds deposited using seamed and seamless rutile flux cored E71T-1 wires.

4.5   EFFECT OF ATMOSPHERIC CONDITION

One of the major issues influencing hydrogen levels in the welds produced by various types of flux-cored wires is the effect of atmospheric exposure. Moisture can be absorbed by a welding consumable even with the greatest care taken during manufacture, packaging and transport. Inadequate or damaged packaging combined with poor storage conditions associated with humid atmosphere can exacerbate the problem and this is a major concern to consumable manufacturers and fabricators. To combat this problem, consumable manufacturers are aiming to develop moisture-resistant electrode flux formulations, which will remain dry when exposed to ambient conditions during welding and storage. Consumable handling procedures are usually provided by manufacturers and commonly specify limited exposure to atmospheric moisture.

The degree to which climatic conditions affect hydrogen absorption by the weld metal depends on the process and the characteristic hydrogen levels of the consumable [Symons 1990]. Some of the important factors include time of exposure, flux composition, the thickness of the flux coating (in the case of MMAW electrodes), and the consumable condition. However, it is the temperature and high relative humidity that are major contributing factors to moisture absorption into MMAW, SAW consumables and FCAW seamed wires. In addition to the above variables, which have a long-term detrimental effect on increasing moisture in the flux, it is also moisture content present in the shielding gas and the immediate atmospheric conditions that can be influential leading to an increase in susceptibility to HACC [Kiefer 1996].

The results of a study by Kiefer (1996) revealed an influence of various dew points for the mixed shielding gas 75Ar-25CO$_2$, as shown in Figure 4. 14.
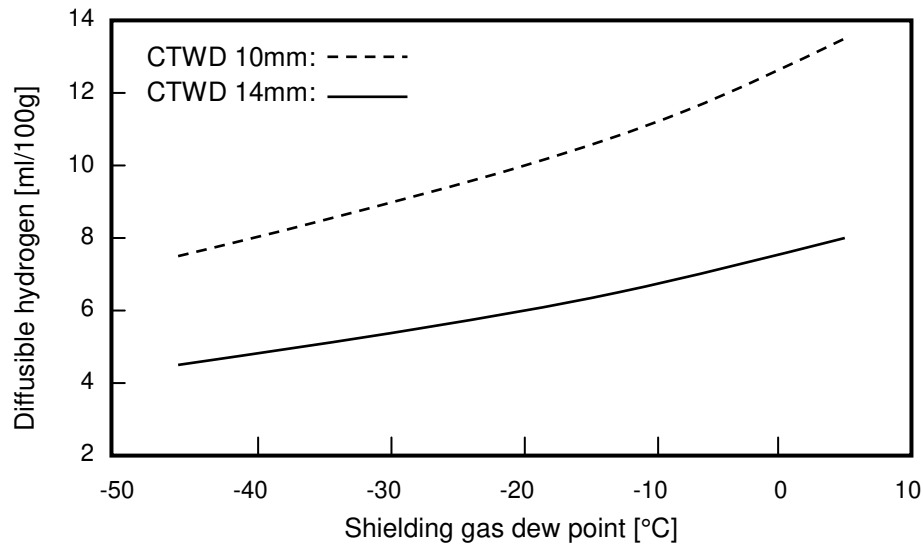

Figure 4. 14   Graph showing the effect of shielding gas dew point on diffusible hydrogen content (after Kiefer 1996).

Both curves indicate an increase of diffusible hydrogen levels at constant heat input of 1.53 kJ/mm over a range of shielding gas dew points for the gas shielded FCAW process.

The contribution of atmospheric conditions to hydrogen content of weld metal deposits for low hydrogen MMAW consumables was extensively studied by Dickehut and Hotz (1991). Their work established a cyclic relationship between the time of year and resultant diffusible hydrogen, where higher hydrogen values were measured during summer and lower values in winter periods. Their study was based over a period of 4 years in the late 1980s, during which time they conducted 1,440 hydrogen tests. A clear link was established between atmospheric water vapour pressure and resultant weld metal diffusible hydrogen levels.

This work subsequently lead into developing a predictive monogram, shown in Figure 4. 15.
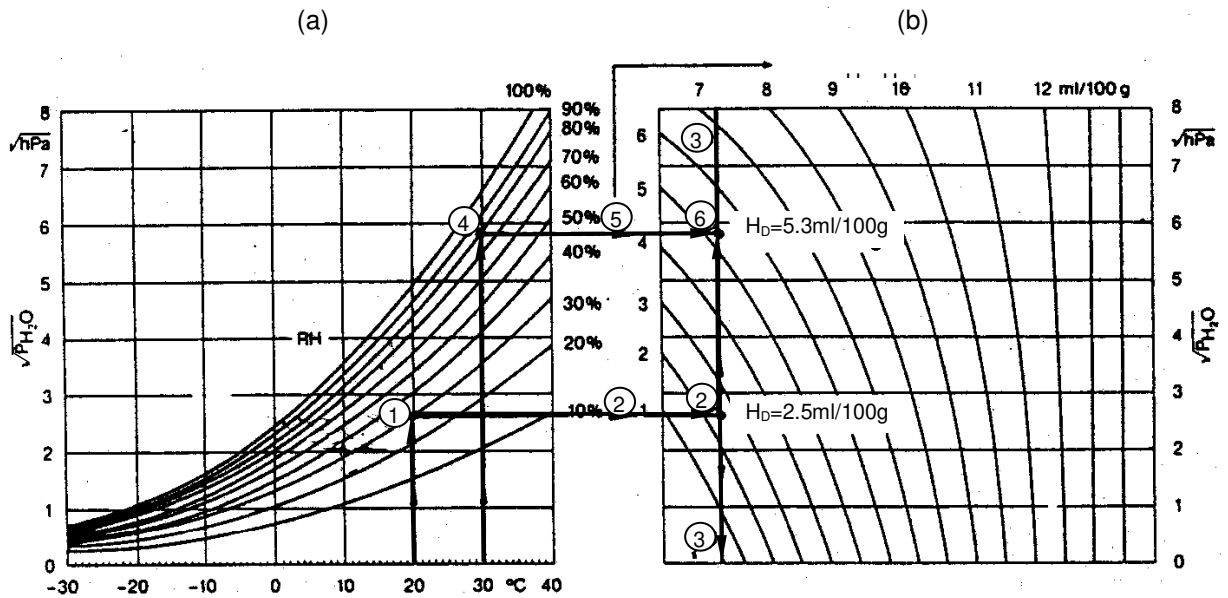
Figure 4. 15   Monograms illustrating the prediction of diffusible hydrogen content in weld metal as a function of atmospheric moisture (after Ruge and Dickehut 1988).

This could be used to predict the diffusible hydrogen at known climatic conditions without the need for testing. The monogram, applicable to basic low hydrogen covered electrodes, demonstrates that as water vapour partial pressure (elevated temperature and humidity) rises, the weld metal hydrogen content is also increased.

The weld metal diffusible hydrogen must be first obtained from known conditions of temperature and humidity (20 °C, 30 %RH) at point [1]. Using the left diagram (a) we plot a horizontal line [2] towards the right diagram (b), marking the point of the known hydrogen value of 2.5 ml/100g. Then draw a vertical line through this point to [3]. From this vertical

line, the predicted hydrogen content $(H_D\downarrow_M)$ can be established for any climate conditions.

So, for example, for temperature 30°C and 80 %RH intercepting in point [4] and drawing

horizontal line [5], the predicted weld metal hydrogen level would be 5.3 ml/100g [6].

Moisture contaminated consumables can significantly affect the weld metal hydrogen content,

even for basic, moisture resistant welding consumables [Chew 1976]. When comparing rutile

flux-cored wire E71 T-1 with basic MMAW electrode E7018, the flux-cored wire revealed

much lower adsorption rate that the MMAW, most probably due to the fact that moisture can

only reach the interior flux through the narrow seam and lower flux-to-metal ratio [Siewert
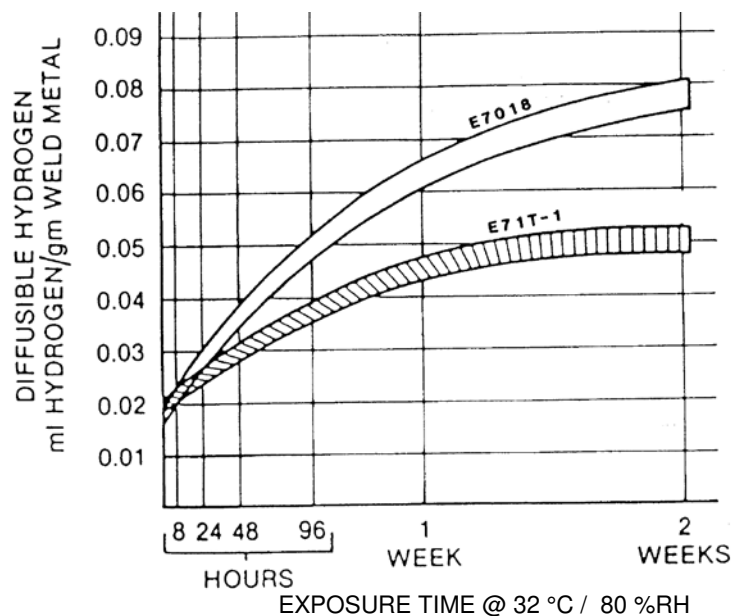
1985], as shown in Figure 4. 16.

Figure 4. 16   Graph comparing moisture adsorption by MMAW basic consumable (E7018) and rutile FCAW wire (E71 T-1) (after Siewert 1985).

A linear increase of weld metal hydrogen content was experimentally observed by increasing

the absolute moisture content in the air [van Wortel 1993]. It was established that by an

increase of 10g H_2O/m^3 air causes an increase of the weld metal hydrogen level by approximately 0.9 ml/100g.

In a similar manner to MMAW consumables, the occurrence of moisture pickup by seamed flux-cored wires at 30 °C / 80 %RH has also been observed [Kuebler et al. 2000], as shown in Figure 4. 17.
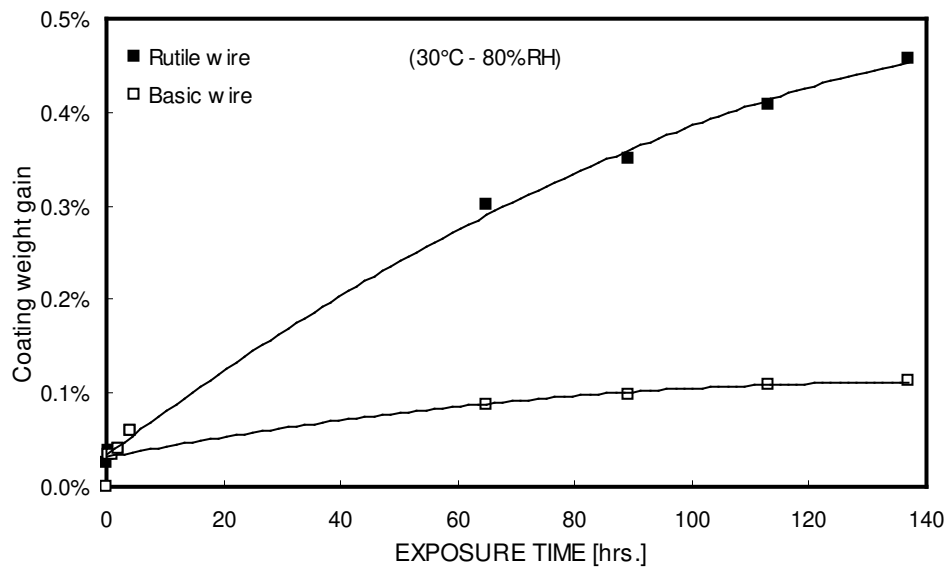
Figure 4. 17   Graph showing a comparison of moisture gain for rutile and basic FCAW wires (after Kuebler et al. 2000).

These results showed two different weight gain rates for rutile and basic wire due to differentiation in the flux formulation used for these wires. Basic wires E71 T-5 were found to be more resistant to increased diffusible hydrogen than rutile E71 T-1 [Harwig et al. 1999 and Pitrun et al. 2001]. The basic flux cored wires with their fluoride based flux system are also known to be tolerant to hydrogen by lowering the partial pressure of hydrogen in the arc

environment. The lower the partial pressure of hydrogen, the lower the equilibrium solubility of hydrogen during welding in the weld pool.

Studies by Harwig et al. (1999) and Pitrun et al. (2001) also concluded that wires of the same classification can yield different diffusible hydrogen levels when exposed to a humid environment due to their flux formulation and type and quality of wire seam joint.

An earlier study by Harwig et al. (1999) examined the effects of atmospheric moisture on hydrogen content of welds deposited by FCAW wires using mixed gas 80Ar-20CO$_2$. For example, one rutile wire was characterized by an increase in diffusible hydrogen from 4 to 8 ml/100g after one week exposure representing 100 % increase. In comparison, the second rutile wire recorded an even higher increase from 8 to 27 ml/100g [Harwig et al. 1999]. After a period of one year of atmospheric exposure the wires were re-tested, and the results confirmed similar values of weld metal diffusible hydrogen. Work by Harwig et al. (1999) concluded that all examined wires, basic (E71 T-5) or rutile (E71 T-1), exposed for a week to 27 °C and 80 %RH, were susceptible to moisture increase.

Long-term exposure tests (one year in their original containers inside of air-conditioned room) also produced welds with higher diffusible hydrogen levels. Interestingly, higher atmospheric humidity, from 5 to 30 g/m^3 of moisture had increased the diffusible hydrogen for CO$_2$ shielding gas only by 2 ml/100g [Levchenko et al. 1978]. Other work by Kiefer (1996) and Ferree (1992), relating to welding with CO$_2$ shielded gas, confirmed that an increase in atmospheric humidity from 10 to 61 %RH at unchanged temperature of 29-31 °C had only a marginal effect on the diffusible hydrogen levels, representing an increase of 1-2 ml/100g.

Obviously, in the gas shielded FCAW process the prediction of diffusible hydrogen levels may be more complicated due to unexpected drafts or other external gas/air turbulences upsetting the protective gas envelope. Poor shielding conditions [Widgery 1994], or an excessive amount of hydrogen taken into the molten weld pool, can also cause the formation of large traces of gas trails often referred to as 'worm-holes' running inside and/or on the outer surface of the weld bead beneath the flux layer.

From the experimental results reported by various researchers on the effects of atmospheric conditions, it is clear that not only are different wire classification (basic and rutile) affected differently, but the wires of the same classification from two manufacturers can react in a different way when exposed to the same atmospheric conditions. When assessing the effect of Ar-CO_2 shielding gas at a particular welding condition, it appears that increased temperature and relative humidity has less effect on diffusible hydrogen level than when using 100 %CO_2 shielded gas. However, considering the results of another study examining the effects of atmospheric exposure on the diffusible hydrogen content [van der Mee 2001], it is unlikely that any single formula will give an absolute prediction for the effect of atmospheric condition on diffusible hydrogen levels. It is apparent that the relationship between interacting variables, such as shielding gas type, atmospheric conditions and different flux formulations, is a complex one, but nevertheless very important for proper consideration of effect on diffusible hydrogen content.

4.6   SU MMARY

HACC represents a significant threat to the integrity of welded steel structures. There have been a number of reviews on the phenomenon of hydrogen cracking in steel weldments that reflect the general understanding that the main factors determining susceptibility to HACC include the presence of diffusible hydrogen, residual stresses and microstructure [Yurioka and Suzuki 1990, Davidson 1995 and Dunne 1999]. The greater part of past work on understanding the mechanism for this phenomenon has concentrated on cracking in the HAZ of the parent metal. Numerous welding standards have been developed to provide guidance on processing parameters for minimization of HACC in the HAZ [AS/NZS 1554.1-2000 and ANSI/AWS D1.1-2000]. However, with a significant progress in developing thermomechanically controlled processed steels resulted in an increased resistance to HACC in the HAZ, and enabled to use of lower preheat temperature during welding fabrication. This improvement in the HACC resistance of parent metal has shifted the problem of cold cracking to the weld metal.

The importance of grouping of welding consumables in accordance to their hydrogen classifications was early recognized in view to have a better control over the amount diffusible hydrogen content in weld metal. However, as a result of some recent cases of transverse weld metal HACC in low strength structural steel fabrications in Australia, research efforts have intensified with a view to better understanding how welding parameters can affect HACC, specifically in the welds deposited using gas shielded FCAW process.

The influence of welding parameters on diffusible hydrogen levels in the weld deposits of flux-cored wires has been a subject of previous work [White et al. 1992, Sierdzinski and

Ferree 1998]. Although these early studies illustrated a great importance of the welding parameters, such as welding current and CTWD on the diffusible hydrogen in weld metal, neither of the studies were examining the effects of welding parameters on the susceptibility of weld metal to cold cracking.

The main aim of the current work was to investigate the effects of FCAW welding parameters, such as welding current, CTWD and shielding gas type on diffusible hydrogen content for single weld bead using seamed and seamless rutile flux-cored wires. Two commercially available, gas shielded, low strength rutile wires as classified in the Australian Standard AS 2203.1-1990, equivalent to the American Standard ANSI/AWS A5.20-95 (the current work adopts the ANSI/AWS A5.20-95 classification of flux cored consumables, where rutile wires are referred to as E71 T-1 and E71 T-1M, rather than more complex AS 2203.1-1990 terminology). Adopting the International Institute for Welding (IIW) benchmarks, the two consumables, described as H5 and H10 were selected for this work containing levels of diffusible hydrogen of <5 ml/100g and <10 ml/100g, respectively. These two wire types are considered to have potentially the most widespread application for FCAW of C and C-Mn steels in the Australian general construction industry.

In order to provide more information on metal transfer and determination of arc length as affected by the welding parameters, the work included an investigation of arc characteristics under typical welding conditions and two shielding gases ($75Ar-25CO_2$ and CO_2), using high speed digital imaging and laser backlighting.

Although there is a considerable amount of experimental data available examining the effects of temperature on susceptibility of various weld metals to HACC using the G-BOP test

[Graville et al. 1974, Mc Parlan et al. 1976, Chakravarti et al. 1989, Hart 1989, Graville et al. 1995 and Atkins et al. 2002], there is no scientific data currently available with respect to cold cracking behaviour in the weld metal affected by welding variables and shielding gases.

In this work, the G-BOP test has been used to investigate significance of welding parameters, such as welding current, CTWD, shielding gases and amount diffusible hydrogen on the susceptibility of deposited weld metal to transverse cracking both H5 and H10 wires.

CHAPTER 5

Experimental Methods, Equipment and Materials

5.1   FCAW WELDING PROCESS

The FCAW process has been available commercially for about 40 years and the welding industry has become well familiar with the benefits of this process, as mentioned in Chapter 4.2. However, there appears to be limited consistency in published experimental data regarding the effects of welding parameters or hydrogen content in deposited weld metal, particularly for low strength carbon steel wires.

The main aim in the present work was to examine the effects of various interacting welding parameters for carbon steel flux-cored wires, which are commonly selected for welding of C and C-Mn steels. The current work was concerned primarily with the determination of hydrogen concentration in deposited weld metal and testing of HACC susceptibility using gas-shielded FCAW process and rutile, low strength welding consumables E71 T-1, with nominal hydrogen contents of 5 and 10 ml/100g.

5.1.1   Welding Equipment

All welding experiments in this study were carried out using a conventional welding power source, a Transmig 400 designed and manufactured by CIGWELD, widely used for continuous gas-shielded wire processes (GMAW and FCAW). The welding machine with flat output characteristic, and a transformer rectifier is shown in Figure 5. 1.

Supply voltage	: 380 – 415 V
Welding arc voltage range	: 16 – 33 V
Operating frequency	: 50 Hz
Number of output voltage step	: 36
Welding current range	: 22 – 400 A
Wire feed speed:	: 2.0 – 20.0 m/min
Duty cycles	: 60% at 350 A
	: 46% at 400 A
Wire diameter range GMAW:	up to 1.6 mm
FCAW :	up to 2.4 mm

Figure 5. 1   Photograph of a conventional welding machine Transmig 400 and the associated manufacturer's specifications.

This 3-phase DC welding machine is generally recognized as a "heavy duty welder" with dual inductance. This welding equipment allows good control of welding parameters, such as welding current, voltage and wire feed speed, using a remotely controlled wire feed speed dial on the wire feeder (Transmig 4R) which is attached on the top of the welding machine.

To allow full control of welding parameters, such as constant travel speed, position of the welding torch and CTWD, the welding torch was fixed onto a traveling mechanism mounted on the top of the frame, which allowed continuous horizontal movement under controlled conditions, as shown in Figure 5. 2.

Figure 5. 2   Photograph showing the welding jig used in the current work with the traveling mechanism located at the top of the frame, with the welding torch firmly attached.

A separate screw mechanism on a mounting console allowed for adjustments for vertical positions as required for various distances between the working piece and contact tip.

As typically used for gas shielded flux cored arc welding, the copper contact tip of the welding torch was positioned 1mm inside of the outside shielding nozzle, as shown in Figure 5. 3. The torch remained in a 90° position relative to the work at all times for all experiments.

In order to maintain acceptable running characteristics at the selected arc voltage of 30 V, the wire feed speed was adjusted for each welding current setting of 280, 300 and 320 A. The arc voltage setting 'Coarse' and 'Fine' positional switches on the front panel of the Transmig 400 welding equipment remained unchanged for all the welding currents used. The front panel

voltage switches were in 'high' and '5' positions, respectively. From these settings, the voltage observed on the welding equipment panel voltmeter varied between 29-30 V. The welding current and voltage values were measured between the welding torch and work piece using a multi-meter for each setting of welding current, CTWD and shielding gas.
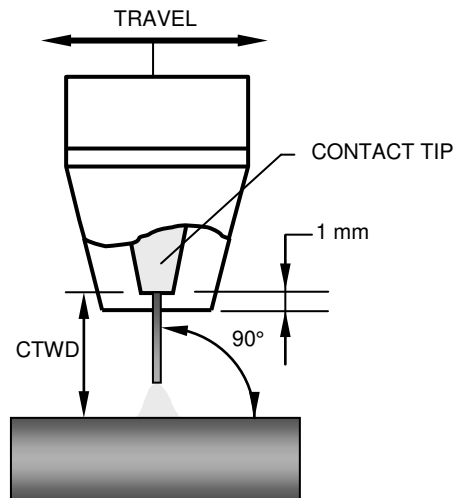
Figure 5. 3   A diagram showing the contact tip position relative to the shielding nozzle used during welding.   [not to scale]

5.1.2   Welding Consumables

In Australia there are two standards for carbon steel flux-cored wires that are commonly used in the industry, ANSI/AWS A5.20-95 and AS 2203.1-1990. However, the wire classification system referred to in these standards and the specification of nominal hydrogen levels vary significantly.

The current work adopts the American ANSI/AWS A5.20-95 classification system for flux-cored consumables, rather than the more complex AS 2203.1-1990 Australian terminology. In this way the low strength rutile consumables used in the current work are referred to as E71T-1 rather than ETP-GMp-W503A as in AS 2203.1-1990. In addition, specification of

hydrogen levels in the current work adopts the ISO 3690-2000 and AS 2203.1-1990 benchmarks, with the wires further designated as H5 and H10, with nominal levels of diffusible hydrogen in deposited weld metal of 5 and 10 ml/100g, respectively. These designations are more common specification levels for consumable hydrogen levels used in Australia.

Two commercially available tubular gas shielded flux cored wires of 1.6 mm in diameter were used in this current work. These two wire types, with their relevant classifications shown in Table 5. 1, are considered to have potentially the most widespread application for flux cored welding of C and C-Mn steels in the Australian general construction industry for all positional applications.

Table 5. 1 An outline of the types of FCAW consumables selected and their all weld metal mechanical properties.

Wire Sample ID	Consumable Classification		Wire Cross-Section
	AS 2203.1	ANSI/AWS 5.20	
H5	ETP-GMp-W503A CM1 (H5)	E71T-1 (H4)	seamless
H10	ETP-GMp-W503A CM1 (H10) ETP-GCp-W503A CM1 (H10)	E71T-1 (H8)	seamed

Mechanical Properties (typical)

Wire Sample ID	Shielding Gas	YS [MPa]	TS [MPa]	Elongation [%]	CVN [J] @ 0 °C	CVN [J] @ -20 °C
H5	75Ar-25CO_2	490	570	26	-	60
	CO_2	-	-	-	-	-
H10	75Ar-25CO_2	480	560	28	110	90
	CO_2	460	530	30	90	75

Both the seamed (H10) and seamless (H5) wires are micro-alloyed rutile types based on a titanium-boron flux composition. The H10 wire is classified for mixed Ar-CO_2 gas used as well as for CO_2 shielding gas, while the H5 wire is not recommended for use with CO_2 shielding gas.

The wires not only significantly differ in the nominal hydrogen levels but also in their cross-section design, as shown in Figure 5. 4. From two wire cross-sections, it is apparent that the butt seam of H10 wire is not fully closed leaving approximately 0.1 mm gap, thereby allowing the ingress of moisture or wire lubricant through seam during the manufacturing process. Similar gaps have been also observed on other wires supplied by different manufacturers.

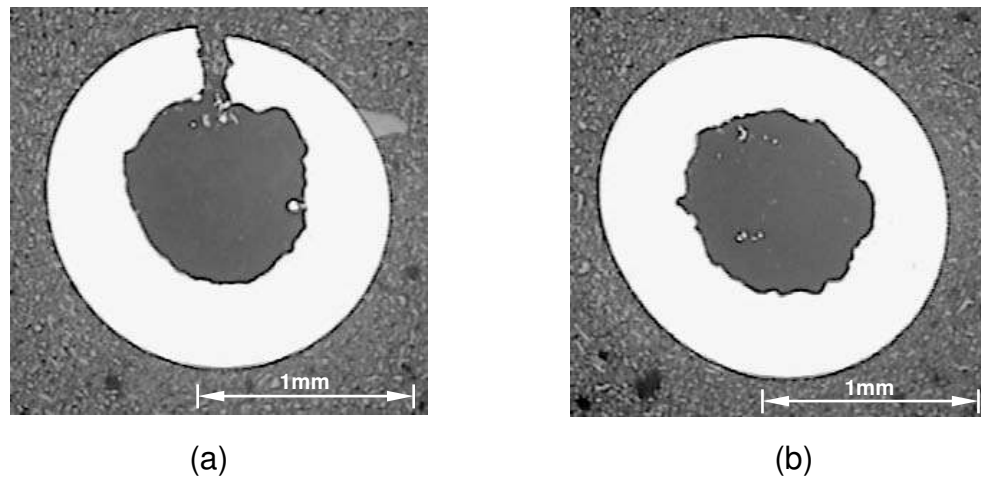(a)   (b)

Figure 5. 4   Photograph showing a cross-section of the (a) seamed H10 consumable and the (b) seamless H5 consumable.

The seamless wire H5 is copper coated to prevent wire surface oxidization and for improving wire feedability, and is not susceptible to the ingress of moisture into its flux core. The manufacturer of the H5 wire refers to hydrogen levels of <2 ml/100g for deposited weld metal when welded straight from the carton or store [http://www.oerlikonweld.com]. Such extremely low hydrogen values represent a considerable cost reduction factor, since lower

preheat temperatures can be employed by fabricators and without increasing the risk of HACC.

The chemical compositions of 'all weld' metal deposits were carried out in accordance to the Australian standard AS 2203.1-1990 for the two wires used in the current work. The calculated carbon equivalent CE_{IIW} and Pcm values, were determined after welding with both mixed 75Ar-25CO$_2$ and CO$_2$ shielding gases are shown in Table 5. 2.

Table 5. 2   Chemical composition of 'all weld' metal deposits of H5 and H10 FCAW consumables, using 75Ar-25CO$_2$ and CO$_2$ shielding gas [element % weight].

	All weld metal analysis of wire samples (shielding gas used)			
	H5		**H10**	
Element	(75Ar-25CO$_2$)	(CO$_2$)	(75Ar-25CO$_2$)	(CO$_2$)
C	0.043	0.050	0.070	0.065
Mn	1.46	1.25	1.41	1.15
Si	0.59	0.47	0.61	0.48
S	0.009	0.010	0.011	0.012
P	0.011	0.011	0.012	0.012
Cr	0.055	0.054	0.027	0.025
Ni	0.051	0.052	0.025	0.024
Mo	0.008	0.008	0.003	0.002
V	0.014	0.013	0.015	0.015
Cu	0.14	0.15	0.029	0.025
Nb	0.011	0.010	0.012	0.010
Ti	0.044	0.042	0.051	0.039
Al	0.008	0.007	0.004	0.003
B	0.0043	0.0032	0.0090	0.0077
N	0.0084	0.0097	0.0042	0.0067
O	0.0430	0.0590	0.0585	0.0545
Fe	Rem.	Rem.	Rem.	Rem.
CE_{IIW}	0.31	0.29	0.32	0.28
Pcm	0.173	0.159	0.210	0.183

(ref: BHP Lab analysis report: M02/3319)

While CE_{IIW} values remain very similar for H5 and H10 wires, the Pcm value for H10 wire sample was noticeably higher for both shielding gases used, most likely due to relatively higher levels of boron in the H10 weld metal deposits. This is shown diagrammatically in Figure 5. 5.
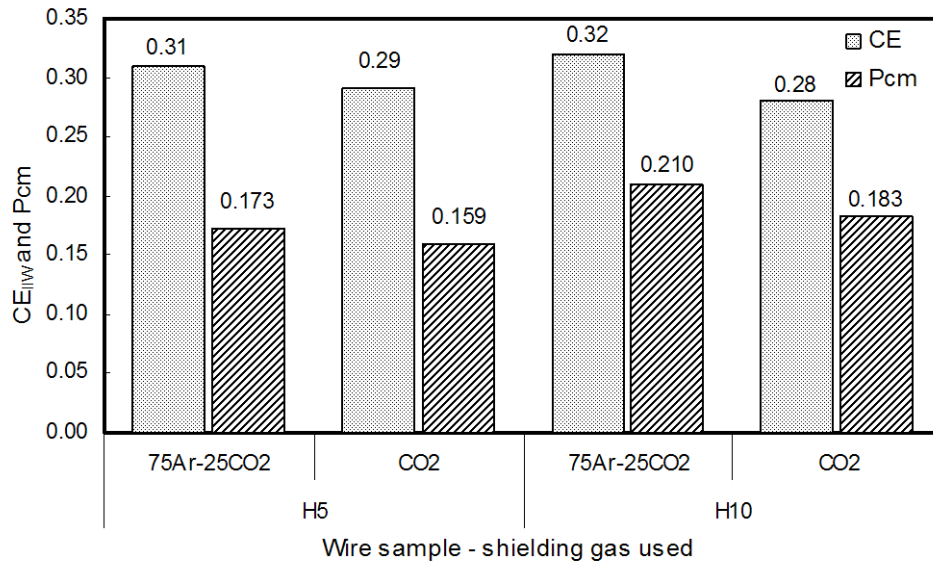

Figure 5. 5   Graph showing the CE_{IIW} and Pcm values for H5 and H10 'all weld' metals welded using 75Ar-25CO$_2$ and CO$_2$ shielding gas (ref: Table 5. 2).

The use of CO$_2$ shielding gas reduced Mn, Si and B recovery resulted in marginally lower CE_{IIW} and Pcm values for both consumables. It should be noted that the CE_{IIW} and Pcm values were calculated from multiple layer 'all weld' metal deposits, as specified in the AS 2203.1-1990 and different values would be obtained from a single weld bead due to the dilution effects.

In order to avoid a variation of results caused by a possible inconsistency between the batches of examined wires, the entire experimental work was carried out by using only one spool from each wire supplied. After completion of each experiment, the wire was re-packed into its

original packaging and stored in dry conditions at ambient temperature. In this way, the effect of long time exposure of wires to varying atmospheric conditions between the experiments was kept to minimum.

5.1.3   Shielding Gas Compositions

Various mixtures of shielding gases will influence the arc transfer physical characteristics, mode of metal transfer, weld bead dimensions, penetration and wetting properties of weld pool, as well as weld metal mechanical properties [Stenbacka et al. 1989, Lucas 1992 and Irving 1994].

In this work, where the main aim of the study was to examine the effects of shielding gases on the hydrogen levels in deposited weld metal and their contribution in cold cracking susceptibility for H5 and H10 wire samples, two types of commonly used shielding gases were used; 75Ar-25CO_2 and welding grade CO_2. Both gas bottles containing 75Ar-25CO_2 and CO_2, which were used during the weld metal hydrogen testing of welding consumables and later for the transverse weld metal cracking susceptibility, were also submitted for moisture analysis at the BOC Gases chemical laboratories. The actual analysis results on moisture content of 75Ar-25CO_2 and CO_2 shielding gases are shown in Table 5. 3.

Table 5. 3   A description of the shielding gases (75Ar-25CO_2 and CO_2) used in the current work, including measures of oxidation potential and moisture content.

Gas type	Cylinder No.	Batch Label	Oxidation Potential (O_2 % + 0.5 x CO_2 %)	Moisture [ppm]
75Ar-25CO_2	AFB 226	070 G22	12.5	2.9 ± 0.5
CO_2	SKA 03083	080 GB	50	25 ± 6

(ref: BOC Gases analysis report: Q2E 21)

The gas supplier confirmed that the moisture results were commercially acceptable and in accordance with the relevant gas manufacturing standards allowing the moisture contents of 40 and 200 ppm maximum for argon and carbon dioxide shielding gases, respectively [AS 4882-2003 and EN 439-1994].

5.2   WELD METAL HYDROGEN ANALYSIS

Measurements of diffusible hydrogen content provide the means of determining the degree to which a given welding consumable is likely to introduce hydrogen into the weld. In this way hydrogen measurements are used to categorize and classify different welding consumables [ISO 3690-2000].

There are two principal ways in which the International Standard [ISO 3690-2000], is intended to be used:

a) to enable a consumable to be classified and to assist in quality control, and

b) to provide information on the levels of weld hydrogen levels arising from the different welding conditions (e.g. wet or dry) or welding parameters (e.g. different welding currents) chosen for each test, so that misunderstanding between these hydrogen levels and classification levels are prevented.

In the current work, hydrogen test pieces were prepared, welded and analysed for diffusible hydrogen content in accordance with ISO 3690-2000: "Welding and allied process – Determination of hydrogen content in ferritic steel arc weld metal".

5.2.1 Testing Equipment and Procedures

The weld metal hydrogen experiments were carried out at CIGWELD welding laboratories in Melbourne, Australia with no control over the atmospheric conditions at the time for each test. The experiments were carried out following a procedure:

 1) Sample preparation:

The center and run-on / run-off test pieces were made from a plain carbon steel equivalent to AS 3678-1999 Grade 250. For removal of residual hydrogen prior to welding, the samples were heat treated at 650 °C ±10 °C in an inert atmosphere, machined by surface grinding and cut to size in accordance with ISO 3690-2000. Each center-piece sample was then uniquely marked and their weight was measured to within an accuracy of ± 0.0001 g.

All test pieces were then degreased using methyl spirit and subsequently washed in an acetone bath. The surface of the samples was then quickly dried using compressed nitrogen gas and to avoid the samples surface contamination they were immediately stored in a furnace with temperature set to 100 °C. This controlled environment allowed the samples to be protected against possibility of surface contamination due to undesirable atmospheric condition when welding of the samples was not undertaken immediately after surface degreasing. Prior to welding, the samples were taken out of the furnace and cooled down to an ambient temperature.

 2) Test assembly:

To enable the quenching that is required for retention of hydrogen in the welded samples immediately after completion of welding, iced water mixture and a solid carbon dioxide and acetone slurry at –78 °C were prepared as quenching medium.

With reference to ISO 3690-2000 and AS/NZS 3752-1996, both standards allow two sizes of welding copper jigs. Smaller jigs are used for welding up to 2 kJmm^{-1} and larger ones where a heat input between 2 and 3 kJmm^{-1} is involved. In this current work, the large type of copper welding jig with a quick release lever clamp, complying with both testing standards, was made available by the Defence Science and Technology Organisation (DSTO) laboratories in Melbourne Australia, as shown in Figure 5. 6.
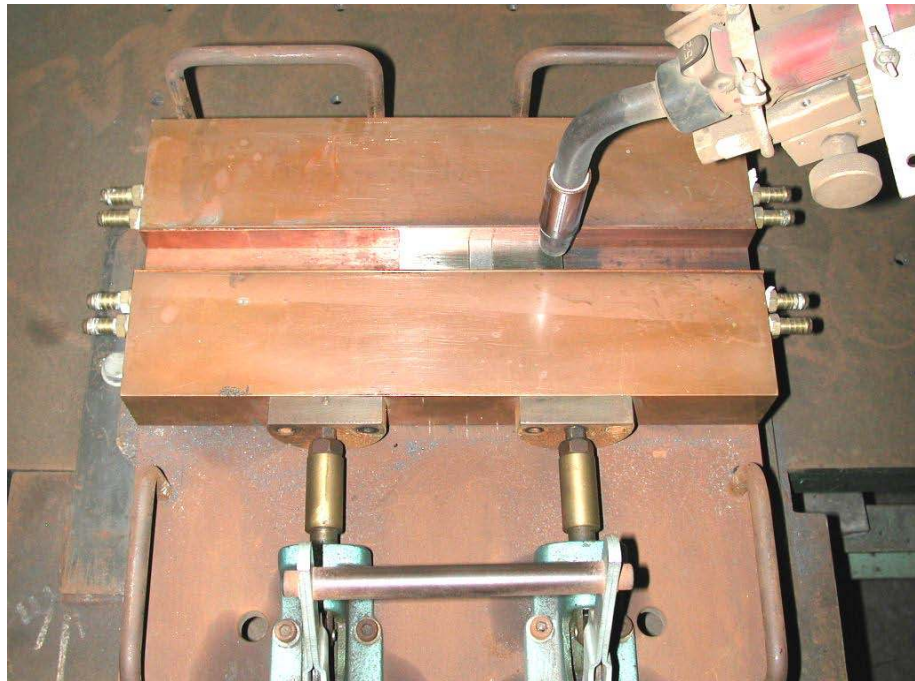

Figure 5. 6   Photograph showing general view of the large welding fixture used and the test piece assembly ready for welding.

Despite the fact that the range of heat inputs used in this current work (1.26 – 1.44 kJmm^{-1}) was less than 2 kJmm^{-1}, the preliminary experiments revealed that the weld deposits were nearly as wide as the actual recommended 15 mm width of sample proposed by the ISO 3690-2000. This weld-to-samples width predicament was resolved by rotating the center piece such

that it was transverse to the welding direction, similarly to the method employed by White et al (1992).

The assembled test pieces with a single weld bead deposited and clamped in the welding jig fixture with 1 mm thick copper shims are shown schematically in Figure 5. 7.
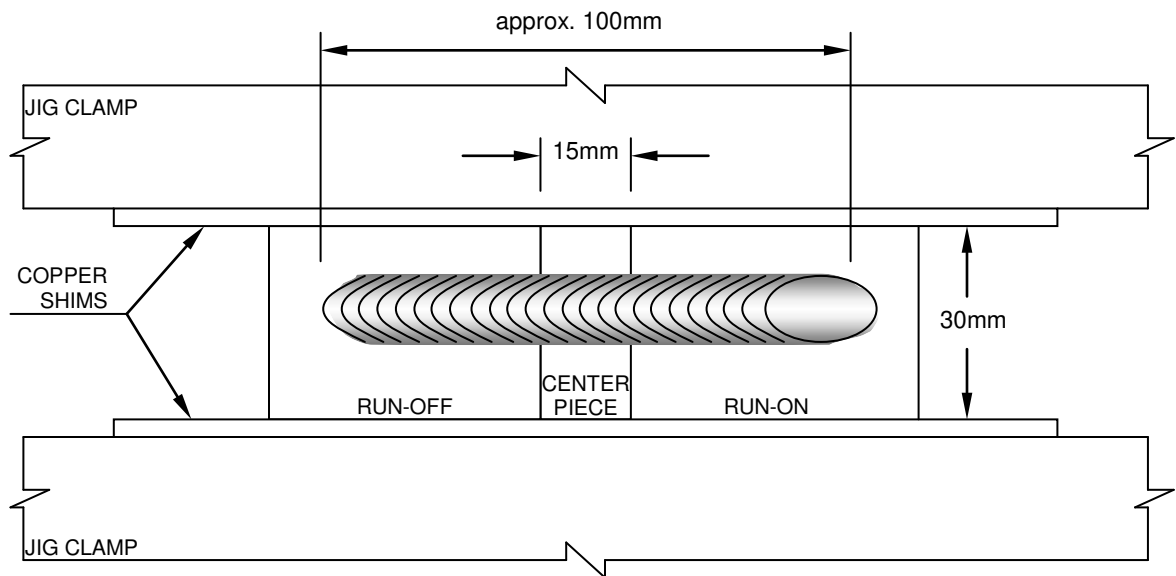

Figure 5. 7   A diagram showing the test piece assembly in the welding test jig and a single weld bead.   [not to scale]

The welding fixture was designed to allow for water cooling if required. However, cooling was not necessary during welding as the welding jig had remained within the temperature limits recommended by the standard.

 3)   Welding and handling of test samples:

Prior to welding of hydrogen test samples, welding parameters (e.g. welding current, CTWD etc.) were adjusted and checked using a dummy test plate. Once the welding parameters were

set, and after recording of atmospheric conditions for each test, welding had proceeded on the hydrogen test samples. After extinction of the arc, the welded test samples were quickly released from the welding jig and immersed as soon as possible into stirred iced water. The samples were then cleaned of flux using a chipping hammer before being immersed in a low-temperature bath containing a solid carbon dioxide and acetone mixture at -78 °C. Samples could be stored in this way for up to three days [ISO 3690-2000].

After about 10 minutes, the welded samples were then taken out from the carbon dioxide slurry and the run-on and run-off extensions were quickly broken away from the center piece used for analysis. The total time that each welded sample was exposed to ambient conditions, including cleaning and removal of run-on run-off blocks, was estimated to be approximately 20 seconds.

Three sets of test samples were made for one set of welding parameters in accordance with ISO 3690-2000. Welding conditions and atmospheric conditions were recorded for each set of samples.

4) Hydrogen analysis and handling:

After all centre pieces were cleaned, the samples were individually taken out from the carbon dioxide and acetone slurry container for the last time and placed into water bath till ice melted on the sample surface, which took between 8-10 seconds. Immediately after this, the sample was placed into acetone and quickly dried with compressed nitrogen. Dried samples were then promptly placed into capsules, attached to the sampler and individually purged using a high purity grade argon gas for 30 seconds and using Oerlikon-Yanako hydrogen analyser model G-1006 at CIGWELD chemical laboratories.

All the test samples were analysed using the gas chromatography method at 150 °C for 6 hours and tested within 2 hours of completion of welding. Three samplers placed in a couple of Oerlikon-Yanako electrical heating furnaces (model GT-1006) set to 150 °C, are shown in Figure 5. 8.

Figure 5. 8   Three samplers placed in the temperature controller electrical furnaces set for 150 °C for 6 hours exposure.

After 6 hours, the samplers were allowed to be cooled down to ambient temperature, and then connected to the hydrogen analyser as shown in Figure 5. 9.

Figure 5. 9   Photograph showing a sampler connected to the Oerlikon-Yanaco Gas Chromatographer (model: G-1006).

According to specified manufacturers procedure by Oerlikon-Yanako, the analyser was calibrated prior to collecting hydrogen accumulated from each capsule. Obtained values of hydrogen were then recorded and sample weights measured to calculate the amount of hydrogen levels in deposited and fused weld metal, as described earlier in Chapter 2.

The measured hydrogen values in this work are expressed in terms of hydrogen in ml/100g of deposited weld metal, H_D, using Equations 2.12 and 2.13 and fused weld metal, H_F, following Equation 2.14.

5.2.2   Welding Parameters

In this work, three welding variables were selected for studying their effects on diffusible hydrogen levels as listed in Table 5. 4. The chosen welding parameters range, were within the recommended ranges from both wire manufactures, and reflect the general industrial practice for welding in downhand position.

Table 5. 4   Matrix of welding parameters investigated in this current work to determine effect on weld metal diffusible hydrogen content in H5 and H10 weld deposits.

Welding Parameter	Testing Range
Welding Current [A]	280 – 300 – 320
CTWD [mm]	15 – 20 – 25
Heat Input [kJ/mm]	1.26 – 1.35 – 1.44
Shielding Gas [18 l/min]	75Ar-25CO_2 and CO_2
Welding Voltage♣ [V]	29 – 30
Travel Speed♣ [mm/min]	400

Notes:

♣ Not investigated parameters

Under the selected welding parameters, the wires generally exhibited good stable arc characteristics with what appeared to be a spray transfer at the optimum welding conditions. No attempts were made to compare the operating characteristics of the individual wires, other than by the arc imaging method described later in this Chapter.

5.2.2.1   Welding Current

In this work, the direct current electrode positive polarity was used at all time, as recommended by the wire classification.

In order to maintain appropriate wire burn-off rate with increasing current, while keeping acceptable arc characteristics for higher welding currents, the wire feed speed had to be increased. The relationship between wire feed speed and welding current is typically described in the form of burn-off curves [Norrish 1992], which predominantly depend on the wire cross sectional area, electrode resistivity and the CTWD, as described in Chapter 4.

The aim of varying welding currents between 280, 300 and 320 A was to find responses in weld metal diffusible hydrogen levels and the significance of welding current in combination with other parameters. The wire feed speed was measured and recorded for each welding condition selected after completion of welding. This was done by measuring the actual length of wire leaving the welding torch without arcing for a period of time.

5.2.2.2   CTWD

The CTWD is defined as the distance between the contact-tip and the work-piece, as shown in Figure 4.11. It includes the wire length from the contact-tip, to the arc entry point and the arc length itself. The longer the CTWD, then the time that the wire spends in the resistive heating zone increases, resulting in enhanced removal of lubricants and moisture on the wire surface and/or from inside the wire. The opportunity to evaporate any residual moisture or decompose any hydrogen-bearing materials on the wire surface is reduced at shorter CTWD.

Since there appears to be some controversy arising from the results of previous research work [White et al. 1992, Kiefer 1996 and Harwig et al. 1999], it is clear that further work is required to more closely define the influence of interrelated physical dimensional parameters, such as the proportion of solid wire and the arc length.

In this current work, three commonly used contact to work distances for downhand welding, 15, 20 and 25 mm, were selected to examine the effect on deposited weld metal hydrogen content.

5.2.2.3   Shielding Gases

The aim of the study was to examine the effects of $75Ar-25CO_2$ and CO_2 shielding gases on the hydrogen levels in deposited weld metal for H5 and H10 wire samples. The gas flow was maintained at 18l/min at all time during all experimental work. The measured moisture levels of $75Ar-25CO_2$ and CO_2 shielding gases used in this current work were 2.9 and 25 ppm, respectively, and were within the gas classification standard [AS 4882-2003 and EN 439-1994].

5.3   G-BOP TESTING

The gapped bead-on-plate (G-BOP) test was selected to study the susceptibility of weld metal to hydrogen transverse cracking. It was chosen since it is a relatively simple procedure, using a bead on plate and is well known as a reliable method for generating transverse cold cracking. Importantly, it allows the use of identical welding parameters as used for the hydrogen testing.

The aim was to observe the effect of preheat temperatures on susceptibility to cold cracking for a range of welding conditions with 'known' hydrogen levels measured in range of reference hydrogen tests.

5.3.1   Equipment and Materials

The G-BOP tests were carried out at CIGWELD welding laboratories using the same welding equipment as for the diffusible hydrogen tests. This enabled the same control of welding parameters, such as constant travel speed, position of welding torch and CTWD.

Further to this, all of the G-BOP experiments were conducted by using the identical spools of wire that were used in the welding trials for the weld metal hydrogen testing. Therefore, other than for the effects of varying atmospheric conditions recorded for each set of test samples, possibility of variation in diffusible hydrogen levels between the two sets of results was reduced.

The G-BOP test samples were prepared from a 50 mm thick rolled plate (BHP heat number *YP116 A1-01*) material equivalent to AS 3678-1999 Grade 250 with a chemical composition as shown in Table 5. 5.

Table 5. 5   Chemical composition of parent material used for G-BOP test.

Element[%]	Analysis type	
	Check	Ladle
C	0.165	0.15
Mn	1.23	1.25
Si	0.34	0.32
S	0.008	0.009
P	0.015	0.014
Cr	0.021	0.023
Ni	0.024	0.024
Mo	0	0.003
V	0	0.004
Cu	0.01	0.007
Nb	0	0.001
Ti	0.018	0.019
Al	0.029	0.028
B	0	0
Sn	0	0.002
Ca	0	0
N	0.0015	0.0028
Fe	Rem.	Rem.
CE$_{IIW}$	0.38	0.37
Pcm	0.240	0.226

5.3.2   Testing Procedure

The G-BOP test configuration is comprised of two blocks firmly clamped together to prevent distortion as a result of the longitudinal stress that develops once the weld bead is deposited across the blocks, as shown in Figure 5. 10.
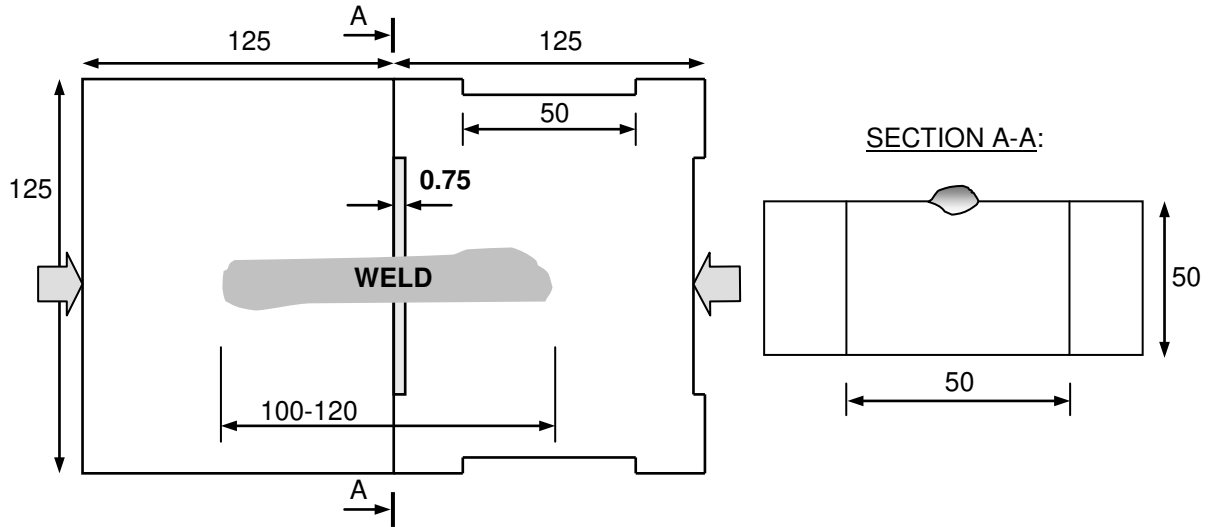
Figure 5. 10   Diagram of G-BOP test. Note: dimensions in millimeters.   [not to scale]

As proposed by Graville et al. (1995), four 0.75 mm deep recesses were machined in one of the mating blocks to introduce a notch so as to initiate transverse weld metal cracking. The multiple recesses enable the use of the same pair of blocks for four weld passes, as shown in Figure 3.31.

Prior to welding, the surfaces of the blocks were surface cleaned by linishing using 60 grid SiC abrasive paper to remove any residual oxide scale present on the steel.

The G-BOP tests were carried out on both H5 and H10 weld deposits using preheat temperatures of 20, 50, 80, 100 and 120 °C. Samples were preheated at temperature for 60 minutes and the furnace temperature was set 10 °C higher, thereby allowing for the time required to align and clamp the block together prior to welding.

Once the temperature of the blocks was stabilized at desired preheat temperature (+10 °C), the mating blocks were quickly joined together by a large clamp manually approximately in the middle of the block thickness. In order to allow a uniform loss of heat through the radiation,

the assembled blocks were rested on two supporting blocks positioned across the block ends,
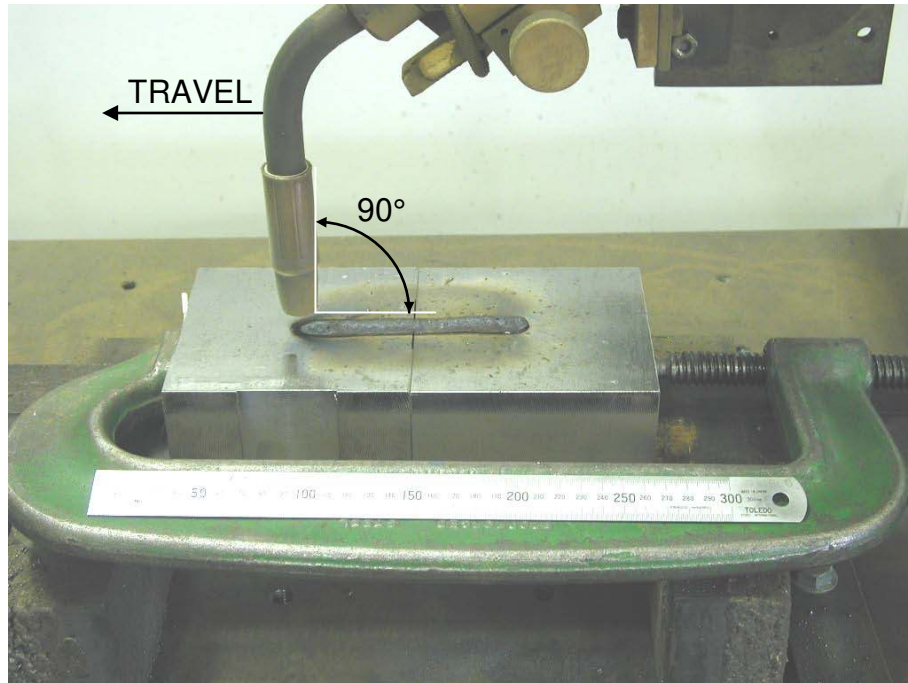
as shown in Figure 5. 11.

Figure 5. 11   Photograph showing a weld bead deposited over the clamped G-BOP test
                   block assembly.

The temperature of the block assembly was continuously measured in the centre of the

assembled blocks and in the vicinity of the 0.75 mm wide recess by using a surface contact

thermocouple.

Once the required welding conditions were established, a weld bead of 100-120 mm in length

was deposited, as shown in Figure 5. 11. Relative humidity and ambient temperature were

recorded for each welded test block. Immediately after completion of welding, the blocks

were allowed to cool down to ambient temperature in still air, while remaining restrained in

the clamp for a minimum period of 72 hours.

After this period of time, the restraining clamp was released and a small area in the vicinity of the weld bead (just over the gap of the two mating halves) was heated up to a dull, cherry red color using a gas flame and maintained for about 10 seconds. This was to heat tint any crack surfaces. The samples were then allowed to cool in still air ambient temperature. Subsequently, the test weld was fractured open by simple bending allowing visual examination of fractured surfaces, as described in Chapter 5.3.4.

5.3.3   Welding Parameters

The objective of this work was to determine the effect of varying welding parameters and shielding gases on the hydrogen induced transverse cracking susceptibility of two low strength rutile FCAW weld deposits. This was achieved by generating various diffusible hydrogen levels with the identical matrix of welding parameters used for weld metal hydrogen testing, as in Table 5. 6.

Table 5. 6   Matrix of welding parameters investigated in G-BOP testing of H5 and H10 weld metals.

Welding Parameter	Testing Range
Welding Current [A]	280 – 300 – 320
CTWD [mm]	15 – 20 – 25
Heat Input [kJ/mm]	1.26 – 1.35 – 1.44
Shielding Gas [18 l/min]	75Ar-25CO_2 and CO_2
Preheat Temperature [°C]	20 – 50 – 80 – 100 – 120
Welding Voltage♣ [V]	29 – 30
Travel Speed♣ [mm/min]	400

Notes:

♣ Not investigated parameters

5.3.4 Cold Crack Percentage Evaluation

In this part of the experimental work, a total of 98 pairs of blocks were welded and examined for cold cracking. The fractured faces of all weld deposits were digitally recorded and visually examined at a magnification of 20x. The proportion of discolored transverse crack area, A_C , and total fused metal area, A_F, were precisely measured by using computer drawing software Autosketch$^®$, as shown in Figure 5. 12.
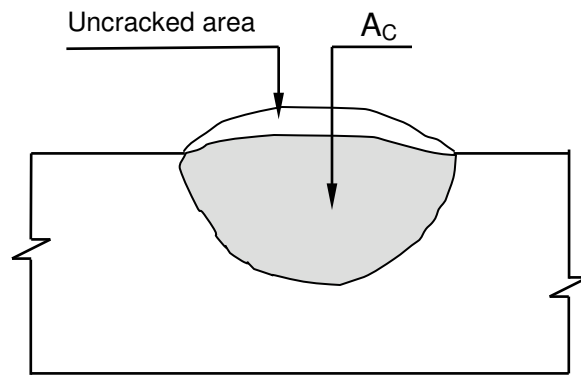

Figure 5. 12   Diagram of the measurement of percentage cracking.

From the measured areas, the percentage cracking was then calculated following Equation 5.1:

$$\text{Percentage cracking} = \frac{A_C}{A_F} \times 100 \qquad (5.1)$$

In addition to the room temperature cracking (RTC), for each set of G-BOP samples the 10 % crack preheat temperature (10 %CPT) and the critical preheat temperature (CPT) were also determined. These values, commonly cited in the literature [Hart 1986 and Chakravarti et al. 1989], are defined as the preheat temperatures required to obtain ≤ 10 % and zero cracking,

respectively. An example of measured and calculated values from the current work is shown in Figure 5. 13.
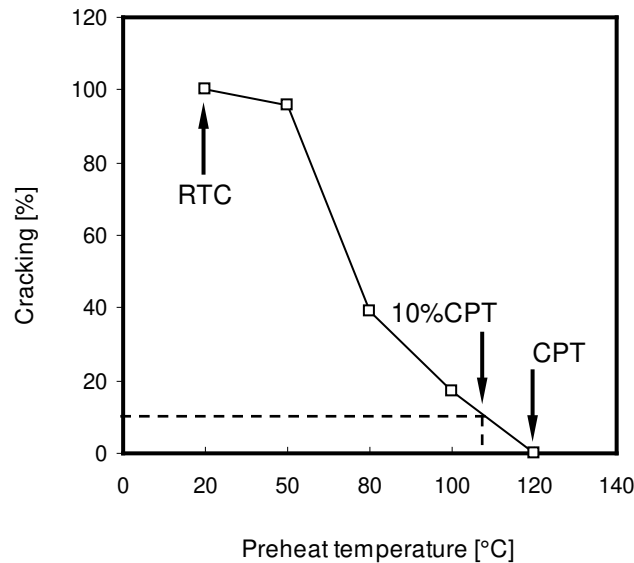

Figure 5. 13   Graph showing an example of G-BOP test results, indicating RTC=100 %, 10 %CPT = 110 °C and CPT = 120 °C values.

5.4   ARC TRANSFER IMAGING

This work was carried out in the welding laboratories at the University of Wollongong, Australia, using laser backlighting and high speed camera digital imaging to capture high quality images of the welding arc and the metal transfer under a range of welding conditions. The objective was to observe changes occurring in the welding arc at different welding conditions, and to investigate their accountability for the diffusible hydrogen variations, which were more noticeable in the H10 weld deposits.

The main purpose of this work was to determine the effect of varying welding parameters and different shielding gases on arc characteristics, with a particular focus on metal transfer mode

and accurate measurement of the arc length. This method allowed the arc length to be clearly established, as shown in Figure 4.11, from which the proportional length of wire in resistive heating zone before it enter the welding arc, l_{RHZ} , could be calculated.

From the measured arc-wire length dimensions, then the time an element of wire spends in resistive heating zone, t_{RHZ}, was subsequently calculated following Equation 5.2:

$$t_{RHZ} = \frac{l_{RHZ}}{WFS} = \frac{CTWD - AL}{WFS} \qquad (5.2)$$

where: t_{RHZ} = time of wire spent in resistive heating zone [s]

l_{RHZ} = length of wire in resistive heating zone [m]

WFS = wire feed speed [m/s]

CTWD= contact tip-to-work distance [m]

AL = arc length [m]

The current work seeks to study the effects welding current on arc characteristics and influence of thermal energy, Q [J], generated in the wire during welding and its effects on the levels of diffusible hydrogen in the deposited weld metal:

$$Q = I^2 R \, t_{RHZ} \qquad (5.3)$$

where: I = welding current [A]

R = electrical resistance ambient temperature [Ω]

and $\qquad R = \dfrac{\rho \times l_{RHZ}}{a} \qquad (5.4)$

where: ρ = electrical resistivity of wire at elevated temperature [Ω.m]

a = cross sectional area of the wire flux core wire sheath [m^2]

Then the thermal energy generated by the wire in Equation 5.3 during continuous welding can be expressed from the experimentally obtained welding parameters as follows:

$$Q = I^2 \times l_{RHZ}^2 \times \frac{\rho}{a} \frac{1}{WFS} \tag{5.5}$$

5.4.1 Equipment and Welding Consumables

In order to obtain an accurate image of the welding arc, the torch had to be fixed in a stable position above an automated lathe table, which was used to move the sample relative to the torch. A LIMAB laser, model RC 15D, with an output power +15 mV and wave length of 535 nm was used for the experiments. The arc images were recorded using a HYSPEED digital camera with an attached NIKON ED lens. Single bead welds were deposited on a 12 mm thick carbon steel plate, cleaned and prepared in a similar manner to those for the diffusible hydrogen and the G-BOP testing. The experimental setup is illustrated schematically in Figure 5. 14.
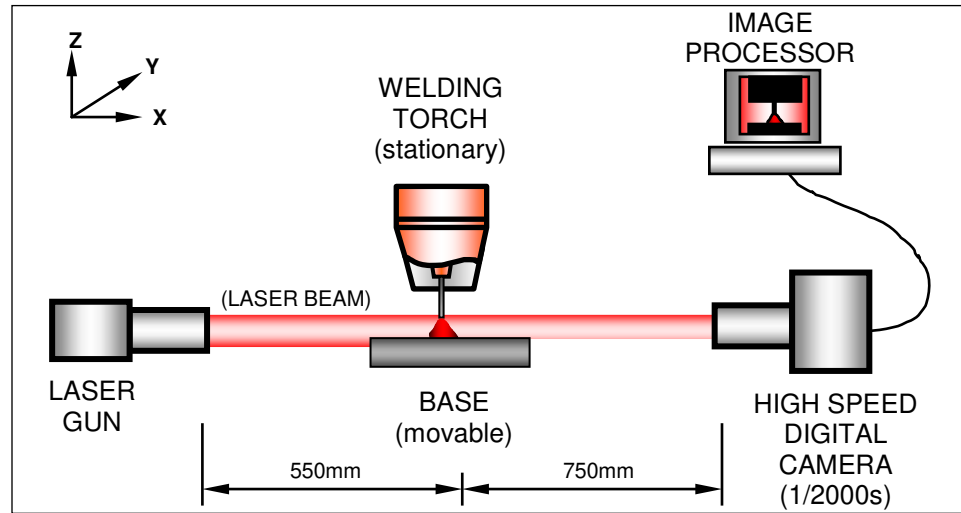
Figure 5. 14   Schematic illustration showing the experimental setup for investigating arc metal transfer.

The tests were carried out using the identical wire spool sample H10 used for weld metal hydrogen testing and for the G-BOP experiments. For the arc imaging experiments, the matrix of selected welding conditions, shown in Table 5. 7, was identical to that used for the weld metal hydrogen testing (Table 5. 4) and G-BOP tests (Table 5. 6).

Table 5. 7   Matrix of welding parameters investigated during arc imaging tests on H10 test welds.

Welding Parameters	
Welding Parameter	Testing Range
Welding Current [A]	280 – 320
CTWD [mm]	15 – 25
Heat Input [kJ/mm]	1.26 – 1.44
Shielding Gas [18 l/min]	75Ar-25CO_2 and CO_2
Welding Voltage♣ [V]	29 – 30
Travel Speed♣ [mm/min]	400

Notes:
♣ Not investigated parameters

5.5   METALLOGRAPHY

The main focus of this work was to determine any significant changes in weld metal microstructure accompanying variation of welding conditions and whether such changes might influence susceptibility to hydrogen cracking. For example, it was investigated whether the varying crack susceptibility of weld metal deposited using H5 and H10 wires is related to weld metal hardness or microstructure.

5.5.1   Hardness Measurements

Samples of welds for Vickers micro-hardness measurements (using 0.5 kg load) and microstructural examination were extracted from both series of H10 and H5 weld deposits, as shown in Table 5. 8.   It was important that the hardness survey and the metallurgical examination of weld metal was carried in zone of the weld that was unaffected by the heat tinting procedure.

The samples were sectioned in two directions to the welding. The first section "A", designated for hardness measurements, was in the transverse direction to the welding. These cross-sections were taken about 10 mm away from the fractured faces to avoid taking hardness measurements in a portion of weld that was thermally by the flame heating required in the G-BOP procedure, allowing for hardness indentations to be taken from the thermally unaffected region of the weld, as shown in Figure 5. 15.

Table 5. 8   Selected weld samples for hardness measurements taken from G-BOP blocks.

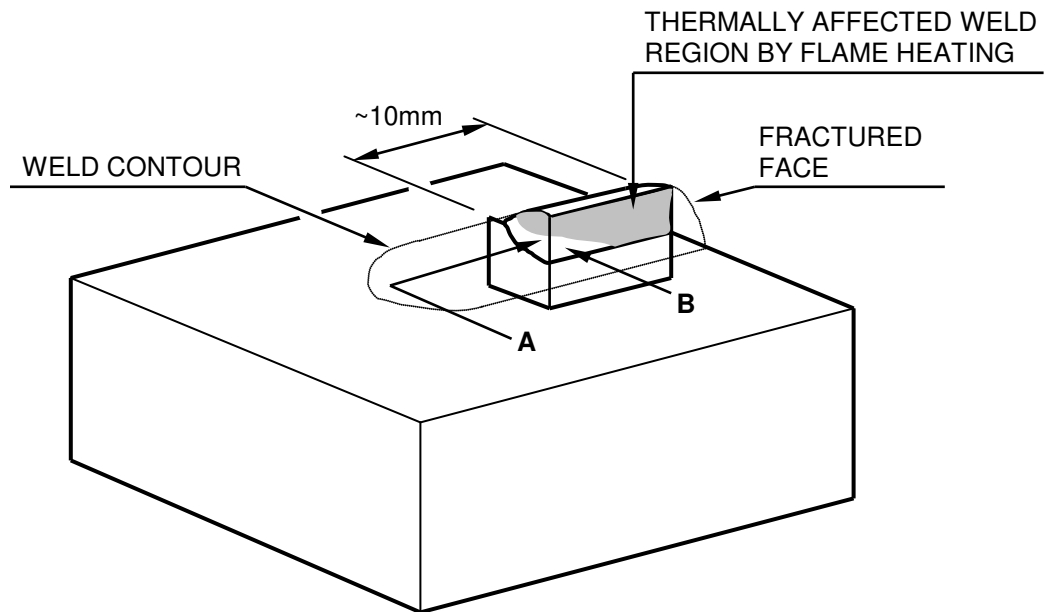| Sample ID	Welding Current [A]	Shielding gas	Preheat [°C]	CTWD [mm]
H10-17-20C	300	CO_2	20	25
H10-17-50C	300	CO_2	50	25
H10-17-80C	300	CO_2	80	25
H10-17-100C	300	CO_2	100	25
H10-8-20A	300	$75Ar-25CO_2$	20	25
H10-8-50A	300	$75Ar-25CO_2$	50	25
H10-8-80A	300	$75Ar-25CO_2$	80	25
H10-8-100A	300	$75Ar-25CO_2$	100	25
H10-11-20C	300	CO_2	20	15
H10-11-50C	300	CO_2	50	15
H10-11-80C	300	CO_2	80	15
H10-11-100C	300	CO_2	100	15
H10-11-120C	300	CO_2	120	15
H10-2-20A	300	$75Ar-25CO_2$	20	15
H10-2-50A	300	$75Ar-25CO_2$	50	15
H10-2-80A	300	$75Ar-25CO_2$	80	15
H10-2-100A	300	$75Ar-25CO_2$	100	15
H10-2-120A	300	$75Ar-25CO_2$	120	15
H10-10-20C	280	CO_2	20	15
H10-12-20C	320	CO_2	20	15
H10-1-20A	280	$75Ar-25CO_2$	20	15
H10-3-20A	320	$75Ar-25CO_2$	20	15
H10-16-20C	280	CO_2	20	25
H10-18-20C	320	CO_2	20	25
H10-7-20A	280	$75Ar-25CO_2$	20	25
H10-9-20A	320	$75Ar-25CO_2$	20	25
H5-17-20C	300	CO_2	20	25
H5-11-20C	300	CO_2	20	15
H5-8-20A	300	$75Ar-25CO_2$	20	25
H5-2-20A	300	$75Ar-25CO_2$	20	15

Figure 5. 15   Schematic diagram of samples for micro-hardness measurements (site A) and weld metal microstructure examination (site B) examined in the thermally unaffected weld metal.   [not to scale]

The samples were metallographically prepared by progressive grinding and mechanical polished on 6 μm and then 1μm finish on diamond pads, and then lightly etched using 2.5 % Nital solution for 30 seconds to reveal weld fusion boundary and weld metal exhibiting regions of unaffected weld metal by the flame.

Hardness measurements were made using Vickers micro-hardness testing equipment (LECO M-400-H1) at the University of Wollongong metallurgical laboratories using a 0.5 kg load. The spacing between indentations was 0.5 mm in vertical down direction in the thermally unaffected region of the weld deposit, as shown in Figure 5. 16.
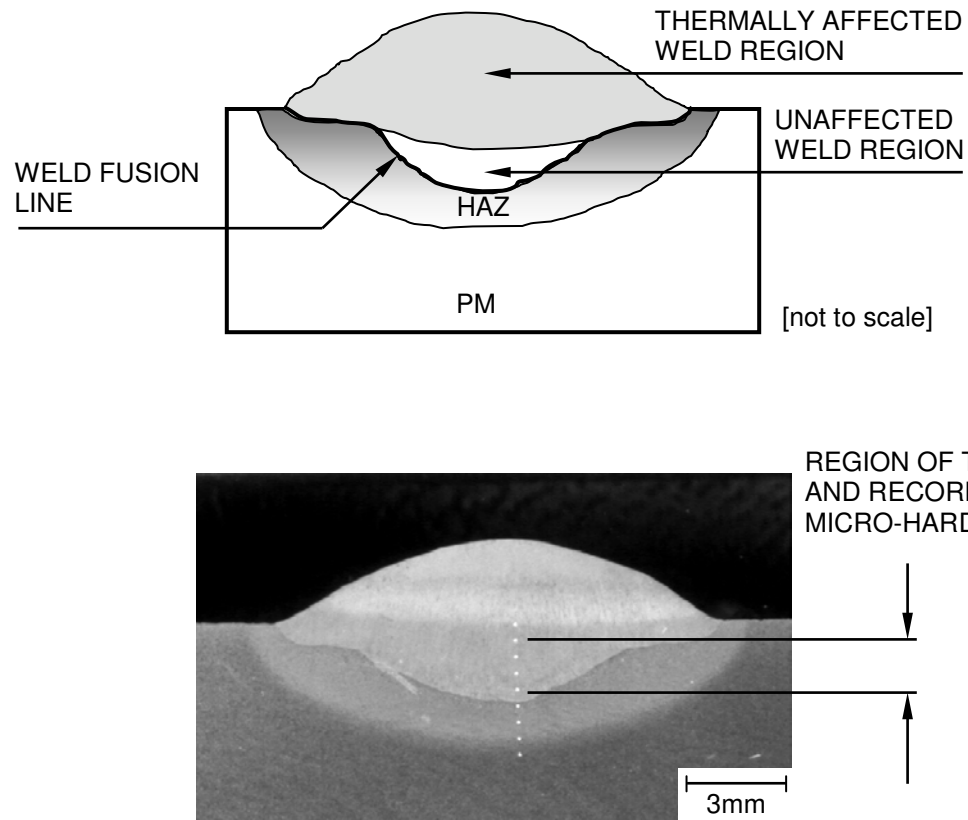
Figure 5. 16　　　Schematic diagram and a typical macrograph illustrating the region of the Vickers micro-hardness measurements taken vertically down across the thermally affected, unaffected weld cross-section and HAZ (site A).

Captured images of all transverse macro-sections were then used further to measure weld metal dilution, as described in following Chapter 5.5.2.

5.5.2　Optical Metallography

Once the micro-hardness measurements were completed, 12 designated weld samples were then selected for further metallurgical examination of the weld to investigate the effects welding conditions, such as welding current, shielding gases, preheat temperature and CTWD

on the weld metal microstructure. In order to investigate the effect of microstructure on weld metal cracking susceptibility, these samples of both H5 and H10 weld deposits were sectioned longitudinally through the center of the weld, as shown in Figure 5. 17. The selected samples, with relevant welding parameters are listed in Table 5. 9.
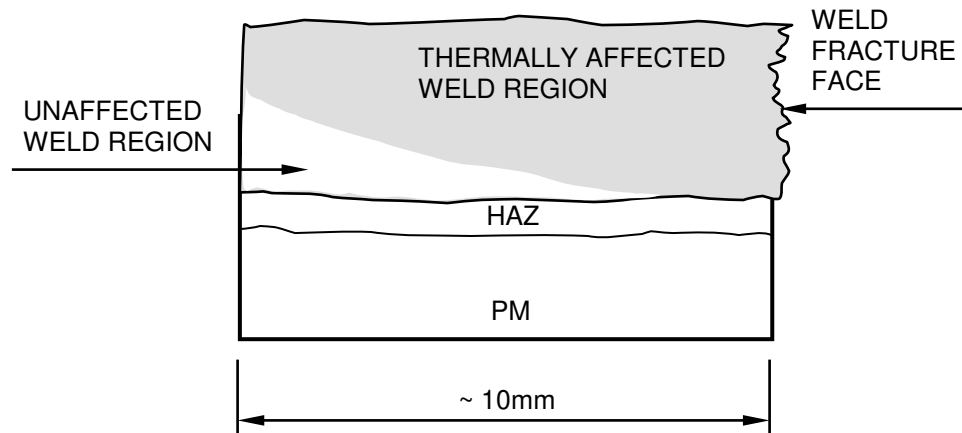

Figure 5. 17   Schematic diagram of the examined weld metal microstructure in the thermally unaffected region (site B).   [not to scale]

Table 5. 9   A listing of G-BOP weld samples selected for microstructural examination.

Sample ID	Welding Current [A]	Shielding gas	Preheat [°C]	CTWD [mm]
H10-10-20C	280	CO_2	20	15
H10-11-20C	300	CO_2	20	15
H10-12-20C	320	CO_2	20	15
H10-11-120C	300	CO_2	120	15
H10-2-20A	300	$75Ar-25CO_2$	20	15
H10-2-120A	300	$75Ar-25CO_2$	120	15
H10-16-20C	280	CO_2	20	25
H10-18-20C	320	CO_2	20	25
H10-7-20A	280	$75Ar-25CO_2$	20	25
H10-9-20A	320	$75Ar-25CO_2$	20	25
H5-17-20C	300	CO_2	20	25
H5-11-20C	300	CO_2	20	15
H5-8-20A	300	$75Ar-25CO_2$	20	25
H5-2-20A	300	$75Ar-25CO_2$	20	15

CHAPTER 6

Results

In this chapter, the results of experimental work will be presented. In order to clarify the effects of welding parameters, such as welding current, CTWD and shielding gas on the H10 and H5 weld deposits, the results in this chapter are presented as follows:

a) diffusible hydrogen analysis,

b) welding arc imaging, and

c) weld metal susceptibility to transverse cold cracking using the G-BOP testing.

6.1 HYDROGEN ANALYSIS

The objective of this work was to obtain the diffusible hydrogen values expressed in terms of deposited and fused weld metal for two rutile flux-cored wires of the same classification, but with different nominal hydrogen levels of 10 and 5 ml/100g for H10 and H5 wire samples, respectively.

The hydrogen testing experiments were designed to study variations in weld metal diffusible hydrogen content associated with varying welding current, CTWD and shielding gas type. For each H10 and H5 wire samples, a total of 36 hydrogen tests of triplicate samples for each condition were prepared and analysed for deposited and fused hydrogen levels in this work. Mean values for deposited and fused weld metal per condition were calculated from the three samples, as shown in Tables 6.1 and 6.2, respectively.

The measured weld bead dimensions for both H10 and H5 wire samples, taken from the cross-sections of weld metal hydrogen test samples, are shown in Tables 6.3 and 6.4. Photographs of cross-sections of the weld metal hydrogen samples are shown in Appendix A.

Table 6. 1   Summary of diffusible hydrogen test results obtained by varying welding current, CTWD and shielding gas for H10 weld deposits.

Sample ID	Welding Current [A]	Heat Input [kJ/mm]	CTWD [mm]	Shielding gas	WFS [m/min.]	Relative humidity and temperature [% - °C]	Actual humidity [gH_2O/kg dry air]	Fused Hydrogen H_F [ml/100g]	Deposited Hydrogen H_D [ml/100g]
H10-1-A	280	1.26	15	$75Ar-25CO_2$	5.35	56-16	6.46	8.4	17.0
H10-2-A	300	1.35	15	$75Ar-25CO_2$	6.20	56-16	6.46	6.8	14.3
H10-3-A	320	1.44	15	$75Ar-25CO_2$	6.90	56-16	6.46	7.5	13.8
H10-4-A	280	1.26	20	$75Ar-25CO_2$	6.20	45-22	7.55	8.0	14.8
H10-5-A	300	1.35	20	$75Ar-25CO_2$	6.86	45-22	7.55	6.3	12.9
H10-6-A	320	1.44	20	$75Ar-25CO_2$	7.45	45-22	7.55	6.5	13.1
H10-7-A	280	1.26	25	$75Ar-25CO_2$	6.65	45-22	7.55	6.9	12.0
H10-8-A	300	1.35	25	$75Ar-25CO_2$	7.40	51-19	7.11	6.3	11.0
H10-9-A	320	1.44	25	$75Ar-25CO_2$	8.20	51-19	7.11	5.5	10.5
H10-10-C	280	1.26	15	CO_2	5.70	49-15	5.31	5.6	11.7
H10-11-C	300	1.35	15	CO_2	6.40	49-15	5.31	5.7	12.7
H10-12-C	320	1.44	15	CO_2	6.80	49-15	5.31	6.2	12.8
H10-13-C	280	1.26	20	CO_2	6.10	49-15	5.31	5.2	9.5
H10-14-C	300	1.35	20	CO_2	7.10	48-20	7.12	5.3	10.7
H10-15-C	320	1.44	20	CO_2	7.80	48-20	7.12	5.4	11.0
H10-16-C	280	1.26	25	CO_2	6.70	48-20	7.12	3.7	8.3
H10-17-C	300	1.35	25	CO_2	7.40	48-20	7.12	4.5	8.4
H10-18-C	320	1.44	25	CO_2	8.65	50-26	10.66	4.7	8.6

Table 6. 2   Summary of diffusible hydrogen test results obtained by varying welding current, CTWD and shielding gas for H5 weld deposits.

Sample ID	Welding Current [A]	Heat Input [kJ/mm]	CTWD [mm]	Shielding gas	WFS [m/min.]	Relative humidity and temperature [% - °C]	Actual humidity [gH_2O/kg dry air]	Fused Hydrogen H_F [ml/100g]	Deposited Hydrogen H_D [ml/100g]
H5-1-A	280	1.26	15	$75Ar-25CO_2$	4.50	50-26	10.66	1.4	3.5
H5-2-A	300	1.35	15	$75Ar-25CO_2$	5.20	50-26	10.66	1.4	3.1
H5-3-A	320	1.44	15	$75Ar-25CO_2$	5.80	50-26	10.66	1.0	2.6
H5-4-A	280	1.26	20	$75Ar-25CO_2$	5.20	47-18	6.16	1.0	2.2
H5-5-A	300	1.35	20	$75Ar-25CO_2$	5.70	47-18	6.16	1.1	2.1
H5-6-A	320	1.44	20	$75Ar-25CO_2$	6.40	47-18	6.16	0.8	1.6
H5-7-A	280	1.26	25	$75Ar-25CO_2$	5.50	47-18	6.16	0.8	1.5
H5-8-A	300	1.35	25	$75Ar-25CO_2$	6.40	61-19	8.51	0.9	1.7
H5-9-A	320	1.44	25	$75Ar-25CO_2$	6.90	61-19	8.51	0.9	1.6
H5-10-C	280	1.26	15	CO_2	4.90	61-19	8.51	0.8	1.9
H5-11-C	300	1.35	15	CO_2	5.20	61-19	8.51	0.6	1.5
H5-12-C	320	1.44	15	CO_2	5.65	61-19	8.51	0.7	1.7
H5-13-C	280	1.26	20	CO_2	5.30	61-19	8.51	0.9	1.8
H5-14-C	300	1.35	20	CO_2	5.80	61-19	8.51	0.6	1.3
H5-15-C	320	1.44	20	CO_2	6.30	61-19	8.51	0.8	1.5
H5-16-C	280	1.26	25	CO_2	5.65	60-19	8.37	0.5	1.1
H5-17-C	300	1.35	25	CO_2	6.20	60-19	8.37	0.4	0.9
H5-18-C	320	1.44	25	CO_2	6.85	60-19	8.37	0.4	0.9

Table 6. 3   Table showing the hydrogen test samples for the H10 welds, with weld bead dimensions deposited using 75Ar-25CO$_2$ and CO$_2$ shielding gas (The values represent an average of 3 samples, as shown in Appendix A).

	75Ar-25CO$_2$					CO$_2$			
Sample ID	Bead height [mm]	Bead width [mm]	Penetration [mm]	Fused weld metal [mm^2]	Sample ID	Bead height [mm]	Bead width [mm]	Penetration [mm]	Fused weld metal [mm^2]
H10-1-A	2.1	12.3	1.8	33	H10-10-C	2.5	12.0	2.3	36
H10-2-A	2.6	12.0	2.8	39	H10-11-C	2.6	11.5	2.6	38
H10-3-A	2.7	12.9	2.1	38	H10-12-C	2.9	12.3	2.9	43
H10-4-A	2.4	11.6	1.7	30	H10-13-C	3.0	11.7	2.1	39
H10-5-A	2.4	12.0	2.3	36	H10-14-C	3.2	12.4	2.8	45
H10-6-A	2.8	12.1	2.4	38	H10-15-C	3.0	12.2	2.4	42
H10-7-A	2.7	11.6	1.6	32	H10-16-C	2.6	11.5	2.6	36
H10-8-A	3.1	12.2	2.2	39	H10-17-C	3.4	12.2	2.6	44
H10-9-A	3.1	12.0	2.5	41	H10-18-C	3.9	11.3	2.9	46

Table 6. 4   Table showing the hydrogen test samples for the H5 welds, with weld bead dimensions deposited using 75Ar-25CO$_2$ and CO$_2$ shielding gas. (The values represent an average of 3 samples, as shown in Appendix A).

	75Ar-25CO$_2$					CO$_2$			
Sample ID	Bead height [mm]	Bead width [mm]	Penetration [mm]	Fused weld metal [mm^2]	Sample ID	Bead height [mm]	Bead width [mm]	Penetration [mm]	Fused weld metal [mm^2]
H5-1-A	2.0	12.5	2.6	36	H5-10-C	2.5	12.3	2.7	41
H5-2-A	2.5	13.5	2.6	40	H5-11-C	2.8	12.2	2.8	42
H5-3-A	2.4	13.6	2.9	46	H5-12-C	3.1	13.3	3.6	52
H5-4-A	2.3	13.2	2.4	39	H5-13-C	2.9	12.1	2.5	41
H5-5-A	2.6	14.5	2.3	44	H5-14-C	3.2	12.5	2.9	49
H5-6-A	3.0	14.4	3.0	51	H5-15-C	3.8	13.1	3.7	55
H5-7-A	3.1	13.6	2.2	44	H5-16-C	2.9	12.3	2.6	43
H5-8-A	2.8	14.0	2.3	45	H5-17-C	3.1	12.4	2.8	44
H5-9-A	3.3	13.8	2.2	44	H5-18-C	3.3	12.8	3.7	46

6.1.1 Effect of Welding Current

An arc running at a given welding current and voltage generates a fixed amount of heat between the parent material and the filler metal and any change which increases one must decrease the other [Widgery 1994]. This principle influences the burn-off behaviour of the wire. It is expected that an increase in welding current will result in an increase in the amount of wire melted and the overall heat input to the base metal, and will also decrease weld metal cooling rates. Consequently, the weld bead width, penetration and reinforcement height are expected to be changed, resulting in a variation of weld metal weight deposited. The effects of welding current on deposited weld metal weight and corresponding diffusible hydrogen content were observed in this work.

The relationship between the wire feed speed and welding current is usually expressed in terms of melting rate, MR, [Norrish 1992]:

$$MR = \alpha A + \frac{\beta\, l\, A^2}{a} \tag{6.1}$$

where: A   = welding current [A]

l   = CTWD [mm]

a   = cross sectional area of wire [mm^2]

α = constant [mmA^{-1}s^{-1}]

β = constant [A^{-2}s^{-1}]

The wire feed speed and welding current, as expressed by melting rate above, are usually expressed in the form of burn-off curves [Norrish 1992]. The relationship between the wire feed speed and welding current is shown graphically in Figure 6. 1. It can be seen that when testing using 15 mm CTWD, the results of wire feed speed for H10 and H5 wires varied.

However, wire feed speed for both wire samples was increasing linearly and by a similar rate of 0.25 m/min per 10 A over the welding current range of 280 , 300 and 320 A.
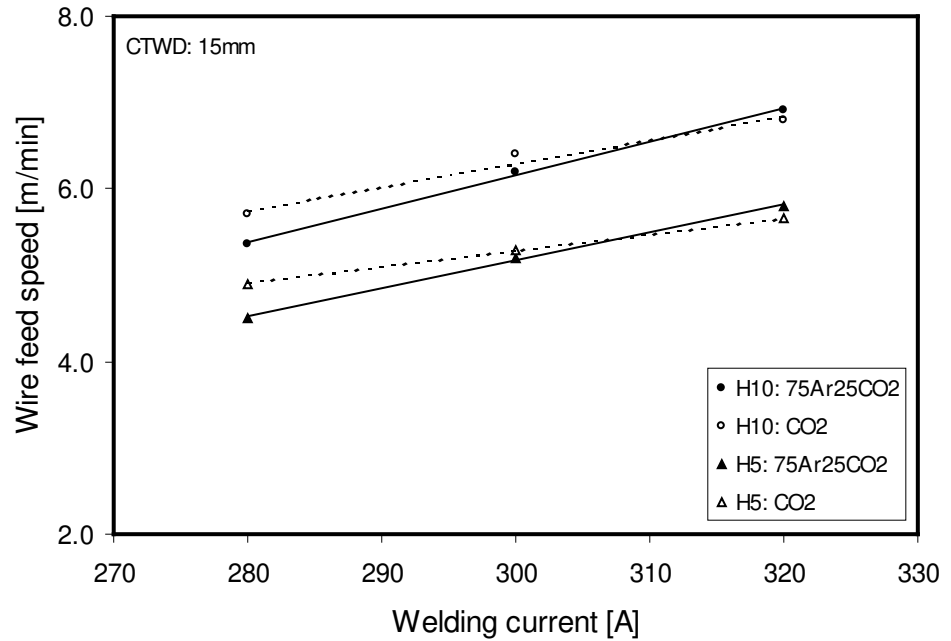
Figure 6. 1   Graph showing the relationship between the wire feed and welding current (280, 300 and 320 A) for H5 and H10 weld deposited using 75Ar-25CO$_2$ and 100 %CO$_2$ shielding gas and 15 mm CTWD.

The wire feed speed was also increased by increasing CTWD within the selected testing range of 15, 20 and 25 mm, and using both shielding gases, as shown in Figures 6.2 and 6.3 using both shielding gases.
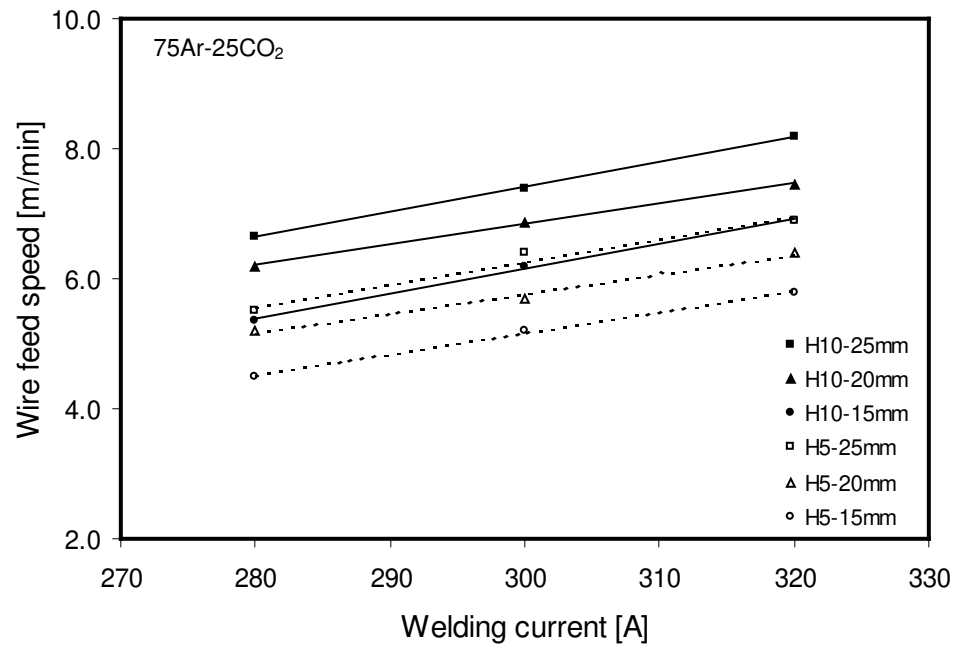
Figure 6. 2   Graph showing the relationship between the wire feed speed and welding current for H5 and H10 weld deposits using $75Ar-25CO_2$ shielding gas and 15, 20 and 25 mm CTWD.
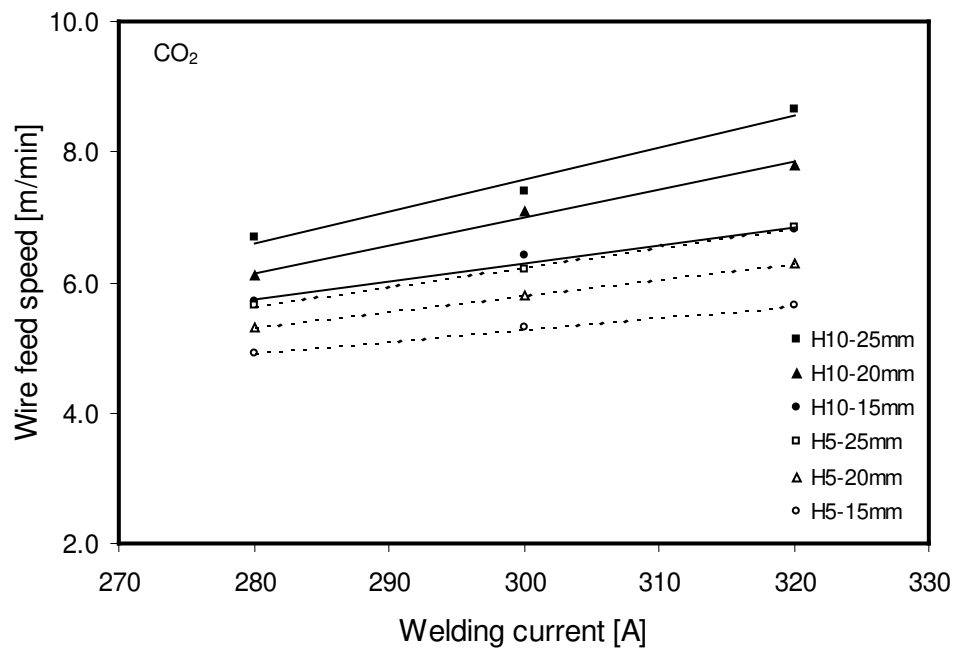
Figure 6. 3   Graph showing the relationship between the wire feed speed and welding current for H5 and H10 weld deposits using CO_2 shielding gas and 15, 20 and 25 mm CTWD.

Generally, higher welding current requires an increase of wire feed speed and this is expected to result in an increase in the amount of deposited weld metal. Understandably, there are also practical difficulties in obtaining a constant weld metal weight for each set of welding parameters. The hydrogen testing standards, ISO 3690-2000 and AS/NZS 3752-1996, determine that the amount of weld metal weight should be proportional to the diffusible hydrogen level (Equation 2.12) and the amount of fused metal (Equation 2.14), and this has no effect on hydrogen levels measured [Sierdzinski and Ferree 1998].

However, work by White et al. (1992) aimed to maintain the standard 4g of deposited weld metal weight at nominal heat input of 1.4 kJ/mm, but found that in order to do so it was necessary to reduce the travel speed with decreasing welding current. The reduced travel speed resulted in an increase of arcing time to deposit a required weld bead length for hydrogen test to be valid. It was suggested that at the arcing time increase from 30 to 57 s, the hydrogen test results might lower the hydrogen results. Also a wide voltage range (17 – 24 V) used by White et al. (1992), had most likely resulted in a large variation of arc length. This effectively could provide a greater opportunity for hydrogen absorption into the molten weld pool.

In order to minimize the possibility of error in diffusible hydrogen test results, caused by inconsistencies in the testing procedure, the travel speed was maintained constant throughout the testing at 400 mm/min. Hence, the weld metal weight variation was predominantly a result of the different welding currents used. The amount of deposited weld metal weight and its relationship to diffusible hydrogen in deposited and fused weld metal is shown in Figure 6. 4. Deposited weld metal weight for all samples in this current work was in the range 2 to 4g.
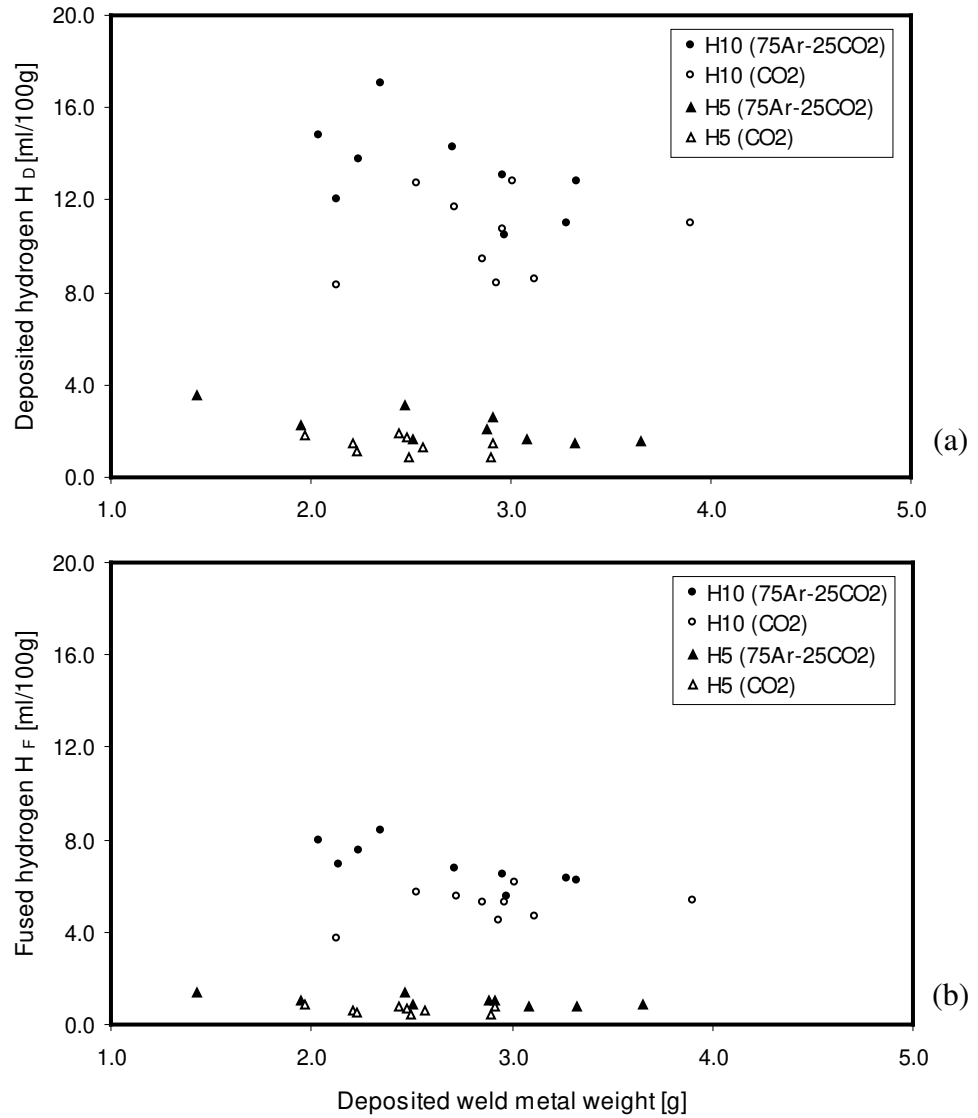
Figure 6. 4   Graphs showing the relationship between the deposited weld metal weight and hydrogen content for H5 and H10 weld (a) deposited and (b) fused using CO_2 shielding gas.

The wide diffusible hydrogen scatter observed in Figure 6. 4 verified there was no significant relationship between weld metal weight and the hydrogen levels measured. The relationship between the weld metal weight and hydrogen content measured in fused metal was also found to be inconclusive with smaller hydrogen values, but of a narrower hydrogen scatter to the deposited weld metal.

The results for diffusible hydrogen contents as a function of welding current (280-320 A), measured at 15 mm CTWD with both shielding gases, are presented in Figure 6. 5. The H5 weld deposits using 75Ar-25CO$_2$ shielding gas showed an insignificant decrease in diffusible hydrogen levels (0.9 ml/100g) with increasing welding current. However, the weld deposits using CO$_2$ shielding gas, the diffusible hydrogen content was unchanged.

The behaviour of the H10 weld deposits was more complex, showing a more significant decrease in diffusible hydrogen (3.2 ml/100g) over the current range for the mixed shielding gas, but less significant increase in hydrogen (1.1 ml/100g) with increasing current for the CO$_2$ shielding gas. Similar relationships between welding current and measured diffusible hydrogen were also observed at 20 and 25 mm CTWD for both wire samples, as shown in Appendix B.
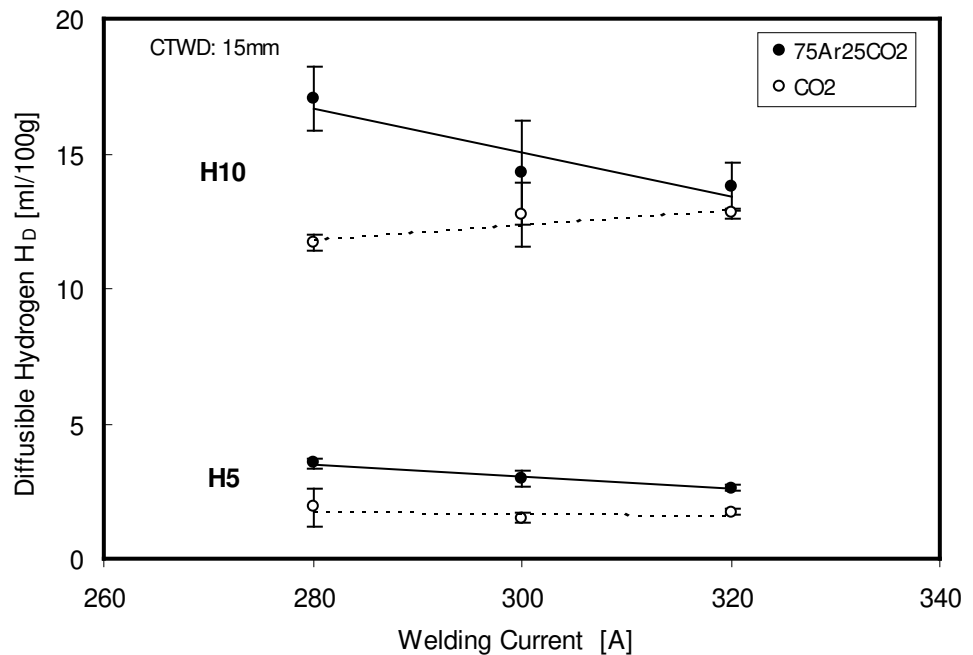
Figure 6. 5   Graph showing the relationship between the welding current and hydrogen levels for H10 and H5 weld deposited using 75Ar-25CO$_2$ and CO$_2$ shielding gases and a CTWD of 15 mm.

The relationships between WFS and diffusible hydrogen levels for the H10 and H5 consumables are shown in Figure 6. 6. For welding with H10 wire under the mixed gas, wire feed speed increased by approximately 1.5 m/min between 280-320 A, for both CTWD values of 15 and 25 mm. The effect was similar for H10 under CO_2 shielding gas, except that the effect was more pronounced for the longer CTWD, increasing WFS by approximately 2 m/min over the current range 280-320 A.

It is apparent that the longer the CTWD, the higher the WFS. From the point of view of removal of moisture and burn-off of lubricants, these two variables are counteracting each other. From the relationship shown in Figure 6. 6, it could be suggested that the extended CTWD allows longer time available to evaporate any residual moisture resulting in reducing diffusible levels of hydrogen in weld deposits, even at higher WFS. It might be also suggested that at CTWD of 25 mm, increasing WFS does not significantly affect the results of weld metal hydrogen levels.

However, this effect is not observed at the CTWD of 15 mm. In this case, the increase in welding current (accompanied by higher WFS), resulted in a significant reduction of diffusible hydrogen for both wires when welded using 75Ar-25CO$_2$ mix gas and marginal increase in diffusible hydrogen in the case of CO_2. This is an important finding requiring further investigation to determine why at the longer CTWD of 25 mm, the increasing welding current and increasing WFS has almost no influence on diffusible hydrogen levels. Whereas, at shorter CTWD of 15 mm, the welding current increase resulted in a significant diffusible hydrogen reduction in welds deposited using 75Ar-25CO$_2$ mix gas and a marginal increase in welds deposited using CO_2. These phenomena were therefore further investigated later in this work by studying the arc images.
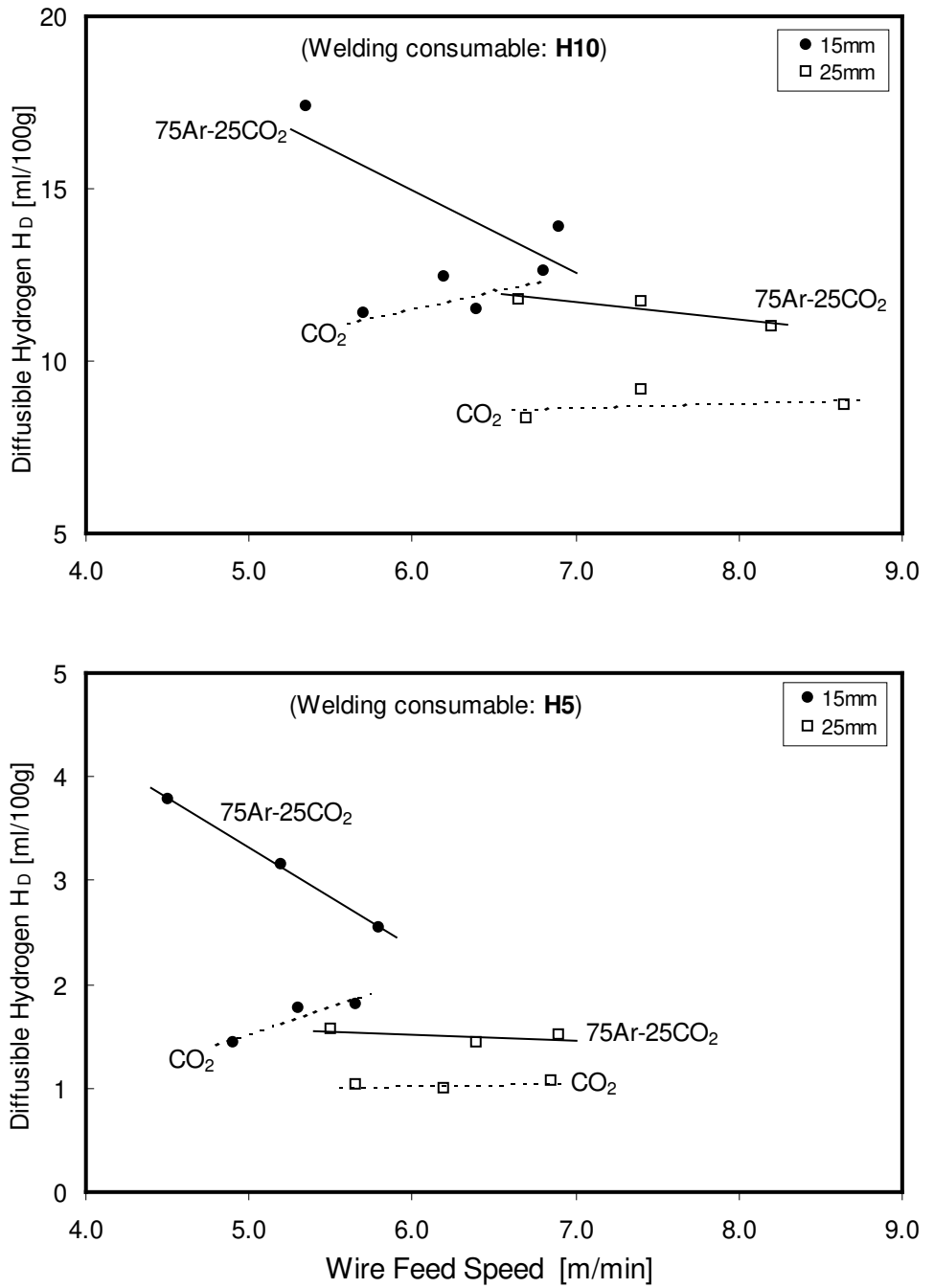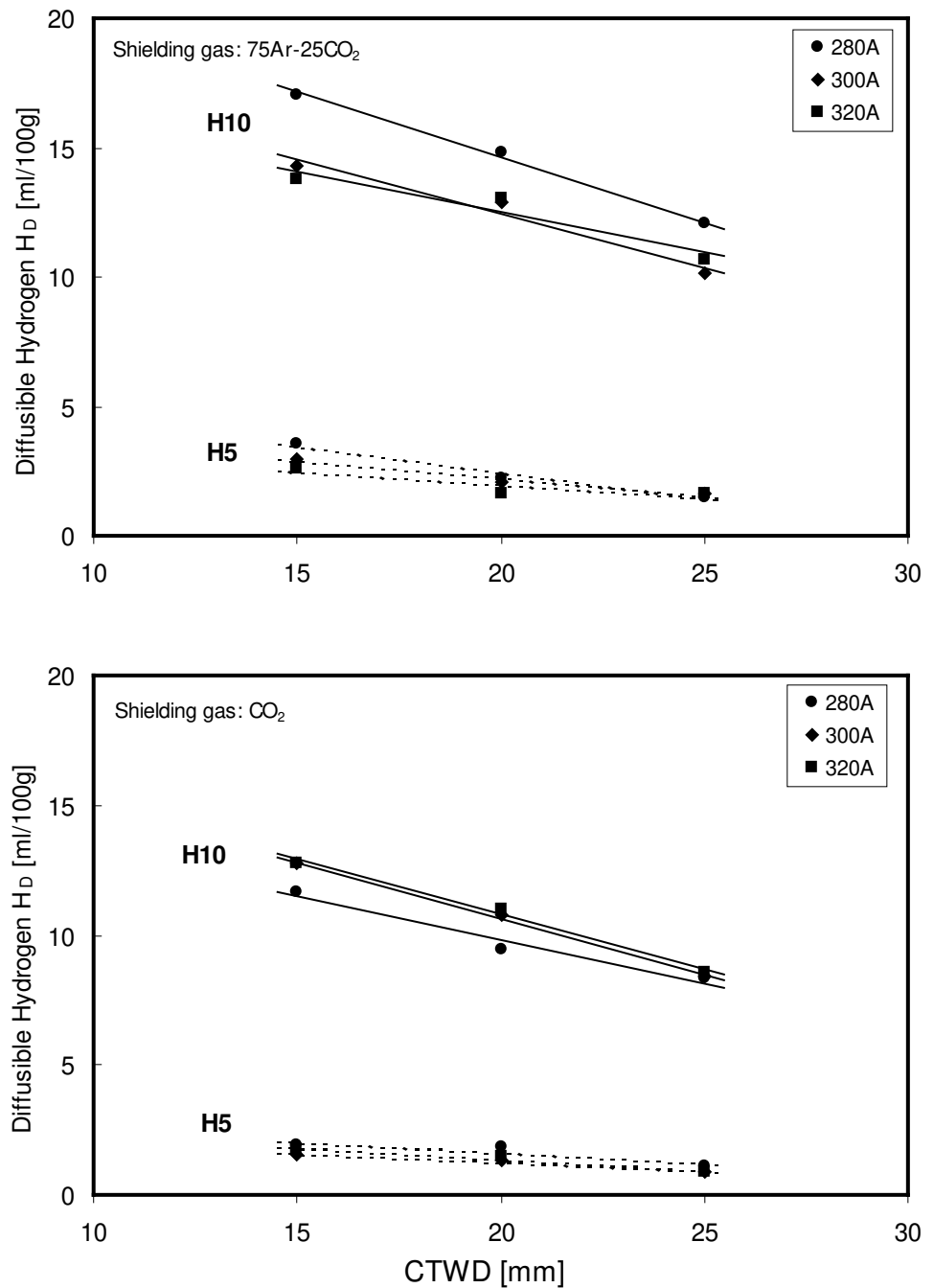
Figure 6. 6   Graphs showing the relationships between the wire feed speed (in welding current range 280-300-320 A) and diffusible hydrogen levels in H10 and H5 welds deposited using 75Ar-25CO$_2$ and CO$_2$ shielding gases and CTWD of 15 and 25 mm.

Overall the results revealed that the H10 wire tended to have higher WFS than the H5 wire under equivalent welding conditions. Although the absolute values of H_D were much lower for the H5 welds, the relationships between WFS, H_D and CTWD seemed to hold true.

6.1.2   Effect of CTWD

From the research work cited in the literature, CTWD has been shown to be a major factor influencing the level of diffusible hydrogen in weld deposits, particularly when using rutile flux cored wires [White et al. 1992 and Kiefer 1996]. In fact, the CTWD appears to be one of the most influential variables affecting the hydrogen levels in weld deposits [Kuebler et al. 2000]. However, it should be noted that the variation of CTWD results in changes to other interacting welding parameters, and this makes the prediction of diffusible hydrogen content more complex.

The effect of CTWD on diffusible hydrogen for both wire weld deposits and shielding gases are presented graphically in Figure 6. 7.   In general, the weld metal diffusible hydrogen (H_D) levels decreased for both wires as the CTWD increased from 15 to 25 mm. This effect was observed for both shielding gas types and under all welding currents. The seamed rutile wire (H10) showed a more significant decrease in the levels of hydrogen with increasing CTWD, compared to the seamless rutile wire (H5). The increase of CTWD from 15 to 25 mm resulted in a reduction of diffusible hydrogen levels of approximately 4-5 ml/100g for the seamed wire for all three welding currents and both shielding gases. The 1-2 ml/100g decrease in H_D seen in the case of the seamless (H5) wire could be considered to be insignificant. Therefore, in absolute terms, the reduction in diffusible hydrogen with increasing CTWD was greater for the H10 wire compared to the H5 wire, presumably because the seam provides a clear

Figure 6. 7   Graphs showing the relationship between the CTWD (in welding current range 280-300-320 A) and diffusible hydrogen levels in H10 and H5 welds deposited using 75Ar-25CO$_2$ and CO$_2$ shielding gases.

mechanism for the removal of entrapped moisture or lubricant residues as the wire passes through the resistive heating zone. It is also possible that there was a difference in the flux formulation between the H10 and H5 wire, resulting in a variation of weld metal chemical composition (particularly in levels of C, Cr, Ni, Cu and B), as show in Table 5.3.

It is reasonable to suggest that an element of wire can spend a longer time in the resistive heating zone when a greater CTWD is selected, thereby allowing more time for pre-drying and removal of lubricant residues on the wire prior to it entering the arc. However, this matter is complicated by the fact that it is necessary to increase WFS in order to maintain constant welding current. As shown in Figure 6. 8, a linear increase of WFS was observed for both wires with increasing CTWD within the welding current range. Increases in WFS of about 1 m/min were observed for each welding current selected when increasing CTWD from 15 to 25 mm. The seamed H10 wire under the higher current condition and under CO_2 shielding gas showed a more dramatic increase in WFS of ~2 m/min with increasing CTWD.

In order to understand the mechanism of CTWD variations on the diffusible hydrogen levels, it was important to calculate the time of wire spent in resistive heating zone time, t_{RHZ}, (Equation 5.2). To determine the t_{RHZ} parameter in this work, it was necessary to measure the arc length (AL), as observed from the welding arc images taken at different CTWD with the known value of and the t_{RHZ}, it is then possible to calculate the thermal energy, Q, (Equation 5.5), generated as a result of resistive heating.
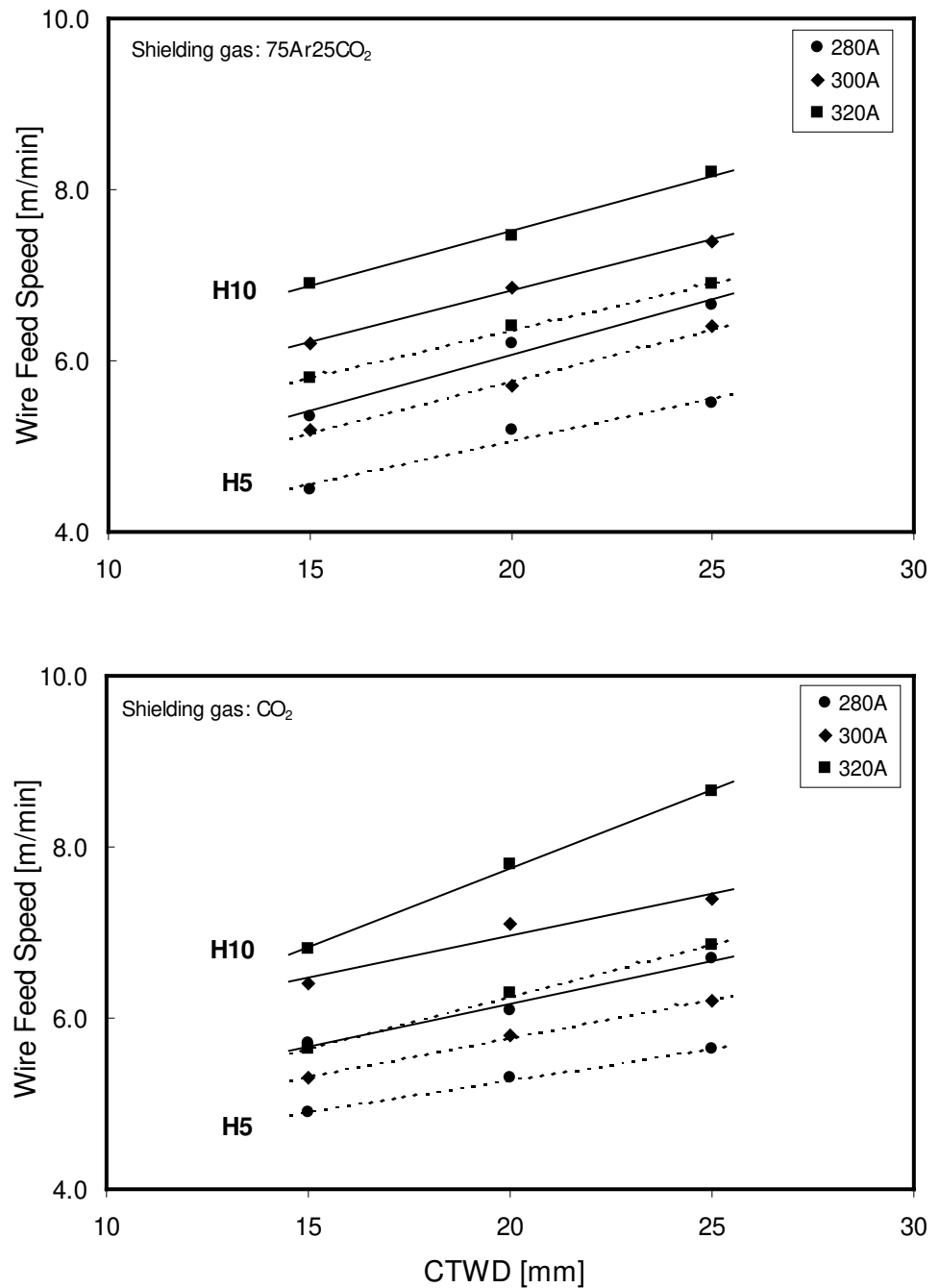
Figure 6. 8   Graphs showing the relationship between the CTWD (in welding current range 280-300-320 A) and WFS for H10 and H5 welds deposited using 75Ar-25CO$_2$ and CO$_2$ shielding gases.

6.1.3 Effect of Shielding Gas

It can be expected that the shielding gas type will not only influence the operating characteristics of the FCAW process, but also the diffusible hydrogen levels in weld deposits [van der Mee 2001].

In the current work, the use of 75Ar-25CO$_2$ mixed gas produced an operating characteristic typical of spray metal transfer. This was particularly noticeable for the H10 wire sample at the lower CTWD of 15 mm. By increasing the CTWD, the arc gradually became less stable, producing undesirable amounts of weld spatter. Under CO$_2$, the arc characteristics appeared to become significantly harsher and unstable, accompanied with dramatic increase in the amount of spatter. Contrary to the observed changes in the arc characteristics during welding of the H10 wire sample using different shielding gases, the H5 wire appeared to have no noticeable reaction to shielding gas change at any selected welding conditions. The arc produced very smooth metal transfer under all conditions for this wire. The results from this work confirm that the shielding gas type can influence the arc characteristics, and that the effect depends on the type of consumable used.

In terms of the effect of shielding gas and diffusible hydrogen, welding with mixed gas 75Ar-25CO$_2$ resulted in higher diffusible hydrogen levels, and in this effect was more pronounced for the seamed H10 wire, as shown in Figure 6. 9. This was observed for every given welding conditions by varying CTWD, welding current and atmospheric conditions at the time of welding, as listed in Tables 6.1 and 6.2.

In contrast with the CO_2 shielding gas, very smooth arc spray transfer characteristics and minimum spatter was observed in the case of 75Ar-25CO_2 welding, particularly noticeable at lower welding current.
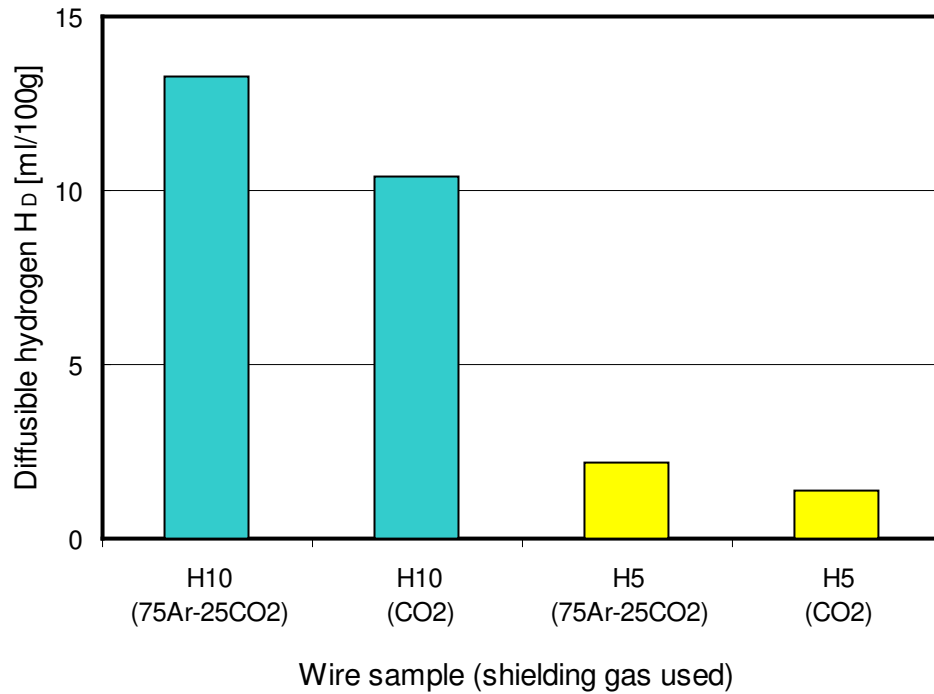
Figure 6. 9   Graph showing the weld metal diffusible hydrogen levels for H10 and H5 weld deposits using 75Ar-25CO_2 and CO_2 shielding gases (each column represents an average of nine triplicate samples welded using welding conditions listed in Tables 6.1 and 6.2).

When welded using 75Ar-25CO_2 shielding gas, the hydrogen levels for H10 wire sample were found to decrease with an increase in the welding current from 280 to 320 A. This was accompanied by deterioration in arc transfer characteristics (more dip-like) and this resulted in an increase in spatter.

The variation of shielding gases was found to contribute to a change of diffusible hydrogen when no noticeable differences were observed in the WFS using different shielding gases for both wires tested (Figure 6. 6). This observation is more noticeable at shorter CTWD of 15 mm and lower welding current of 280 A.

In general, welding under CO_2 produces reduced hydrogen levels, particularly for the seamed H10 consumable. However, the results are not entirely consistent for all conditions. For example, when welding with 100 %CO_2 shielding gas, the hydrogen levels tended to increase with welding current rather than decrease as was the case under 75Ar-25CO_2 shielding gas. Therefore, more information is required with respect to arc characteristics so that the mechanism responsible for these observations can be more clearly defined.

6.1.4   Effect of Atmospheric Conditions

The absorption of hydrogen into the molten weld metal is virtually unavoidable during arc welding, although the amount of hydrogen absorbed will vary significantly depending on the type of process, consumable used and its exposure to atmospheric conditions. The latter is well documented for the flux-cored wires exposed to detrimental atmospheric conditions for extended periods of time [Harwig et al. 1999 and Pitrun et al. 2001]. However, it is also important to understand how the atmospheric conditions during welding may affect the measured diffusible hydrogen results for gas shielded flux-cored wires in the 'as received' condition.

In this work, a total of 36 diffusible hydrogen tests were carried out over the period of 24 days during an April – May period, with atmospheric conditions typical for Melbourne at this time of the year. For both H10 and H5 wires, the relative humidity and temperature at the time of

welding was recorded for every set of welding conditions listed in Tables 6.1 and 6.2, with

relative humidity and temperature range between 47-61 % and 15-26 °C respectively, and

absolute moisture weight ranging between 5.31 and 10.66 g/kg of dry air.

From the relatively wide range of atmospheric conditions recorded during the hydrogen

welding trials, and with varying welding parameters, the effect of atmospheric conditions was

not clearly demonstrable. The relationship between the relative humidity and diffusible

hydrogen in deposited welds for both H10 and H5 wires is shown in Figure 6. 10. A large

scatter, particularly noticeable for the H10 weld deposits, using both shielding gases,

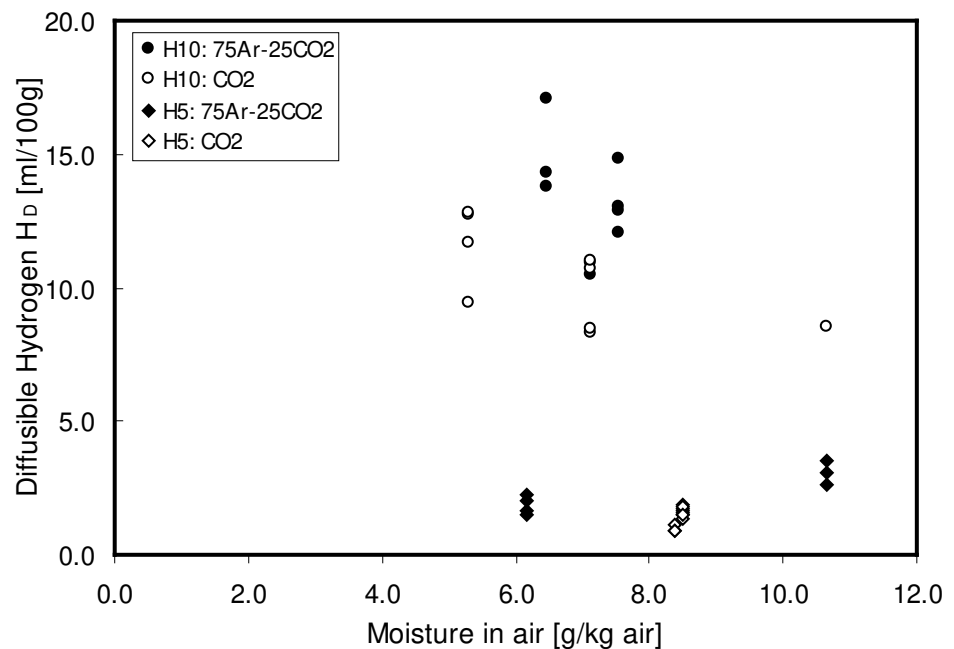characterized their relationship.
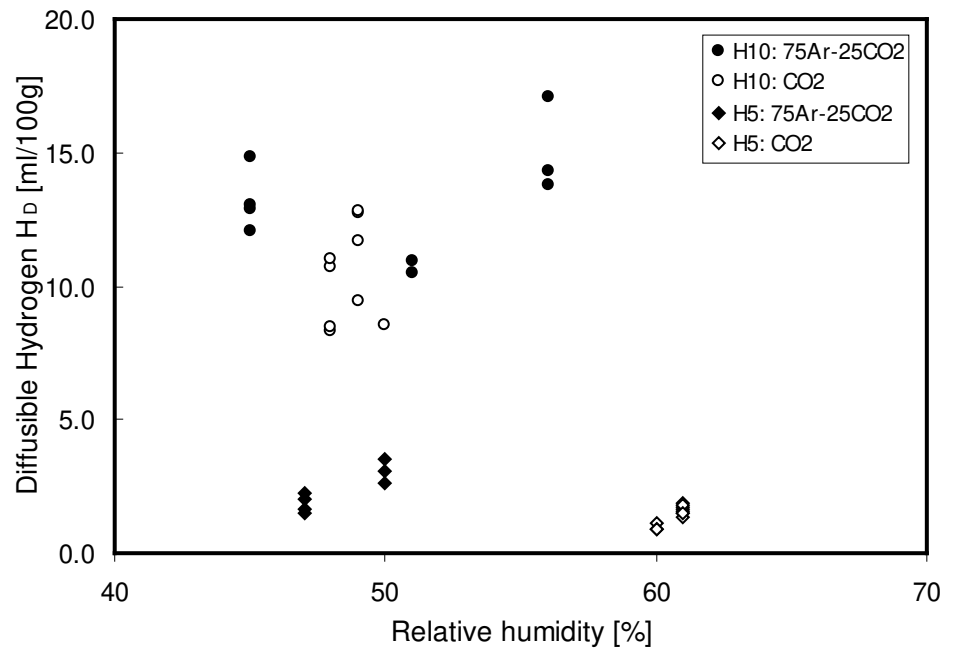
Figure 6. 10   Graph showing the relative humidity measured during welding for
diffusible for H10 and H5 weld deposits using $75Ar-25CO_2$ and CO_2
shielding gases hydrogen testing between April - May 2002.

This shows that varying welding parameters for each set of welding conditions appears to be more influential, and making it more difficult to observe the commonly accepted phenomenon that rising relative humidity results in the diffusible hydrogen increase [Kiefer 1996 and Feree 1992]. There was no apparent increase of diffusible hydrogen contents in the H5 welds even when the relative humidity was increased from 47 to 61 %.

Moisture content in the atmosphere is known to contribute to increase of diffusible hydrogen levels in weld metal [Siewert 1985]. In this current work, the actual moisture content, expressed in grams of water in 1 kg of dry air, was calculated for each hydrogen test. The relationship between the absolute moisture (5.3-10.7 g/kg dry air) and the diffusible hydrogen in the H10 and H5 weld deposits was not clear, as shown in Figure 6. 11.

Figure 6. 11   Graph showing the relative humidity measured during welding for diffusible for H10 and H5 weld deposits using 75Ar-25CO_2 and CO_2 shielding gases hydrogen testing between April - May 2002.

Once again, this is most likely due to changes of welding parameters for each test, which appear to be more significant than the atmospheric conditions at the time of welding. From these results, it is apparent that in order to study the effects of only atmospheric conditions on the diffusible hydrogen levels in weld deposits, the welding parameters should remain unchanged.

The results of study by van der Mee (2001) demonstrated that weld deposits using gas shielded rutile flux-cored wires (1.2 mm diameter, E71 T-1) with high levels of relative humidity (80 – 90 %), atmospheric temperatures (10-35 °C) and moisture content in the air (7-33 g/kg dry air), the weld metal diffusible hydrogen content raised from 3.7 to 6.4 ml/100g, representing 73 % increase.

However, it should be noted that van der Mee (2001), was able to demonstrate the effects of atmospheric moisture on the diffusible hydrogen in weld metal over a wider range of moisture content than in this current work, which was between 5.3 and 10.7 g/kg dry air. The range of moisture content measured during this work is shown diagrammatically in Figure 6. 12.
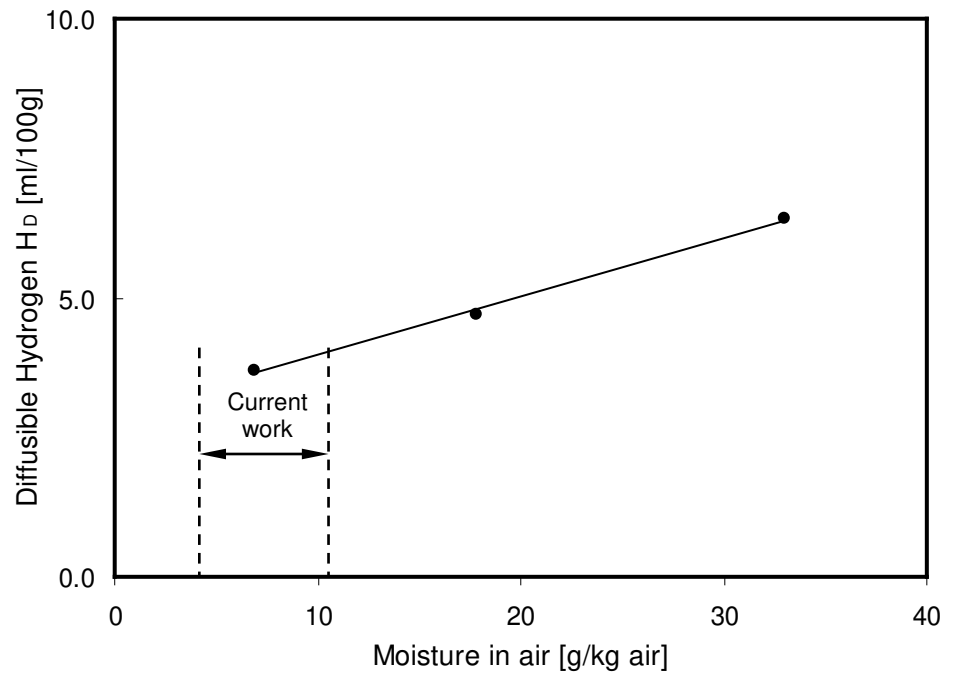
Figure 6. 12   Graph showing the relationship atmospheric moisture, represented by the content of moisture in dry air, and the weld metal diffusible hydrogen levels for welds deposited using rutile flux cored wire E71 T-1, with a nominal weld metal hydrogen content of 5 ml/100g (after van der Mee 2001).

Although the prime objective of this work was to study the effects of welding parameters and not atmospheric conditions on the weld metal diffusible hydrogen content, the results of work by Nolan and Pitrun (2003), using E71 T-1 (H10 classification) also indicate a minor increase of diffusible hydrogen in weld deposits at atmospheric conditions, characterized by relatively smaller increases in relative humidity and temperature. This observation suggests that further work would be very valuable, especially studying the significance of atmospheric conditions on diffusible hydrogen for weld deposits using rutile wires with nominal hydrogen levels of 10 ml/100g.

6.2   ARC TRANSFER IMAGES

The greater the heat generated through increased welding current, the greater is the WFS required to accommodate the greater burn-off rate of the electrode. This counteractive effect reduces the time available for temperature increase due to resistive heating. An exact relationship between current, t_{RHZ} and resistance heating energy, Q, is not possible without an accurate assessment of arc length.

The consumable investigated for this part of the work was a seamed rutile wire H10 and, importantly, it was deposited using the same welding equipment as for all previous experiments. A total of 10 sets of welding parameters were selected to examine metal transfer and arc dimensions, as listed in Table 6. 5.

Table 6. 5   Matrix of welding parameters investigated for arc imaging tests on the H10 consumable.

Sample	Welding current [A]	Voltage [V]	Travel speed [mm/min.]	Heat input [kJ/mm]	Shielding gas [18l/min]	CTWD [mm]	Deposited Hydrogen H_D [ml/100g]
H10-1-A	280	30	400	1.26	$75Ar-25CO_2$	15	17.0
H10-7-A	280	same	same	1.26	$75Ar-25CO_2$	25	12.0
H10-3-A	320	same	same	1.44	$75Ar-25CO_2$	15	13.8
H10-9-A	320	same	same	1.44	$75Ar-25CO_2$	25	10.5
H10-10-C	280	same	same	1.26	CO_2	15	11.7
H10-16-C	280	same	same	1.26	CO_2	25	8.3
H10-12-C	320	same	same	1.44	CO_2	15	12.8
H10-18-C	320	same	same	1.44	CO_2	25	8.6

The average measured values of l_{RHZ}, AL, t_{RHZ}, Q and with hydrogen levels extracted from equivalent conditions in earlier part of this work, for each set of welding conditions are also presented.

6.2.1 Effect of Welding Current

Regarding the effect of welding current on arc characteristics and hydrogen content, arc images for welding at CTWD of 15 mm using both shielding gases and welding currents of 280 and 320 A, are shown in Figure 6. 13. It can be seen that under these conditions and for 75Ar-25CO_2 shielding gas, an increase in current results in a slight decrease of 16 % in t_{RHZ} (0.13 to 0.11s), but a 37 % decrease in arc length (3.8 to 2.4 mm). This, as expected, resulted in an increase of 28 % in heat generated energy (52.5-76.3 J). This effect is accompanied by a decrease in diffusible hydrogen from 17.0 to 13.8 ml/100g, representing a 23 % decrease. It would appear in this case that the reduction in diffusible hydrogen is primarily a result of the decreased arc length, which reduces the potential for dissociation of moisture or organic residues and absorption of hydrogen into the molten weld pool.

Under CO_2 shielding gas, the measured parameters appeared to be less affected by the welding current increase. A slight decreases in t_{RHZ} (from 0.14 to 0.12 s) and in arc length (from 1.5 to 1.4 mm), and with marginal increase of 11 % in the heat energy Q (from 71.6 to 79.5 J) in the wire. Figure 6. 14 shows the effect of welding current increase from 280 to 320 A and generated heat at CTWD of 15 and 25 mm welded using both shielding gases. It appears that welding current has a less significant effect on the increase of heat energy when compare to the CTWD increase for both shielding gases used. This is demonstrated by the slight increase in diffusible hydrogen levels, from 11.7 to 12.8 ml/100g, which is probably insignificant.
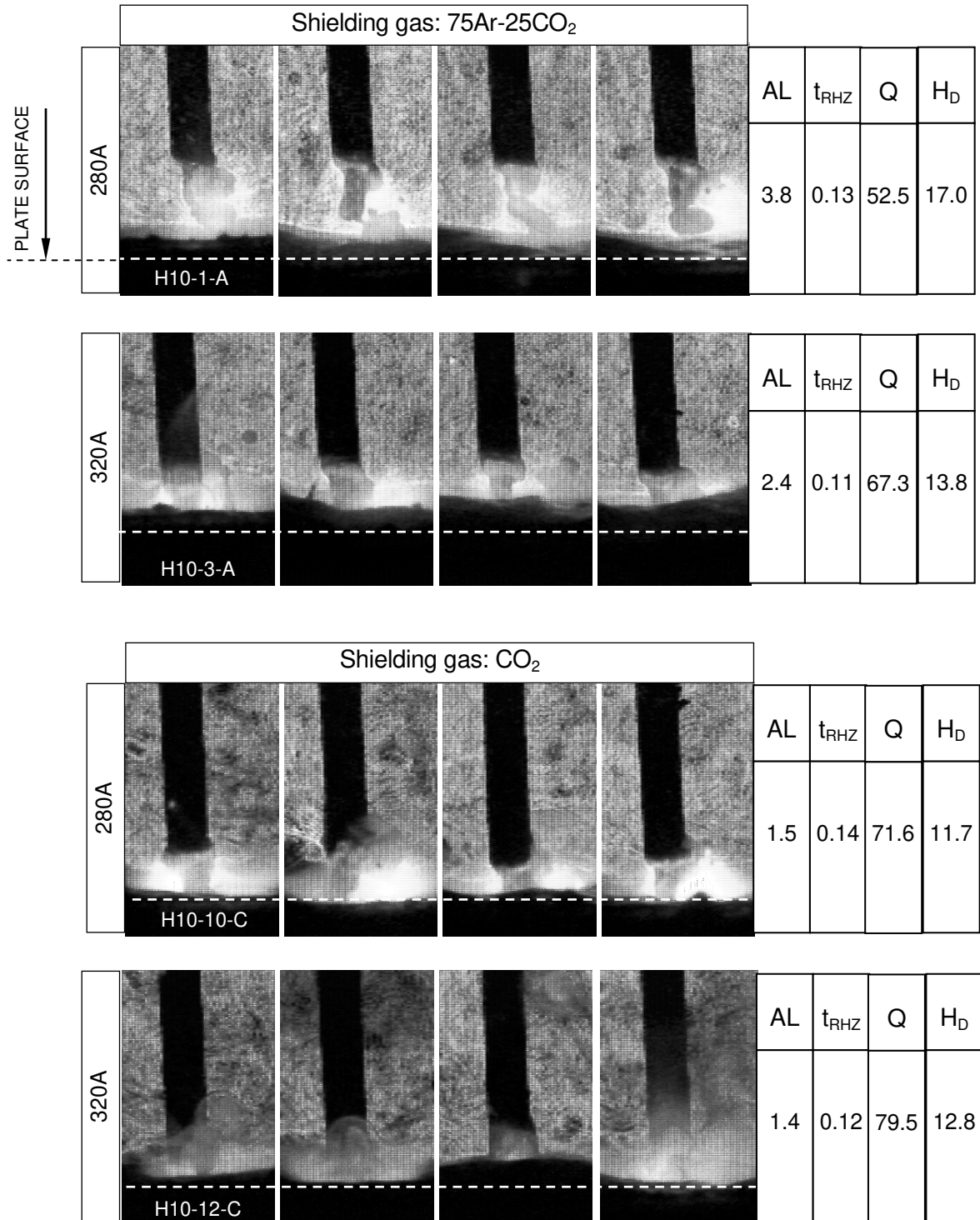
Figure 6. 13   Table showing the effect of welding current (280 and 320 A) on arc characteristics using $75Ar-25CO_2$ and CO_2 shielding gas at 15 mm CTWD. AL [mm], t_{RHZ} [s], Q [J] and H_D [ml/100g].
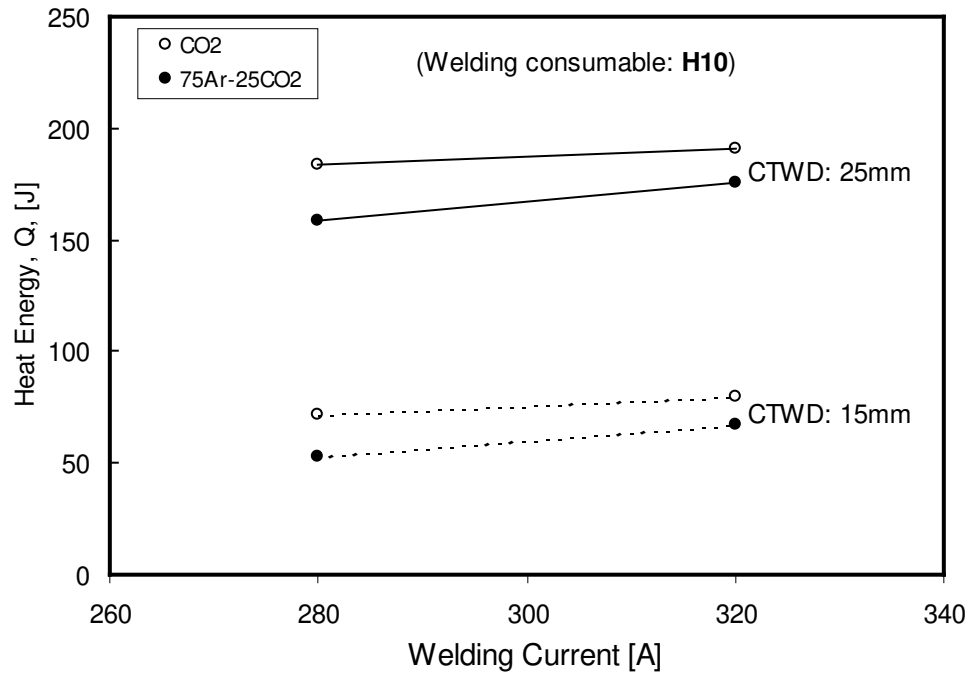
Figure 6. 14   Graph showing the relationship between welding current (280 and 320 A) and generated heat, Q, at CTWD of 15 and 25 mm for 75Ar-25CO$_2$ and CO$_2$ shielding gases.

While previous work has reported an increase in diffusible hydrogen levels with increasing welding current explained by a transition from globular metal to spray-like metal transfer [White et al. 1992 and Kiefer 1996], in the current work, the results of the arc imaging confirmed that the metal transfer remained globular within the welding current of 280-320 A.

6.2.2   Effect of CTWD

Typical arc images for the H10 wire, welded using CTWDs of 15 and 25 mm and both shielding gases, are shown in Figure 6. 15. Under constant welding conditions of 280 A, 29-30 V and CTWD 15 mm, and with 75Ar-25CO$_2$ shielding gas the arc length (AL) and the time in the resistive heating zone (t_{RHZ}) were found to be 3.8 mm and 0.13 s, respectively, and the

measured diffusible hydrogen content was 17.0 ml/100g. With the higher CTWD of 25 mm, t_{RHZ} was increased by 54% to 0.20 s and arc length decreased to 3.2 mm, accompanied by a decrease in diffusible hydrogen content to 12.0 ml/100g. The most significant increase, from 52.5 to 159.0 J, was found in the wire heat energy. This amount of heat generated in the wire, represented by a 300 % was likely to be most accountable for the 17 % decrease in weld metal diffusible hydrogen content.

In the case of welding with similar conditions under CO_2 shielding gas also shown in Figure 6. 15, a similar increase of 50 % in t_{RHZ} from 0.14 to 0.21 s was observed for the increase in CTWD from 15 to 25 mm. However, in this case, the arc length remained unchanged with increasing CTWD, but the diffusible hydrogen was reduced from 11.7 to 8.3 ml/100g, represented by 29 % decrease. Similar as for the mixed gas, there was a significant increase (275 %) of heat energy released from 71.6 to 184.0 J.

These results confirm that increasing CTWD (from 15 to 25 mm) causes an increase in the time interval that the wire resides in the resistive heating zone, t_{RHZ}, and significant increase of heat generated energy, Q, in the wire. This effectively results in lower values of diffusible hydrogen in deposited weld metal. The decrease in arc length with CTWD, observed when welding with mixed gas, is likely to have also contributed to the reduced hydrogen level.

				AL	t_{RHZ}	Q	H_D
				3.8	0.13	52.5	17.0

H10-1-A

				AL	t_{RHZ}	Q	H_D
				3.2	0.20	159.0	12.0

H10-7-A

				AL	t_{RHZ}	Q	H_D
				1.5	0.14	71.6	11.7

H10-10-C

				AL	t_{RHZ}	Q	H_D
				1.5	0.21	184.0	8.3

H10-16-C
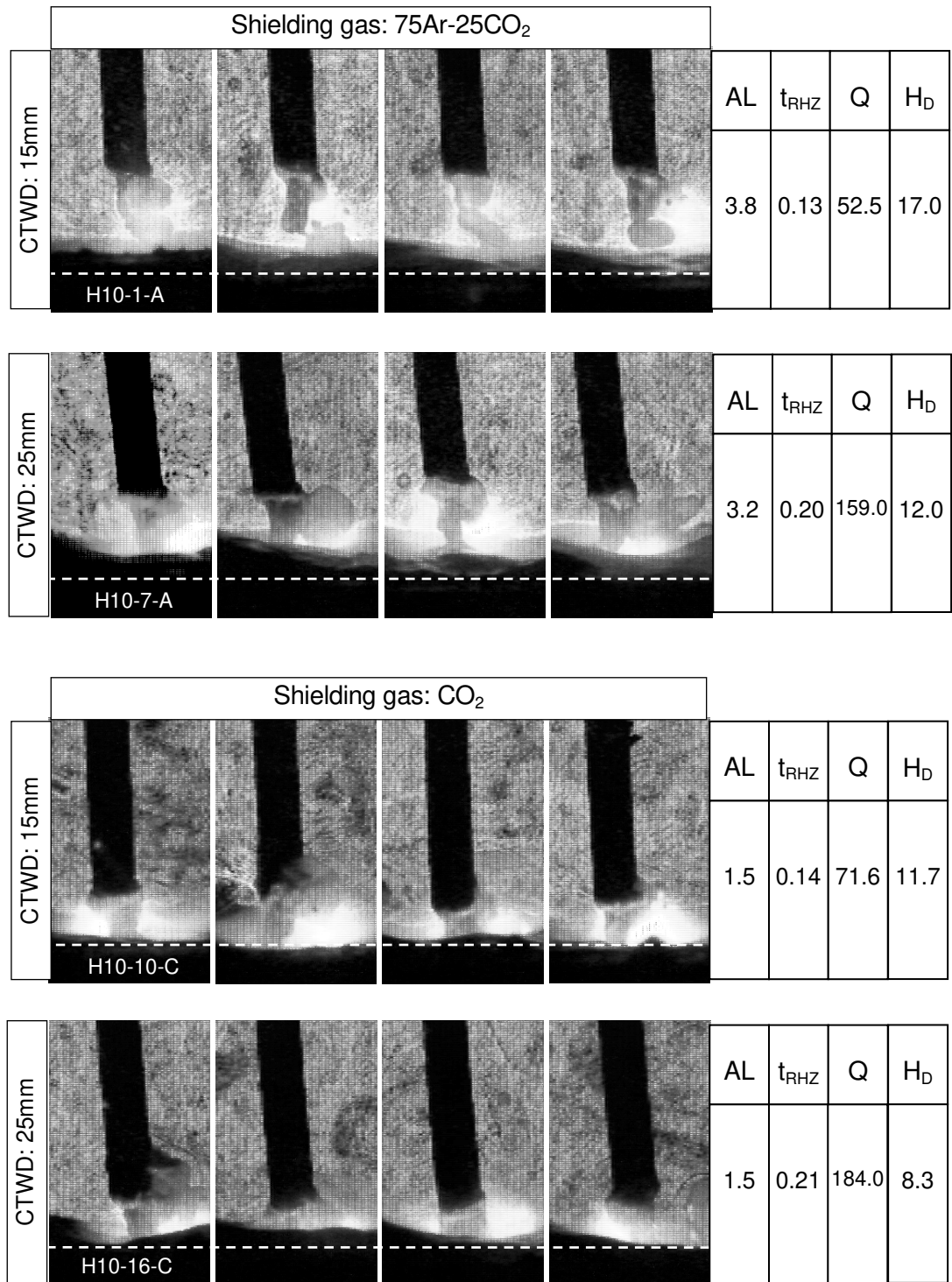
Figure 6. 15   Table showing the effect of CTWD (15 and 25 mm) on arc characteristics using 75Ar-25CO$_2$ and CO$_2$ shielding gas at welding current of 280 A. AL [mm], t_{RHZ} [s], Q [J] and H_D [ml/100g].

However, the fact that hydrogen was reduced for both shielding gases, despite a constant arc length being observed in the case of CO_2 shielding gas, suggests that the dominant mechanism for reduction in diffusible hydrogen levels with increasing CTWD is the increase in t_{RHZ} (50 %) and heat energy generated (an increase of up to 260 %).

When comparing the effects of welding current and CTWD on the diffusible hydrogen, the results indicates that the effect of increasing the CTWD has a more significant effect on reduction of diffusible content compared to that of the welding current. This is most likely due to the relatively small increases of heat energy accompanying the increase in welding current, compare to those generated by the increase in CTWD. This relationship is shown in Figure 6. 16.
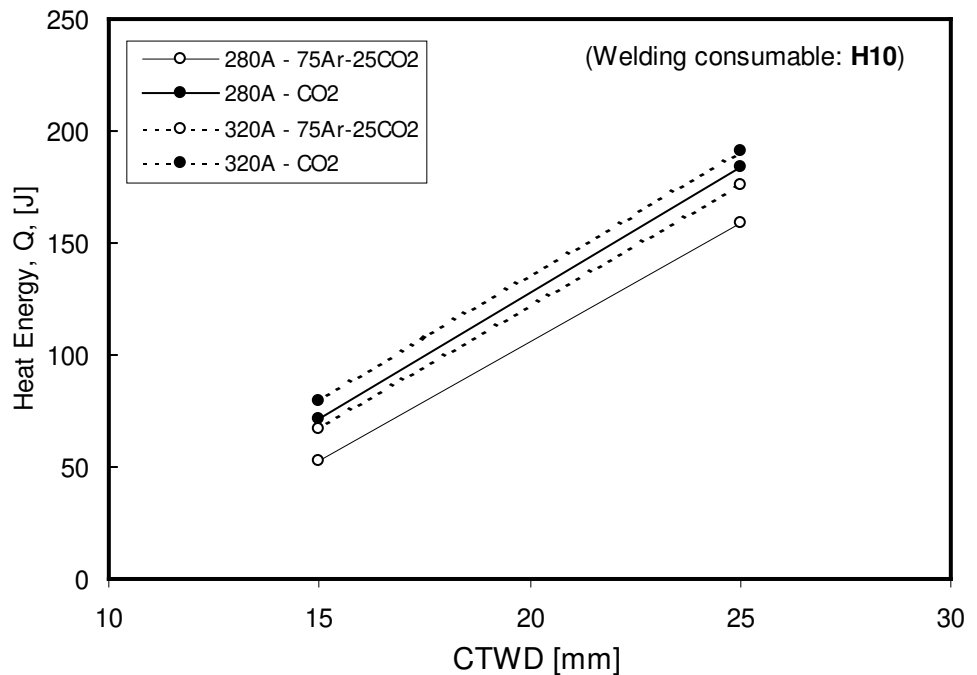
Figure 6. 16   Graph showing the relationship between CTWD (15 and 25 mm) and generated heat, Q, at welding current of 280 and 320 A for 75Ar-25CO$_2$ and CO$_2$ shielding gases.

During welding trials on the effect of CTWD, arc destabilization was noted with increasing CTWD. The results from this part of the work on arc imaging did not reveal obvious cause for this effect. Arc length was observed to decrease with increasing CTWD under mixed gas shielding, but there was no clear change in the mode of metal transfer.

6.2.3 Effect of Shielding Gas

The relationships between the arc length and welding current, and between t_{RHZ} and welding current, for welding under mixed and CO_2 gas are shown diagrammatically in Figure 6. 17 and Figure 6. 18, derived from the preceding arc images.

For welding under mixed gas, the arc length is significantly decreased with increasing welding current resulting in a decrease in hydrogen. This effect is more pronounced for the shorter CTWD, suggesting that the increased arc length allows greater opportunity for hydrogen to be absorbed into deposited weld metal. The t_{RHZ} was found to decrease with increasing welding current under all conditions investigated.

For CO_2 welding, the measured arc lengths were significantly shorter than those observed when using 75Ar-25CO_2 shielding gas. Generally for CO_2 welding, the changes in welding current and CTWD had a little effect on the arc length (see Figure 6. 17).

The effect of shielding gas on arc characteristics can be concluded from Figures 6.16 and 6.17. For example, for welding current of 280 A and CTWD of 15 mm, changing from mixed gas to CO_2 shielding gas resulted in an insignificant increase in t_{RHZ}, but a very significant decrease in arc length from 3.8 to 1.5 mm (140 % decrease). This change of arc length was accompanied by a decrease in diffusible hydrogen content from 17.0 to 11.7 ml/100g.
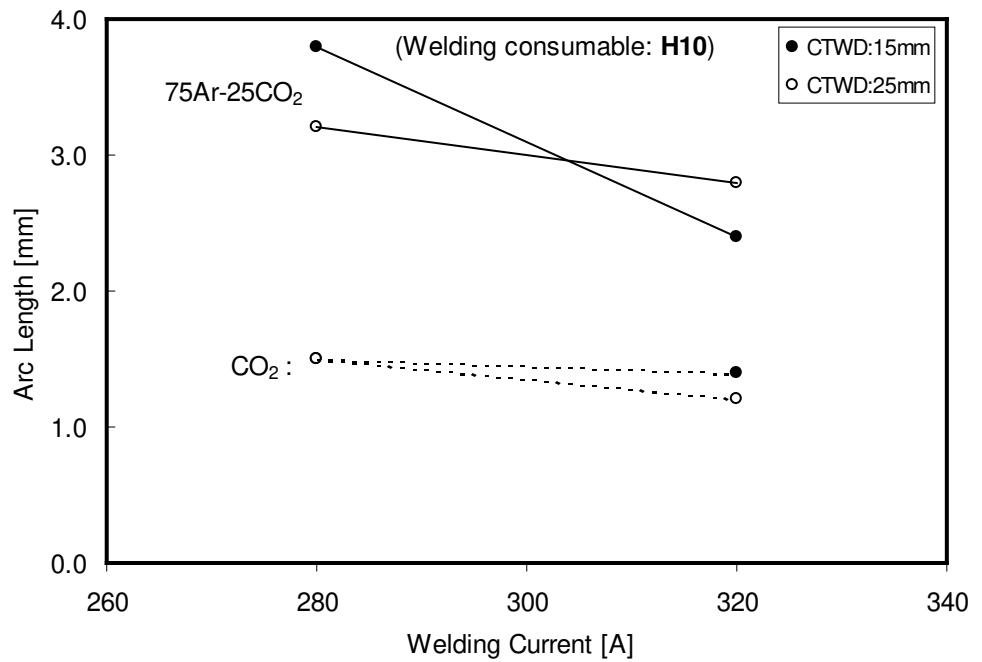
Figure 6. 17   Graph showing the relationship between welding current and arc length at CTWD of 15 and 25 mm for 75Ar-25CO$_2$ and CO$_2$ shielding gases.
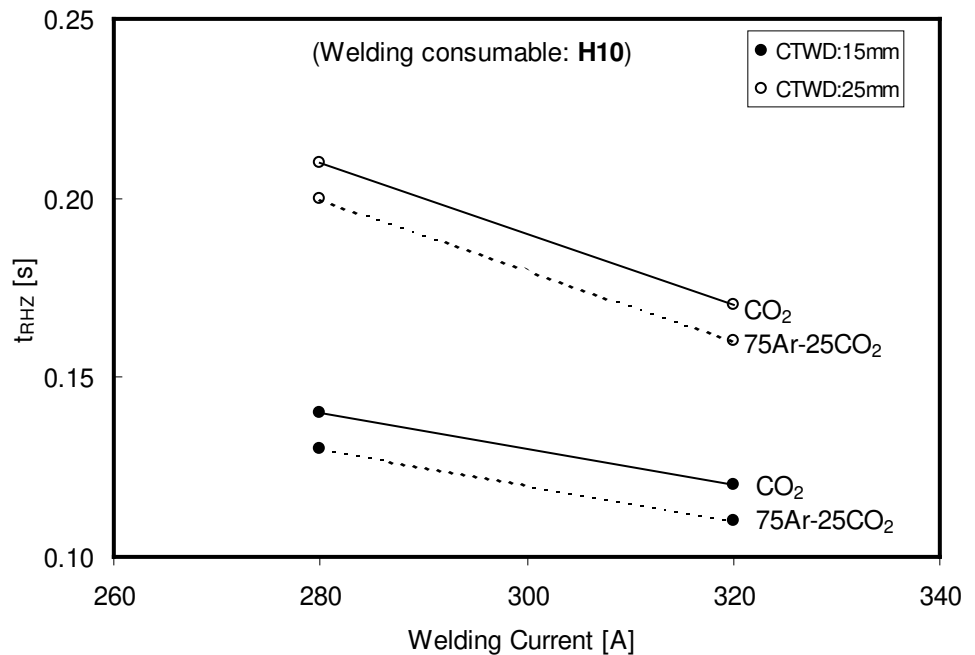

Figure 6. 18   Graph showing the relationship between welding current and time in resistive heating zone, t$_{RHZ}$, at CTWD of 15 and 25 mm for 75Ar-25CO$_2$ and CO$_2$ shielding gases.

Similarly, a significant reduction of AL (113 % decrease) was observed for 25 mm CTWD, under CO_2 shielding gas, but the t_{RHZ} did vary significantly with the change of shielding gas.

The effect of increasing the heat energy on the weld metal diffusible hydrogen levels (at unchanged welding current of 280 A) are shown in Figure 6. 19. It is apparent that the levels of resistive heat generated in the wire, for both CTWD of 15 and 25 mm, were found to be increasing by the change of shielding gas from $75Ar-25CO_2$ to CO_2.
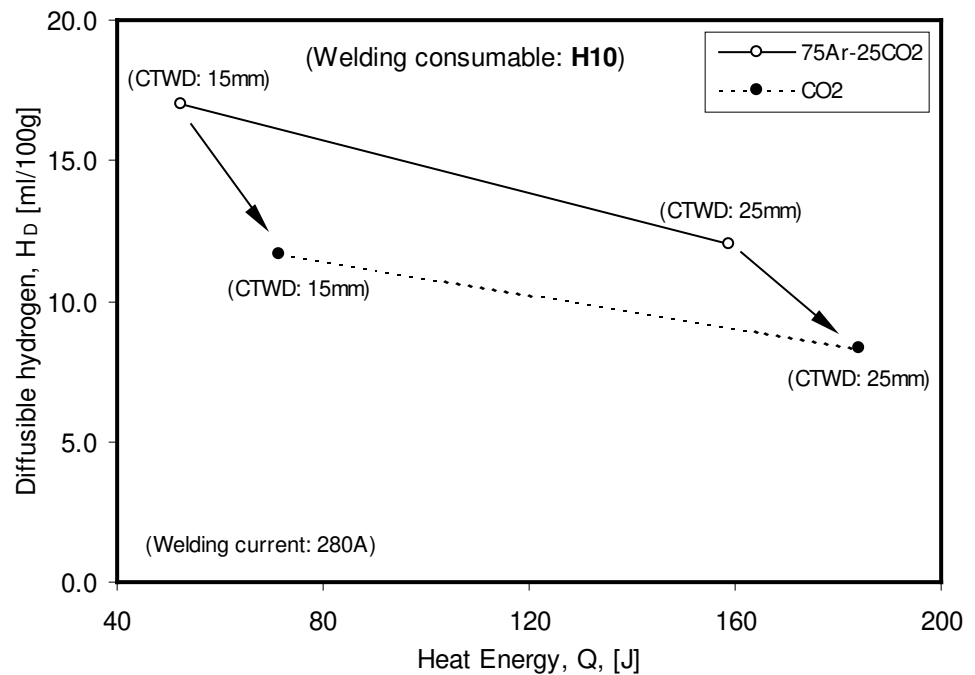
Figure 6. 19   Graph showing the relationship between heat energy, Q, and diffusible hydrogen levels in H10 weld deposits at CTWD of 15 and 25 mm for $75Ar-25CO_2$ and CO_2 shielding gases.

Another important factor to consider is the effect of CO_2 content in the shielding gas on the oxidation potential of the atmosphere in the arc. The oxidation potential (OP) is related to the content of oxygen and carbon dioxide in the arc according to Equation 4.5, [Norrish and Richardson 1988]. It has been shown that an argon-based shielding gas becomes more oxidizing as CO_2 content is increased, with a rapid increase in oxidizing potential in shielding gases containing over 25 % CO_2. Since monatomic hydrogen in the arc can be oxidized, and therefore neutralized in the terms of its absorption into the weld pool, the higher levels of CO_2 in the shielding gas are likely to lead to reduced levels of diffusible hydrogen in the weld deposits [Kiefer 1996].

From the current results, it is apparent that the shielding gas plays an important role in facilitating the pickup of hydrogen from the arc atmosphere. For example, it is seen that in the case of the H10 wire, welding under mixed gas results in significantly higher levels of diffusible hydrogen, associated with a significant increase in the arc length, as illustrated in Figure 6. 20. These results suggest that although OP is understandably influential, arc length is an important factor in determining hydrogen uptake due to the shielding gas change. Presumably, the increase in arc length provides more opportunity for hydrogenous compounds to ionize, thereby providing the source of monatomic hydrogen for absorption into the weld metal.
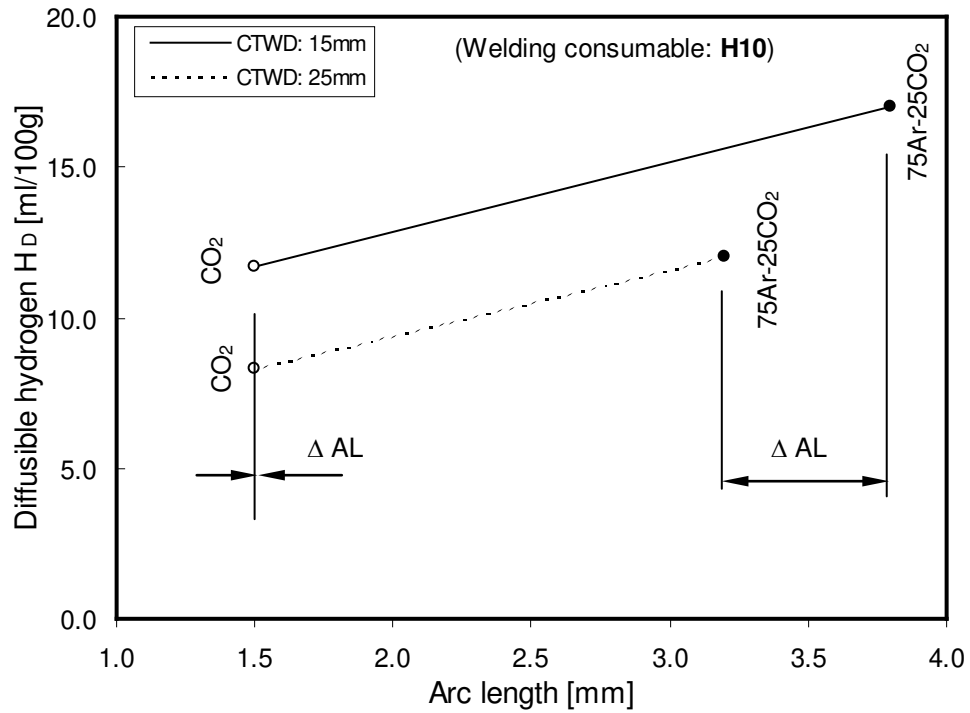
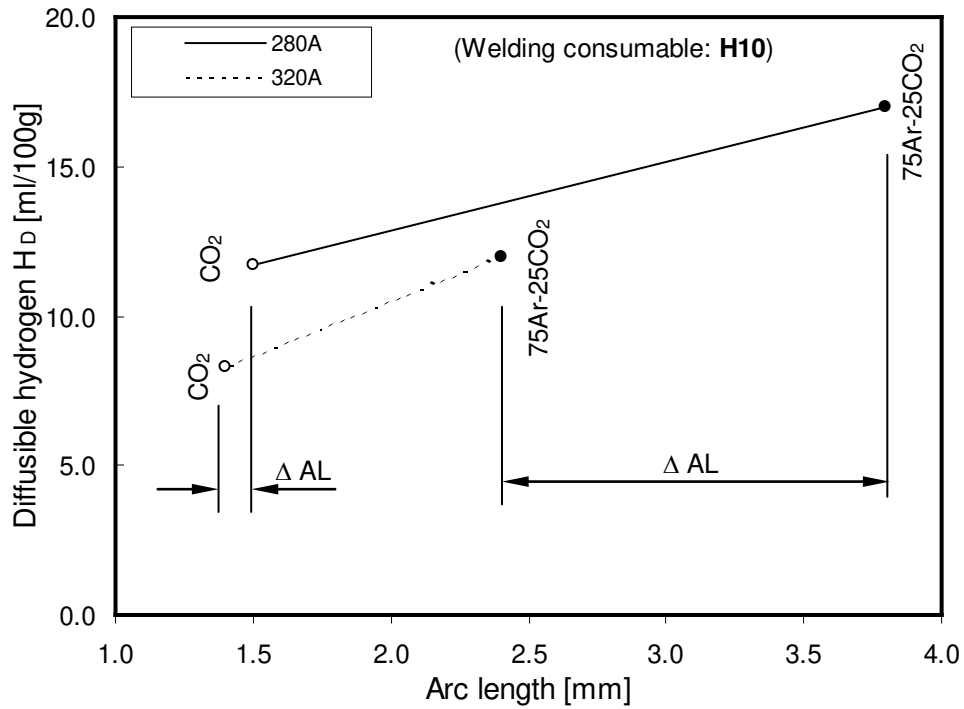Figure 6. 20   Graph showing the relationship between arc length and diffusible hydrogen levels in H10 welds deposited using welding current of 280 A, CTWD of 15 and 25 mm and using $75Ar-25CO_2$ and CO_2 shielding gases.

The results of this work suggest that when welding under the $75Ar-25CO_2$ shielding gas, the AL is significantly increased, particularly noticeable at the lower welding current of 280 A, resulting in a significant increase of diffusible hydrogen, as shown in Figure 6. 21.   This diagram also illustrates that by increasing welding current the arc length is reduced, ΔAL, for both shielding gases, and corresponding to a reduction of diffusible hydrogen. However, this decrease of arc length is more evident during welding under $75Ar-25CO_2$ shielding gas, where AL was significantly reduced from 3.8 to 2.4 mm.

Figure 6. 21   Graph showing the relationship between arc length and diffusible hydrogen levels in H10 welds deposited at CTWD of 15 mm, welding current of 280 and 320 A and using $75Ar-25CO_2$ and CO_2 shielding gases.

However, it is also clear that the mixed gas provides a more stable medium for the hydrogen ions, such that they remain active in the arc atmosphere and are better able to be absorbed in the weld pool. It is suggested that the higher oxidation potential of the CO_2 shielding gas results in reduced availability of ionic hydrogen in the arc.

The results obtained from the arc imaging experiments are summarized in Table 6. 6. Hydrogen levels obtained were higher when using $75Ar-25CO_2$ shielding gas at all comparable welding currents and CTWD combinations. For the particular H10 wire investigated, the calculated values of t_{RHZ} were also found to be similar between shielding gases $75Ar-25CO_2$ and CO_2 for all combinations of welding conditions. In contrast, the values

of AL and Q under comparable welding conditions were found to significantly decrease and increase respectively, when welding with CO_2 shielding gas. This was accompanied by a significant decrease in diffusible hydrogen levels.

Table 6. 6   Matrix of welding parameters and values investigated on arc imaging.

Selected welding parameters				Measured Values				
Shielding gas [18 l/min]	Welding Current [A]	Voltage [V]	CTWD [mm]	WFS [m/min]	t_{RHZ} [s]	Average Arc Length [mm]	Heat Energy Q [J]	Diffusible Hydrogen levels H_D [ml/100g]
75Ar-25CO$_2$	280	29-30	15	5.35	0.13	3.8	52.5	17.0
	320		15	6.90	0.11	2.4	67.3	13.8
	280		25	6.65	0.20	3.2	159.0	12.0
	320		25	8.20	0.16	2.8	175.6	10.5
CO$_2$	280	29-30	15	5.70	0.14	1.5	71.6	11.7
	320		15	6.80	0.12	1.4	79.5	12.8
	280		25	6.70	0.21	1.5	184.0	8.3
	320		25	8.65	0.17	1.2	191.4	8.6

Finally it should be noted that under most welding parameters and shielding gases selected in this work, the weld metal hydrogen content measured for H10 seamed rutile wire did not comply with its hydrogen classification, as specified by the wire manufacturer, except when using a combination of the longest CTWD of 25 mm and CO_2 shielding gas (see Figure 6. 6). The H5 seamless wire produced weld metals that easily complied with the hydrogen levels specified by the manufacturer for all welding conditions investigated.

6.3   G-BOP TESTING

The effects of welding parameters on susceptibility of the weld metal to transverse HACC was investigated by conducting a series of G-BOP cold cracking tests.

The results from testing of H10 and H5 weld metals using a range of preheat temperatures are summarized in Tables 6.7, 6.8, 6.9 and 6.10. The corresponding fracture faces of H10 and H5 weld deposits are shown in Appendix C. The G-BOP test results for H10 weld metal show cold cracking at all combinations of welding parameters selected at the no-preheat condition of 20 °C. In contrast, the H5 weld metals exhibited no cracking at room temperature. Therefore, the examination of H5 at higher preheat temperatures was not pursued.

Table 6. 7   Percentage of cold cracking for H10 welds deposited using 75Ar-25CO$_2$ shielding gas at various preheat temperatures.

Sample	Welding parameters			Preheat temperature [°C]					H$_D$ [ml/100g]
				20	**50**	**80**	**100**	**120**	
	Welding current [A]	Shielding gas [18 l/min]	CTWD [mm]	Percentage cracking [%]					
H10-1-A	280		15	100	100	88	0	-	17.0
H10-4-A	280		20	100	98	16	18	0	14.8
H10-7-A	280		25	100	100	29	0	-	12.0
H10-2-A	300		15	100	96	39	17	0	14.3
H10-5-A	300	75Ar-25CO$_2$	20	100	100	53	11	0	12.9
H10-8-A	300		25	100	100	31	0	-	11.0
H10-3-A	320		15	97	70	18	0	-	13.8
H10-6-A	320		20	100	82	36	4	-	13.1
H10-9-A	320		25	94	83	30	0	-	10.5
RH [%] – Temperature [°C]				50 - 17	37 - 18	45 - 25	28 - 26	44 - 22	

Table 6. 8   Percentage of cold cracking for H10 welds deposited using CO$_2$ shielding gas at various preheat temperatures.

Sample	Welding parameters			Preheat temperature [°C]					H$_D$ [ml/100g]
				20	**50**	**80**	**100**	**120**	
	Welding current [A]	Shielding gas [18 l/min]	CTWD [mm]	Percentage cracking [%]					
H10-10-C	280		15	89	57	24	0	-	11.7
H10-13-C	280		20	88	50	38	16	0	9.5
H10-16-C	280		25	67	66	38	12	0	8.3
H10-11-C	300		15	58	37	17	0	-	12.7
H10-14-C	300	CO$_2$	20	76	65	0	0	-	10.7
H10-17-C	300		25	67	70	27	16	0	8.4
H10-12-C	320		15	25	0	0	0	-	12.8
H10-15-C	320		20	75	48	22	13	0	11.0
H10-18-C	320		25	73	70	26	8	0	8.6
RH [%] – Temperature [°C]				44 - 22	44 - 22	45 - 25	42 - 26	44 - 22	

Table 6. 9   Percentage of cold cracking for H5 welds deposited using 75Ar-25CO$_2$ shielding gas at various preheat temperatures.

	Welding parameters			Preheat temperature [°C]					H$_D$ [ml/100g]
				20	**50**	**80**	**100**	**120**	
Sample	Welding current [A]	Shielding gas [18 l/min]	CTWD [mm]	Percentage cracking [%]					
H5-1-A	280		15	0	-	-	-	-	3.5
H5-4-A	280		20	0	-	-	-	-	2.2
H5-7-A	280		25	0	-	-	-	-	1.5
H5-2-A	300		15	0	-	-	-	-	3.1
H5-5-A	300	75Ar-25CO$_2$	20	0	-	-	-	-	2.1
H5-8-A	300		25	0	-	-	-	-	1.7
H5-3-A	320		15	0	-	-	-	-	2.6
H5-6-A	320		20	0	-	-	-	-	1.6
H5-9-A	320		25	0	-	-	-	-	1.6
RH [%] – Temperature [°C]				42 - 17	-	-	-	-	

Table 6. 10   Percentage of cold cracking for H5 welds deposited using CO$_2$ shielding gas at various preheat temperatures.

	Welding parameters			Preheat temperature [°C]					H$_D$ [ml/100g]
				20	**50**	**80**	**100**	**120**	
Sample	Welding current [A]	Shielding gas [18 l/min]	CTWD [mm]	Percentage cracking [%]					
H5-10-C	280		15	0	-	-	-	-	1.9
H5-13-C	280		20	0	-	-	-	-	1.8
H5-16-C	280		25	0	-	-	-	-	1.1
H5-11-C	300		15	0	-	-	-	-	1.5
H5-14-C	300	CO$_2$	20	0	-	-	-	-	1.3
H5-17-C	300		25	0	-	-	-	-	0.9
H5-12-C	320		15	0	-	-	-	-	1.7
H5-15-C	320		20	0	-	-	-	-	1.5
H5-18-C	320		25	0	-	-	-	-	0.9
RH [%] – Temperature [°C]				42 - 17	-	-	-	-	

6.3.1   Effect of Welding Current

According to the literature, the diffusible hydrogen content is dependent on the welding current [White et al. 1992, Sierdzinski and Ferree 1998]. Both studies recorded an increase of diffusible hydrogen levels due to welding current increase. This was observed in weld deposits using rutile flux cored wires welded using mixed shielding gases. However, the weld metal susceptibility to cold cracking was not reported.

The plotted results of the G-BOP tests show a clear relationship between the susceptibility of weld metal cracking and welding current, as shown diagrammatically in Figure 6. 22 and in Appendix D. From the diagrams presented, it is apparent that the welding current effects the weld metal cracking differently with varying combinations of other welding conditions. Perhaps the most noticeable difference is that the welding current increase from 280, 300 and 320 A, when using $75Ar-25CO_2$ shielding gas, appears to have very little effect on percentage cracking at room temperature at all CTWD tested. Despite the significant differences in the weld metal hydrogen content range from 10.5 to 17.0 ml/100g, the values of room temperature cracking (RTC) eight out of ten G-BOP samples revealed 100 % cracking. Only two samples, H10-3-A and H10-9-A, produced using the highest welding current of 320 A, exhibited 97 and 94 %RTC, respectively.

As expected, by introducing the preheat temperature from 50, 80 100, and 120 °C, the percentage of cold cracking was reduced. This effect is perhaps most noticeable at the shortest CTWD of 15 mm, using $75Ar-25CO_2$ shielding gas, as shown in Figure 6. 22, diagram (A15).
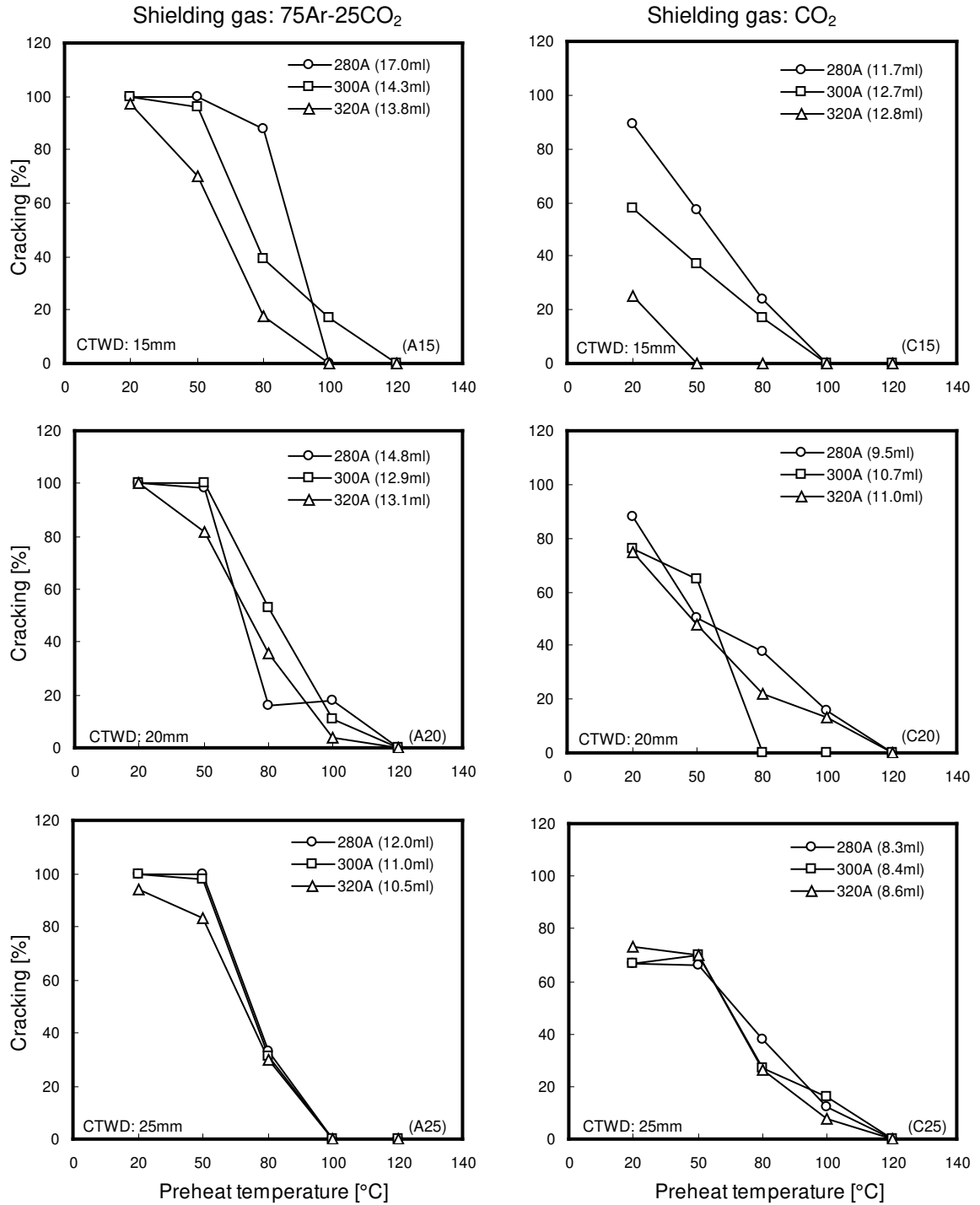
Figure 6. 22   Graphs showing the percentage cracking for H10 weld metal in G-BOP tests, using 75Ar-25CO$_2$ and CO$_2$ shielding gases at welding currents 280, 300 and 320 A and CTWD of 15, 20 and 25 mm.

Here, the plotted lines for each current level are further apart than those plotted in diagram (A25), for a CTWD of 25 mm. This was most likely due to the relatively lower and wider range of hydrogen levels for weld metal produced at 15 mm CTWD (13.8-17.0 ml/100g) rather than at 25 mm CTWD (10.5-12.0 ml/100g).

It should be noted that the weld metal deposited using the lowest welding current of 280 A at 15 mm CTWD contained the maximum amount of diffusible hydrogen in weld metal (17.0 ml/100g for sample H10-1-A) and also exhibited a significantly higher percentage of cracking up to the preheat temperature of 80 °C. This observation confirms an expectation based on the earlier reported results in this work on weld metal diffusible hydrogen levels. An increasing welding current reduces the weld metal diffusible hydrogen levels (see Figure 6. 5) and its susceptibility to cold cracking when welded using 75Ar-25CO$_2$ shielding gas and CTWD of 15 mm.

When comparing the diagrams (A15) and (A25), it is suggested that an increase in welding current tends to result in reduced susceptibility of weld metal to cold cracking. This was particularly noticeable at the shorter CTWD of 15 mm and at preheat temperatures over the ambient. An increase in CTWD, accompanied by lower hydrogen levels, results in a reduced influence of welding current. It is apparent that the preheat temperature increase is the major contributor to reduction of percentage of cracking in this case, suppressing the cracking more consistently at all welding currents.

The percentage cracking observed, when using CO$_2$ shielding gas, showed a more complex relationship with welding current, particularly at the shortest CTWD of 15 mm. The increase of welding current, which resulted in an increase of weld metal diffusible hydrogen content

(see Figure 6. 5), produced a significant and unexpected reduction of weld metal susceptibility to cold cracking at room temperature, as shown in Figure 6. 22 diagram C15. This effect was also observed when preheating was employed. Possible explanations for this phenomenon are either the geometry of the G-BOP welds cross sections, as shown in Figure 6. 23, or differences in weld metal microstructure. The fused weld metal profiles varied significantly with welding current increase at the 20 °C preheat. For example, the sample deposited using the lowest welding current of 280 A was characterized by a very flat and wide bead profile (89 %RTC), whereas the sample welded using high welding current of 320 A (25 %RTC) is characterized by deeper penetration and a higher bead height. Increase in preheat temperature appears to suppress this effect and the weld deposit contours gradually become more even.

Welding Conditions: Sample: 'H10'
Shielding gas: CO_2
CTWD: 15 mm
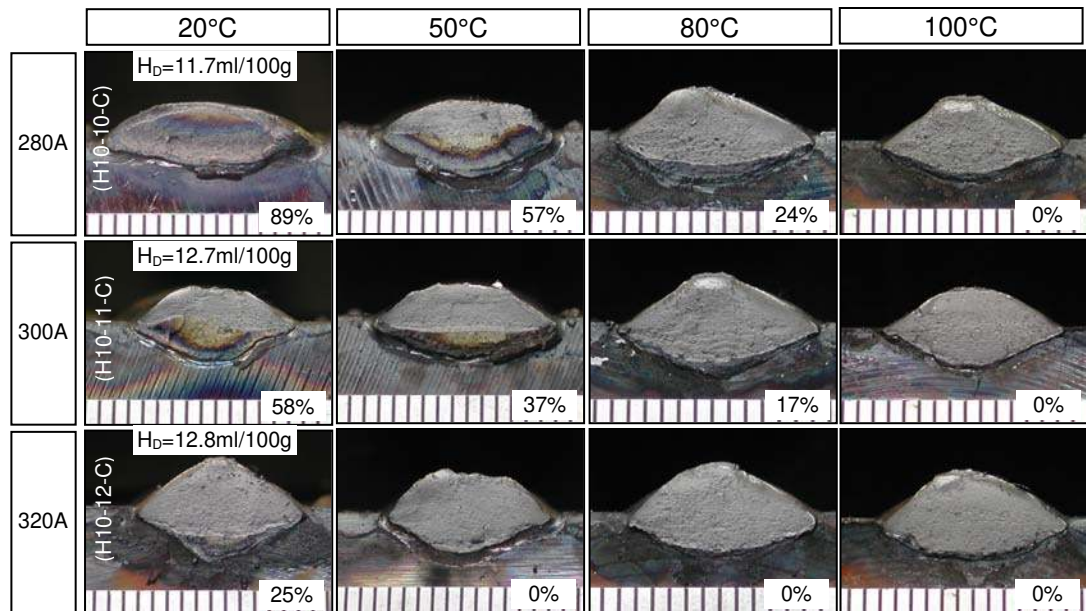
Figure 6. 23   Photograph showing the G-BOP fracture faces with cracking percentage of H10 weld metal deposited at preheat temperatures 20, 50, 80 and 100 °C using CO_2 shielding gas and CTWD of 15 mm.

Although the diffusible hydrogen levels range is relatively very narrow (11.7-12.8 ml/100g), the increase in welding current was found to be beneficial and significantly reduce the weld metal cold cracking susceptibility at all preheat temperatures examined in this work. At the lowest CTWD of 15 mm the welding current appears to be the governing variable in reduction of cracking percentage at 20, 50 and 80 °C preheat temperature.

When comparing the diagrams (C15) and (C25) shown in Figure 6. 22, it is apparent that an increase in welding current at the shortest CTWD of 15 mm can significantly reduce the susceptibility of the weld metal to cold cracking at all preheat temperatures, even for a very narrow range of 11.7-12.8 ml/100g in diffusible hydrogen content. However, for an increase of CTWD from 15 to 25 mm, with weld metal containing relatively lower hydrogen levels and closer range of weld metal diffusible hydrogen of 8.3-8.6 ml/100g, the change in welding current change has an insignificant effect.

6.3.2   Effect of CTWD

The effect of CTWD from 15 to 25 mm on cracking susceptibility is best illustrated in Figure 6. 22, where the results clearly illustrate the strong relationship between the CTWD and weld metal percentage cracking. Increasing CTWD, associated with a decrease in diffusible hydrogen was found to reduce the percentage of cold cracking. Although the CTWD appears to be a significant variable in the hydrogen measurements, it appears that its significance on weld metal hydrogen cracking varied by between the $75Ar-25CO_2$ and CO_2 shielding gas.

Regardless of weld metal diffusible hydrogen levels at ambient temperature, the CTWD increase had no effect on percentage of RTC reduction at this temperature when welded using $75Ar-25CO_2$ shielding gas. The majority of G-BOP samples exhibited close to 100 %RTC.

However, when using CO_2 shielding gas the weld metal cracking was found to be more complex, as shown in Figure 6. 22 diagrams (C15), (C20) and (C25). Interestingly, at the CTWD of 15 mm using CO_2 shielding gas (see diagram C15), there appears to be a wide scatter of in the RTC caused by the welding current. It should be noted that the weld metal hydrogen levels varied marginally between 11.7-12.8 ml/100g, but by increasing welding current the percentage of RTC was decreasing from 89, 58 and 25 %. By increasing of preheat temperature to 50, 80 and 100 °C, the variation of RTC parameter was gradually narrowed (C15). It should be noted that welds deposited using the welding current of 320 A, containing the highest level of diffusible hydrogen (12.8 ml/100) exhibited the smallest amount of cracking percentage (25 %) at 20 °C (see Figure 6. 23).

Although it may be generally recognized that CTWD significantly contributes to the reduction in weld metal diffusible hydrogen reduction, the results of this current work show that the lowest percentage of RTC in weld metal was found in weld deposited using CTWD of 15 mm and CO_2 shielding gas, with the largest measured diffusible hydrogen range between 11.7 - 12.8 ml/100g (see Figure 6. 22, diagram C15). Despite the smallest diffusible hydrogen range (8.3- 8.6 ml/100) being measured in welds deposited using the CTWD of 25 mm and CO_2 shielding gas (see Figure 6. 22, diagram C25), the effect of the preheat temperature increase was not as responsive as for welds deposited using the CTWD of 15 mm and the same shielding gas.

6.3.3   Effect of Shielding Gas

The results of this work revealed that the shielding gas not only affects the measured hydrogen levels, as shown in Figure 6. 9, and the arc characteristics (see Figure 6. 13), but also the weld

metal susceptibility to transverse cold cracking, as shown diagrammatically in Figure 6. 24 at various preheat temperatures.

Independent of the welding parameters, such as CTWD and welding current, the weld metal deposited using the mixed 75Ar-25CO$_2$ shielding gas generally exhibited a larger percentage of cracking than for the CO$_2$ shielding gas at room temperature. At preheat temperatures of 50 and 80 °C, the decrease of percentage of cracking was more noticeable under CO$_2$ shielding gas at CTWD of 15 mm, as shown in Figure 6. 24 (a). However, further increase of preheat temperature from 80 and 100 °C resulted in a significant decrease of weld metal cracking when using mixed shielding gas 75Ar-25CO$_2$. Despite the fact that the RTC values were significantly lower when using carbon dioxide shielding gas in all G-BOP samples, the critical preheat temperatures at which no cracking is observed were found to be similar under both shielding gases.
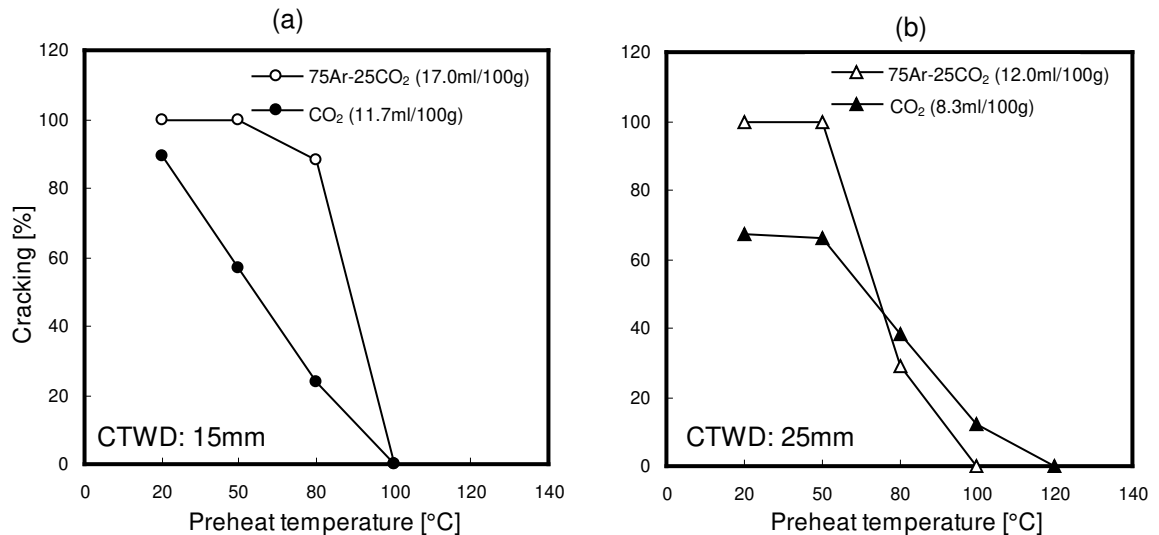
Figure 6. 24   Graphs showing the percentage cracking for H10 weld metal in G-BOP tests, using 75Ar-25CO$_2$ and CO$_2$ shielding gases at constant welding current 280 A and CTWD of (a) 15 mm and (b) 25 mm.

A different relationship between percentage of cracking and shielding gas was observed at CTWD of 25 mm, shown in Figure 6. 24 (b). At room temperature, the weld metal deposited using CO_2 shielding gas was again characterized by significantly less cracking. In comparison with the 75Ar-25CO$_2$ deposit with 100 %RTC, the weld deposited using the carbon dioxide shielding gas exhibited only 67 %RTC. A more rapid decrease in percentage of cracking was observed as preheat temperature was increased from 50 and 80 °C on welds deposited using the 75Ar-25CO$_2$ shielding gas. This steeper reduction of cracking percentage in samples using mixed gas resulted in no cracking at 100 °C, whereas in CO_2 shielding gas the cracking continued to appear until the preheat temperature of 120 °C.

Figure 6. 25 illustrates the effect of weld metal diffusible hydrogen levels and its cracking susceptibility at room temperature for 75Ar-25CO$_2$ and CO_2 shielding gas deposits. It is apparent that CO_2 shielding gas deposits exhibited a lesser amount of RTC than 75Ar-25CO$_2$ shielding gas deposits. Although the ranges of hydrogen levels partly overlap, the percentage cracking at room temperature was significantly lower in welds deposited using CO_2 shielding gas. This finding not only illustrates the differences in diffusible hydrogen generated in weld metal by the two shielding gases, 75Ar-25CO$_2$ and CO_2, but also demonstrates the weld metal sensitivity to cold cracking. Two points placed outside of the expected band represent weld samples H10-11-C and H10-12-C. Although the deposited welds exhibited relatively small variation in the diffusible hydrogen levels (see Table 6. 8), the welds showed noticeably different contour variation to other weld beads, as shown in Figure 6. 23 that could affect the G-BOP test results.
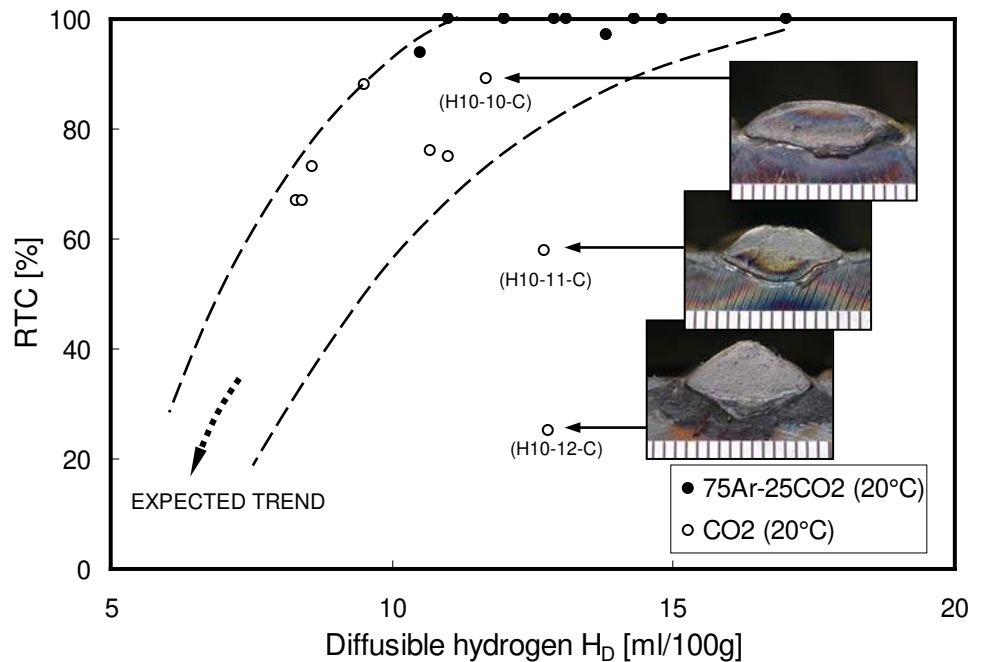
Figure 6. 25   Graph showing the percentage cracking at room temperature for H10 weld
                  metals deposited using 75Ar-25CO$_2$ and CO$_2$ shielding gases.

It is important to note, however, that by increasing preheat temperature, the samples welded

using 75Ar-25CO$_2$ exhibited a steeper reduction of percentage of cracking to the CO$_2$ weld

deposits (see Figure 6. 22 (A25) and (C25)), especially in samples welded using a CTWD of

25 mm.

6.3.4   RTC vs 10 %CPT

Room temperature cracking (RTC) and 10 % of crack preheat temperature (10 %CPT)

generally show the same ranking of behaviour, but because higher hydrogen levels often give

100 %RTC, the 10 %CPT values are often used [Hart 1986]. All the results of H10 weld

samples using 75Ar-25CO$_2$ and CO$_2$ shielding gases showing 10 %CPT are listed in Tables

6.11 and 6.12, respectively.

Table 6. 11   G-BOP test results for H10 welds deposited using 75Ar-25CO$_2$ shielding gas, including H$_D$ (in ascending order), RTC and 10 %CPT.

Sample	Welding current [A]	CTWD [mm]	Atm. Cond. RH [%]- [°C]	H$_D$ [ml/100g]	RTC [at 20 °C]	10 %CPT [°C] (nearest to 5 °C)
H10-9-A	320	25	50 - 17	10.5	94	95
H10-8-A	300	25	-	11.0	100	95
H10-7-A	280	25	-	12.0	100	95
H10-5-A	300	20	-	12.9	100	100
H10-6-A	320	20	-	13.1	100	95
H10-3-A	320	15	-	13.8	97	90
H10-2-A	300	15	-	14.3	100	110
H10-4-A	280	20	-	14.8	100	110
H10-1-A	280	15	-	17.0	100	100

Table 6. 12   G-BOP test results for H10 welds deposited using CO$_2$ shielding gas, including H$_D$ (in ascending order), RTC and 10 %CPT.

Sample	Welding current [A]	CTWD [mm]	Atm. Cond. RH [%]-[°C]	H$_D$ [ml/100g]	RTC [at 20 °C]	10 %CPT [°C] (nearest to 5 °C)
H10-16-C	280	25	44 - 22	8.3	67	100
H10-17-C	300	25	-	8.4	67	110
H10-18-C	320	25	-	8.6	73	100
H10-13-C	280	20	-	9.5	88	110
H10-14-C	300	20	-	10.7	76	80
H10-15-C	320	20	-	11.0	75	100
H10-10-C	280	15	-	11.7	89	90
H10-11-C	300	15	-	12.7	58	85
H10-12-C	320	15	-	12.8	25	40

The results for the H10 welds deposited using the 75Ar-25CO$_2$ shielding gas, characterized by higher diffusible hydrogen levels, display also high cracking susceptibility at room temperature compare to those deposited using CO$_2$ shielding gas (see Figure 6. 25). However, as illustrated in Figure 6. 26, the welds deposited using both 75Ar-25CO$_2$ and CO$_2$ shielding gas revealed a similar values of 10 %CPT parameter ranging between 95-110 °C. This finding demonstrates that although the welds deposited using CO$_2$ shielding gas exhibited a higher resistance to cold cracking to those deposited using 75Ar-25CO$_2$ shielding gas at room temperature, an increase of preheat temperature resulted that both welds showed similar resistance to cold cracking expressed by the 10 %CPT parameter. Note that a isolated point, representing weld sample H10-12-C, was relatively different in the contour to the other weld beads and also exhibited the lowest amount of cold cracking at room temperature (25 %RTC).
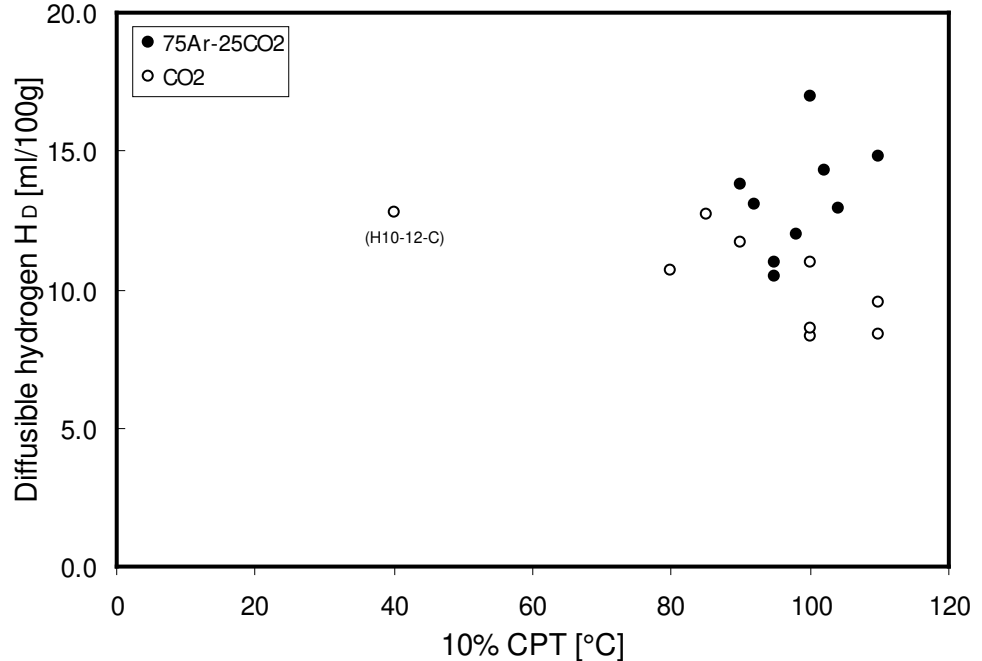
Figure 6. 26   Graph showing the relationship between 10 %CPT and diffusible hydrogen levels for G-BOP welds deposited using H10 wires, welded using 75Ar-25CO$_2$ and CO$_2$ shielding gases.

The data of G-BOP test results for H10 welds deposited using 75Ar-25CO$_2$ and CO$_2$ shielding gases, as listed in Table 6. 11 and Table 6. 12, the relationship between the %RTC and the 10 %CPT is shown in Figure 6. 27. Although the relationship between the two parameters is not very clear, the diagram illustrates that a given conditions, which the weld metal is containing a higher amount of cracking at room temperature, %RTC, (welds deposited using 75Ar-25CO$_2$) does not necessary require significantly higher preheat temperature to eradicate cracking. This observation suggests that the levels of diffusible hydrogen in welds deposited using 75Ar-25CO$_2$ and CO$_2$ shielding gas can affect the responsiveness of weld metal to cold cracking above the ambient temperature.
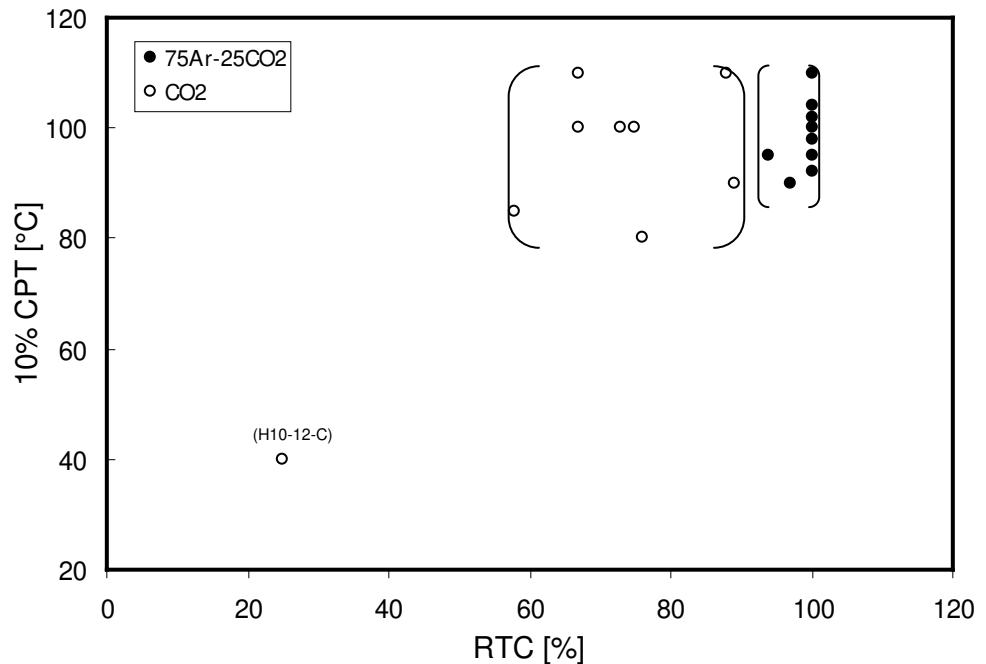
Figure 6. 27   Graph showing the relationship between room temperature cracking and 10 %CPT for G-BOP welds deposited using H10 wires, welded using 75Ar-25CO$_2$ and CO$_2$ shielding gases.

6.3.5   Weld Metal Hardness

For each of the H10 and H5 weld metals, micro-hardness measurements (using 0.5 kg load) were taken from combinations of welding parameters consisting of welding current (280, 300 and 320 A), CTWD (15 and 25 mm), shielding gases (75Ar-25CO_2 and CO_2) and preheat temperatures (20, 50, 80, 100 and 120 °C). The hardness results are average values of a minimum of five measurements taken.

A gradual decrease of weld metal hardness with increasing preheat temperature was observed, as shown in Figure 6. 28. The hardness results indicated that the samples welded using mixed gas 75Ar-25CO_2 exhibited a greater reduction of hardness than the samples welded using CO_2 shielding gas. For example, this reduction in hardness from the preheat temperature of 20 to 120 °C, represented a decrease of 22 and 7 HV0.5kg for 75Ar-25CO_2 and CO_2 shielding gas, respectively.

In general, the H10 welds deposited using 75Ar-25CO_2 revealed higher hardness values to those using CO_2 shielding gas. This effect was more apparent at lower preheat temperatures of 20 and 50 °C, but at higher temperatures the difference was found to be only marginal and decreasing with increasing preheat temperature. Since the G-BOP samples of H5 weld metal exhibited no cracking at room temperature and no welding was carried out at higher preheat temperatures, the effects of increasing preheat temperatures on H5 weld deposit hardness could not be presented here.

The hardness measurements of weld metals deposited using H5 and H10 wires reacted similarly to a change in shielding gas when using a given welding condition at 20 °C. This is shown in Figure 6. 29 for welds deposited using a welding current of 300 A and CTWD of 25 mm for both H5 and H10 wires.
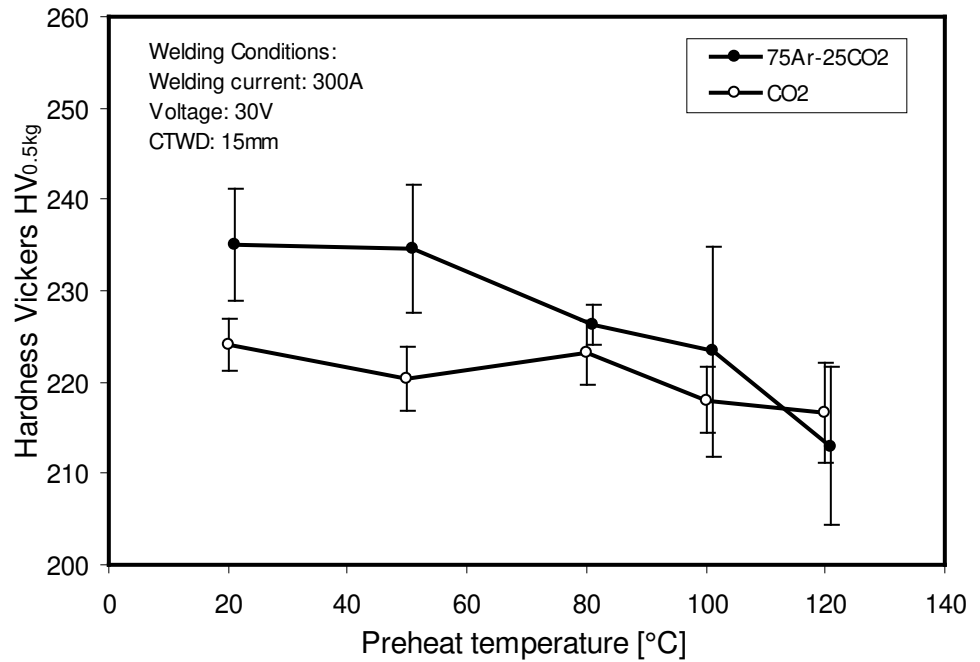
Figure 6. 28   A plot of hardness values for G-BOP weld deposited using H10 wire at various preheat temperatures and using 75Ar-25CO_2 and CO_2 shielding gas.
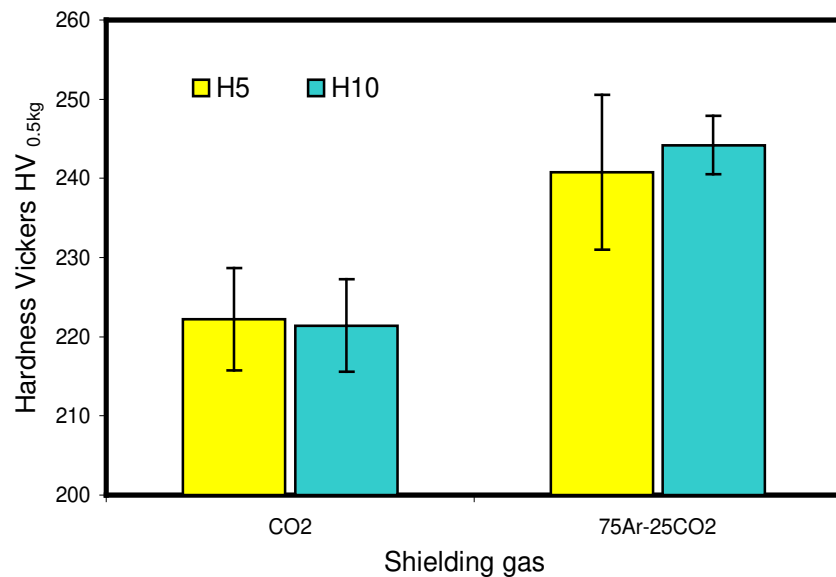
Figure 6. 29   A plot of hardness values for G-BOP welds deposited using H5 and H10 wires both welded at ambient temperature with a welding current of 300 A, CTWD of 25 mm and the two shielding gases.

Both welding consumables exhibited a similar hardness increase (20 HV0.5kg) due to shielding gases change from CO_2 to 75Ar-25CO$_2$.

The relationships between the welding current and hardness values for H10 welds deposited at the preheat temperature of 20 °C, CTWD of 25 mm, and both shielding gases are shown in Figure 6. 30. The weld metal hardness was found to increase with increasing welding current using CO_2 shielding gas, whereas increase in welding current from 280 to 320 A resulted in an increase of weld metal micro-hardness from 215 to 233 HV0.5kg. However, the weld metal hardness remained unchanged in welds deposited using 75Ar-25CO$_2$ shielding gas.
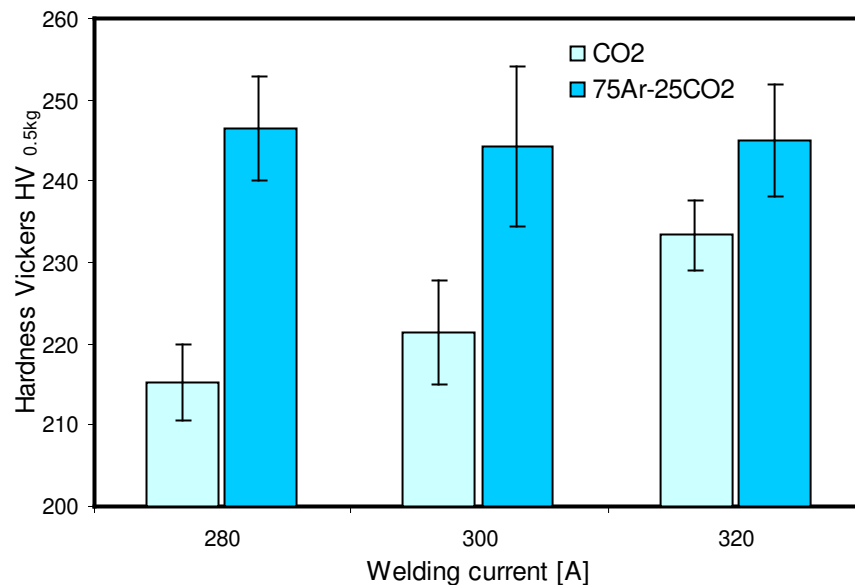
Figure 6. 30   A plot of hardness values for G-BOP welds deposited using the H10 wire at various welding currents (280, 300 and 320 A) using CO_2 and 75Ar-25CO$_2$ shielding gases, CTWD of 25 mm and preheat temperature of 20 °C.

The results of weld metal hardness confirmed that there was a consistent difference in weld metal hardness for welds deposited using CTWDs of 15 and 25 mm and 75Ar-25CO$_2$

shielding gas. This effect was observed for both H5 and H10 weld deposits. The results, shown in Figure 6. 31, revealed a marginal but consistent weld metal hardness increase of around 5 % with an increase in CTWD for 15 to 25 mm. This effect was only observed in welds deposited using the $75Ar-25CO_2$ shielding gas.
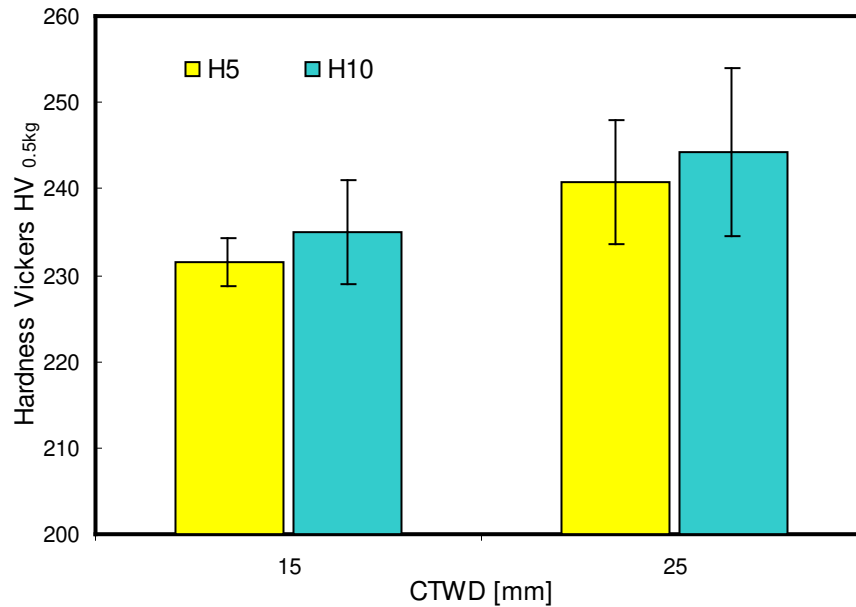
Figure 6. 31   A plot of hardness values for G-BOP welds deposited using H5 and H10 wires with CTWD of 15 and 25 mm. Welding current 300 A, shielding gas $75Ar-25CO_2$, preheat temperature 20 °C.

In summary, weld metal hardness was found to be reduced by an increase in preheat temperature for both shielding gases, although the effect was more pronounced for the mixed gas.

Weld metal hardness was also affected by welding current, CTWD and type of shielding gas. For example, when welding with $75Ar-25CO_2$ shielding gas, the increasing welding current was found to increase the hardness values. However, when using CO_2 shielding gas, the weld

metal hardness remained unaffected. In general, H5 and H10 weld metals deposited using 75Ar-25CO$_2$ shielding gas exhibited higher hardness values to weld metals deposited using CO$_2$ under all welding conditions. An increase in CTWD was found to result in an increase in weld metal hardness for both H5 and H10 weld deposits.

6.3.6   Weld Metal Microstructure

The weld metal deposits may contain several microstructures that are dependent on the chemical composition of a welding consumable, and cooling rates of the weld metal [Alcantra and Rogerson 1984].

In this current work, the microstructures of the G-BOP test samples were examined for both H5 and H10 welds deposited using identical welding parameters. The chemical compositions of the H5 and H10 weld deposits, (see Table 5.2). When comparing the weld metal composition the H5 deposit exhibited higher levels of Cr and Ni, but lower content of Cu, B and C. The higher content of carbon and boron content in the H10 to the H5 weld deposits might be contributing to higher Pcm parameter and hardness values in weld metal when welded using identical welding parameters (see Figure 6. 31). The microstructures of weld metals deposited with different welding current, shielding gases, CTWDs and preheat temperatures were examined. Detailed welding parameters for all selected samples are listed in Table 5.9.

Typical microstructures of all weld deposits consisted from elongated prior austenite grains with varying amounts of grain boundary ferrite, PF(G), fine ferrite side plates, FS(A), and grains consisting of acicular ferrite, AF. Typical micrographs of the H10 and H5 weld metal deposits are shown in Figure 6. 32 (a) and (b) respectively.
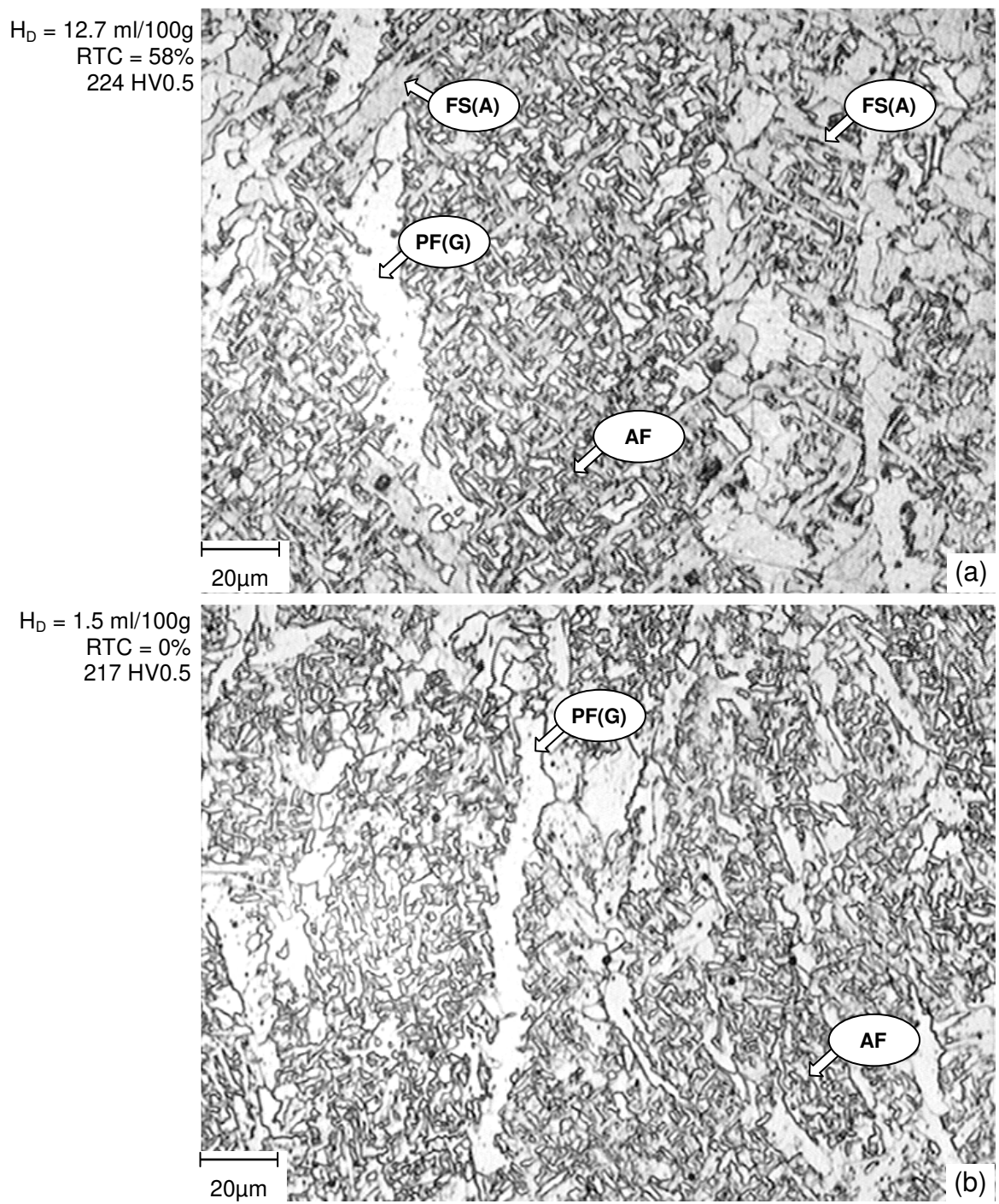
Figure 6. 32   Micrographs showing the H10 (a) and H5 (b) weld metal deposits (welding current: 300 A, CTWD: 15 mm, shielding gas: CO_2, preheat temperature: 20 °C).

When comparing two weld metal micrographs, the H10 microstructure appeared to contain wider bands of boundary ferrite with formation of aligned second phase and coarser acicular ferrite formations. The H10 weld metal microstructure exhibited relatively larger non-metallic particles.

For H10 weld deposits produced by the same shielding gas, there were only marginal differences in microstructure for different preheat temperatures. The weld metal deposited at 20 °C exhibited similar amount of ferrite aligned second face FS(A) to those deposited at 120 °C. It appears that the higher preheat temperature resulted in break down of AF, but allowed for a development of Widmanstätten ferrite side plates FS(SP), as shown in Figure 6. 33. There was less obvious PF(G) phase observed in the welds deposited at 120 °C.

Optical examination of the weld deposits produced with 75Ar-25CO$_2$ and CO$_2$ shielding gases revealed no significant microstructural variations. Other than for finely dispersed ferrite aligned second phase FS(A) found in weld deposit microstructure using 75Ar-25CO$_2$ shielding gas, the microstructures were similar in appearance. This is illustrated in micrographs shown in Figure 6. 32(a) and Figure 6. 33(a).

The results of microstructural examination of three samples (see Figure 6. 23), where a higher welding current had resulted in higher diffusible hydrogen levels in weld deposits, but an unexpectedly significant reduction of the RTC from 89 to 25 %, revealed no apparent differences in weld metal microstructures.
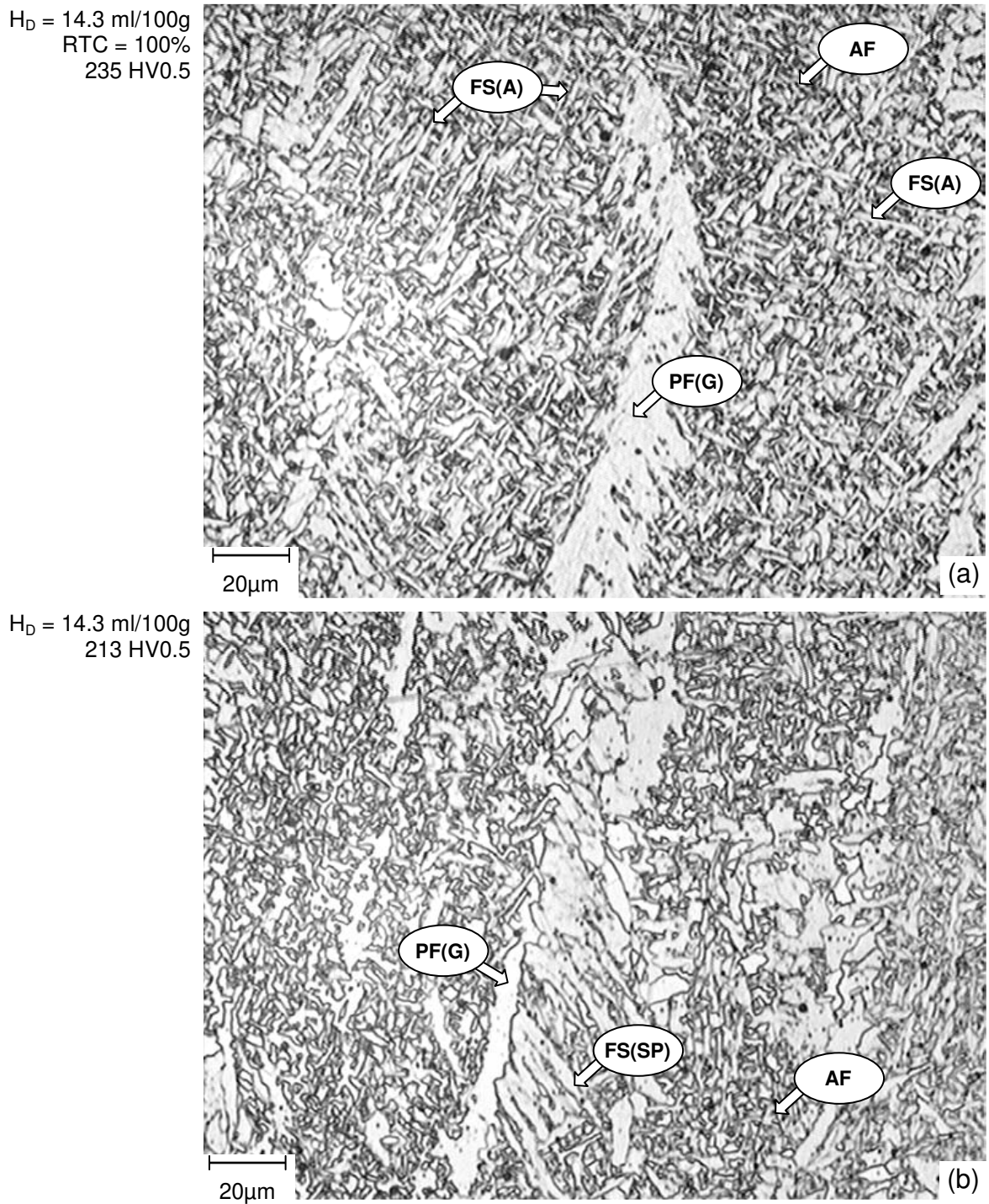
Figure 6. 33   Micrographs   showing the H10 weld metals deposited at 20 °C (a) and 120 °C (b) using welding current: 300 A, CTWD: 15 mm, shielding gas: 75Ar-25CO$_2$, preheat temperature: 20 °C.

Knowing that lower heat input or higher cooling rates can result in microstructural refinement, such as smaller prior austenite grains, reduction of grain boundary ferrite and finer acicular ferrite [French and Bosworth 1997], there were no significant microstructural changes observed in any of the weld metal deposits when varying welding current (280, 300 and 320 A) and CTWD (15 and 25 mm) within the ranges investigated. This is most likely due to relatively small variation of these welding parameters when comparing to those used by French and Bosworth (1997).

The micrographs of all weld metal deposits are shown in Appendix E.

CHAPTER 7

Discussion

The results of experimental work as presented in Chapter 6 demonstrate different levels of diffusible hydrogen are obtained in weld deposits through variation of welding parameters. The influence of welding parameters on weld metal susceptibility to transverse cold cracking will be also discussed in this Chapter. The results will be discussed according to:

7.1 The effects of welding parameters such as welding current, CTWD and shielding gas on levels of diffusible hydrogen in deposited weld metal when using low strength H5 and H10 flux-cored rutile wires.

7.2 The susceptibility of weld metal to hydrogen cracking and the effect of preheat temperature.

7.1 HYDROGEN ANALYSIS

7.1.1 Effect of Welding Current

Considering the introduction of the FCAW process more than four decades ago, it is surprising that the relationship between the welding current and the levels of diffusible hydrogen in weld metal is not more clearly defined. As a result, this topic has been the subject of considerable research for the last decade.

An early work by White et al. (1992) was one of the first studies to examine the relationship between welding current and weld metal diffusible hydrogen using rutile, basic and metal cored flux-cored wires. In regards to the rutile E71 T-1 wires (1.2 mm diameter), the authors suggest that the increase in welding current from 160 to 280 A resulted in a reduction of diffusible hydrogen as a result of an increase of resistive heating in the wire. However, it was

also noted that the increase of welding current was proportional to a considerable increase in WFS. Therefore, the reduction of time available for resistive heating at higher WFS would reduce the time available for removal of hydrogenous compounds.

Sierdzinski and Ferree (1998), also examined a rutile wire E71 T-1, (1.6 mm in diameter), and also reported an increase in diffusible hydrogen levels with as increase in welding current from 210 to 300 A. The authors are in agreement with the explanation by White et al. (1992), but suggest that the hydrogen levels depend on the arc metal transfer mode. Although not examined in detail, the authors propose that a higher welding current generates a finer spray droplet transfer with a larger surface area for interaction with the moisture contained in the arc atmosphere. However, this was without any supporting experimental evidence in relation to the metal transfer mode.

Harwig et al. (1999) also reported an increase in hydrogen content from 2.3 to 11.6 ml/100g with an increase in welding current from 140 to 345 A, using 1.2 mm diameter E71 T-1 rutile wire. However, the arc voltage was adjusted to maintain a constant arc length of 6.35 mm.

Contrary to these findings, Kiefer (1996) examined the effects of moisture contamination in shielding gas and welding parameters on diffusible hydrogen, and found that the effect of current on diffusible hydrogen is also influenced by CTWD. Both variables are strongly interacting. The author suggested it is the CTWD and not welding current, that is the more dominant variable affecting the diffusible hydrogen in weld metal.

The results of this current work examining the effects of welding current show a slight decrease of hydrogen at higher welding currents. However, it is suggested that to assess the influence of the welding current independently of other parameters might be misleading. An

explanation can be found with consideration of the other inter-active welding parameters, as listed in Table 7. 1. The results of listed studies with varying welding parameters are plotted in Figure 7. 1.

Table 7. 1   The welding parameters used to study the effects of welding current (using E71 T-1 rutile wires) on diffusible hydrogen as selected by various authors.

Work by	Welding parameters						Diffusible hydrogen H_D [ml/100g]
	Wire dia. [mm]	Welding current [A]	Arc voltage [V]	CTWD [mm]	Shielding gas	Arc length [mm]	
White et al. (1992)	1.2	160 210 260	25 27 29	25 25 25	80Ar-20CO$_2$	NR NR NR	4.4 5.3 8.7
Harwig et al. (1999)	1.2	179 240 275	27.9 32.1 37.2	22.2 22.2 22.2	80Ar-20CO$_2$	6.35 6.35 6.35	3.8 4.3 7.6
Kiefer (1996)	1.2	158 220	22 23	19.1 19.1	75Ar-25CO$_2$	NR NR	6.0 4.2
This work	1.6	280 300 320	30 30 30	25 25 25	75Ar-25CO$_2$	3.2 NR 2.8	12.0 11.0 10.5

NR: not recorded

The work of White et al. (1992) and Harwig et al. (1999) shows that an increase in the welding current results in an increase in hydrogen. The results in this current work and some results of work by Kiefer (1996) indicate an opposite effect. In comparison with this current work and work by Kiefer (1996), it is apparent that the first two authors used a broader arc voltage range.
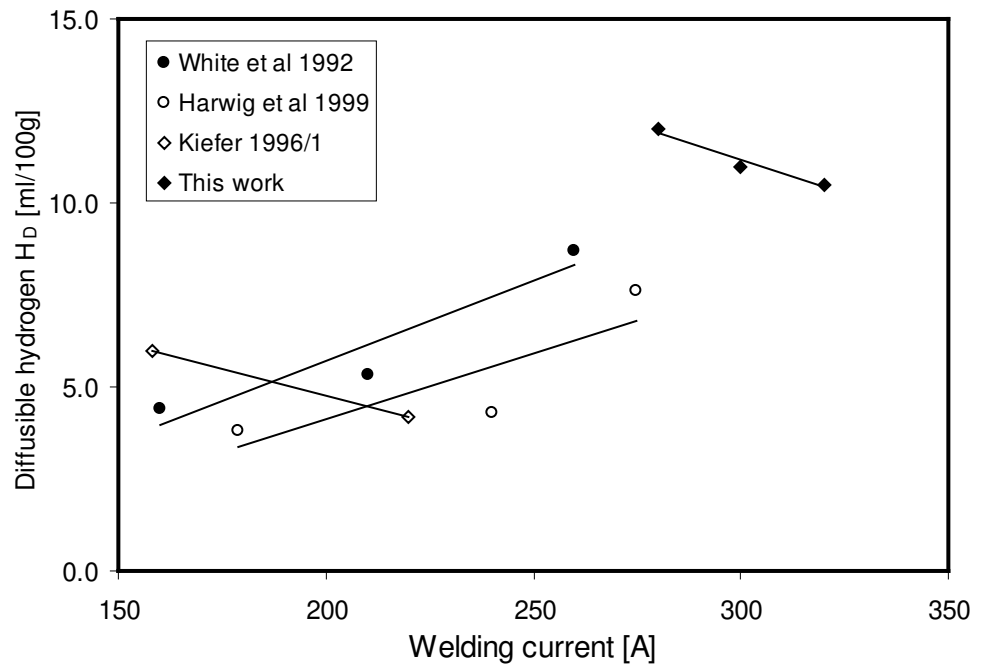
Figure 7. 1   The relationship between welding current and diffusible hydrogen in weld deposits using a rutile E71 T-1 wire, and Ar-CO_2 gas mixtures.

The intention of the current work was to minimize the effects of arc voltage, and focus only on a narrower range of welding currents (280-320 A), typical of industrial use on the wires of interval in the current work. In this range of welding current, the arc voltage was maintained within a range of 29-30 V during all tests to maintain acceptable running arc characteristics. Therefore, in order to directly compare the results of present and past work, the effects of arc voltage must be considered. Analyzing the results of welding current and the arc voltage and their influence on diffusible hydrogen from work by Kiefer (1996), it is obvious that the change of diffusible hydrogen appears to respond not only to variation of welding current, but also to the arc voltage change. Although an increasing welding current resulted in higher diffusible hydrogen levels in weld deposits in the work of White et al. (1992) and Harwig et al.

(1999), a higher arc voltage produces a longer arc length which potentially may contribute to an increased absorption of hydrogen from the arc atmosphere [Kiefer 1996].

A similar increase in diffusible hydrogen with an increase in voltage was reported recently by Kuebler (2003). In this case, single weld beads were deposited at an increasing arc voltage from 27 to 33 V, at constant welding current (200 A) and CTWD (20 mm) under $75Ar-25CO_2$ shielding gas. The increase of arc voltage resulted in an increase of diffusible hydrogen from 4.0 to 5.6 ml/100g in weld metal deposited using 1.2 mm diameter rutile flux-cored wire E81T1-Ni1. Although in terms of an increased amount of diffusible hydrogen (1.6 ml/100g) this does not represent a very significant increase, it should be recognized that this consumable failed its nominal level classification H5 when welding with the higher arc voltage of 33 V. This supports the suggestion that the arc voltage and arc length are influential and, therefore, that welding current is not the only parameter accountable for hydrogen level variation. A relationship between the arc voltage and diffusible hydrogen was also suggested by Kiefer (1996), but no detailed study of arc transfer behaviour was carried out in this case. From the study by Harwig et al. (1999), where the arc length was maintained constant at 6.35 mm through a wide range of arc voltage (27.9-37.2 V), it was suggested that only welding current was responsible for increase in diffusible hydrogen. From these observations, it is apparent that more experimental work is needed to study these interactive effects on diffusible hydrogen levels in welds, particularly in regard to the relationship between the welding current and arc voltage.

In order to define the effects of welding current on diffusible hydrogen in weld deposits, one of the objectives of this current work was to examine the relationship between welding current in connection with the AL, Q and the arc metal transfer. The relationship between the welding

current and AL, Q, arc metal transfer mode and diffusible hydrogen is shown in Figure 7. 2.

As expected, an increase of welding current from 280 to 320 A resulted in an increase of Q

from 52.5 to 67.3 J, representing 28 % increase. The increasing values of Q support the theory

that increasing welding current results in an increase of heat generated in the wire, therefore

promoting the removal of hydrogenous compounds on the wires surfaces. In this current work,

the hydrogen content in weld metal was found to decrease with increasing welding current at a

given welding conditions, contrary to the theory proposed by White et al. (1992).
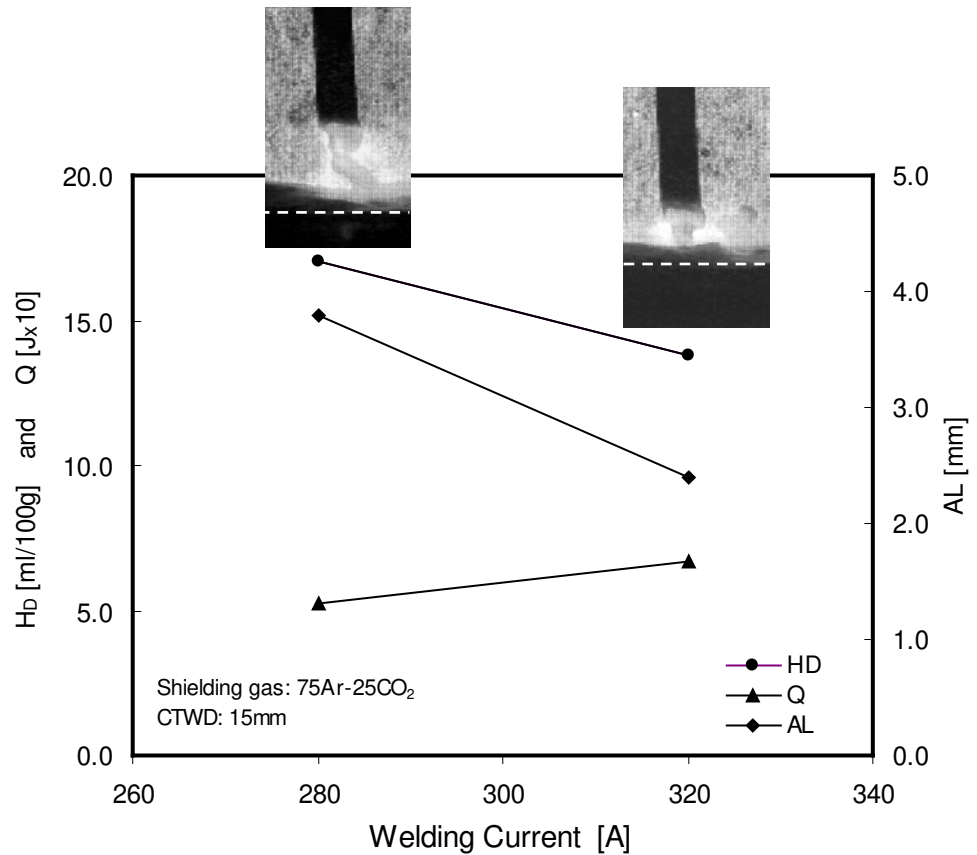
Figure 7. 2   The relationship between welding current, generated heat energy, Q, and
arc length, AL, and observed arc metal transfer in relation to the hydrogen
levels when welded using 75Ar-25CO$_2$ shielding gas and CTWD of
15 mm. (note: dashed line represents the plate surface).

It is apparent that increasing welding current is accompanied by a higher WFS, which subsequently leads to a higher wire burn off rate, but more importantly, resulting in a change of arc length, as shown in Figure 7. 2. By examining the high-speed arc images, the current work has established that by increasing welding current, the arc length has shortened significantly from 3.8 down to 2.4 mm, representing a 37 % reduction. This decrease of AL corresponded to a decrease in diffusible hydrogen from 17.0 to 13.8 ml/100g (reduction of 19 %). These results support the suggestion that arc length is an important parameter for study of diffusible hydrogen levels in weld deposits. The typical arc images presented in Figure 7. 2 show that, other than for an increase of the AL, there was no apparent change in arc metal transfer as the welding current was increased. Although, some variations in sound effects of the arcs during the trials were noted, the high-speed camera failed to find any evidence of fine spray droplets in the plasma arc column. This suggests the reduction of diffusible hydrogen with the increase in welding current was predominantly due to the reduction of arc length in the case of $75Ar-25CO_2$ shielding gas. It is also apparent that generated heat energy, Q, had contributed to this reduction of diffusible hydrogen.

However, when welding using CO_2 shielding gas, a different relationship between welding current and weld metal hydrogen was found. By increasing the welding current from 280 to 320 A, the values of diffusible hydrogen were increased from 11.7 to 12.8 ml/100g, representing an increase of about 9 %. Figure 7. 3 shows the relationship between the AL, Q, arc metal transfer mode and samples of arc images. In this case, an increase in welding current resulted also increasing of Q from 71.6 to 79.5 J, representing 11 %. However, in comparison to the mixed shielding gas, the AL was found to be significantly reduced and almost constant with increasing welding current (1.5 to 1.4 mm).

It is apparent that the values of AL and Q, relating to the welding current increase, are the key variables responsible for the decrease in hydrogen at higher welding current in welds deposited using 75Ar-25CO$_2$ shielding gas. In contrast, under CO$_2$ shielding gas a marginal increase in diffusible hydrogen from 11.7 to 12.8 ml/100g with increasing welding current is observed despite a small increase in Q, and a small decrease in the arc length from 1.5 to 1.4 mm. This suggests that other influential factors affect the kinetics of absorption of hydrogen in the arc plasma, such as the temperature sensitivities of competing oxidation reactions.
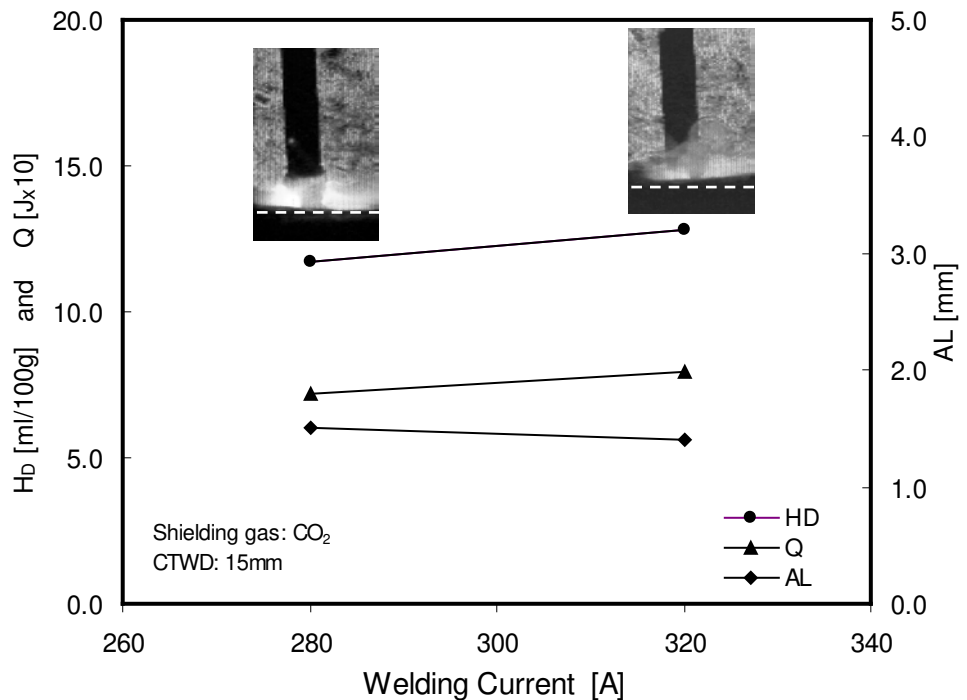
Figure 7. 3   The relationship between welding current, generated heat energy, Q, and arc length, AL, and observed arc metal transfer in relation to the hydrogen levels when welded using CO$_2$ shielding gas and CTWD of 15 mm. (note: dashed line represents the plate surface).

7.1.2   Effect of CTWD

The results of this current work show an agreement with generally accepted theory that a change of CTWD can significantly influence the weld metal hydrogen levels. The results of this current work show that the hydrogen content in weld deposits decreased with increasing CTWD. In general, the weld metal diffusible hydrogen content H_D decreased for both wires (H5 and H10) as the CTWD increased from 15 to 25 mm (see Figure 6.7). However, the H10 weld deposits showed a more significant decrease in the levels of diffusible hydrogen with increasing CTWD, compared to the seamless rutile wire H5 welds.

It is generally accepted that, t_{RHZ} is increased by extending the CTWD. This allows a longer time for any hydrogenous compounds, such as moisture or wire lubricants to burn-off and/or evaporate, particularly applicable in the case of H10 seamed wire. Although, the relationship between the CTWD and t_{RHZ} is accepted, there appears to be no supporting confirmation in the literature referring to this relationship proposed by White et al. (1992) and Kiefer (1996). It is important to note that this relationship is further complicated by the WFS interaction. Increases of about 1m/min in WFS were required when increasing the CTWD from 15 to 25 mm for each welding current selected, as shown in Figure 6.8.

It is clear that an element of wire can spend a longer time in the resistive heating zone when a greater CTWD is selected. In order to determine the effect of t_{RHZ} parameter and calculate the generated heat energy of wire, it is vital to measure the arc length accurately, without the interference of radiation generated by the plasma surrounding the wire tip. For both shielding gases, the increase of CTWD from 15 to 25 mm, represented significant increases of t_{RHZ} and Q at both welding currents of 280 and 320 A (see Table 6.6).

The seamed rutile wire (H10) showed a more significant decrease in the levels of diffusible hydrogen with increasing CTWD, compared to the seamless rutile wire (H5). The increase of CTWD from 15 to 25 mm resulted in a reduction of H_D levels of approximately 4-5 ml/100g for the seamed wire for all three welding currents (280, 300 and 320 A) and both shielding gases. The corresponding decrease of diffusible hydrogen for weld metal produced from seamless wire was 1-2 ml/100g. These results indicate that increasing CTWD clearly reduce H_D in weld metal and it is therefore inferred that in general this condition is conducive to reduction of the hydrogen content in the arc plasma and/or the rate of absorption of hydrogen into the weld metal droplets in arc. The relatively large reduction of diffusible hydrogen content for the H10 wire with increasing CTWD probably arises from the relatively high initial hydrogen content of the wire due to possibility of moisture increases through seam after manufacture and because the seam provides a clear pathway for the removal of entrapped moisture or lubricant residues as the wire passes through the resistive heating zone, and therefore allowing for an increase of the heat energy (see Figures 6.16 and 6.19).

7.1.3   Effect of Shielding Gas

It is well known that the shielding gas can affect the arc characteristics, mode of metal transfer, wetting properties and physical dimensions of molten weld pool. Although the main function of shielding gas is to protect and stabilize the plasma arc from the surrounding atmosphere, the variation in chemical composition of shielding gases influences subsequent reactions in the plasma arc and molten weld metal.

The results of this current work, studying the effects of 75Ar-25CO$_2$ and CO$_2$, confirmed that shielding gas can influence not only the arc characteristics, but also have a noticeable effect on levels of diffusible hydrogen in weld deposits.

In general, the results showed that, when welding using 75Ar-25CO$_2$, the levels of diffusible hydrogen in weld deposits were higher compared to CO$_2$. This applied for both consumables, but was more noticeable for the H10 welds, as shown in Figure 6.9. This was accomplished despite that the CO$_2$ shielding gas had about 10 times higher levels of moisture content to that measured in the mixed gas (see Table 5.3).

Even with an identical set of welding parameters there were apparent sound differences observed during the welding trials using two different shielding gases. Although when welding with the mixed gas, the arc was characterized by a smooth arc 'spray' transfer, the arc transfer was more 'dip-like' under CO$_2$. However, examined high-speed camera images found no significant variation in the arc metal transfer which appeared to remain globular at all welding conditions examined.

The AL values, measured from the high-speed camera digital images, were significantly reduced at all welding parameters when changing from 75Ar-25CO$_2$ to CO$_2$ shielding gas, as illustrated in Figure 6.17. However, despite what appeared to be a smooth arc spray transfer for 75Ar-25CO$_2$ shielding gas, in fact, there was no evidence of finely dispersed droplets in any of the digital images taken at any of the welding conditions selected.

For a given set of welding conditions, the WFS did not seem to be significantly affected by a change in the shielding gas (see Figure 6.6). Therefore, more information is needed with respect to arc length, so that l$_{RHZ}$ and corresponding heat energy in respect to composition of

shielding gases, so they can be accurately establish and their relationship to diffusible hydrogen content properly considered.

At increasing welding current 280-300-320 A, the levels of diffusible hydrogen were found to decrease in weld metal deposited under 75Ar-25CO$_2$, but marginally increase under CO$_2$ shielding gas. This was found in welds deposited at the all CTWD's examined (see Figure 6.5 and Appendix B). Although no arc images were taken from the H5 wire, its weld deposits revealed a similar response in hydrogen levels at both examined shielding gases.

7.1.4   Effect of Atmospheric Conditions

The series of hydrogen tests conducted during two months of April-May 2002 were undertaken using a wide range of welding parameters, but without control of atmospheric conditions. During this period of year, the relative humidity and atmospheric temperature varied between 47-61 % and 15-26 °C respectively. It was expected that by varying the primary welding parameters, such as welding current, CTWD and shielding gases, the sole effects of atmospheric conditions would not be possible to determine in the main part of this study.

However, the work conducted during a round robin series by Nolan and Pitrun (2003) considered the effects of atmospheric conditions on the weld metal diffusible hydrogen of E71 T-1 weld metal. The relative humidity and measured values of diffusible hydrogen in welds deposited are shown in Figure 7. 4, where the diffusible hydrogen content was found to increase with an increased in relative humidity. The relative humidity increase from 31 to 45 % (temperature range 21-24 °C) appeared to result in an increase of weld metal hydrogen

levels from 10.4 to 18.9 ml/100g in welds deposited using an identical set of welding parameters.
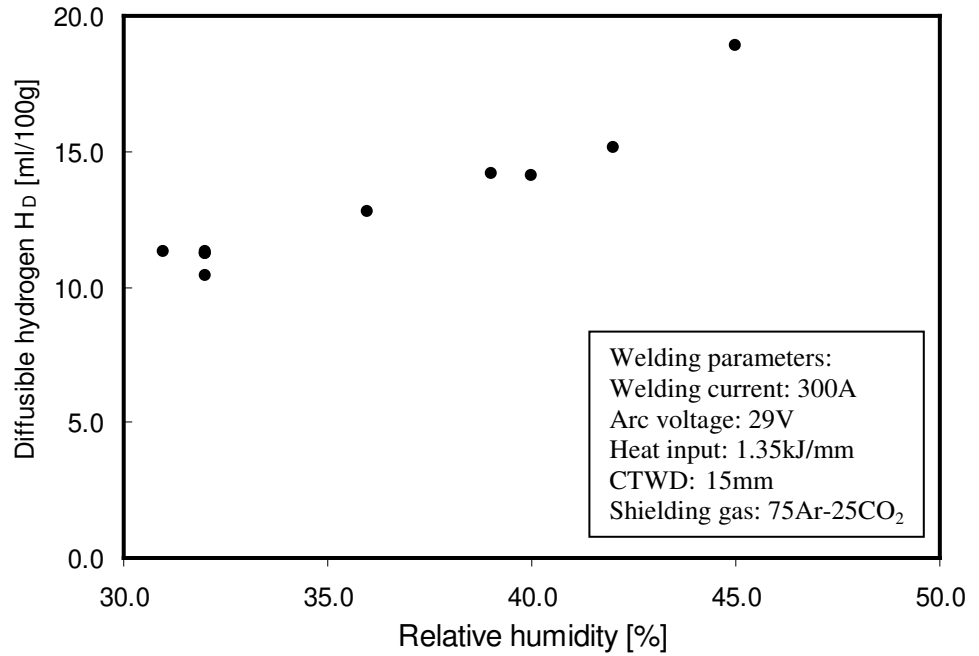
Figure 7. 4   Graph showing the relationship between relative humidity and diffusible hydrogen for E71 T-1 weld deposits (after Nolan and Pitrun 2003).

It should be noted that this significant increase of 55 % in diffusible hydrogen was measured at relatively moderate atmospheric conditions. It would be expected that with more extreme atmospheric conditions commonly encountered in Australia, often in vicinity of 90 %RH [http://www.bom.gov.au], the levels of diffusible hydrogen in weld metal might be expected to be even higher.

Figure 7. 6 shows the relationship between the absolute moisture content and its effect on diffusible hydrogen. As for the relative humidity, the moisture increase by 1 g in 1 kg of dry air resulted in a significant increase of weld metal hydrogen levels. The effect of atmospheric

conditions is an important factor worthy of further investigation in order to facilitate improved prediction of diffusible hydrogen levels in welds deposited using gas shielded flux-cored wires.
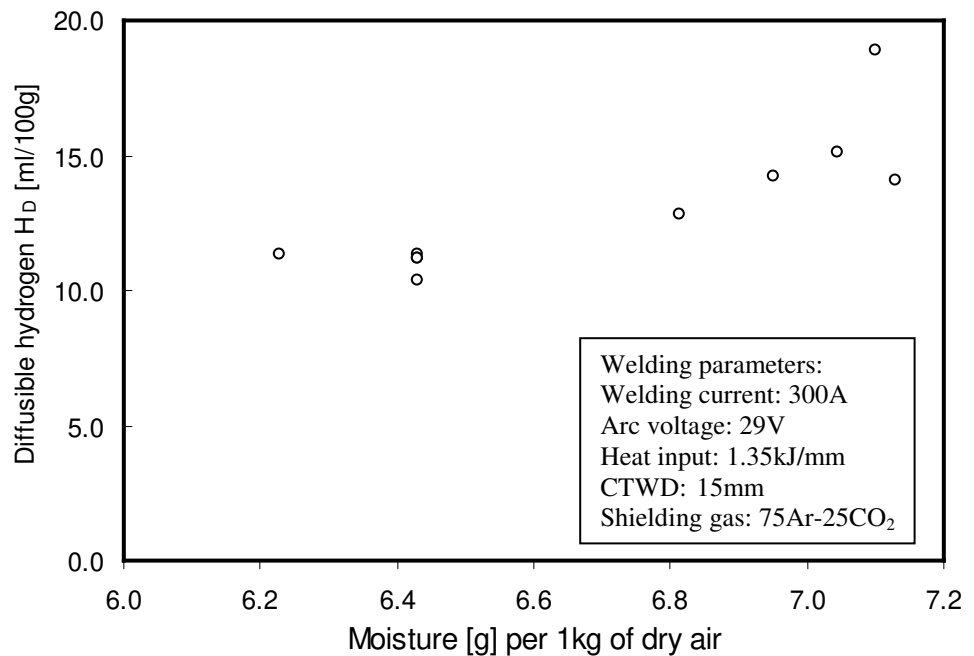
Figure 7. 5   Graph showing the relationship between absolute moisture and diffusible hydrogen for E71 T-1 weld deposits (after Nolan and Pitrun 2003).

The aim of any future work should focus on a development of hydrogen predictive monograms similar to those established by Ruge and Dickhurt (1988) for the MMAW process. However, in comparison with the MMAW, such predictive monograms for FCAW process will be more complicated by inter-active welding parameters, such as welding current, WFS, AL, t_{RHZ}, CTWD, Q and shielding gases.

7.1.5   Accuracy and Reproducibility

To determine the accuracy of hydrogen testing, the testing standards ISO 3690-2000 and AS/NZS 3752-1996 propose a statistical comparison of a series of identical test welds, divided into two groups, where one group is analyzed by primary method and the second group by the alternative method. The standards also recommend to carry the diffusible hydrogen tests over a range of hydrogen levels from 5 to 15 ml/100g, or higher. It is recommended that nine tests are carried out using both methods [ISO 3690-2000 and AS/NZS 3752-1996]. From the commercial point of view, it is apparent that this might be a lengthy and expensive procedure. Therefore, to benchmark the accuracy of the diffusible hydrogen tests performed, the manufacturers adopted more practicable measure expressed as standard deviation (STDV).

The results of diffusible hydrogen tests in this current work, examining two rutile wires H5 and H10, demonstrate differences in the ranges of diffusible hydrogen in the respective weld metal deposits, but also higher STDV values for the H10 wire. The results for the H5 consumable were within the nominal diffusible hydrogen levels ($\leq$5 ml/100g), but the weld deposits for the H10 wire yielded a much wider spread of diffusible hydrogen levels.

Considering that each set of 3 results was under constant conditions and their weld deposits were analyzed using identical gas chromatography hydrogen analyzer and preparation procedure, these results suggest that the two wires may exhibit different accuracy levels when expressed in terms of the standard deviation. The diffusible hydrogen levels of weld deposits for both flux cored wires H10 and H5 are shown diagrammatically in Figure 7. 6.
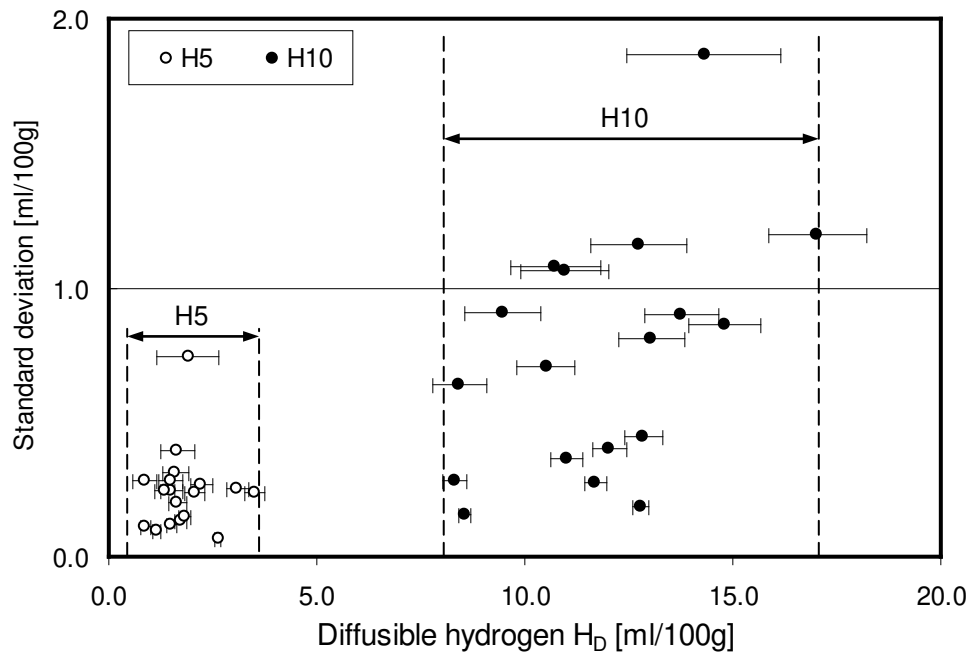
Figure 7. 6   Graph showing the relationship between the diffusible hydrogen and the standard deviation values calculated for H10 and H5 weld deposits.

A series of repeated welds will also provide information on the reproducibility of the testing method. Generally, it is accepted that reproducibility of results within a variation of ± 1 ml/100g can account for environmental factors, welding parameters, inter-laboratory variability [Kotecki 1992], and different testing methods employed [Nolan and Pitrun 2003].

The results of this current work appeared to be well within the range of ± 1 ml/100g for in the welds deposited using the H5 wire. However, five out of eighteen hydrogen tests for the H10 weld deposits yielded diffusible hydrogen levels with a variation of greater than ± 1 ml/100g (see Figure 7. 6). McParlan and Graville (1976) also observed a larger scatter of FCAW hydrogen test results.

The results of the round robin test conducted by Nolan and Pitrun (2003), using the identical gas chromatography analyzer as used in this current work, confirmed its reproducibility variation of ±1 ml/100g when comparing the diffusible hydrogen results obtained by primary method and other laboratories in Australia.

The procedure for welding and storage of test pieces was consistent across all sample sets. It is estimated that each sample was quenched in iced water within approximately 5 seconds of the completion of welding. The total time that each welded sample was exposed to ambient conditions, including cleaning and removal of run-on run-off blocks, from the iced water was estimated to be approximately 20 seconds. The time between storage and testing when the sample was exposed to ambient conditions varied between 45 to 60 seconds. Considering that these conditions were within the range of testing conditions, as recorded by Nolan and Pitrun (2003), it is safe to say that any additional error resulting from the hydrogen testing procedure used in this current work would be insignificant.

7.2 G-BOP TESTING

In this section, the influence of welding current, CTWD, shielding gas, and preheat temperature will be discussed to understand their influence on the susceptibility to weld metal cold cracking. Prior to discussing the results of the G-BOP tests, it should be noted that the experiments were carried in the same welding laboratory as used earlier during the hydrogen testing, and without controlling the atmospheric conditions at the time of welding. Since in this current work, the aim was to simulate atmospheric conditions which would be close to the conditions experienced in the field, there was no attempt made to establish the significance of

this variable against other controllable variables, such as welding current, CTWD, shielding gas and preheat temperature. Nevertheless, the effects of the atmospheric conditions should not be discounted when assessing either the levels of diffusible hydrogen in weld metal or its susceptibility of to HACC.

7.2.1   Effect of Welding Current

Although earlier work by White et al. (1992) and Sierdzinski and Ferree (1998) experimentally established that an increase in welding current results in an increase of weld metal diffusible hydrogen no further work was undertaken to define the effect of increased hydrogen levels in relation to the susceptibility to weld metal cold cracking.

As shown in the G-BOP test results from the current work, where the percentage cracking for the H10 weld metal was examined, there appears to be some disagreement in the suggestion that increasing levels of hydrogen caused by an increase in welding current will result in a higher percentage of cold cracking. As shown diagrammatically in Figures 6.22, (A15) and (C15), there are noticeable differences between the sensitivity of weld metal to HACC when deposited using 75Ar-25CO$_2$ and CO$_2$ shielding gas. When using 75Ar-25CO$_2$ shielding gas (diagram A15), increasing welding current from 280, 300 and 320 A results in a lowering of diffusible hydrogen levels from 17.0 to 14.3 and 13.8 ml/100g, respectively. This subsequently results in a lowering of the percentage of cracking, most noticeably at the preheat temperatures of 50 and 80 °C. In the case of CO$_2$ shielding gas, the increase in the welding current resulted in a marginal increase of diffusible hydrogen, but a significant lowering in the percentage of cold cracking. This phenomenon was most notable at the CTWD of 15 mm (see Figure 6.22, C15). At greater CTWD of 20 and 25 mm, the difference between cracking

behaviour at varying welding currents were found less substantial and fairly consistent at the largest CTWD of 25 mm under all preheat conditions. As discussed earlier, an increase of CTWD resulted in a linear increase of WFS (see Figure 6.8). The welding current and CTWD increases then result in a higher melting rate, MR, (see Equation 6.1) and most likely producing various weld contours, as discussed later in this Chapter and shown in photographs of the G-BOP fracture faces (see Appendix C).

When examining the weld bead profiles deposited at 20 °C and using CO_2 shielding gas, the welding current increase from 280 to 320 A resulted an increase of heat input from 1.26 to 1.44 kJ/mm and significantly different weld bead cross sections, as shown in Figure 7. 7.

(a)   (b)
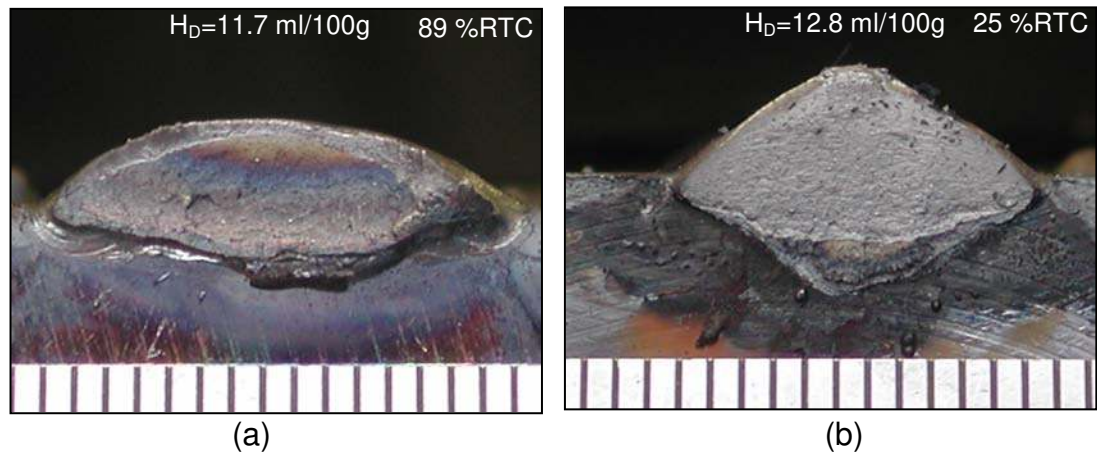
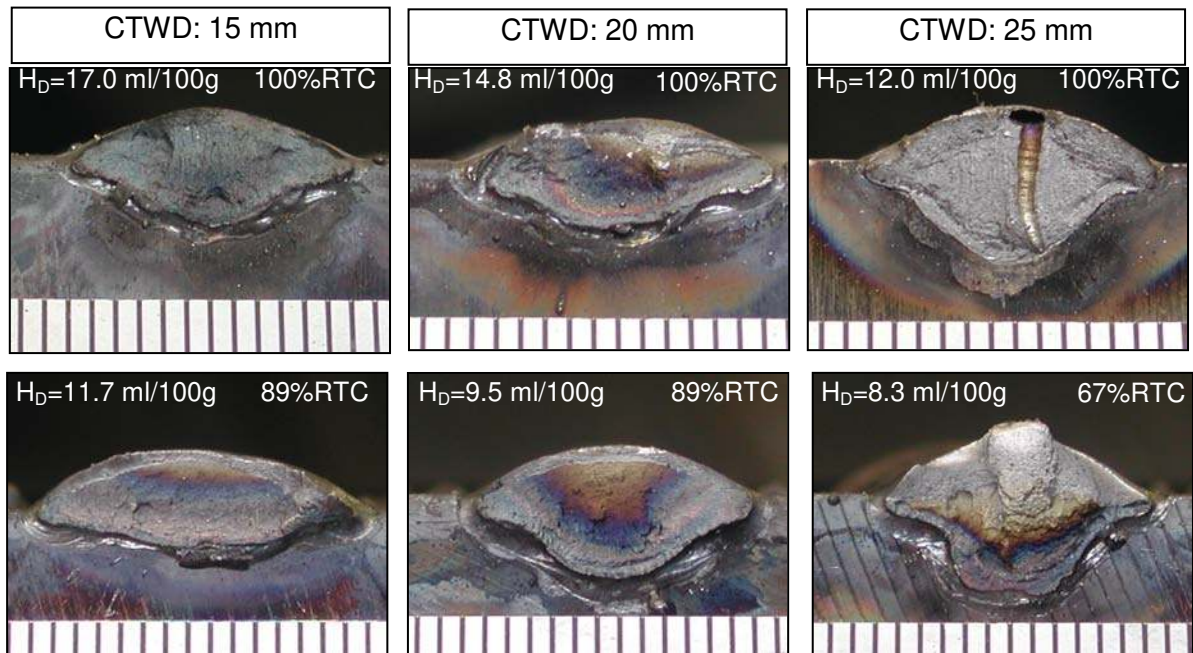Figure 7. 7   Photographs showing the G-BOP fracture faces of H10 weld metal deposits at preheat temperature of 20 °C using CO_2 shielding gas, CTWD of 15 mm and welded using welding of (a) 280 A and (b) 320 A.

It is known that higher heat input and preheat temperature result in decreasing of weld metal cooling rates, as this was observed in the instrumented G-BOP tests [Garville et al. 1974]. This consequently allows for more hydrogen to diffuse out from the weld deposit. When comparing the two weld bead sections (see Figure 7. 7), the weld deposited using the 280 and 320 A

produced similar cross sectional areas of fused metal of 52 and 56 mm^2, respectively. However, there were significant differences noticed in the weld bead contours. In the case of a weld deposited at lower welding current of 280 A, the depth of penetration and its height were 2.5 mm for both parameters, whereas in the case of weld deposit using welding current of 320 A, the values of bead penetration and height were significantly higher at 3.9 and 3.5 mm, respectively.

Although not examined in this current work, this variation of weld bead contour may be an important factor when defining the heat flow and longitudinal stresses along the weld and cooling rates. Further work in this area by computer modelling with FEA would be very valuable in providing some insight into the influence of weld bead geometry and cracking behaviour in G-BOP testing method.

Other than for the H10 welds deposited using CO_2 shielding gas at the shortest CTWD of 15 mm (see Figure 6.22 diagram C15), there was no clear relationship between the welding current increases and the amount of cracking at room temperature. It is apparent that the %RTC appeared to be unaffected by the change in diffusible hydrogen content, as found in weld metals deposited using 75Ar-25CO_2 and CO_2 shielding gases, respectively (see Figure 6.5). Although it is difficult to establish the exact cause of phenomenon, it is likely that different atmospheric conditions at the time of diffusible hydrogen measurements (see Table 6.1) and the G-BOP testing (see Table 6.11) might contribute to this effect.

7.2.2   Effect of CTWD

The effect of CTWD on the cracking percentage in welds deposited using 75Ar-25CO_2 and CO_2 shielding gases is shown in Figure 7. 8. Although the results of this current work clearly

demonstrate that increasing CTWD results in a linear decrease of weld metal diffusible hydrogen in both H5 and H10 weld deposits and when using both shielding gas (see Figure 6.7), the correlation between the CTWD and weld metal susceptibility to cold cracking is less pronounced. This is shown in an example of welds deposited at welding current of 280 A, where the weld metal percentage of cracking in welds deposited at CTWD of 15, 20 and 25 mm when using the 75Ar-25CO_2 shielding gas, did not reveal any significant percentage cracking decrease to reflect lowered diffusible hydrogen content from 17.0 to 12.0 ml/100g at room temperature. A similar observation was found in the higher welding currents of 300 and 320 A. (see Appendix D). However, at preheat temperature of 80 °C, the welds deposited at CTWD of 20 and 25 mm revealed a significant decrease of percentage of cracking from down to 16 and 29 %, respectively, compared to that deposited at CTWD of 15 mm which exhibited 88 % of cracking. The welds deposited using CO_2 shielding gas and containing relatively lower levels of diffusible hydrogen (8.3-11.7 ml/100g) revealed a smaller amount of cracking at 20 and 50 °C preheat temperatures.
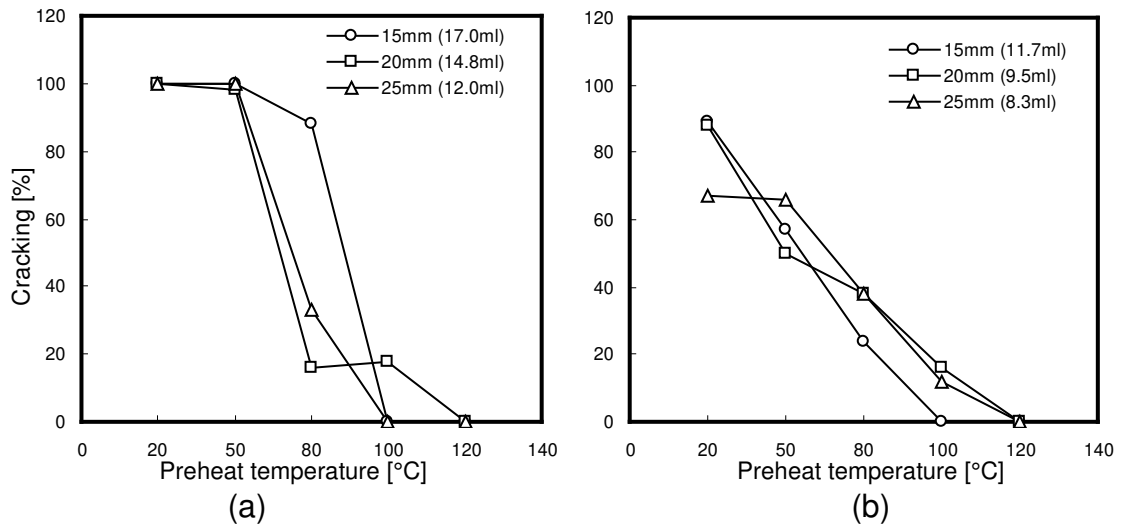
Figure 7. 8   Graphs showing the percentage cracking for H10 weld metal in G-BOP tests, using (a) 75Ar-25CO_2 and (b) CO_2 shielding gases at welding current of 280 and CTWD of 15, 20 and 25 mm.

The profile of the G-BOP test weld beads varied significantly with CTWD. This was expected since the WFS had to be increase by about 1m/min. to maintain required welding current with the increase of the CTWD from 15 to 25 mm. Examples of different weld profiles, produced using a welding current of 320 A, are shown in Figure 7. 9.

For both shielding gases the weld penetration was noticeably increased by the CTWD. The cracking percentage of these six weld deposits is shown diagrammatically in above Figure 7. 8. These images demonstrate the effects of the CTWD increase on larger weld bead cross sections and a deeper weld penetration.

CTWD: 15 mm	CTWD: 20 mm	CTWD: 25 mm
H_D=17.0 ml/100g 100%RTC	H_D=14.8 ml/100g 100%RTC	H_D=12.0 ml/100g 100%RTC
H_D=11.7 ml/100g 89%RTC	H_D=9.5 ml/100g 89%RTC	H_D=8.3 ml/100g 67%RTC

Figure 7. 9   Photographs showing the G-BOP fracture faces of H10 weld metal deposited at CTWD of 15, 20 and 25 mm with preheat temperature of 20 °C using (top row) 75Ar-25CO$_2$ and (bottom row) CO$_2$ shielding gas and welded using welding current of 320 A.

7.2.3 Effect of Shielding Gas

As discussed earlier in Chapter 7.1.3, the shielding gas not only influences the arc characteristics, but also affects the levels of diffusible hydrogen in weld deposits. The results of current work has shown higher levels of diffusible hydrogen in welds deposited using 75Ar-25CO_2 shielding gas as compared to CO_2 (see Figure 6.9).

The shielding gas containing CO_2 results in a variation of weld metal chemical and mechanical properties. This can also influence the weld metal hardness [Schumann and French 1994]. Hart (1986) has suggested that the resistance to cold cracking is primarily related to the hardness for weld deposits containing relatively higher levels of diffusible hydrogen (10 ml/100g). However in the case weld metal with lower levels of diffusible hydrogen levels (5-10 ml/100g), the microstructural characteristics appears to be more important than hardness in influencing crack resistivity.

A similar observation was made in this current work when examining the FCAW weld deposits and their susceptibility to cold cracking when using two different shielding gases. In general, the Vickers micro-hardness results in this current work established that for all H10 and H5 weld metal deposits studied the average hardness values were higher by about 20 HV0.5 when welded using mixed gas 75Ar-25CO_2 (see Figure 6.26). The relationship between the shielding gas used, the weld metal hardness and its susceptibility to HACC cracking was examined on G-BOP weld samples using the H5 (4 off) and H10 (12 off) weld deposits welded with identical welding conditions, but with different shielding gas employed. From the results examining the effect of shielding gas on the susceptibility of weld metal cracking, it was found that weld metal deposited using 75Ar-25CO_2 exhibited higher average hardness values to those observed when using CO_2 shielding gas. Not only did the

75Ar-25CO$_2$ shielding gas result in a higher average weld metal hardness, but it also resulted in an increase of weld metal susceptibility to cold cracking at the room temperature, as shown in Figure 7. 10. The results indicate that for the H10 welds deposited using 75Ar-25CO$_2$ shielding gas, containing H$_D$ ≥ 10 ml/100g and hardness values >235 HV0.5, most of the these welds exhibited 100 %RTC. However, in the case of the H10 welds deposited using CO$_2$ shielding gas, which resulted in a lower hardness values <235 HV0.5, the range of % cold cracking at room temperature was lower at between 25-89 %. It is important to note that in the case of the welds deposited using the CO$_2$ shielding gas, there appeared to be no clear relationship between the weld metal hardness and diffusible hydrogen levels. For example, weld metal with 213 HV0.5 containing H$_D$=11.7 ml/100g revealed 89 %RTC, whereas the weld metal with Vickers hardness of 225 HV0.5, containing H$_D$=12.7 ml/100g exhibited significantly lower percentage of cold cracking of 25 %RTC only. It can be suggested that using the identical welding consumable and shielding gas, will likely result in an identical chemical and composition of the deposited weld metal. Given that these two welds were deposited also using identical welding parameters, except welding current 280 and 320 A (see Figure 7. 7), then it appears that the deeper penetration and the contour of fused metal at 320 A results in a reduction of hydrogen cracking in weld metal at room temperature. Although this finding is in agreement with the recognised relationship between the arc energy and HAZ hydrogen cracking, it is contrary to the weld metal hydrogen cracking observed by Pargeter (1992) investigating multi-pass weld deposits. It should be noted that the hydrogen diffusion path is more significant in multi-pass, particularly deposited using high arc energy weld deposits than in the single-pass G-BOP test, when HACC occurs beneath the final layer.

A more detailed study would be useful, in particular the influence of geometric effects of weld

bead in the single-pass G-BOP test using modeling techniques, such as FEA.
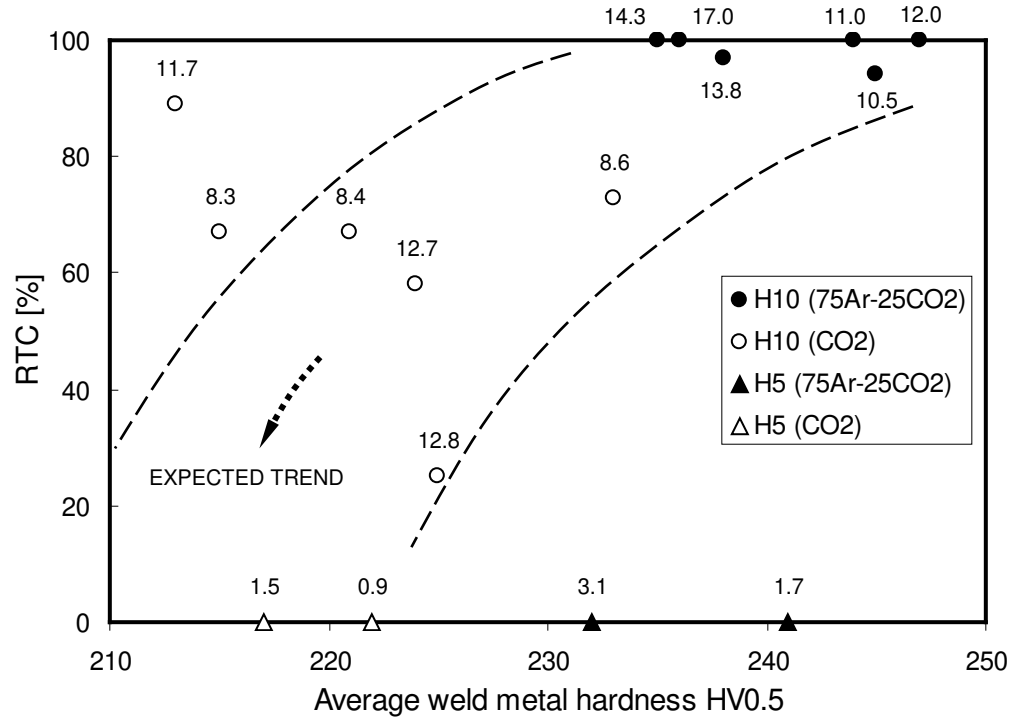
Figure 7. 10   A plot of hardness values and weld metal cold cracking at room
temperature for G-BOP welds deposited using H10 and H5 wires, welded
using 75Ar-25CO$_2$ and CO$_2$ shielding gases. Numbers next to the markers
represent relevant weld metal diffusible hydrogen levels H$_D$ [ml/100g].

7.2.4 Effect of Preheat Temperature

The main aim of the application of preheat is to control the cooling rate during weld

solidification and solid state transformations, so as to ensure sufficient time for removal of

hydrogen from the weld metal. The results of this work, examining the G-BOP test welds,

confirmed that preheat plays an important role when avoiding HACC. For example, the

percentage of cold cracking in G-BOP test welds decreased with increasing preheat

temperature. For the H10 deposits welded using the 75Ar-25CO$_2$ shielding gas, the percentage of weld metal cracking decreased most markedly at 80 °C, and crack free welds were obtained within the preheat temperatures of 100-120 °C. For the H10 welds using the CO$_2$ shielding gas and deposited at the CTWD of 15 and 20 mm, the reduction of cracking percentage was observed earlier at 50 °C. However, the welds deposited using the CTWD of 25 mm and containing the lowest range of diffusible hydrogen levels (8.3-8.6 ml/100g) no reduction of cracking was observed. This finding suggests that an increase in preheat temperature from 20 to 50 °C appears to be more beneficial in welds containing relatively higher levels of diffusible hydrogen deposited at the CTWD of 20 mm, but even more significant at the shortest CTWD of 15 mm with the weld metal diffusible levels range between 11.7-12.8 ml/100g. However, crack free weld deposits were obtained within the preheat temperatures of 100-120 °C and similar as for the welds deposited using the 75Ar-25CO$_2$ shielding gas.

In general, for the H10 welds deposited using 75Ar-25CO$_2$ and CO$_2$ shielding gases, the preheating offered two recognizable benefits resulting in reduced susceptibility to cold cracking; enhanced hydrogen diffusion (where the hydrogen has an extended time to diffuse out of the weld metal before reaching critical temperature) and reduced weld metal hardness. There appears to be a relationship between the rates of reduction of weld metal hardness and cracking percentage. Firstly, the H10 welds deposited using 75Ar-25CO$_2$ exhibited a higher percentage of RTC than those when using CO$_2$ shielding gases (see Figure 6.22). Secondly, with increasing of preheat temperature the weld metal hardness was decreasing more rapidly to those welds deposited with CO$_2$ shielding gases (see Figure 6.28). This second effect of hardness reduction, more pronounced in the welds using 75Ar-25CO$_2$ shielding gas, is believed to result in more rapid reduction of cold cracking in these deposits. An example of this relationship is illustrated in Figure 7. 11.
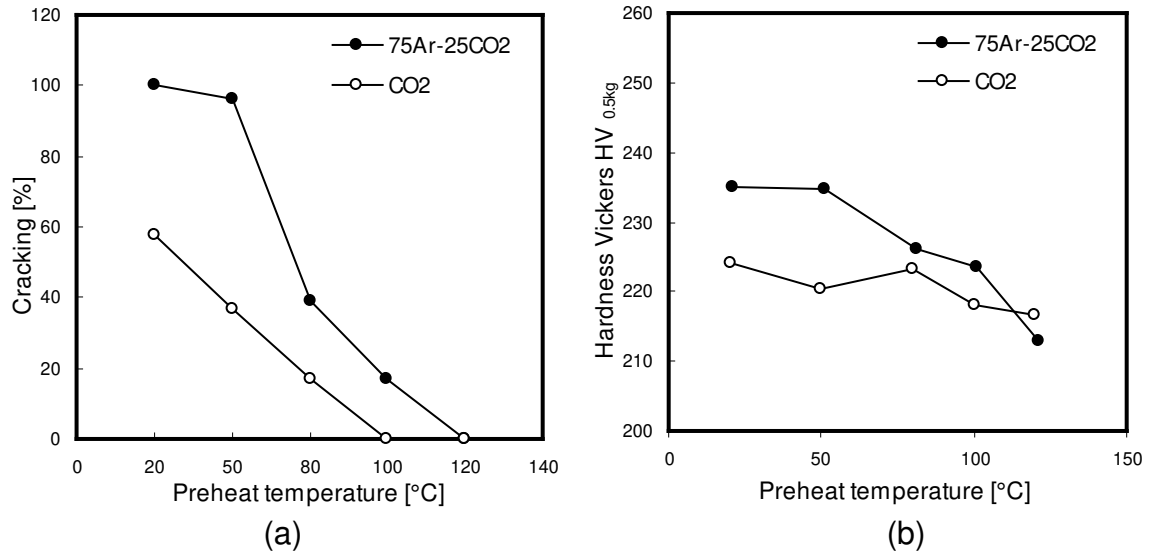
Figure 7. 11   Graph showing the relationship between preheat temperature and (a) the percentage cracking and (b) hardness for H10 weld metal in G-BOP tests using $75Ar$-$25CO_2$ and CO_2 shielding gases. Both welds were deposited using identical welding current and CTWD of 300 A and 15 mm, respectively.

The remaining question is to address the possibility that differences in weld metal microstructure might be apparent due to an increase in preheat temperature. The microstructures of relevant weld metals samples from Figure 7. 11, show typical structures for a low strength carbon steel weld metal composition.

The observe the effects of preheat temperature on microstructures of welds deposited at 20 and 120 °C, using $75Ar$-$25CO_2$ and CO_2 shielding gases are shown in Figures 7.12 and 7.13, respectively.   In general, the weld metal microstructures deposited using $75Ar$-$25CO_2$ and CO_2 shielding gases consisted of similar appearance of grain boundary ferrite, PF(G), fine ferrite side plates, FS(A), and acicular ferrite, AF, within the original austenitic grain. Minor refinements in the amount and thickness of PF(G) and amount of FS(A) were noticed when

comparing the microstructures of weld samples deposited at 20 and 120 °C preheat temperature and deposited using 75Ar-25CO$_2$ shielding gas (see Figure 6.33). This observation may partly explain the corresponding reduction in the hardness measurements from 235 to 213 HV0.5, as shown in Figure 7. 11. The weld metal hardness reduction and decreased cooling rates due to increasing preheat temperature had a beneficial effect on a reduction of hydrogen cold cracking. Slower cooling rates resulting from a higher preheat temperature also promote formation of softer phase products and a reduction of thermal stress changes [McParlan et al. 1976].
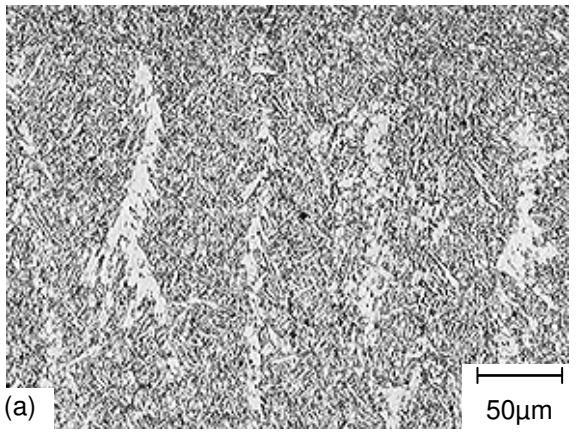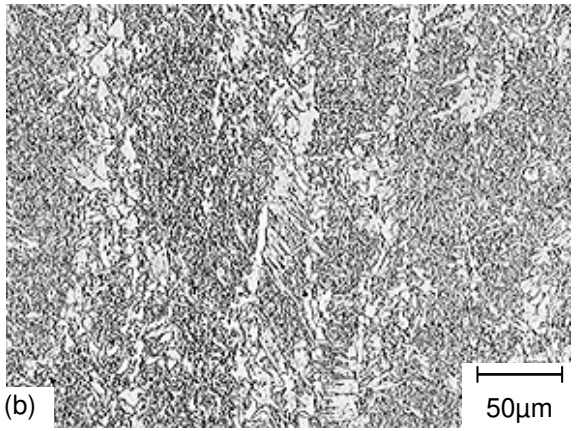
Wire sample:	H10
Welding current [A]:	300
CTWD [mm]:	15
Shielding gas:	75Ar-25CO$_2$
Weld metal H$_D$ [ml/100g]:	14.3
Preheat temperature [°C]:	**20**
Percentage cracking [%]:	100
Vickers hardness HV 0.5kg:	235
Sample:	H10-2-20A

Wire sample:	H10
Welding current [A]:	300
CTWD [mm]:	15
Shielding gas:	75Ar-25CO$_2$
Weld metal H$_D$ [ml/100g]:	14.3
Preheat temperature [°C]:	**120**
Percentage cracking [%]:	0
Vickers hardness HV 0.5kg:	213
Sample:	H10-2-120A

Figure 7. 12   Micrographs showing the H10 weld metal deposits using identical welding current (300 A), CTWD (15 mm), shielding gas 75Ar-25CO$_2$ deposited at preheat temperature of (a) 20 °C and (b) 120 °C.
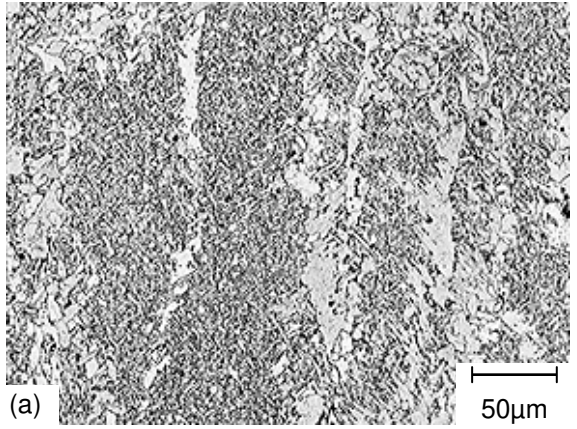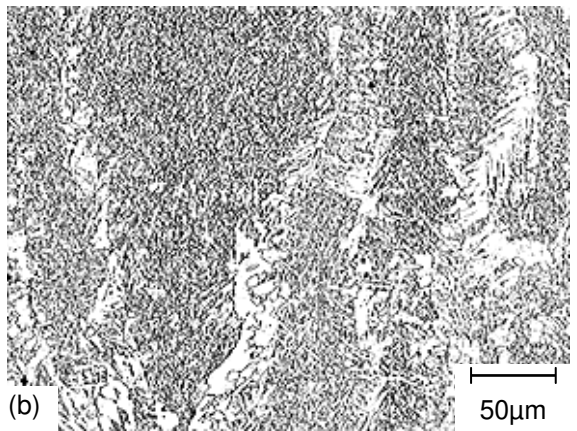
Wire sample:	H10
Welding current [A]:	300
CTWD [mm]:	15
Shielding gas:	CO_2
Weld metal H_D [ml/100g]:	12.7
Preheat temperature [°C]:	**20**
Percentage cracking [%]:	58
Vickers hardness HV 0.5kg:	224
Sample:	H10-11-20C

(a)   50µm

Wire sample:	H10
Welding current [A]:	300
CTWD [mm]:	15
Shielding gas:	CO_2
Weld metal H_D [ml/100g]:	12.7
Preheat temperature [°C]:	**120**
Percentage cracking [%]:	0
Vickers hardness HV 0.5kg:	217
Sample:	H10-11-120C

(b)   50µm

Figure 7. 13   Micrographs showing the H10 weld metal deposits using identical welding current (300 A), CTWD (15 mm), shielding gas CO_2 and deposited at preheat temperature of (a) 20 °C and (b) 120 °C.

7.2.5   RTC vs 10 % CPT

The results of this work show that at given welding conditions and hydrogen contents, two types of weld metals exhibiting different amount of cracking at room temperature may require different preheat temperature in order to achieve <10 % cracking. For example, all but two welds deposited with the H10 wire under 75Ar-25CO$_2$ shielding gas exhibited 100 %RTC, with the other two showing marginally lower percentage of 94 and 97 %. The majority of the

welds deposited using the same consumable but CO_2 shielding gas showed significantly lower values of RTC, ranging between 25-90%.

The results indicate the same welding consumable deposited using different shielding gases can results in a different response to preheat temperature. This is an important finding that can influence the selection of shielding gases, particularly with regard to the weld metal resistance to HACC for a given preheat temperature selected for production.

Although there appears to be no clear correlation between RTC and 10 %CPT, the results suggest that the welds deposited using the same welding consumable but using different shielding gas may generate similar diffusible hydrogen levels but respond differently to preheat temperature. As a consequence of this, a different preheat temperature may be needed to obtain crack-free weld deposits when using different shielding gases.

7.2.6   Accuracy and Errors

One of the objectives of this work was to establish the effects of three welding parameters, such as welding current, CTWD and shielding gases on diffusible hydrogen levels in deposited weld metals using seamed and seamless flux cored wires. These experiments were carried out with no control over the atmospheric conditions at the time of welding during two months when different atmospheric conditions were experienced between the tests (see Tables 6.1 and 6.2). Considering this, it was accepted that this uncontrollable variable during the testing might influence the diffusible hydrogen contents in weld metals. Since this work was not aimed investigate the effects of atmospheric conditions, no attempt was made in this work to study the significance of this variable. It should be also noted that the diffusible hydrogen data obtained from weld deposits were directly transferred and used for the assessment of the

weld metal susceptibility to cold cracking using the G-BOP test. Although using matching welding parameters, when conducting the series of G-BOP cold cracking tests, the atmospheric conditions (see Tables 6.7, 6.8, 6.9 and 6.10) varied to those during the diffusible hydrogen testing (see Tables 6.1 and 6.2). The transfer of diffusible hydrogen results and their direct correlation to cold cracking observed in this study might be likely source of error. Therefore, a consideration for the future work should be given to investigate the effects of atmospheric conditions and their significance on the levels of diffusible hydrogen in welds deposited using gas shielded FCAW process in the atmosphere controlled environment. To carry out both tests at the same time might eliminate this variable. However, if more extensive study is required such as in this work, this option would not be practicable when the atmospheric conditions may vary on day-to-day basis.

The results of this work do not indicate a clear relationship between the amount of diffusible hydrogen in weld deposits and the amount of cold cracking. This was further complicated by the contours of the weld beads, caused by an increase of welding current from 280 to 320 A (see Figure 7. 7). This example of comparing two weld deposits contained 11.7 and 12.8 ml/100g, but exhibited 89 and 25 %RTC, respectively indicates also a need to consider the contour of the single weld beads when examining the susceptibility of weld metal cracking using the G-BOP test. Finite element modelling of a series of weld deposits consisting of flatter-to-convex or deeper-to-shallower or smaller-to-larger weld bead profiles, may indeed assist in determining the significance of the weld bead contour as a potential error for the G-BOP test.

The results of this work, examining the effects of welding parameters on diffusible hydrogen and weld metal susceptibility to HACC indicate a need for future work examining the effects

of diffusible hydrogen concentration and its distribution across the deposited weld metal when

using the G-BOP tests to predict cracking in production welds.

CHAPTER 8

Conclusions

The current work has illustrated the importance of welding parameters and shielding gas on the level of diffusible hydrogen in rutile E71 T-1 flux-cored weld deposits. The results suggest that these interacting welding parameters can determine the levels of hydrogen in weld deposits, which subsequently may influence the presence of HACC. The interactions between these welding parameters are complex, resulting in not only changes in the diffusible hydrogen content in weld metal and metal arc transfer, but also the amount of cold cracking observed in the self restrained G-BOP tests. From the results of this work, the following conclusions can be drawn:

1. An increase of CTWD resulted in a decrease in diffusible hydrogen content for both consumables H10 and H5 under all welding current levels (280, 300 and 320A) and both shielding gases 75Ar-25CO$_2$ and CO$_2$. The effect was more significant for the seamed H10 wire. It is concluded that the dominant mechanism for reduction in diffusible hydrogen levels with increasing CTWD is the increase in the amount of heat energy Q released in the resistive heating zone.

2. The effect of welding current on diffusible hydrogen content is influenced by the shielding gas used. Under most combinations of wire and shielding gas used, a relatively insignificant effect on diffusible hydrogen was observed, with a decrease in the case of the seamless H5 wire under both shielding gases. The H10 wire under mixed gas showed a significant decrease in diffusible hydrogen (17.0 – 13.8 ml/100g) with increasing welding current. In the case of the H10 wire, this can be explained in terms of the arc length, as observed by high speed digital photography. Under mixed gas, the increase in welding current resulted in a significant decrease in AL (3.8 - 2.4 mm), while under CO$_2$ the change arc length was minimal (1.5 – 1.4 mm). This suggests that the reduction of arc

length at increased welding current reduces the amount of dissociation of hydrogenous compounds in the arc and the amount of hydrogen absorbed from a shorter welding arc into the weld metal. However, more experimental work would be required to study the arc behaviour in relation to the temperature distribution and hydrogen dissociation within the arc to support this conclusion.

3. The type of shielding gas used also has an important effect on hydrogen content. The CO_2 shielding gas resulted in lower levels of diffusible hydrogen for all combinations of CTWD and welding current investigated. It is concluded that the reduced arc length under CO_2 shielding gas is primarily responsible for this effect, providing less opportunity for hydrogenous compounds to decompose and for monatomic hydrogen to be absorbed into the weld metal. It is also likely that the higher oxidation potential of the CO_2 shielding gas reduces the availability of ionic hydrogen in the arc. In comparison, the 75Ar-25CO_2 shielding gas provides a longer arc column and a more stable medium for the hydrogen ions, increasing the probability of absorption into the weld pool.

4. For the H10 wire, the type of shielding gas influenced the effect of welding current on diffusible hydrogen content at constant CTWD. For the mixed gas, a significant decrease in diffusible hydrogen occurred with increasing welding current; and this effect can be explained at least in part by the effect of increased I^2R heating and reduced arc length on the quantity of heat released, Q, in the resistive heating zone, l_{RHZ}. The reduced arc length also serves to reduce the droplet residence time in the arc plasma, resulting in reduced hydrogen pickup. In contrast, the H10 consumable under CO_2 shielding gas showed an increase in diffusible hydrogen with increasing welding current despite a small increase in Q. Since the arc length remained unchanged with increasing welding current, other factors

affecting the kinetics of absorption of hydrogen in the arc plasma, such as the temperature sensitivities of competing reactions, should be considered accounting for the observed increase in diffusible hydrogen with increasing welding current.

5. The examination of arc metal transfer arc images using the H10 seamed rutile wire, confirmed globular transfer for all combinations of welding current (280-320 A), CTWD (15-25 mm), voltage (29-30 V) and shielding gases selected in this work. There was no evidence of spray transfer mode at these welding conditions.

6. From the range of atmospheric conditions recorded during the hydrogen testing trials, relative humidity of 47-61 % and temperature of 15-26 °C, the sole effect of these atmospheric conditions on diffusible hydrogen levels was difficult to demonstrate. This was due to variation of welding parameters and shielding gases for each set of hydrogen test samples.

7. Under most welding parameters and shielding gas as selected in this work, as recommended by the consumable manufacturer, the weld metal hydrogen content measured for the H10 seamed rutile wire did not comply with its hydrogen classification, except when using a combination of the longest CTWD of 25 mm and CO_2 shielding gas. The H5 seamless wire produced weld metals which all complied with the hydrogen levels specified by the manufacturer for all welding conditions investigated.

8. Shielding gas composition also influenced the chemical composition in weld deposits. For both welding consumables H10 and H5 their welds deposited using 75Ar-25CO$_2$ shielding gas exhibited higher CE_{IIW} and Pcm values when comparing with the weld metal deposited using CO_2 shielding gas. This correlated well with a higher hardness

found in the welds from the G-BOP tests. The measured hardness results indicate that weld metals deposited using identical welding parameters and under $75Ar-25CO_2$ exhibited about 20 HV 0.5kg higher hardness values to those deposited using CO_2.

9. In most cases, 100 % cracking was observed in most of the G-BOP test welds deposited using the H10 wire at room temperature. Although this finding correlated well with the results of diffusible weld metal hydrogen tests, an exception was found for the case of the welds deposited using CO_2 shielding gas, the lowest CTWD of 15 mm and a narrow range of diffusible hydrogen (11.7-12.8 ml/100g). Under these conditions, the most marked decrease in cracking percentage was found at room temperature with a significant reduction from 89 to 25 % resulting from an increase in welding current from 280 to 320A. Since there appeared to be no significant variations in the weld metal microstructures, hardness or diffusible hydrogen levels, this effect is explained in terms of fused weld metal geometry. However, in order to confirm this suggestion it would be recommended to investigate this finding by FEA computer modelling.

10. In contrast to the H10 wire weld metals, the H5 weld deposits exhibited no cracking at room temperature under any welding conditions investigated.

11. The results of the G-BOP tests conducted at room temperature indicate that the susceptibility of weld metal to HACC was reduced in welds deposited using CO_2 shielding gas for all combinations of CTWD and welding current investigated. This is explained in terms of marginally lower levels of measured diffusible hydrogen in welds deposited using CO_2 shielding gas, and lower hardness values.

12. Increasing of preheat temperature was shown to decrease the percentage of cracking in the H10 weld deposits in all cases. The effect of preheat temperature increase (20, 50, 80, 100 and 120 °C) was most likely a result of decreasing the hydrogen concentration. The preheat temperature increase from 20 to 120 °C, resulted in only a reduction of weld metal hardness of 22 and 7 HV 0.5 kg for welds deposited using $75Ar-25CO_2$ and CO_2 shielding gas, respectively. This observation suggests that the increase in preheat temperature is the major contributor to a reduction in susceptibility to weld metal cracking.

13. An increasing welding current was found to reduce the weld metal diffusible hydrogen levels but not its susceptibility to cold cracking in the G-BOP tests welds when deposited at 20 °C preheat temperature, using $75Ar-25CO_2$ shielding gas and CTWD of 15 mm. In the case of the G-BOP tests welds deposited under CO_2 shielding gas, an increasing welding current resulted a significant reduction of cold cracking at room temperature at CTWD of 15 mm. This effect was less evident at the higher CTWD's.

14. The increase in welding current resulted in different hardness values for weld metal deposited at ambient temperature with $75Ar-25CO_2$ and CO_2 shielding gases. As mentioned previously, the weld metal deposited with mixed shielding gas, showed relatively higher hardness values that were unaffected by increases in welding current. However, for the weld metal deposited using CO_2 shielding gas, the hardness values were found to increase from 215 to 233 HV 0.5kg with an increase in welding current.

15. Although the CTWD appears to be a significant variable in the hydrogen measurements, its effect on the weld metal hydrogen cracking varied between welds deposited with $75Ar-25CO_2$ and CO_2 shielding gas. An increase in CTWD had no effect on the RTC % at room

temperature when welded using 75Ar-25CO$_2$ shielding gas, since the majority of these G-BOP samples exhibited close to 100 %RTC. However, when using CO$_2$ shielding gas, the percentage of RTC decreased with increasing CTWD.

16. From the examination of the weld metal microstructures deposited with H10 and H5 wires, there were some minor microstructural changes observed which would indicate an influence on the weld metal susceptibility to HACC. The weld metal microstructure of H10 wire contained wider bands of boundary ferrite with formation of aligned second phase and coarser acicular ferrite. The weld microstructure of H5 wire exhibited narrower bands of grain boundary ferrite with finely dispersed acicular ferrite.

17. Changes in weld metal microstructures were observed in H10 weld metal deposited using 75Ar-25CO$_2$ shielding gas at 20 and 120 °C preheat temperature. An increase of preheat temperature resulted in a reduction of ferrite with aligned second phase, but also encouraged development of grain boundary ferrite and Widmanstätten ferrite side plates. These microstructural changes were accompanied with a reduction in weld metal hardness, as mentioned above.

18. The results of this work indicate that weld metal containing diffusible hydrogen of $\geq$10 ml/100g is highly susceptible to cold cracking at room temperature. The results of the G-BOP tests indicate that the same welding consumable (H10) deposited using different shielding gases can show different responses to preheat temperature, the preheat temperature of 120 °C was still required to decrease the cracking to $\leq$10 % for both welds deposited using 75Ar-25CO$_2$ and CO$_2$ shielding gases.

19. The current work was not successful in revealing a relationship between the amount of diffusible hydrogen in weld deposits and the amount of cold cracking found in the G-BOP tests. Although this might be partly due to direct correlation of diffusible hydrogen measurements and the results of the G-BOP tests welded under different atmospheric conditions, further work examining the effects of the weld bead geometry resulting from different welding current and CTWD should be considered under controlled atmospheric conditions. This would provide new and valuable insights into the G-BOP testing and its validity for studying the cracking susceptibility of weld metal produced by an identical consumable, but deposited under different welding conditions.

20. Based on the results of this work, on the effects of welding parameters on levels of diffusible hydrogen in weld metal deposited using gas shielded rutile flux-cored wires, a number of the changes are proposed to AS3752-1996, AS2203.1-1990 and ISO3690-2000. In particular the standards should address:

    a) The specification of the CTWD for the diffusible hydrogen testing should be conducted for the minimum electrode extension, as recommended by the manufacturer, and

    b) where more than one shielding gas is recommended for a given cored consumable, tests shall be conducted under each and every recommended gas at the minimum recommended electrode extension.

REFERENCES

ABSON, D.J.: 'An investigation of hydrogen-induced cracking behaviour during welding of two high strength structural steels' TWI Report 507, April 1995

ABSON, D.J.: 'Non-metallic inclusions in ferritic steel weld metals – a review' Welding in the World, Volume 27, No.3/4, 1989, pp 76-101.

ALAM, N., DUNNE, D., SQUIRES, I., BARBARO, F.J. and FENG, B.: 'Weldment cold cracking – the effect of hydrogen and other factors' Proceedings of the Seminar, Melbourne, October 1996, pp 49-60.

ALAM, N., CHEN, H.L.L. and DUNNE, D.: 'Fracture morphology of hydrogen-assisted cold cracking in steel weldments' Australasian Welding Journal, Volume 42, 1st Quarter, 1997, pp 43-47.

ALBERT, S.K, REMASH, C., MURUGESAN, N., GILL, T.P.S., PERIASWAMI, G. and KULKARNI, S.D.: 'A new method to measure the diffusible hydrogen content in steel weldments using a polymer electrolyte based hydrogen sensor' Welding Journal, July 1997, pp 251-255s.

ALCANTRA, N.G. and ROGERSON, J.H.: 'A prediction diagram for preventing hydrogen – assisted cracking in weld metal' Welding Journal, April 1984, pp 116-122s.

ALLEN, D.J., CHEW, B. and HARRIS, P.: 'The formation of chevron cracks in submerged arc weld metal' Welding Journal, July 1982, pp 212-220s.

ALEXANDROV, B.T.: 'Evaluation of the influence of hydrogen on cold cracking formation in welded joints' IIW doc.No: IX-2020-02.

ALEXANDROV, B.T.: 'Hydrogen diffusion coefficient and modelling of hydrogen behaviour in welded joints of structural steels' IIW doc.No: IX-2063-03.

ANSI/AWS A4.3-93: 'Methods for Determination of the Diffusible Hydrogen Content of Martensitic, Bainitic and Ferritic Steel Weld Metal Produced by Arc Welding'

ANSI/AWS A5.20-95: 'Specification for carbon steel electrodes for flux cored arc welding'

ANSI/AWS D1.1-2000: 'Structural welding code – steel'

API Recommended Practice 4009, April 1977.

AS 2203.1-1990: 'Cored electrodes for arc welding - ferritic steel electrodes'

AS 2207-1994: 'Non-destructive testing – Ultrasonic testing of fusion welded joints in carbon and low alloy steel'

AS 2812-1985: 'Welding, brazing and cutting of metals – glossary of terms'

AS 3597-1993: 'Structural and pressure vessel steel - Quenched and tempered plate'

AS 3678-1999: 'Structural steel – hot rolled plates, floor plates and slabs'

AS 4882-2003: 'Shielding gases for welding'

AS/NZS 1554.1-2000: 'Structural steel welding - welding of steel structures'

AS/NZS 1554.4-1995: 'Structural steel welding - welding of high strength quenched and tempered steels'

AS/NZS 3752-1996: 'Welding – methods for determination of the diffusible hydrogen content of ferritic weld metal produced by arc welding'

AS/NZS 3992-1998: 'Pressure equipment – welding and brazing qualification'

ASM Handbok: 'Welding, brazing and soldering' Volume 6, 1993.

ATKINS, G., THIESSEN, D., NISSLEY, N. and ADONYI, Y.: 'Welding process effects in weldability testing of steels' Welding Journal, April 2002, pp 61-68s.

BAILEY, N., COE, F.R., GOOCH, T.G., HART, T.H.M., JENKINS, N. and PARGETER, R.J.: 'Welding without hydrogen cracking' TWI, Abington Publishing, Cambridge, 2nd edition, 1995.

BANG, K. and AHN, Y.: 'Weldability of direct quenched, low-carbon, Ti-B containing steels' Welding Journal, April, 1997, pp 151-155s.

BARBARO, F.J.: 'Types of hydrogen cracking in pipeline girth welds' Proceedings of the 1st International conference, Wollongong, March 1999.

BEACHAM, C.D.: 'A new model for hydrogen-induced cracking' Metallurgical Transactions, Volume 3, February 1972, pp 437-451.

BERGHEAU, J.M., BOITOUT, F. and MANGIALENTI, G.: 'Predictive simulation of welding and heat treatment with SYSWELD+® presented capabilities and evolution' ESI Group, Proceedings of HANPAM, 1997, pp 236-243.

BERNSTEIN, I.M. and THOMPSON, A.W.: 'Effect of metallurgical variables on environmental fracture of steels' International Metals Review, December 1976, pp 279-285.

BISALLOY STEELS Pty Ltd: 'Welding' Finlay Preece publication, May 1997.

BLACK, N.: 'Shielding gas selection for short arc welding carbon and low alloy steels' pp 109-119.

BLACKMAN, S.A., RIVAS, S., GREIG, A., TIZANI, W., WHITEHEAD, A. and BERTASO, D.: 'Automated FCAW for tubular structures' http://www.nottingham.ac.uk, 2002, pp 1-11.

BS 7363-1990: 'Methods for controlled thermal severity (CTS) test and bead-on-plate (BOP) test for welds'

CHAKRAVARTI, A.P. and BALA, S.R.: 'Evaluation of weld metal cold cracking using the G-BOP test' Welding Journal, January 1998, pp 1-8s.

CAMPBELL, W.P.: 'Effect of aluminium on HAZ cold cracking in C-Mn steels' Welding Journal, May 1975, pp 154-161s.

CHEN, L.: 'Characterisation of transverse cold cracking in weld metal of a high strength quenched and tempered steel' PhD Thesis, University of Wollongong, 1999.

CHEW, B.: Moisture and regain by some basic covered electrodes' Welding Journal, May, 1976, pp127-134s.

CHOO, W.Y. and LEE, J.Y.: 'Thermal analysis of trapped hydrogen in pure iron' Metallurgical Transactions, Volume 13A, January 1982, pp 135-140.

CHOO, W.Y., LEE, J.Y, CHO, C.G. and HWANG, S.H.: 'Hydrogen solubility in pure iron and effects of alloying elements on the solubility in the temperature range 20 to 500°C' Journal of Materials Science, Volume 16, 1981, pp 1285-1292.

COE, F.R.: 'The comparison of hydrogen levels' IIW doc.No: II-A-305-72.

COMMONWEALTH BUREAU OF METEOROLOGY web site: http://www.bom.gov.au

COTTRELL, C.L.M.: 'Controlled thermal severity cracking test simulates practical welded joints' Welding Journal, June 1953, pp 257-272s.

CZARNECKI, J.: Preventing the effects of moisture contamination on flux-cored wire' Phoenix International, http://www.phx-international.com

DALLAM, C., QUINTANA, M. and van der MEE, V.: 'Capabilities and limitations of FCAW-S, IIW doc.No: XII-1646-00.

DAVIDSON, J.L. and PHILLIPS, R.: 'Flux cored arc welding consumables: a user perspective' Proceedings of the 1st International conference, Wollongong, March 1999.

DAVIDSON, J.L.: 'Hydrogen-induced cracking of low carbon – low alloy steel weldments' Material Forum, 19, 1995, pp 35-76.

DAVIDSON, J.L.: 'Advances in hydrogen management: the science based design of low hydrogen consumables for future' Australasian Welding Journal, Volume 43, 3rd Quarter, 1998, pp 33-39.

DAVIDSON, J.L, LYNCH, S.P. and MAJUMDAR, A.: 'The relationship between hydrogen-induced cracking resistance, microstructure and toughness in high strength weld metal' Proceedings of the Seminar, Melbourne, October 1996, pp 21-34.

de LOACH, J.J., NULL, C., FIORE, S. and KONKOL, P.: 'The right welding wire could help the U.S. Navy save millions' Welding Journal, June 1999, pp 55-58.

de MEESTER, B.: 'Development of base materials for welding' Science and Technology of Welding and Joining, Volume 6, No.3, 2001, pp 159-167.

DICKEHUT, G. and HOTZ, U.: 'Effect of climatic conditions on diffusible hydrogen content in weld metal' Welding Journal, January 1991, pp 1-6s.

DITCHBURN, R.J., SCALA, C.M. and DIXON, B.F.: 'Comparison of techniques for non-destructive inspection in thick section welds of pressure vessel steel' Proceedings of the ICPVT-2000 conference, Sydney, 2000.

DIXON, B.F. and TAYLOR, J.S.: 'Control of hydrogen cracking in Collins class submarine welds' Proceedings of the Seminar, Melbourne, October 1996, pp 125-144.

DOUMANIDIS, C.C. and HARDT, D.E.: 'Simultaneous in-process control of heat affected zone and cooling rate during arc welding' Welding Journal, May 1990, pp 186-196s.

DUNNE, D.: A review of the theoretical and experimental background of hydrogen assisted cold cracking of steel weldments' Proceedings of the 1st International Conference on weld metal hydrogen cracking in pipeline girth welds, Wollongong, March 1999, pp.3-11.

DuPONT, J.N. and MARDER, A.R.: 'Thermal efficiency of arc welding process' Welding Journal, December 1995, pp 406-416s.

DÜREN, C.F.: 'Prediction of the hardness in the HAZ of HSLA steels by means of the C-equivalent' Select conference on hardenability of steels, Derby, UK, May, 1990.

EASTERLING, K.: 'Introduction to the physical metallurgy of welding' Butterworths Monograms in Metals, Butterworths and Co. Ltd., 1983.

EBERT, H.W.: 'Advances in flux cored electrodes reflected in new classifications' Welding Journal, February 1998, pp 53-54.

EDWARDS, G.R. and LIU, S.: 'Recent developments in HSLA steel welding' Proceedings on 'Advances in Welding Metallurgy', First US-Japan Symposium - AWS/JWS/JWES, San Francisco, U.S.A, June 1990, pp 215-293.

EN 439-1994: 'Welding consumables – shielding gases for arc welding and cutting'

EN 758-1997: 'Welding consumables – tubular cored electrodes for manual metal arc welding with and without a gas shield of non alloy and fine grain steels – classifications.

EN 1011.1-1998: 'Welding – recommendations for welding of metallic materials – general guidance for arc welding'

EN 1011.2-2001: 'Welding – recommendations for welding of metallic materials – arc welding of ferritic steels'

EN 10 113-1993: 'Hot rolled products in weldable fine grain structural steels'

EASTERLING, K.: 'Introduction to the physical metallurgy of welding' Butterworths, London, 1983.

EVANS, G.M.: 'The effect of nickel on the microstructure and properties of C-Mn all weld metal deposits' IIW doc.No: II-A-791-89.

EVANS, G.M.: 'Microstructure and properties of ferritic steel welds containing Al and Ti' Welding Journal, August 1995, pp 249-261s.

EVANS, G.M. and CHRISTENSEN, N.: 'Micro-fissuring of multi-run mild steel weld metal' British Welding Journal, October 1963, pp 508-515.

EVANS, G.M. and CHRISTENSEN, N.: 'Correlation of weld metal hydrogen content with HAZ embrittlement' Metal Construction and British Welding Journal, March 1971, pp 188-189.

EVANS, G.M.: 'Effect of aluminium and nitrogen on Ti-B containing steel welds' Welding Journal, October 1997, pp 431-441s.

FALS, H.C. and TREVISAN, R.E.: 'Acoustical emission characterisation of the fracture mode of hydrogen assisted cracking in high strength low alloy steel weldment by flux cored arc welding process' Proceedings of OMAE 17th International conference, Lisbon, 1998.

FANG, C.K., ASIBU, E.K. and BARBER, J.R.: 'Acoustic emission investigation of cold cracking in gas metal arc welding of AISI 4340 steel' Welding Journal, June 1995, pp 177-184s.

FARRAR, J.C.M. and DOLBY, R.E.: 'An investigation into lamellar tearing' Metal Construction and British Welding Journal, February 1969, pp 32-39.

FERREE, S.F.: 'New and improved cored wires for welding high strength steels' Proceedings of PACRIM WELDCON conference, 1992, Paper 11.

FERREE, S.F.: 'New generation of cored wires creates less fume and spatter' Welding Journal, December 1995, pp 45-49.

FRANCIS, R.E., JONES, J.E. and OLSON, D.L.: ' Effect of shielding gas oxygen activity on weld metal microstructure of GMA welded microalloyed HSLA steel' Welding Journal, November 1990, pp 408-415.

FRENCH, I.E.: 'Low temperature impact properties of multi-pass welds steel' Australasian Welding Journal, Volume 43, 4th Quarter 1998, pp 27-29.

FRENCH, I.E. and BOSWORTH, M.R.: 'Special basic flux-cored wire for all-positional pulsed welding' Welding Journal, March 1997, pp 120-124s.

GEDEON, S.A. and EAGAR, T.W.: 'Thermochemical analysis of hydrogen absorption in welding' Welding Journal, July 1990, pp 264-271s.

GEDEON, S.A. and EAGAR, T.W.: 'Assessing hydrogen assisted cracking fracture in high strength steel weldments' Welding Journal, June 1990/1, pp 213-220s.

GRANJON, H.: Metal Construction and British Welding Journal, January 1969, pp 509-515.

GRANJON, H.: 'Cold cracking in welding of steels' International symposium on cracking and fracture in welds, Proceedings Japan Welding Society, 1971, IB, 1.1.

GRAVILLE, B.A., BAKER, R.G. and WATKINSON, F.: 'Effect of temperature and strain rate on hydrogen embrittlement of steel' British Welding Journal, June 1967, pp 337-342.

GRAVILLE, B.A.: 'A survey of weld metal hydrogen cracking' Welding in the World, Volume 24, No.9/10, pp 190-198,1986.

GRAVILLE, B.A.: ' Cold cracking in welds in HSLA steels' Proceedings of International conference, Rome, 1978, pp 85-101.

GRAVILLE, B.A.: 'Interpretive report on weldability tests for hydrogen cracking of higher strength steels and their potential for standardization' Welding Research Council, Bulletin 400, April 1995.

GRAVILLE, B.A. and McPARLAN, M.: 'Weld metal cold cracking' Metal Construction and British Welding Journal, February 1974, pp 62-63.

GREGORY, N.: 'Why do welds crack?' TWI Bulletin 4, July/August 1991, pp 34-37.

GRONG, O. and KLUKEN, A.O.: 'Microstructure and properties of steel weld metals' Key Engineering Materials, Volume 69 and 70, 1992, pp 21-46.

GUNNET, R.: 'Method for measuring triaxial residual stress' Welding Research Abroad, Volume 4, No.10, 1958, pp 17-25.

HARRISON, R.P.: 'TOFD study of two steel plates' Report No: R01m023, Australian Nuclear Science and Technology Organization, May 2001.

HART, P.H.M.: 'Resistance to hydrogen cracking in steel weld metals' Welding Journal, January 1986, pp 14-22s.

HART, P.H.M.: 'Weld metal hydrogen cracking' TWI Research Bulletin, November 1978, pp 320-324.

HART, P.H.M. and EVANS, G.M.: 'Hydrogen content of single and multipass steel welds' Welding Journal, February 1997, pp 74-80s.

HART, P.H.M.: 'Hydrogen cracking – its cause, costs and future occurrence' Proceedings of the 1st International conference, Wollongong, March 1999.

HART, P.H.M. and HARRISON, P.L.: 'Compositional parameters for HAZ cracking and hardening in C-Mn steels' Welding International, Volume 5, No.4, 1991, pp 521-536s.

HARWIG, D.D, LONGERNECKER, D. and CRUZ, J.: 'Effects of welding parameters and electrode atmospheric exposure on the diffusible hydrogen content of gas shielded flux cored arc welds' Welding Journal, September 1999, pp 314-321s.

HIRAI, Y., HIRO, T. and TSUBOI, J.: 'Behaviour of hydrogen in arc welding (Report 2) – sources of hydrogen in a shielded metal arc welding' Transactions of the Japan Welding Society, Volume 5, No.2, September 1974, pp 3-8.

HIRTH, J.P.: 'Effects of hydrogen on the properties of iron and steel' Metallurgical Transactions, Volume 11A, June 1980, pp 861-889.

HOFFMEISTER, H. and MATTHIÄ, A.: ' the effects of test conditions on hydrogen assisted weld cracking of StE 355, StE 465 and StE 690 high strength steels' IIW doc.No. IX-1621-90.

HOFFMEISTER, H. HARNESHAUG, S. and ROAAS, S.: 'Investigation of the conditions for weld metal hydrogen cracking of low carbon offshore steels by the IRC weldability test' Material technology, steel research, Volume 58, No.3, 1987, pp 134-141.

HONG, J.K, TSAI, C.L. and DONG, P.: 'Assessment of numerical procedures for residual stress analysis of multi-pass welds' Welding Journal, September 1998, pp 372-382s.

HORIKAWA, K., Akazawa, J., Matusi, S. and Ohkuma.Y.: 'Correlation of various weld cracking tests' IIW doc.No: IX-966-76.

HRIVŇÁK, I.: 'Theory of weldability of metals and alloys' Materials Science Monographs 74, Elsevier, 1992.

HUGHES, R.K. and RITTER, J.C.: 'Micromechanisms of cleavage fracture in high strength steel weld metal' Proceedings of the WTIA conference, Adelaide, August 1995. pp 73-78.

International Institute of Welding: 'Guide to the light microscope examination of ferritic steel weld metals' IIW doc.No: IX-1533-88.

IRVING, B.: ' Trying to make some sense out of shielding gases' Welding Journal, May 1994, pp 65-70.

IRVING, B.: 'Weld cracking takes on some new twists' Welding Journal, August 1998, pp 37-40.

ISO 3690-2000: 'Welding and allied processes – determination of hydrogen content in ferritic steel arc weld metal' 2nd edition.

ITO,Y. and BESSYO, K.: Weldability formula of high strength steels related to heat affected zone cracking' IIW doc.No: IX-467-68.

Japan Welding Engineering Society: 'Relation between hydrogen content by IIW and JIS methods' IIW doc.No: II-698-74.

Japan Welding Engineering Society: 'Methods of measurements for hydrogen evolved from steel welds' IIW doc.No: II-1073-86.

JENKINS, N., Hart, P.H.M.H. and PARKER, D.H. 'An Evaluation of Rapid Methods for Diffusible Weld Hydrogen', Welding Journal, January 1997, pp 1-101s.

JILONG, Ma and APPS, R.L.: 'MIG transfer discovery of importance to industry' Welding and Metal Fabrication, September 1982, pp 307-316.

JIS Z3118-1992: 'Methods of measurement for hydrogen evolved from steel welds'

JIS Z3158-1996: 'Method of y-groove cracking test'

JONES, A.R. and HART, P.H.M.: 'Improving procedure prediction to avoid hydrogen cracking when welding C-Mn steels' TWI Report 225, October 1983.

JONES, A.R.: 'An evaluation of the production welding aspects of flux-cored wires' TWI Report 174, February 1982.

JUBB, J.E.M., CARRICK,L. and HAMMOND, J. ' Metal Construction and British Welding Journal, February 1969, pp 58-63.

KASUAYA, T., HASHIBA, Y., OKHITA, S. and FUJI, M.: 'Hydrogen distribution in multi-pass submerged arc weld metals' Science and Technology of Welding and Joining, Volume 6, No.4, 2001, pp 261-266.

KIEFER, J.H.: 'Effects of moisture contamination and welding parameters on diffusible hydrogen' Welding Journal, May 1996, pp 155-161s.

KIEFER, J.H.: 'Bead tempering effects on FCAW heat affected hardness' Welding Journal, November 1995, pp 363-367s.

KIHARA, H., SUZUKI, N. and NAKAMURA, N. 'Welding Journal, January, Volume 41, 1962, pp 36-48s.

KINSEY, A.J.: 'The welding of structural steels without preheat' Welding Journal, April 2000, pp 79-88s.
KINSEY, A.J.: 'Weld metal hydrogen cracking during welding 450 MPa yield strength steel using tubular cored electrodes' TWI Report 655, October 1998.

KINSEY, A.J.: 'Heat affected zone hydrogen cracking of Mn-Mo steels when welding with tubular cored wires' TWI Report 7316-01/96/923.3, 1996.

KOMIZO, Y and FUKADA, Y.: 'Toughness improvement in weld metal of carbon and HSLA steels in Japan' pp 227-250.

KONKOL, P.J., WARREN, J.L and HEBERT, P.A.: 'Weldability of HSLA-65 steel for ship structures' Welding Journal, September 1998, pp 361-371s.

KOSEKI, T., OHKITA, S. and YURIOKA, N.: 'Thermodynamic study of inclusion formation in low alloy steel weld metals' Science and Technology of Welding and Joining, Volume 2, No.2, 1997, pp 65-69.

KOTECKI, D.J.: 'Hydrogen reconsidered' Welding Journal, August 1992, pp 35-43.

KOTECKI, D.J.: 'Hydrogen measurement and standardisation' Proceedings of the Seminar, Melbourne, October 1996, pp 87-102.

KUEBLER, R., PITRUN, M. and PITRUN, I.: 'The effect of welding parameters and hydrogen levels on the weldability of high strength Q&T steel welded with FCAW consumables' Australasian Welding Journal, Volume 45, 1st Quarter, 2000, pp 38-47.

KUEBLER, R.: Private communication, June 2003.

KUROKAWA, T., NAGAOKA, S. and HASHIMOTO, T.: 'Characteristics of newly developed flux-cored wire for mild and high tensile strength steels' Kobelco, Technology Review No.21, April 1998, pp 30-34.

KUWANA, T. and SATO, Y.: 'Effect of manganese on oxygen absorption by steel weld metal during arc welding' IIW doc.No. IX-1593-90.

KYTE, W.S. and CHEW, B.: 'Postweld heat treatment for hydrogen removal' Welding Journal, February 1979, pp 54-58s.

LANCASTER, J.F.: 'Metallurgy of welding' 6th edition, 1999.

LANFORD, W.A.: 'MeV ion beam analysis for hydrogen' Proceedings of the Seminar, Melbourne, October 1996, pp 103-112.

LAZOR, R.B. and GRAVILLE, B.A.: 'Effect of microalloying on weld cracking in low carbon steels' Canadian welder and fabricator, Volume 74, July 1983, pp 21-23.

LEE, H.W. and KANG, S.W.: 'A study on transverse weld cracks in 50mm thick steel plate with SAW process' Journal of Japan Welding Society, Volume 15, No.4, 1997, pp 563-573.

LEE, H.W., KANG, S.W. and UM, D.S.: 'A study on transverse weld cracks in thick steel plate with the FCAW process' Welding Journal, December 1998, pp 503-510s.

LEE, H.W., KANG, S.W.: 'The relationship between residual stress and transverse weld cracks in thick steel plate' Welding Journal, August 2003, pp 225-230s.

LEE, J.L. and LEE, J.Y.: 'The interaction of hydrogen with the interface of Al_2O_3 particles in iron' Metallurgical Transactions A, Volume 17A, December 1986, pp 2183-2186.

LEE, J.L. and LEE, J.Y.: 'Hydrogen trapping in AISI 4330 steel' Metal Science, Volume 17, September 1983, pp 426-432.

LEONARD, A.J., GUNN, R.N. and GOOCH. T.G.: 'Hydrogen cracking of ferritic-austenitic stainless steel weld metal' Proceedings of Stainless steel world duplex America 2000 conference, USA, February – March 2000.

LEVCHENKO, A.M., PETROV, G.L. and SINYAKIN, V.P. 'The effect of air humidity on the hydrogen content of single-pass welded joints' Welding production, 1978, pp 23-26.

LI, H. and NORTH, T.H.: 'Hydrogen absorption and hydrogen cracking in high strength weld metal' Key Engineering Materials, Volumes 69 and 70, 1992, pp 95-112.

LI, J.C.M. and LIU, C.T.: 'Crack nucleation in hydrogen embrittlement' Scripta Metallurgica et Materialia, Volume 27, 1992, pp 1701-1705.

LIN, Y.C., and PERNG, J.Y.: 'Effect of welding parameters on residual stress in type 420 martensitic stainless steel' Science and Technology of Welding and Joining, Volume 2, No.3, 1997, pp 129-132.

LIU, S.: 'Metallography of HSLA steel weldments' Key Engineering Materials, Volumes 69 and 70, 1992, pp 1-20.

LUCAS, W.: 'Choosing a shielding gas – part 2' Welding and Metal Fabrication, July, 1992, pp 269.

LUNDIN, C.D., GILL, T.P.S., QIAO, C.Y.P., WANG, Y. and KHAN, K.K.: 'Weldability of low carbon micro-alloyed steels for marine structures' Welding Research Council, Bulletin 359, December 1990.

LYNCH, S.P.: 'Comments on evidence for the discontinuity of hydrogen assisted fracture in mild steel' Scripta Metallurgica et Materialia, Volume 26, 1992, pp 153-156.

LYNCH, S.P.: 'Overview No.74. Environmentally assisted cracking: Overview of evidence for an adsorption-induced localised-slip process' Acta Metallurgica, Volume 36, No. 10, 1988, pp 2639-2661.

MAKARA, A.M.: 'Cold transverse cracks in low-alloy high strength welds' Avtomaticheskaja Svarka, Volume 11, 1971, pp 1-4.

MATHARU, I.S. and HART, P.H.M.: 'Heat affected zone (HAZ) hydrogen cracking behaviour of low carbon equivalent C-Mn steels' TWI Report 290, November 1985.

MATSUDA, F., NAKAGAWA, H. and SHINOKAZI, K.: Trans. of JWRI, 8, 1979, pp 113-119.

MATSUDA, F., NAGAKAWA, H., SHINOZAKI K., MORIMOTO, H. and MATSUMOTO, T: 'Effect of oxygen on cold cracking susceptibility in weld metal of high strength steel' Transaction of JWRI, Volume 14, No.2, 1985, pp 135-142s.

MATSUSHITA, M. and LIU, S.: 'Hydrogen control in steel weld metal by means of fluoride additions in welding flux' Welding Journal, October 2000, pp 295-303s.

McKEOWN, D.: 'Hydrogen and its control in weld metal' Metal Construction, Volume 17, October 1985, pp 655-661.

McMAHON, C.J. Jr.: 'The role of solute segregation in promoting the hardenability of steel' Metallurgical Transactions A, Volume 11A, March 1980, pp 531-535.

McPARLAN, M. and GRAVILLE, B.A.: 'Hydrogen cracking in weld metals' Welding Journal, April 1976, pp 95-102s.

MIKULA, J.: 'The role of hydrogen in the initiation of cold cracking (Part 1)' Welding International, Volume 8, (10), 1994, pp 761-765.

MOORE, E.M. and McINTYRE, D.R.: 'Common misconceptions about hydrogen-induced cracking' Material Performance, Volume 37, October 1998, pp 77-81.
MOTA, J.M. and APPS, R.L. :' "Chevron cracking" – a new form of hydrogen cracking in steel weld metal' Welding Journal, July 1982, pp 222-228s.

MUNDRA, K., deBROY, T., BABU, S.S. and David, S.A.: ' Weld metal microstructure calculations from fundamentals of transport phenomena in the arc welding of low-alloy steels' Welding Journal, April 1997, pp 163-171s.

MUNNS, I.J. and SCHNEIDER C.R.A.: 'The reliability of radiography of thick sections welds' Proceedings of the Conference, Review in quantitative non-destructive evaluation, Montreal, Canada, July 1999, pp 1-10.

NAKAMURA, M. and FURUBAYASHI, E.: 'Effect of grain size on crack propagation of high strength steel in gaseous hydrogen atmosphere' Materials Science and Technology, Volume 6, July 1990, pp 604-610.

NEVASMAA, P.: 'Controlling factors affectiong hydrogen cold cracking in high strength multi-pass weld metals: Comparison of the cracking test results between SMAW and SAW welds' IIW doc.No. IX-2027-02.

NEVASMAA, P.: 'Hydrogen cold cracking in high strength multi-pass weld metal – predicting the cracking risk and necessary precautions for safe welding' IIW doc.No. IX-2066-03.

NF A89-100-1991: 'Welding and allied processes. Cold cracking on implants. Test method'

NISHITO, Y., YOSHIDA, Y. and MUIRA, Y. Japan Welding Society, Volume 44, No.4, 1975, pp 345-350.

NOLAN, D. and PITRUN, M.: 'A comparative study of diffusible hydrogen test methods' Australasian Welding Journal, Volume 48, 4th Quarter, 2003, pp 36-41.

NORRISH, J.: 'Advanced welding processes' Institute of Physics Publishing, ISBN 0-85274-326-2, 1992.

NORRISH, J. and RICHARDSON, I.M.: ' Metal transfer mechanism' Welding & Metal Fabrication, 56, (1), 1988.

OERILKON web site: *http://www.oerlikonweld.com*

OKUDA, N., OGATA, Y., NISHIKAWA, Y., AOKI, T., GOTO, A. and ABE, T.: 'Hydrogen-induced cracking susceptibility in high strength weld metal' Welding Journal, May 1987, pp 141-146s.

OKUMARA, T. and HORIKAWA, K.: 'Transverse cracks in submerged-arc welding of 80 kg/mm^2 tensile strength steel' Paper IA7, 1st International Symposium of Japan Welding Society, Tokyo, November 1971, pp 1-17.

OLSON, D.L., MAROEF, I., LENSING, C., SMITH, R.D., WANG, W.W., LIU, S. WILDEMAN, T. and EBERHART, M.: 'Hydrogen management in high strength steel weldments' Proceedings of the Seminar, Melbourne, October 1996, pp 1-19.

ONSØIEN, M., PETERS, D.L., OLSON, D.L. and LIU, S.: 'Effect of hydrogen in an argon GTAW shielding gas: Arc characteristics and bead morphology' Welding Journal, January 1995, pp 10-15s.

ORIANI, R.A.: 'The diffusion and trapping of hydrogen in steel' Acta Metallurgica, Volume 18. January 1970, p 147-157.

PARGETER, R.J.: 'Effects of arc energy, plate thickness and preheat on C-Mn steel weld metal hydrogen cracking' TWI Report 461, November 1992.

PARGETER, R.J.: 'Hydrogen – a moving target' TWI Bulletin, January/February, 1993, pp 14-15.

PARK, Y.D., MAROEF, I.S., LANDAU, A. and OLSON, D.L.: 'Retained austenite as a hydrogen trap in steel welds' Welding Journal, February 2002, pp 27-35s.
PETCH, N.O. and STABLES, P.: 'Delayed fracture of metals under static load' Nature 169, 1952, pp 842-843.

PICK, R.J., NORTH, T.H. and A.G. GLOVER, A.G.: 'Full-scale weldability testing of large diameter line pipe' Canadian Mining and Metallurgy Bulletin, January 1982, pp 122-127.

PITRUN, M., DAVIDSON, J.L., KENNY, C.J., WITTKE, P.J. and CORNISH, N.: 'Factors affecting the hydrogen content of weld metal deposited by flux cored arc welding consumables' Australasian Welding Journal, Volume 46, 1st Quarter, 2001, pp 33-38.

POKHODNYA, I.K. and SHVACHKO, V.I: 'Physical nature of hydrogen-induced cold cracks in welded joints in structural steels' IIW doc.No. IX-1970-00.

POKHODNYA, I.K., STEPANYUK, S.N. and SHVACHKO, V.I.: 'Role of temperature in hydrogen-induced cracking of structural steels and welded joints' The Paton Welding Journal, February 2000, pp 2-7.

POKHODNYA, I.K.: 'Hydrogen behaviour in welds joints' Proceedings of the Seminar, Melbourne, October 1996, pp 145-181.

POWELL, G.L.F. and HERFURTH, G.: 'Charpy V-notch properties and microstructures of narrow gap ferritic welds of a quenched and tempered steel plate' Metallurgical and Materials Transactions A, Volume 29A, November 1998, pp 2775-2784.

PRESSOUYRE, G.M.: 'Trap theory of hydrogen embrittlement' Acta Metallurgica, Volume 28, 1980, pp 895-911.

PUSSEGODA, L.N, GRANVILLE, B.A. and MALIK, L.: 'Delayed cracking in naval structures steels' National Defence Canada, Unclassified Report No.CR97/420, May, 1997.

QUINTANA, M.A. and KOTECKI, D.J.: 'Achievements and perspectives for the new millennium' 53rd IIW Annual Assembly, July 2000.

REEVE, L.: 'A summary of reports of investigations on selected types of high strength steels' Trans. Inst. Welding, April 1940, pp 177-202.

RIPLEY, M.: 'Residual stress measurement using neutrons' Welding Technology Institute Australia and Australian Nuclear Science and Technology Organization seminar, Melbourne, February 2002.

RITTER, J.C., DIXON, B.F., PHILLIPS, R.H., HUGHES, R.K. and DAVIDSON, J.L.: 'Experience with welding technology on HSLA steel in the Collins submarine' Proceedings of the DSTO Conference, Melbourne, March 2002, pp 1-17.

ROELENS, J.B.: 'Determination of residual stresses in submerged arc multi-pass welds by means of numerical simulation and comparison with experimental measurements' Mathematical Modelling of Weld Phenomena 2, pp 227-241.

RUGE, J. and DICKEHUT, G.: 'Method of predicting the content of diffusible hydrogen in the weld metal under the influence of atmospheric moisture' IIW doc.No. II-A-754-88.

SAF & AIRLIQUIDE web site: *http://www.saf-airliquide.com*

SALTER, G.R.: 'Hydrogen absorption in arc welding' British Welding Journal, Volume 6, October 1963, pp 316-325.

SATOH, K. and MATSUI, S.: IIW doc.No. IX-574-68.

SATO, M., SUDA, K. and NAGASAKI, H.: 'How to weld using flux-cored wires' Welding International, Volume 11, April 1997, pp 264-272.

SAVAGE, W.F., NIPPES, E.F. and SZEKERES, E.S.: 'Hydrogen induced cold cracking in a low alloy steel' Welding Journal, September 1976, pp 276-283s.

SCHUMANN, G.O. and FRENCH, I.E.: 'Influence of welding variables on weld metal mechanical and microstructural properties from flux-cored and solid wires of E80/90 strength level' Proceedings of the conference, Adelaide, August 1995, pp 37-44.

SCHUMANN, G.O. and FRENCH, I.E.: 'Influence of welding variables on weld metal from microalloyed, rutile flux cored wires' CRC for MW&J, Project No. 93-05, January 1994.

SCHWINN, V., STREISSELBERGER, A. and BAUER, J.: 'Various approaches to different demands of low alloy steels with specified HIC resistance' Proceedings from NACE International Annual conference and corrosion show, Boston, 1995, paper No. 66, pp 1-16.

SÉFÉRIAN, D.: 'The metallurgy of welding' Chapman and Hall London, 1962.

SHIM, Y., FENG, Z., LEE, S., KIM, D., JAEGER, J., PAPRITAN J.C. and TSAI, C.L.: 'Determination of residual stresses in thick-section weldments' Welding Journal, September 1992, pp 305-312s.

SHINOZAKI, H., WANG, X. and NORTH, T.H.: 'Effect of oxygen on hydrogen cracking in high-strength weld metal' Metallurgical Transactions A, Volume 21A, May 1990, pp 1287-1297.

SHIRALI, A.A. and MILLS, K.C.: 'The effect of welding parameters on penetration in GTA welds' Welding Journal, July 1993, pp 347-353s.

SHVACHKO, V.I.: 'Cold cracking of structural steel weldments as reversible hydrogen embrittlement effect' International Journal of Hydrogen Energy, Volume 25, 2000, pp 473-480.

SIERDZINSKI, M.S. and FERREE, S.E.: 'New flux cored wires control diffusible hydrogen levels' Welding Journal, February 1998, pp 45-48.

SIEWERT, T.A.: 'Moisture in welding filler materials' Welding Journal, February 1985, pp 32-41.

SMITH, S.D. and BLUNT, F.J.: 'An application of a simple numerical model for hydrogen diffusion in multi-pass submerged arc welds in C-Mn steels' 1993.

SMITH II, R.D., LANDIS, G.P., MAROEF, I., OLSON, D.L. and WILDEMAN, T.R.: 'The determination of hydrogen distribution in high strength steel weldments, Part 1: Laser ablation methods' Welding Journal, May 2001-1.

SMITH II, R.D., BENSON, D.K., MAROEF, I., OLSON, D.L. and WILDEMAN, T.R.: 'The determination of hydrogen distribution in high strength steel weldments, Part 2: Opto-elecronic diffusible hydrogen sensor' Welding Journal, May 2001-2.

Smithell Metals Reference Book, Butterworths & Co. Publishing, 6th edition, 1983.

STEMVERS, M.: 'Cored wire benefits' Proceedings of the ESAB Seminar: Welding of steels using flux-cored wires, Slovak Technical University, Trnava, April 2001, pp 11-20.

STENBACKA, N. and PERSSON, K.A.: 'Shielding gases for gas metal arc welding' Welding Journal, November 1989, pp 41-47.

STOUT, R.D., TOR, S.S., McGEADY, L.J. and DOAN, G.E.: 'Quantitative measurement of the cracking tendency in welds' Welding Journal, September 1946, pp 522-531s.

STOUT, R.D.: 'Post weld heat treatment of pressure vessels steels' Welding Research Council, Bulletin 302, 1985, pp 1-14.

SUZUKI, H., INAGAKI, M. and NAKAMURA, H.: 'Effects of restraint and hydrogen on root cracking of high strength steel welds' IIW doc. No. IX-408-64.

SUZUKI, H.: 'Cold cracking and its prevention in steel welding' Transactions of the Japan Welding Society, Volume 9, No.2, 1978, pp 82-91.

SUZUKI, H. and YURIOKA, N.: 'Tetsu to Hagané' Journal Iron Institute Japan, Volume 67, October 1982, pp 1657-1699.

SUZUKI, H. and YURIOKA, N.: 'Prevention against cold cracking by the hydrogen accumulation cracking parameter P_{HA}' Transactions of the Japan Welding Society, Volume 14, No.1, 1983, pp 40-52.

SYMONS, H.O.: 'Weld metal hydrogen – a review of its determination and other control aspects for the 1900s' Australasian Welding Journal, 3rd Quarter, 1990, pp 21-26.

TAKAHASHI, E., IWAI, K. and HORITSUJI, T.: 'Relationship between occurrence of the transverse cracking' Journal of Japan Welding Society, Volume 48, No.10, 1979, pp 865-872.

TANAKA, J. and NAKAGAWA, H.: Journal of Japan Welding Society, Volume 41, No.8, 1972, pp 915-924.

TARLINSKI, V.D.: Avtomaticheskaja Svarka, No. 27, June, 1974, pp 16-20.

TCHAIKOVSKY, M. and SQUIRES, I.: 'Hydrogen activity coefficients in the weld zone' Proceedings of the Seminar, Melbourne, October 1996, pp 75-86.

The Welding Institute TWI web side: http://www.twi.co.uk

THOMPSON, A.W. and BERNSTEIN, I.M.: 'Microstructure and hydrogen embrittlement' Proceedings of the International Conference, Moran, 1980, pp 291-303.

THIBAU, R. and BALA, S.R.: 'Influence of electroslag weld metal composition on hydrogen cracking' Welding Journal, April 1983, pp 97-104s.

TROIANO, A.R.: 'The influence of hydrogen on the mechanical behaviour of steel' The Iron and Steel Institute, Special report No.73, 1962.

TYAGI, V.K., FRENCH, I.E. and BEE.J.V.: 'Understanding the influence of alloy additions on microstructural and mechanical properties of weld metal from gas-shielded processes' Australian Welding Research report CRC No.20, December 1996. pp 1-26.

UWER, D. and HÖHNE, H.: 'Characterisation of the cold cracking behaviour of steels during welding' Welding and Cutting Volume 43, 4, 1991, pp 195-199.

UWER, D. and DEGENKOLBE, J.: 'Thermal cycles in arc welding calculation of cooling times' IIW doc.No. IX-987-76.

van der MEE, V.: 'Effect of atmospheric storage condition on weld metal diffusible hydrogen content of gas shielded cored wires. A brief study for IIW Sub-Commission II-A' IIW doc.No. II-1437-01.

van VLACK, L.H.: 'Elements of materials science' 2nd edition, 1964.

van WORTEL, J.C.: 'Reproducibility and reliability of hydrogen measurements at a level of less than 5ml/100g deposited weld metal (SMAW)' IIW doc.No. II-1212-93.

VAIDYA, V.V.: 'Shielding gas mixtures for semiautomatic welds' Welding Journal, September 2002, pp 43-48.

VASUDEVAN, R. STOUT, R.D. and PENSE, A.W.: 'Hydrogen assisted cracking in HSLA pipeline steels' Welding Journal, September 1981, pp 155-168s.

VIGILANTE, G.N., UNDERWOOD, J.H., CRAYON, D., TAUSCHER, S., SAGE, T. and TROIANO, E.: 'Hydrogen induced cracking tests of high strength steels and nickel-iron base alloys using the bolt-loaded specimen' Proceedings of the Seminar, Melbourne, October 1996, pp 61-73.

VILLAFUERTE, J.: 'Understanding contact tip longevity for gas metal welding' Welding Journal, December 1999, pp 29-35.

VISMAN, V.: 'Weld metal HACC in thick section, low strength multi-pass FCAW', Honours thesis, University of Wollongong, Australia, 2002.

VUIK, J.: 'An update of the state-of-the-art of weld metal hydrogen cracking' Welding in the World, Volume 31, 5, 1993, pp 23-32.

WANG, D. and APPS, R.L.: 'Hydrogen induced cold cracking in high strength steel weld metal' Proceedings of International Conference, Helsingor, Denmark, May 1991. pp 485-446.

WATANABE, M. and SATOH, K.: Japan Society Naval Architects 1962, pp 487-496.

WEBER, R.A.: 'Detection of hydrogen in the welding arc' Proceedings of the Seminar, Melbourne, October 1996, pp 113-123.

WEGRZYN, T.: 'Effect of oxygen on the toughness of low-carbon, low-hydrogen steel weld metal' Welding International, Volume 6, (9), 1994, pp 683-689.

Welding Technology Institute of Australia (WTIA): 'The weldability of steels' Technical Note 1, 1994.

Welding Technology Institute of Australia (WTIA): 'Welding and fabrication of quenched and tempered steel' Technical Note 15, 1996.

Welding Technology Institute of Australia (WTIA): 'Welding stainless steels' Technical Note 16, 1985.

WHITE, D., POLLARD, G. and GEE, R.: 'The effect of welding parameters on diffusible hydrogen levels in cored wire welding' Welding and Fabrication, June 1992, pp 209-216.

WIDGERY, D.J.: 'Tubular wire welding' Abington Publishing, ISBN 1 85573 088 X, 1994.

WILDASH, C., COCHRANE, R.C., GEE, R. and WIDGERY, D.J.: 'Microstructural factors affecting hydrogen induced cold cracking in high strength steel weld metal' Proceedings of the International Conference, Leeds, 1999, pp 745-750.

WILDASH, C., GEE, R. and COCHRANE, R.: 'Design a microstructure to resits HIC in HS steels' Welding & Metal Fabrication, April, 2000, pp 15-20.

WONG, R., BLACKBURN, J., DeLOACH J. and DENALE, R.: 'Welding induced hydrogen in US Navy structural steels' Proceedings of the Seminar, Melbourne, October 1996, pp 35-48.

YURIOKA, N.: 'Comparison of preheat predictive methods' IIW doc.No. IX-2025-02.

YURIOKA, N., SUZUKI, H., OHSHITA, S. and SAITO, S.: 'Determination of necessary preheating temperature in steel welding' Welding Journal, June 1983, pp 147-153s.

YURIOKA, N. and SUZUKI, H.: 'Hydrogen assisted cracking in C-Mn and low alloy steel weldments' International Materials Reviews, Volume 25, April 1990, pp 217-249.

YURIOKA, N. and KASUYA, T.: 'A chart to determine necessary preheat in steel welding' Welding in the World, Volume 35, No.5, 1995, pp 31-38.

YURIOKA, N., OHSHIDA, S. and NAKAMURA, H.: 'An analysis of hydrogen accumulation at weld heat affected zone' Hydrogen in metals Proceedings of second JIM international symposium, 1979.

ZAPFFEE, C.A. and SIMS, C.E.: 'Hydrogen embrittlement, internal stress, and defects in steels' Trans. AIME 145, 1941, pp 225-259.

ZHANG, Z., MARSHALL, A.W. and HOLLOWAY, G.B.: 'Flux cored arc welding the high productivity process for P91 steels' 3rd EPRI conference on Advances in Materials Technology for Fossil Power Plants, 1st – 6th April 2001, University of Wales, Swansea, USA.

APPENDICES

Appendix A:

Cross-sections of the hydrogen test samples for the H10 deposits.

Sample ID

H10-18-C

H10-17-C

H10-16-C

H10-15-C

H10-14-C

H10-13-C

H10-12-C

H10-11-C

H10-10-C

H10-9-A

H10-8-A

H10-7-A

H10-6-A

H10-5-A

H10-4-A

H10-3-A

H10-2-A

H10-1-A
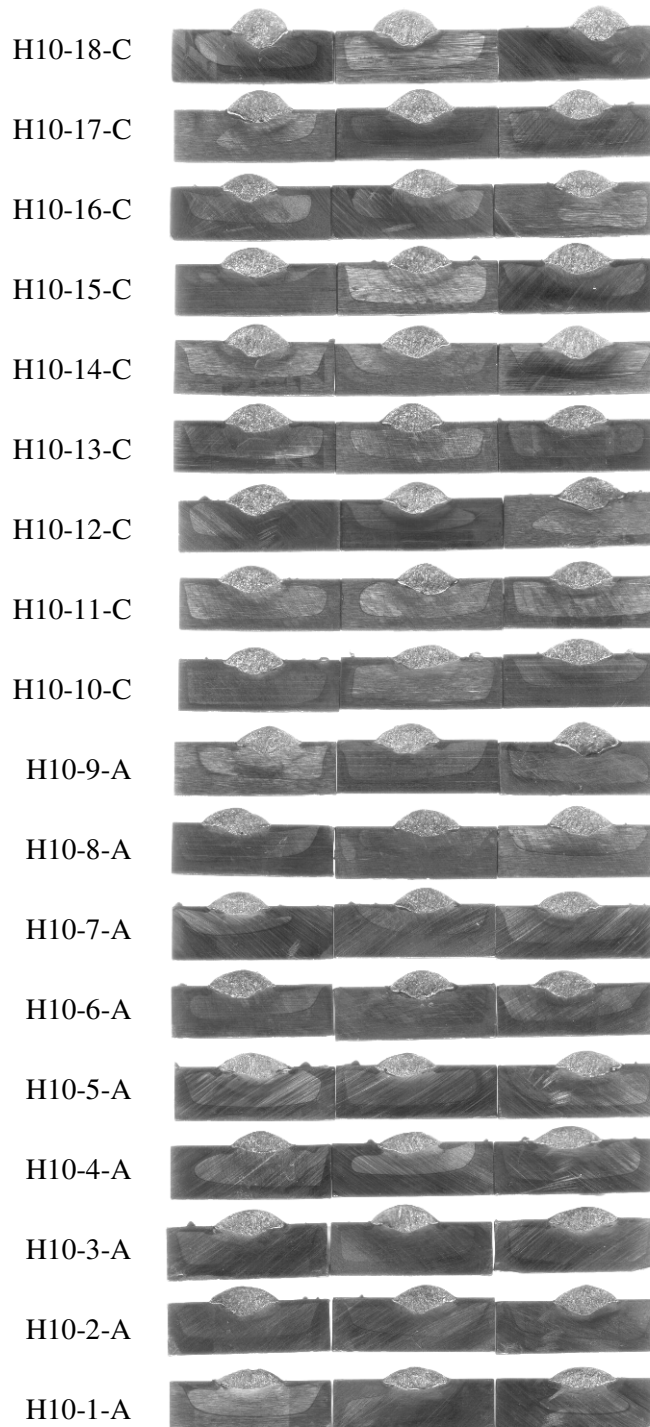
Cross-sections of the hydrogen test samples for the H5 deposits.

Sample ID
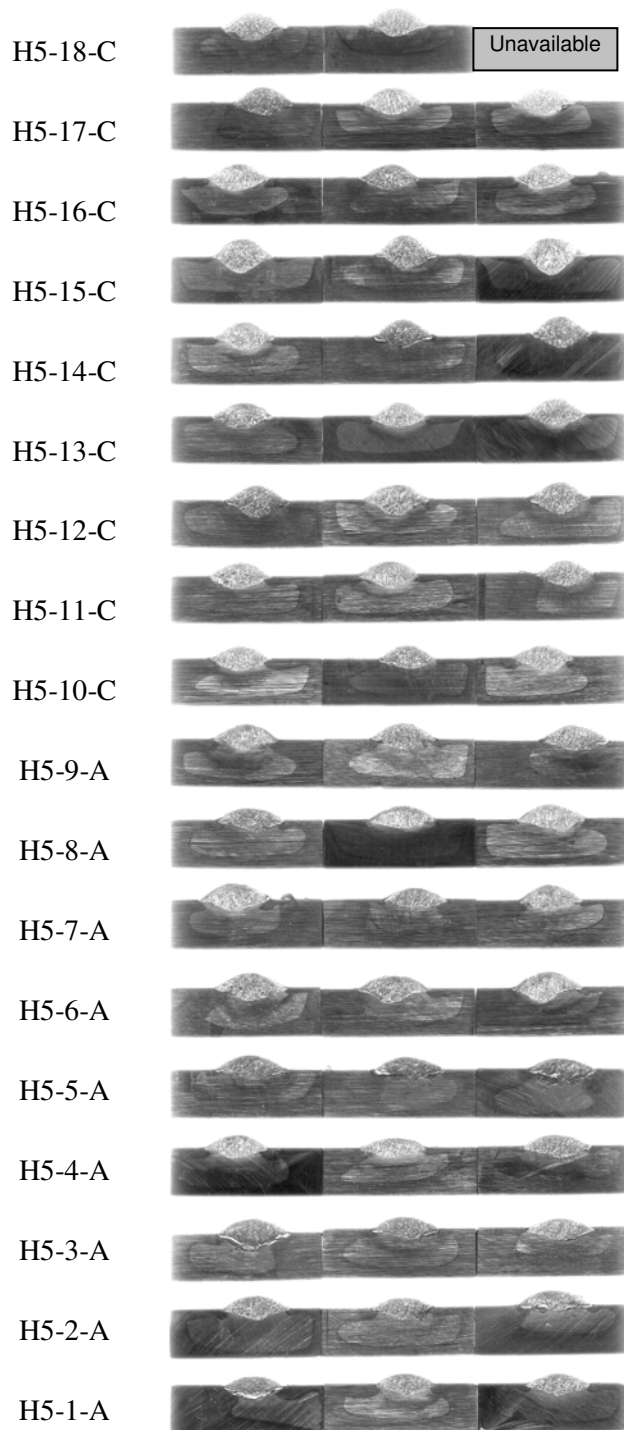
Appendix B:

Graphs showing the relationship between the welding current and hydrogen levels for H10 and H5 welds deposited using 75Ar-25CO_2 and CO_2 shielding gases at CTWD of 20 and 25mm.
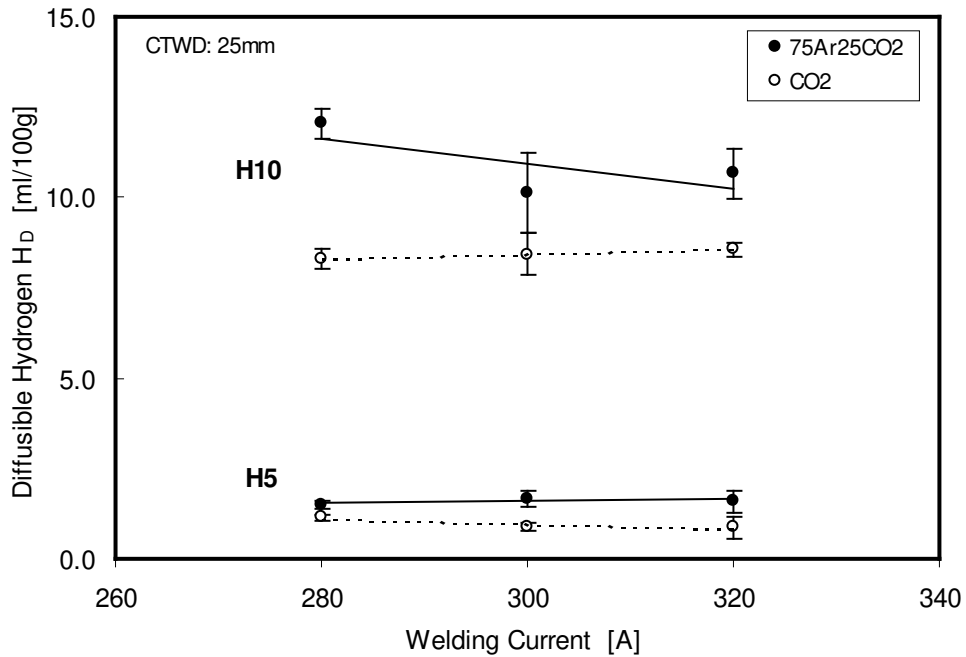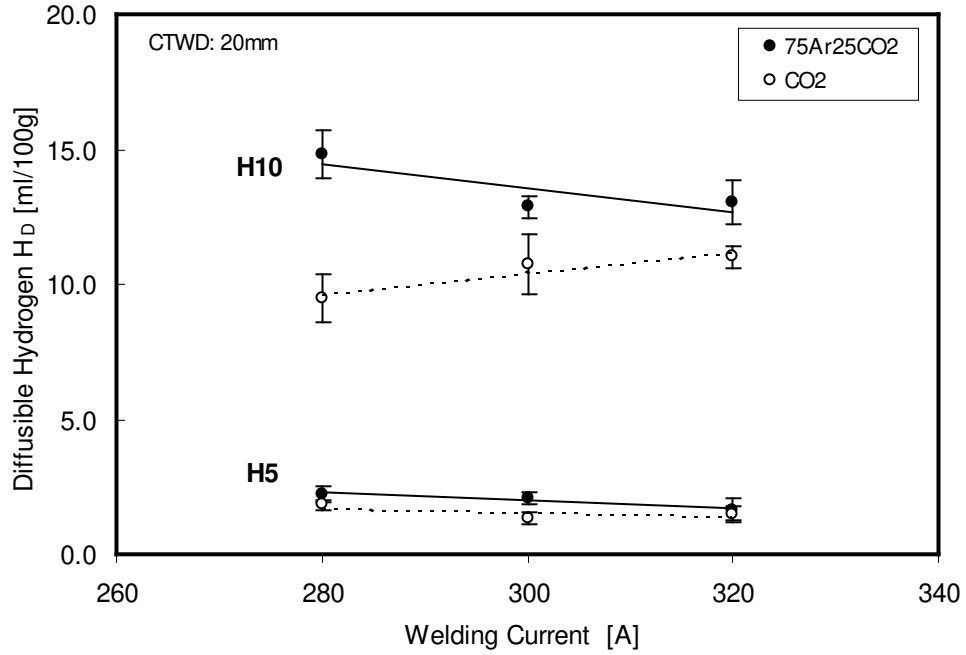
Appendix C:

G-BOP fracture faces of H10 and H5 weld deposits using a range of preheat temperatures (20, 50, 80, 100, and 120 °C) and two shielding gases (75Ar-25CO_2 and CO_2), as listed in Tables 6.7, 6.8, 6.9 and 6.10.
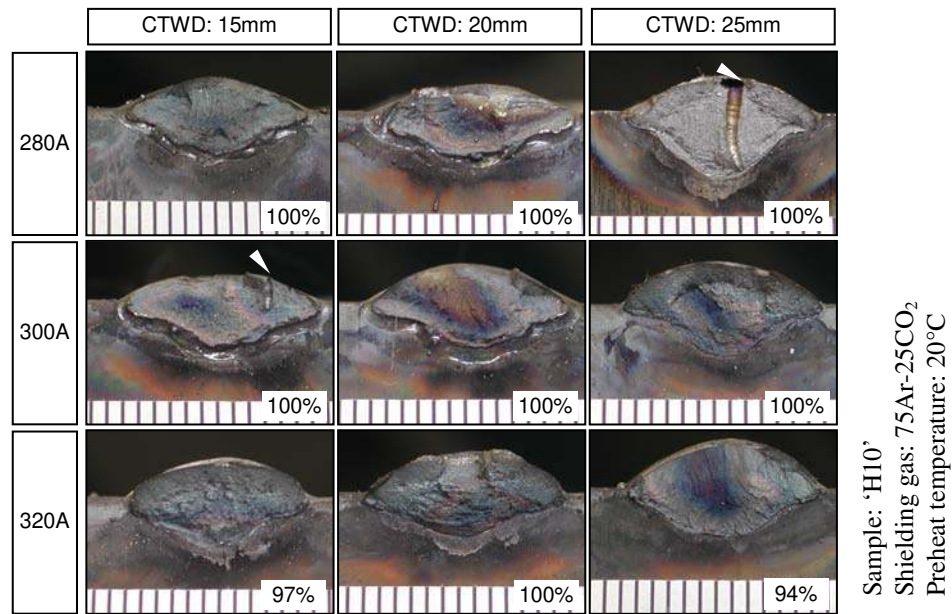
Photographs of the fracture faces of H10 weld deposits at preheat temperature of 20 °C and using 75Ar-25CO_2 shielding gas.
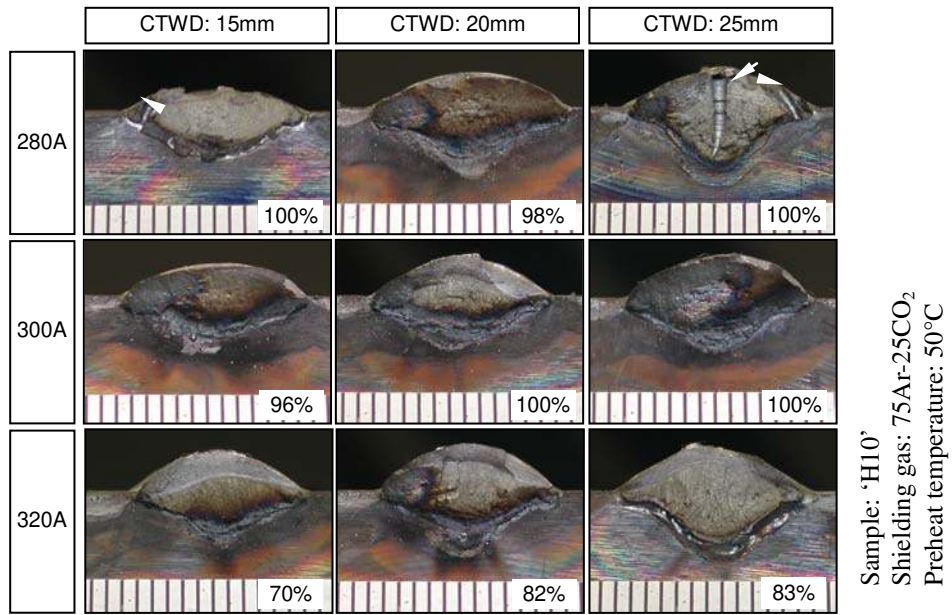
Photographs of the fracture faces of H10 weld deposits at preheat temperature of 50 °C and using 75Ar-25CO₂ shielding gas.
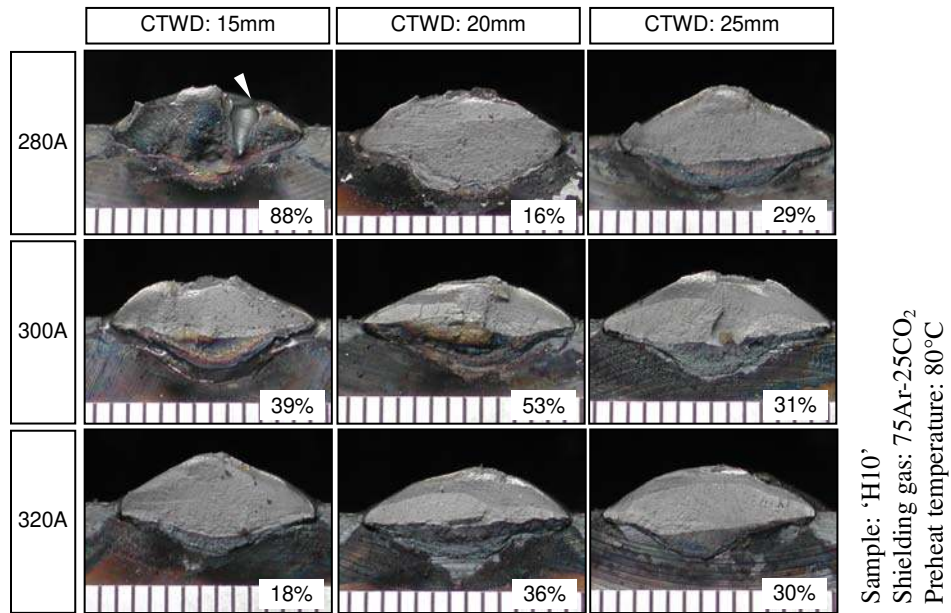
Photographs of the fracture faces of H10 weld deposits at preheat temperature of 80 °C and using 75Ar-25CO₂ shielding gas.
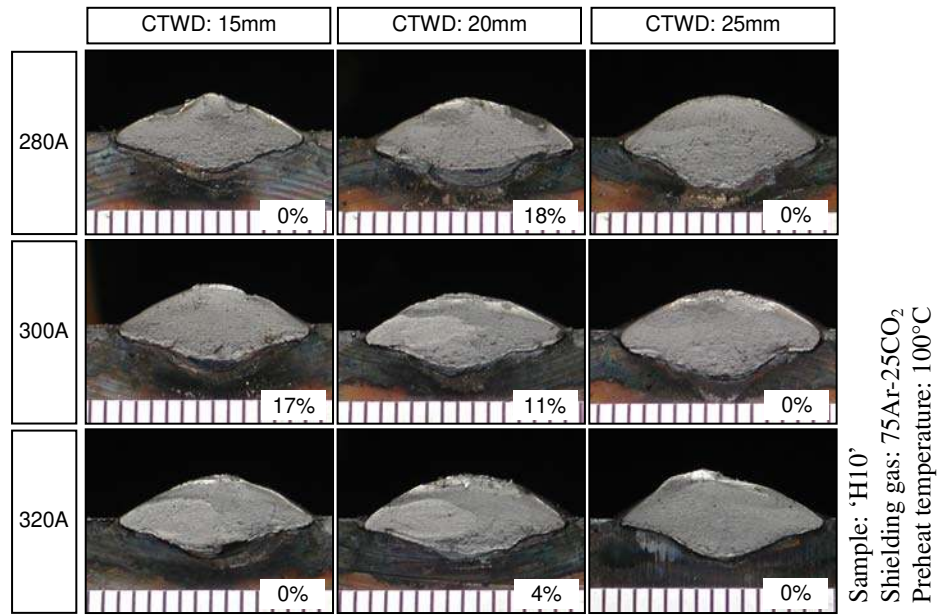
Photographs of the fracture faces of H10 weld deposits at preheat temperature of 100 °C and using 75Ar-25CO$_2$ shielding gas.
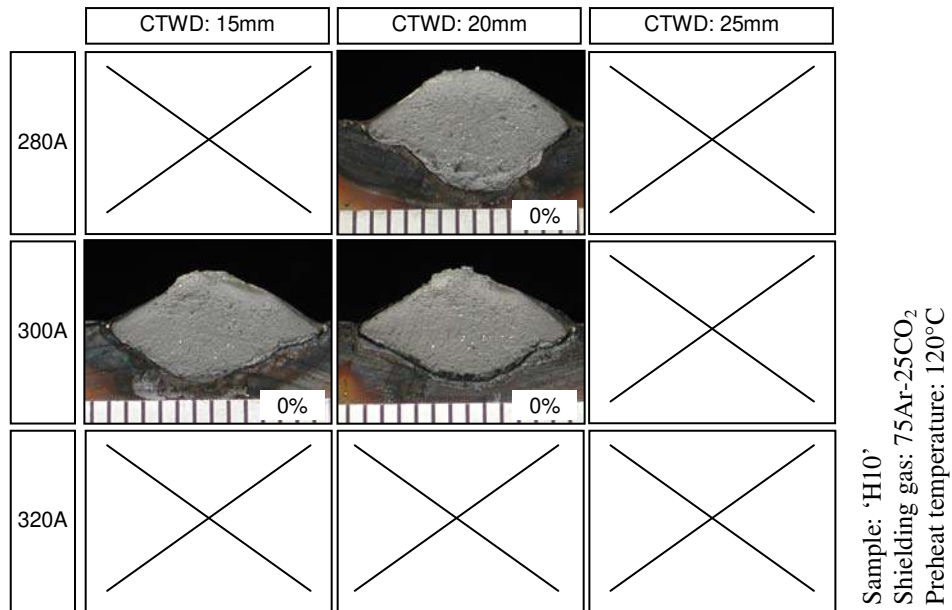
Photographs of the fracture faces of H10 weld deposits at preheat temperature of 120 °C and using 75Ar-25CO$_2$ shielding gas.
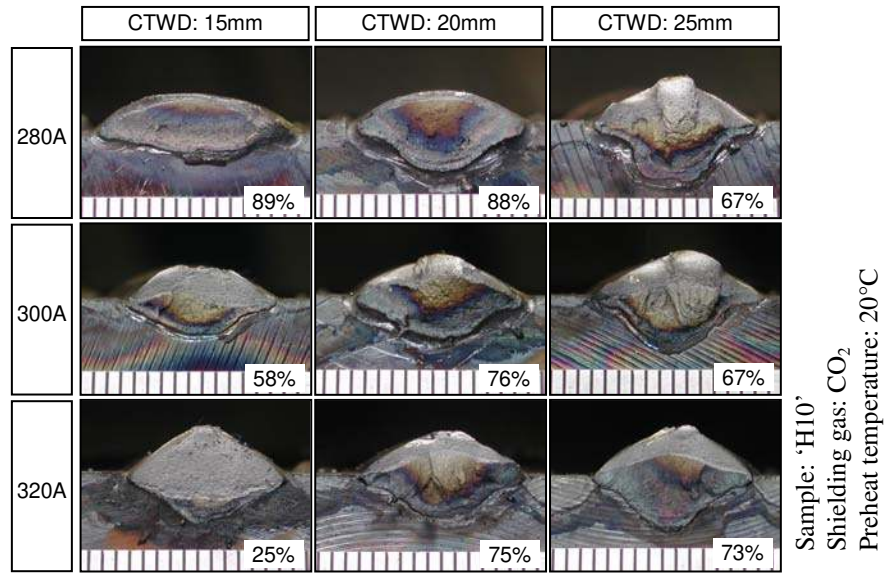
Photographs of the fracture faces of H10 weld deposits at preheat temperature of 20 °C and using CO_2 shielding gas.
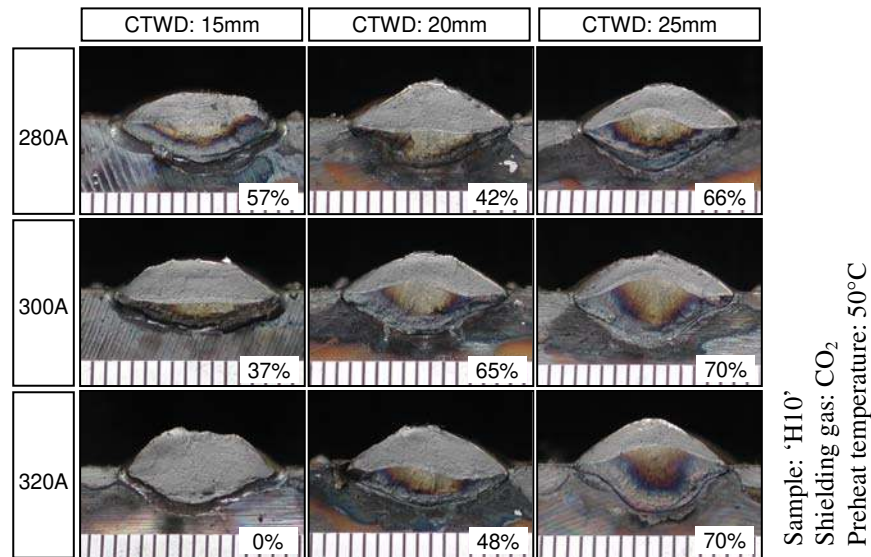
Photographs of the fracture faces of H10 weld deposits at preheat temperature of 50 °C and using CO_2 shielding gas.
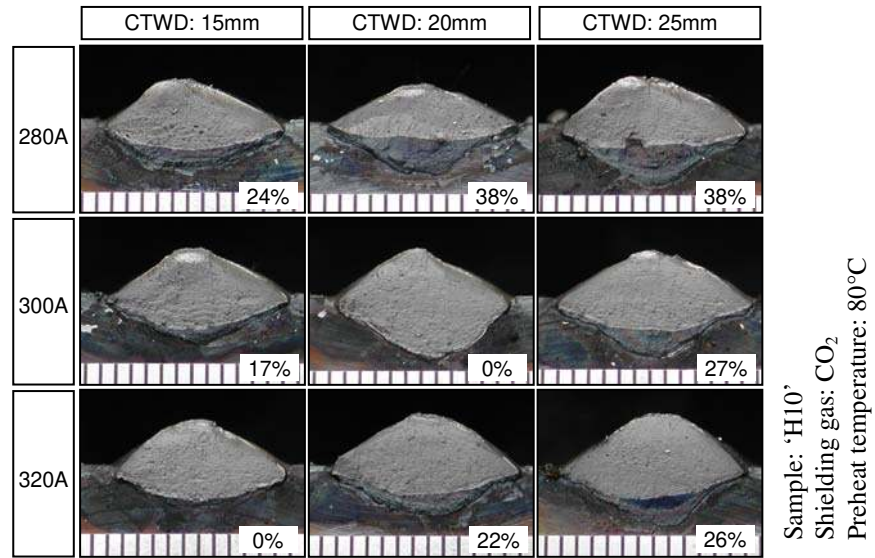
Photographs of the fracture faces of H10 weld deposits at preheat temperature of 80 °C and using CO_2 shielding gas.
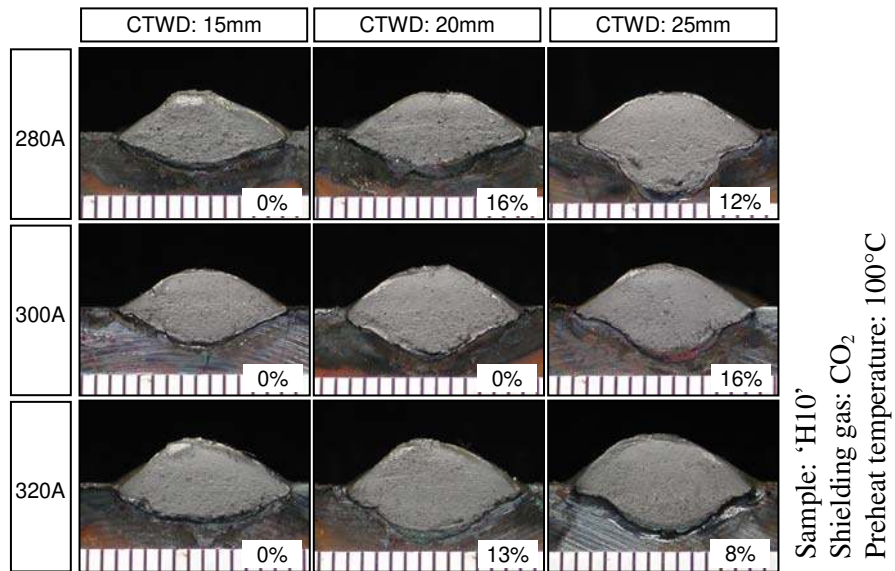
Photographs of the fracture faces of H10 weld deposits at preheat temperature of 100 °C and using CO_2 shielding gas.
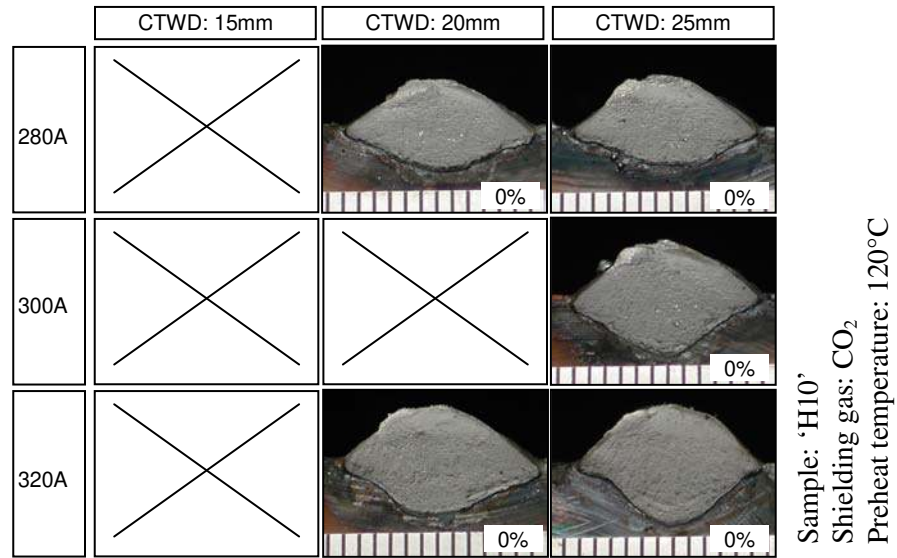
	CTWD: 15mm	CTWD: 20mm	CTWD: 25mm
280A		0%	0%
300A			0%
320A		0%	0%

Sample: 'H10'
Shielding gas: CO_2
Preheat temperature: 120°C

Photographs of the fracture faces of H10 weld deposits at preheat temperature of 120 °C and using CO_2 shielding gas.

	CTWD: 15mm	CTWD: 20mm	CTWD: 25mm
280A	0%	0%	0%
300A	0%	0%	0%
320A	0%	0%	0%

Sample: 'H5'
Shielding gas: 75Ar-25CO_2
Preheat temperature: 20°C
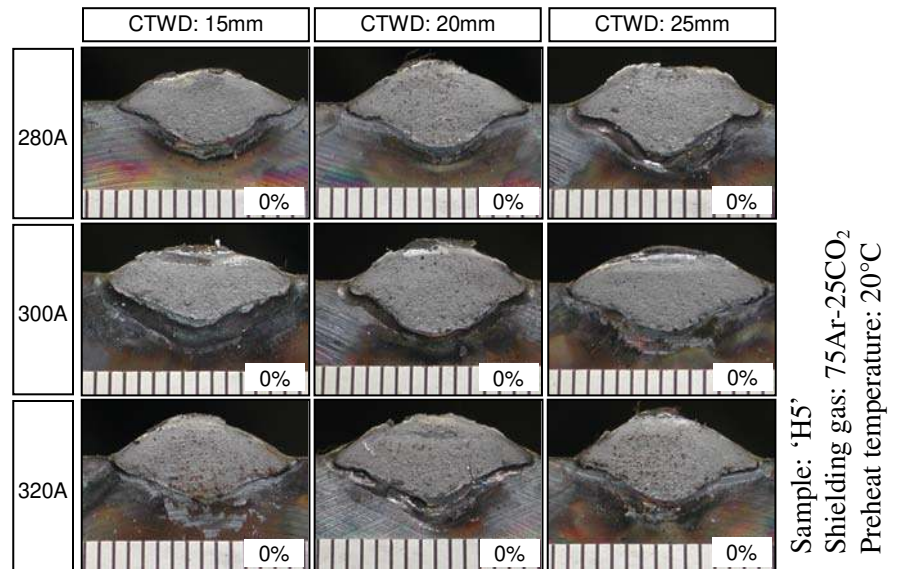
Photographs of the fracture faces of H5 weld deposits at preheat temperature of 20 °C and using 75Ar-25CO_2 shielding gas.
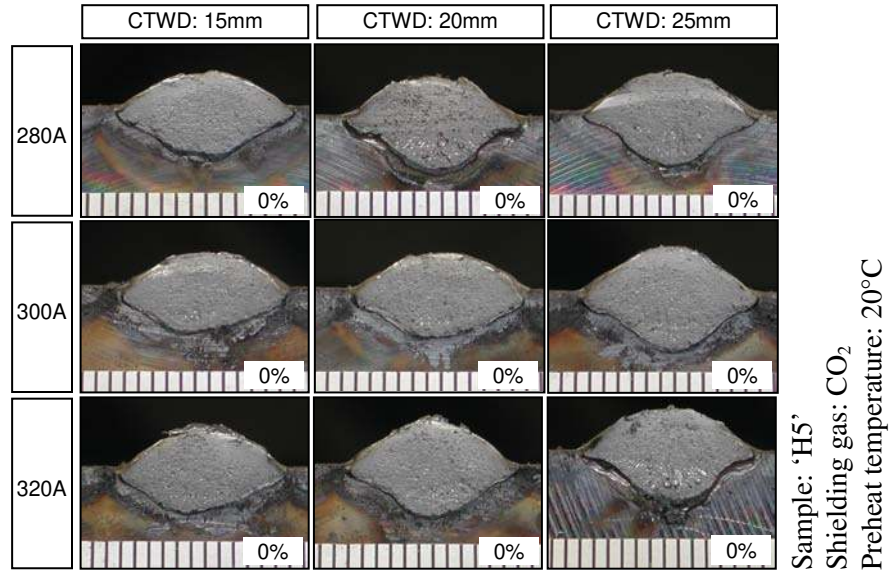
Photographs of the fracture faces of H5 weld deposits at preheat temperature of 20 °C and using CO_2 shielding gas.
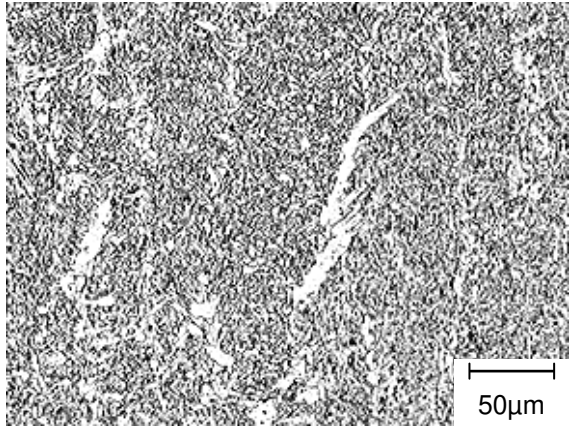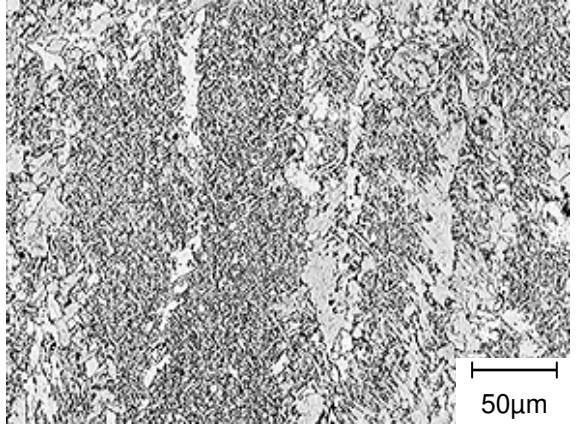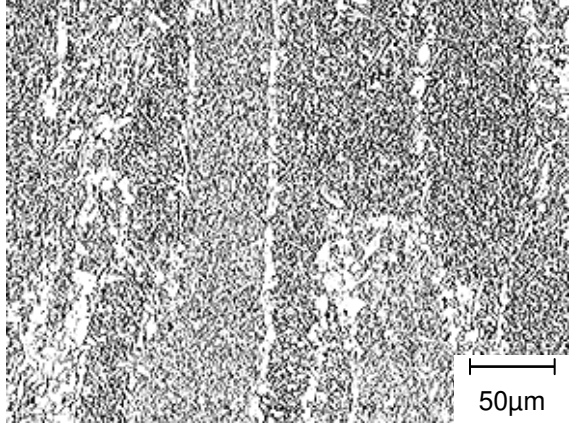
Appendix D:

Graphs showing the percentage of cracking for H10 weld metal in G-BOP tests, using 75Ar-25CO$_2$ and CO$_2$ shielding gases at CTWD of 15, 20 and 25 mm and welding currents of 300 and 320 A (for data refer to Table 6.7 and 6.8).
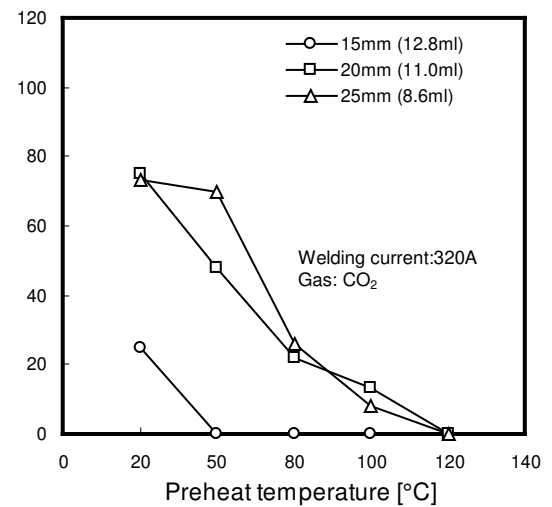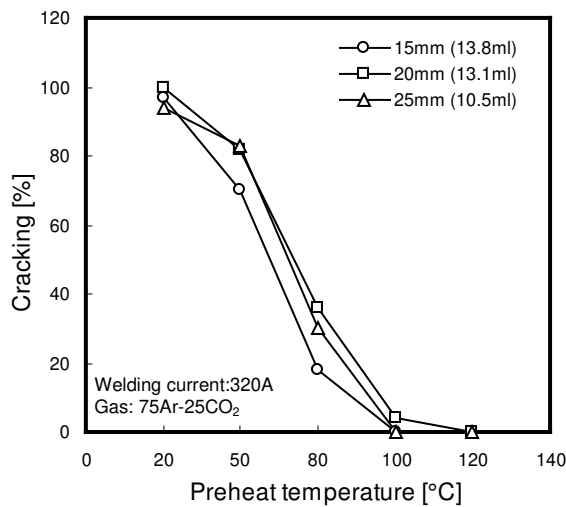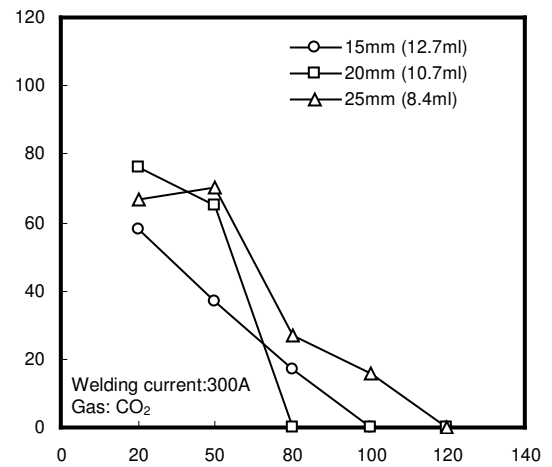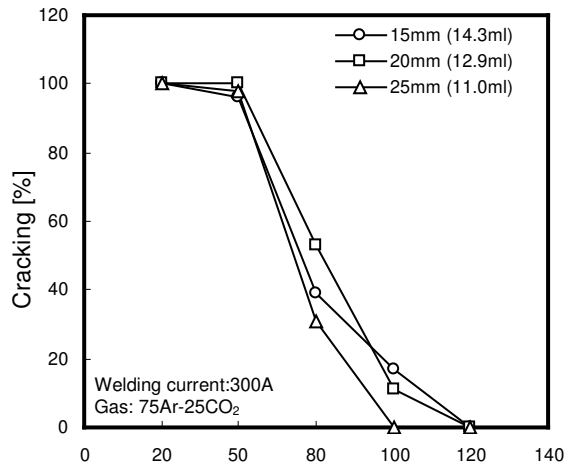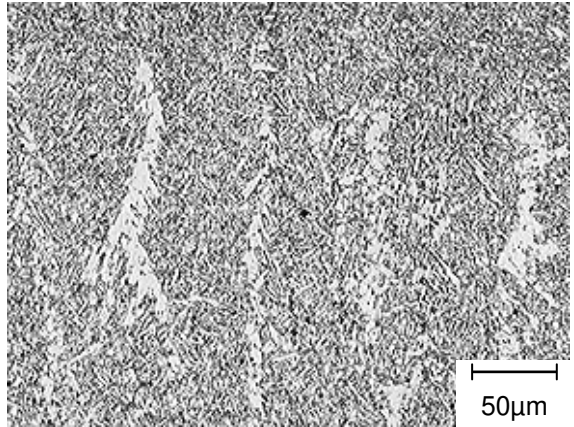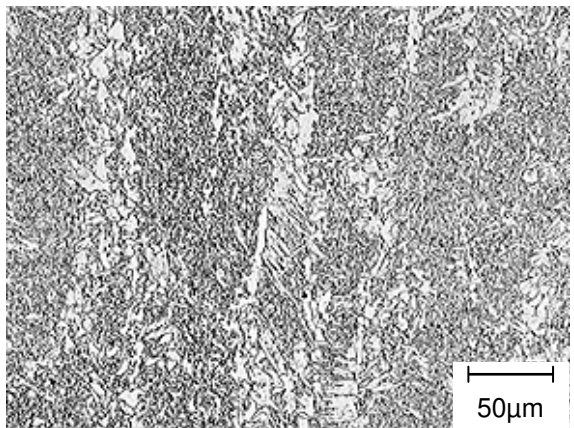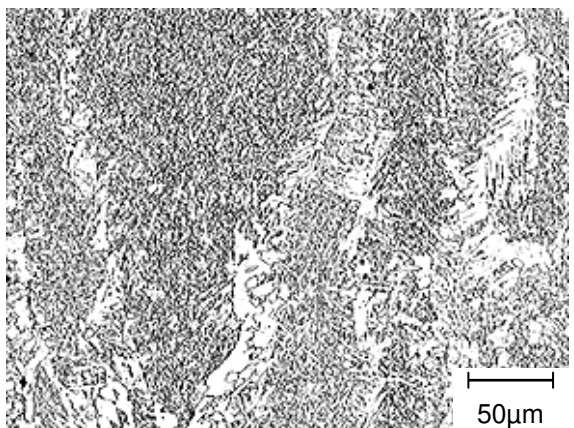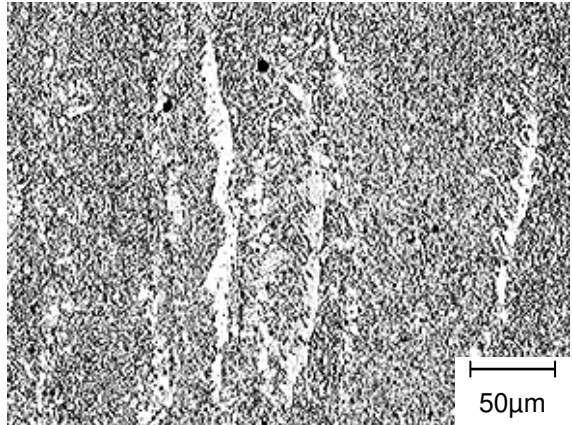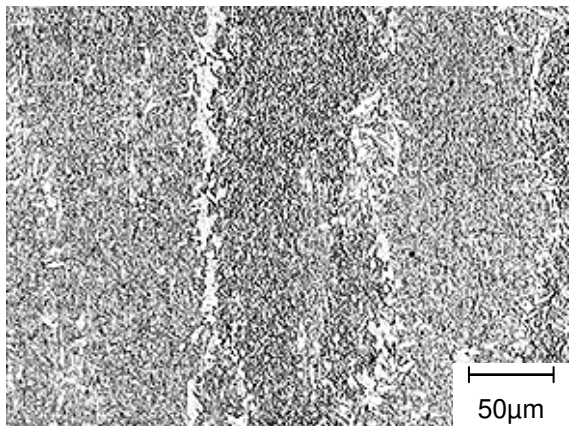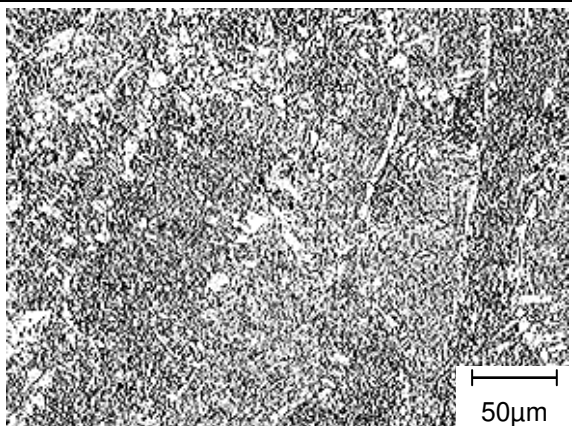
Appendix E:
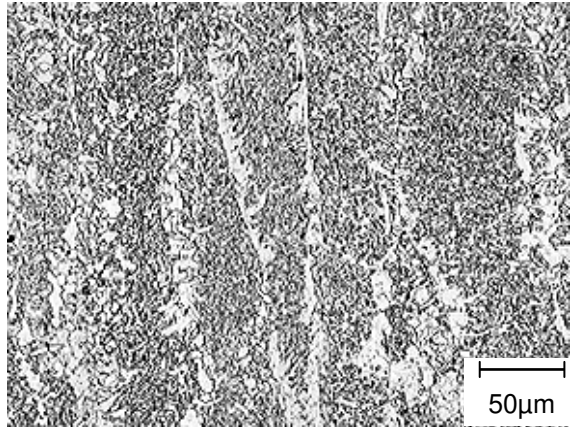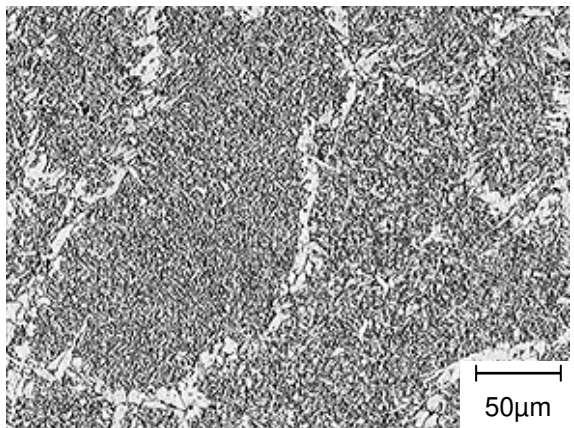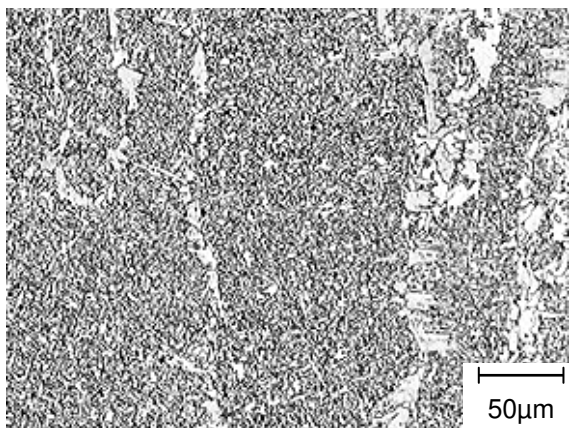
Micrographs showing the H10 and H5 weld deposits from G-BOP test samples using range of welding parameters, as listed in Table 5.9.

Wire sample:	H10	
Welding current [A]:	280	
CTWD [mm]:	15	
Shielding gas:	CO_2	
Weld metal H_D [ml/100g]:	11.7	
Preheat temperature [°C]:	20	
Percentage cracking [%]:	89	
Vickers hardness HV 0.5kg:	215	
Sample:	H10-10-20C	50µm
Wire sample:	H10	
Welding current [A]:	300	
CTWD [mm]:	15	
Shielding gas:	CO_2	
Weld metal H_D [ml/100g]:	12.7	
Preheat temperature [°C]:	20	
Percentage cracking [%]:	58	
Vickers hardness HV 0.5kg:	224	
Sample:	H10-11-20C	50µm
Wire sample:	H10	
Welding current [A]:	320	
CTWD [mm]:	15	
Shielding gas:	CO_2	
Weld metal H_D [ml/100g]:	12.8	
Preheat temperature [°C]:	20	
Percentage cracking [%]:	25	
Vickers hardness HV 0.5kg:	233	
Sample:	H10-12-20C	50µm

Wire sample:	H10	
Welding current [A]:	300	
CTWD [mm]:	15	
Shielding gas:	75Ar-25CO_2	
Weld metal H_D [ml/100g]:	14.3	
Preheat temperature [°C]:	20	
Percentage cracking [%]:	100	
Vickers hardness HV 0.5kg:	235	
Sample:	H10-2-20A	50µm
Wire sample:	H10	
Welding current [A]:	300	
CTWD [mm]:	15	
Shielding gas:	75Ar-25CO_2	
Weld metal H_D [ml/100g]:	14.3	
Preheat temperature [°C]:	120	
Percentage cracking [%]:	0	
Vickers hardness HV 0.5kg:	213	
Sample:	H10-2-120A	50µm
Wire sample:	H10	
Welding current [A]:	300	
CTWD [mm]:	15	
Shielding gas:	CO_2	
Weld metal H_D [ml/100g]:	12.7	
Preheat temperature [°C]:	120	
Percentage cracking [%]:	0	
Vickers hardness HV 0.5kg:	217	
Sample:	H10-11-120C	50µm

Wire sample:	H10	
Welding current [A]:	280	
CTWD [mm]:	25	
Shielding gas:	CO_2	
Weld metal H_D [ml/100g]:	8.3	
Preheat temperature [°C]:	20	
Percentage cracking [%]:	67	
Vickers hardness HV 0.5kg:	215	
Sample:	H10-16-20C	
Wire sample:	H10	
Welding current [A]:	320	
CTWD [mm]:	25	
Shielding gas:	CO_2	
Weld metal H_D [ml/100g]:	8.6	
Preheat temperature [°C]:	20	
Percentage cracking [%]:	73	
Vickers hardness HV 0.5kg:	233	
Sample:	H10-18-20C	
Wire sample:	H10	
Welding current [A]:	280	
CTWD [mm]:	25	
Shielding gas:	75Ar-25CO_2	
Weld metal H_D [ml/100g]:	12.0	
Preheat temperature [°C]:	20°C	
Percentage cracking [%]:	100	
Vickers hardness HV 0.5kg:	247	
Sample:	H10-7-20A	

Wire sample:	H10	
Welding current [A]:	320	
CTWD [mm]:	25	
Shielding gas:	75Ar-25CO$_2$	
Weld metal H$_D$ [ml/100g]:	10.5	
Preheat temperature [°C]:	20	
Percentage cracking [%]:	94	
Vickers hardness HV 0.5kg:	245	
Sample:	H10-9-20A	
Wire sample:	H5	
Welding current [A]:	300	
CTWD [mm]:	25	
Shielding gas:	CO$_2$	
Weld metal H$_D$ [ml/100g]:	0.9	
Preheat temperature [°C]:	20	
Percentage cracking [%]:	0	
Vickers hardness HV 0.5kg:	222	
Sample:	H5-17-20C	
Wire sample:	H5	
Welding current [A]:	300	
CTWD [mm]:	15	
Shielding gas:	CO$_2$	
Weld metal H$_D$ [ml/100g]:	1.5	
Preheat temperature [°C]:	20	
Percentage cracking [%]:	0	
Vickers hardness HV 0.5kg:	217	
Sample:	H5-11-20C	

Wire sample:	H5	
Welding current [A]:	300	
CTWD [mm]:	25	
Shielding gas:	$75Ar-25CO_2$	
Weld metal H_D [ml/100g]:	1.7	
Preheat temperature [°C]:	20	
Percentage cracking [%]:	0	
Vickers hardness HV 0.5kg:	241	
Sample:	H5-8-20A	
Wire sample:	H5	
Welding current [A]:	300	
CTWD [mm]:	15	
Shielding gas:	$75Ar-25CO_2$	
Weld metal H_D [ml/100g]:	3.1	
Preheat temperature [°C]:	20	
Percentage cracking [%]:	0	
Vickers hardness HV 0.5kg:	232	
Sample:	H5-2-20A	

PUBLICATIONS

1. PITRUN, M., NOLAN, D. and DUNNE D.: 'Correlation of welding parameters and diffusible hydrogen content in rutile flux-cored arc welds' Australasian Welding Journal, Volume 49, 1st Quarter, 2004.

2. NOLAN, D. and PITRUN, M.: 'A comparative study of diffusible hydrogen test methods' Australasian Welding Journal, Volume 48, 4th Quarter, 2003.

3. NOLAN, D. and PITRUN, M.: 'Diffusible Hydrogen Testing in Australia' IIW doc.No. IX-2065-03. (accepted for publication in Welding in the World)
    (presented at the 56th Annual Assembly – Bucharest, Romania, July 2003)

4. PITRUN, M., NOLAN, D. and DUNNE D.: 'Diffusible hydrogen content in rutile flux-cored arc welds as a function of welding parameters' IIW doc.No. IX-2064-03.
    (accepted for publication in Welding in the World)
    (presented at the 56th Annual Assembly – Bucharest, Romania, July 2003)

5. PITRUN, M.: 'The influence of welding parameters on diffusible hydrogen content in weld metal deposited using the FCAW process' Proceedings of Welding Technology Institute of Australia, International Conference – Melbourne, 18-19 March 2002.

6. PITRUN, M.: 'Cold cracking' Proceedings of Welding Technology Institute of Australia, Conference – Adelaide, 8-10 October 2001.

7. PITRUN, M., DAVIDSON, J.L., KENNY, C.J., WITTKE, P.J. and CORNISH, N.: 'Factors affecting the hydrogen content of weld metal deposited by flux cored arc welding consumables' Australasian Welding Journal, Volume 46, 1st Quarter, 2001, pp 33-38.

8. KUEBLER, R., PITRUN, M. and PITRUN, I.: 'The effect of welding parameters and hydrogen levels on the weldability of high strength Q&T steel welded with FCAW consumables' Australasian Welding Journal, Volume 45, 1st Quarter, 2000, pp 38-47.